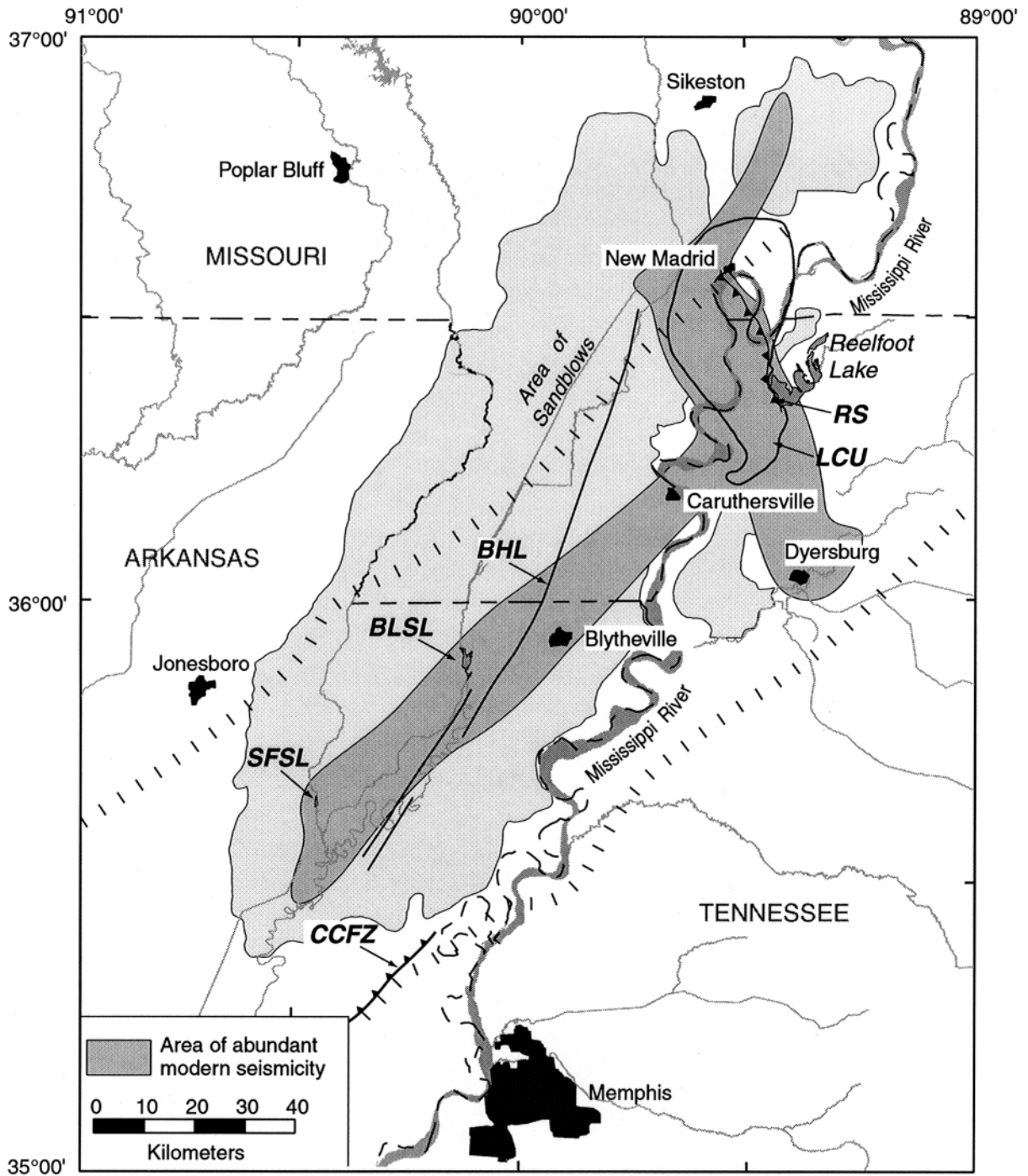


s:\7900\7935\7935.000\03_0109_eesp\fig_2.1-16(04).ai (2003-03-26, 17:20)

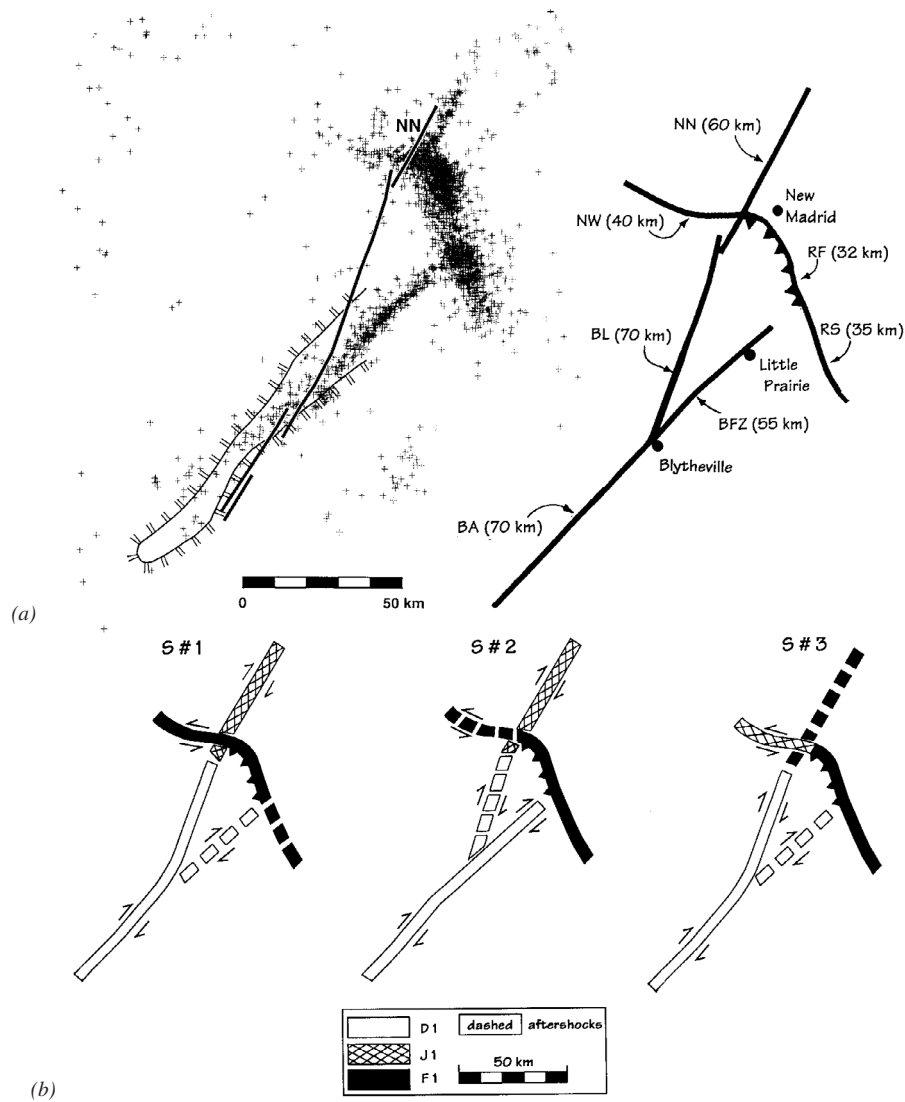


Light shaded area shows location of abundant sand blows and medium shaded area shows location of abundant modern seismicity. Selected features are: LCU, Lake County uplift; RS, Reelfoot scarp; BLSL, Big Lake sunklands; SFSL, St. Frances sunk-lands ; BHL, Bootheel lineament ; CCFZ, Crittenden County fault zone.

From Crone and Wheeler (2000).

Seismic Hazards Report for the EGC ESP Site
**Schematic Diagram Showing the Reelfoot Scarp and Selected Features
 in the Area of the New Madrid Seismic Zone**

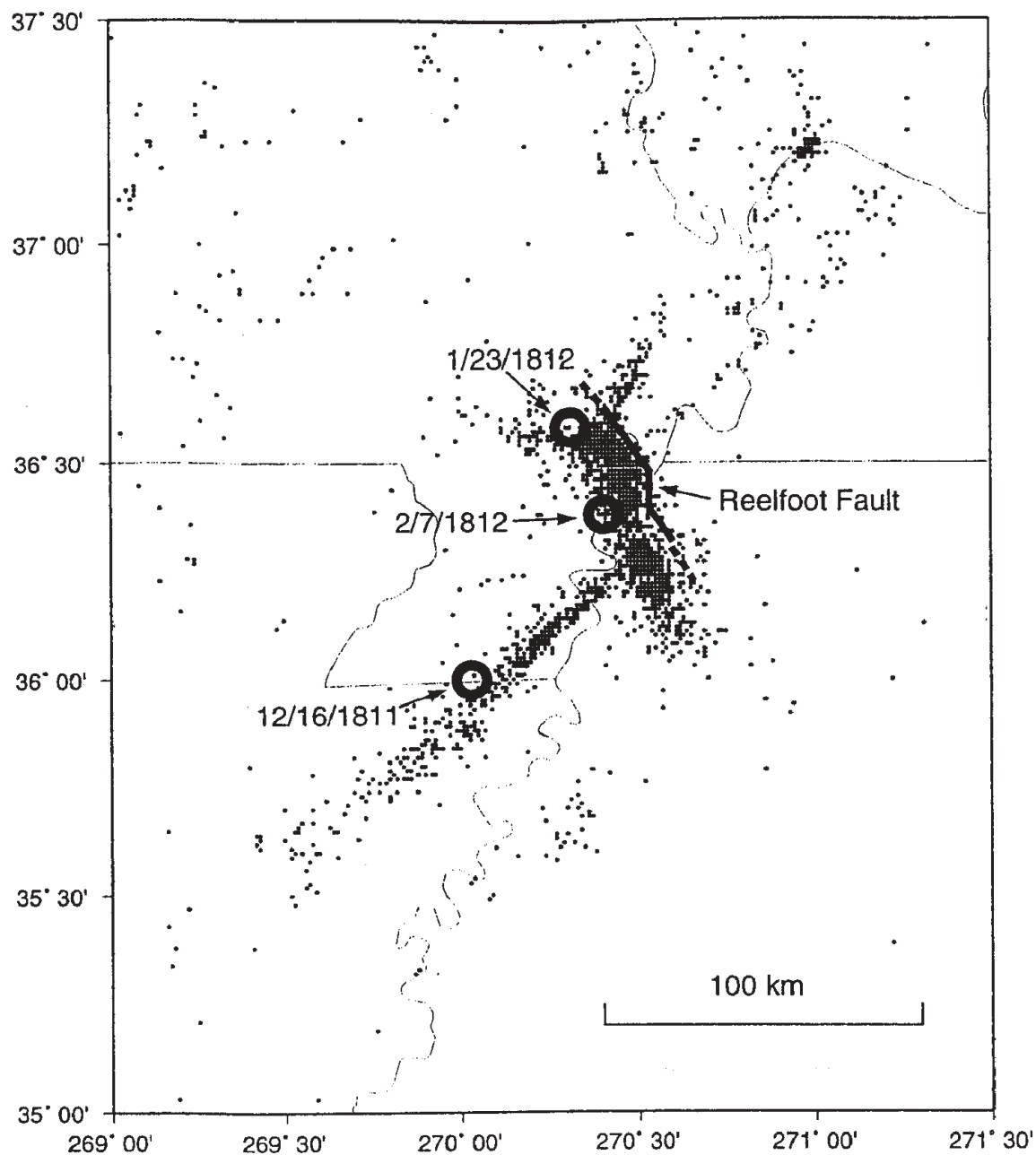
Figure
2.1-21



(a) Fault segmentation of the NMSZ. Seismicity of the NMSZ, the Blytheville arch, and the Bootheel lineament/NN fault (left) yield the seven segments (right) identified as: BA, Blytheville arch; BFZ, Blytheville fault zone; BL, Bootheel lineament; NW, New Madrid west; NN, New Madrid north; RF, Reelfoot fault; RS, Reelfoot south. Segments NW and RS are defined solely from seismicity.

(b) Possible fault rupture scenarios (S#1, S#2, S#3) for the 1811-1812 D1, J1, and F1 earthquake sequences, using the seven fault segments of (a). Based on historical and physical constraints, the D1 principal event must rupture BA, and the F1 principal event must rupture RF in all scenarios. S#1 is the favored scenario.

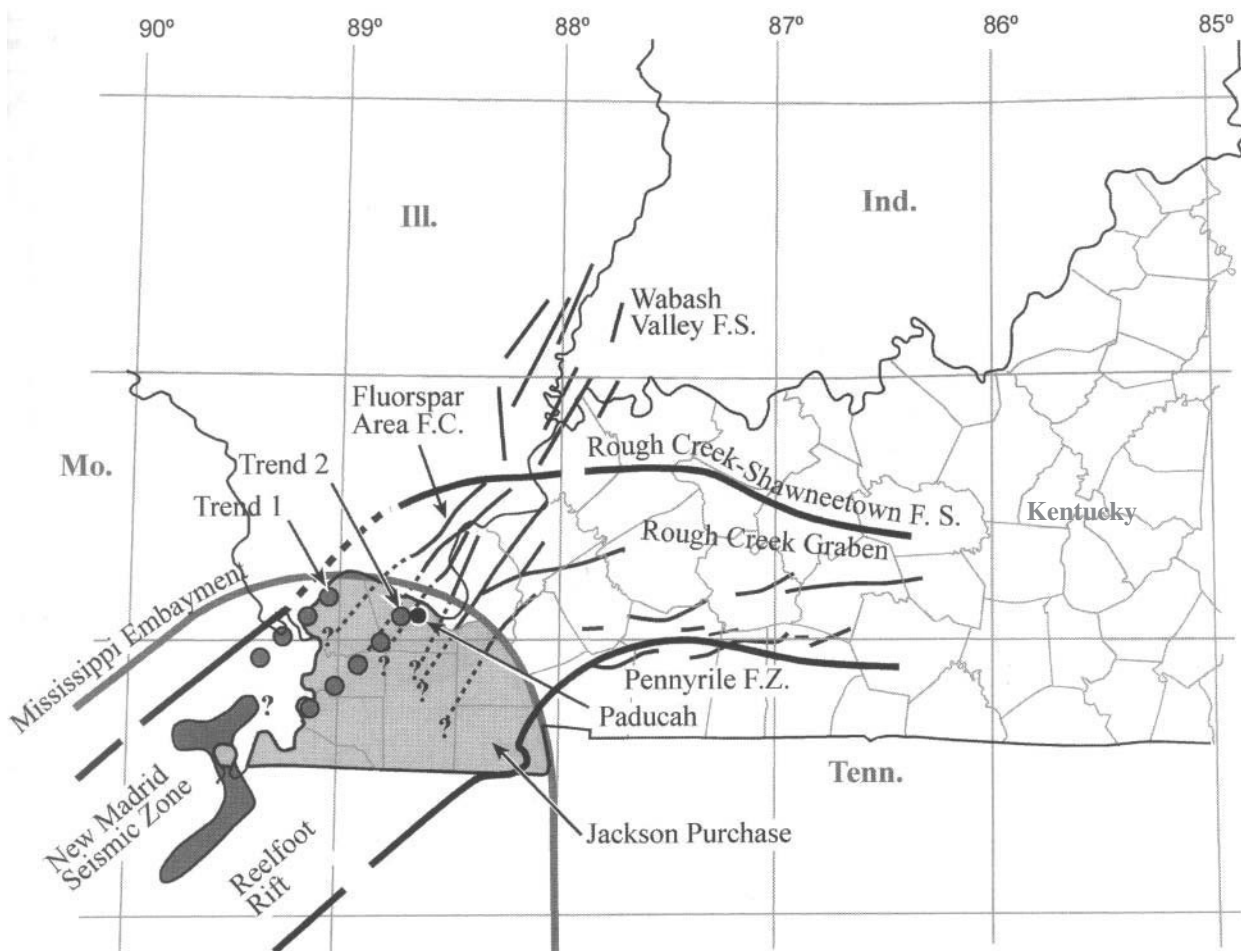
From Johnston and Schweig (1996)



From Hough et al. (2000)

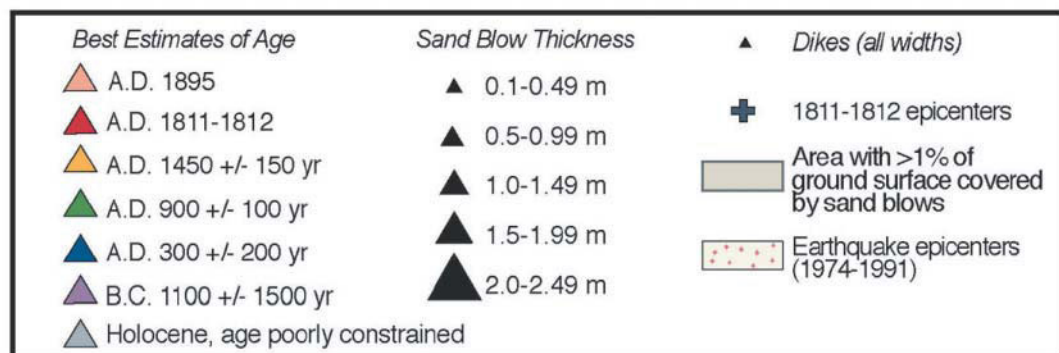
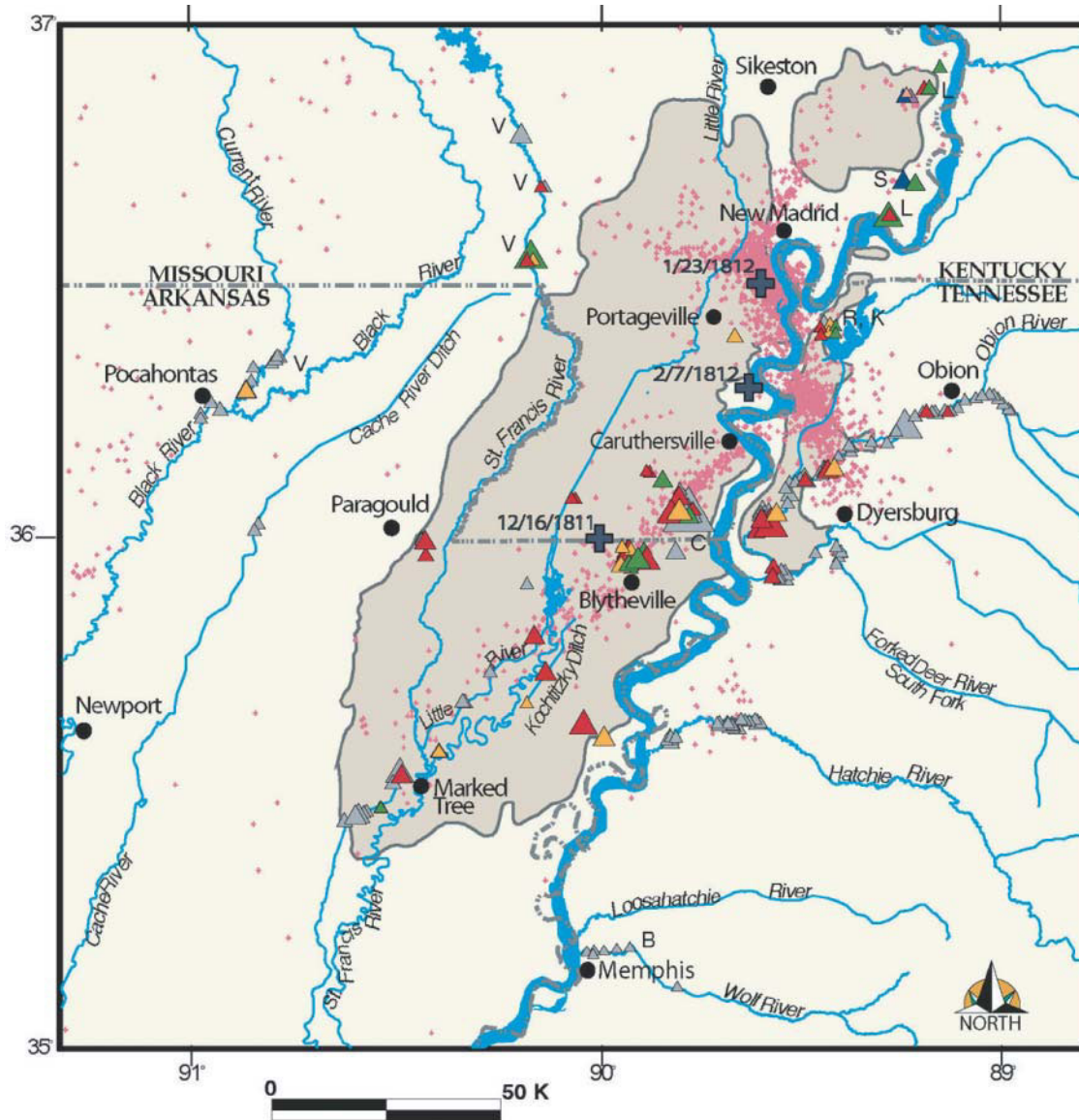
Seismic Hazards Report for the EGC ESP Site
**Map Showing Location of New Madrid Seismic Zone
 as Illuminated by Seismicity Between 1974 and 1996**

Figure
2.1-23



Major structural features (modified from Koda and Nelson, 1997). The lines of shaded circles represent the locations of Wheeler's (1997) trends 1 and 2 seismicity in relation to the New Madrid seismic zone and the study area.

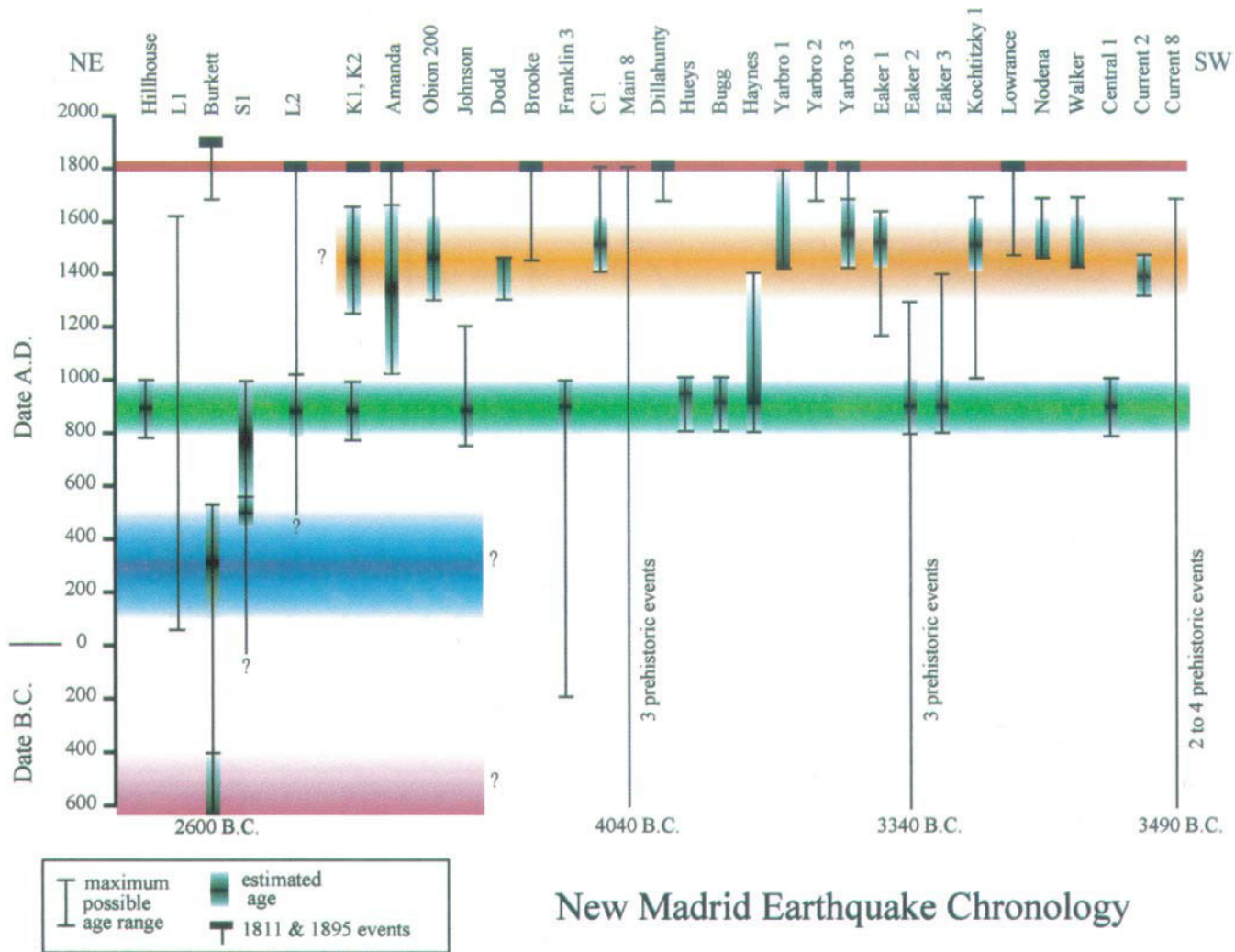
From Woolery and Street (2002)



From Tuttle et al. (2002)

Seismic Hazards Report for the EGC ESP Site
**Map of New Madrid Seismic Zone Showing
 Estimated Ages and Measured Sizes of Liquefaction Features**

Figure
2.1-25

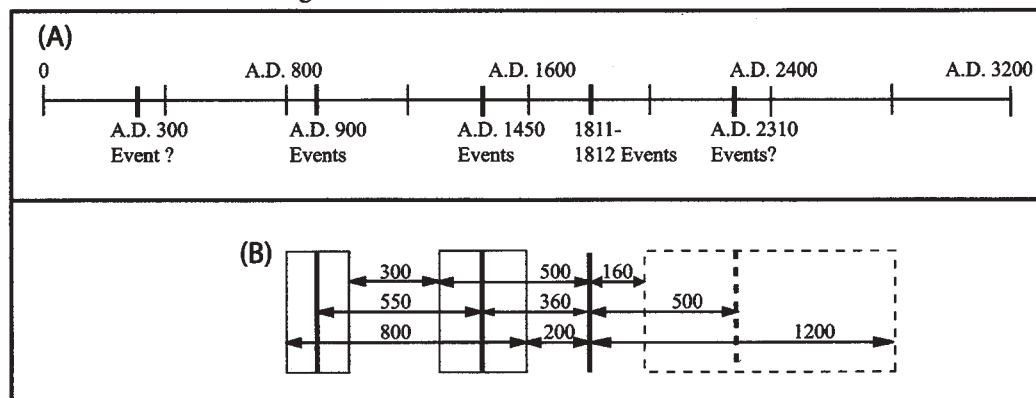


From Tuttle et al. (2002)

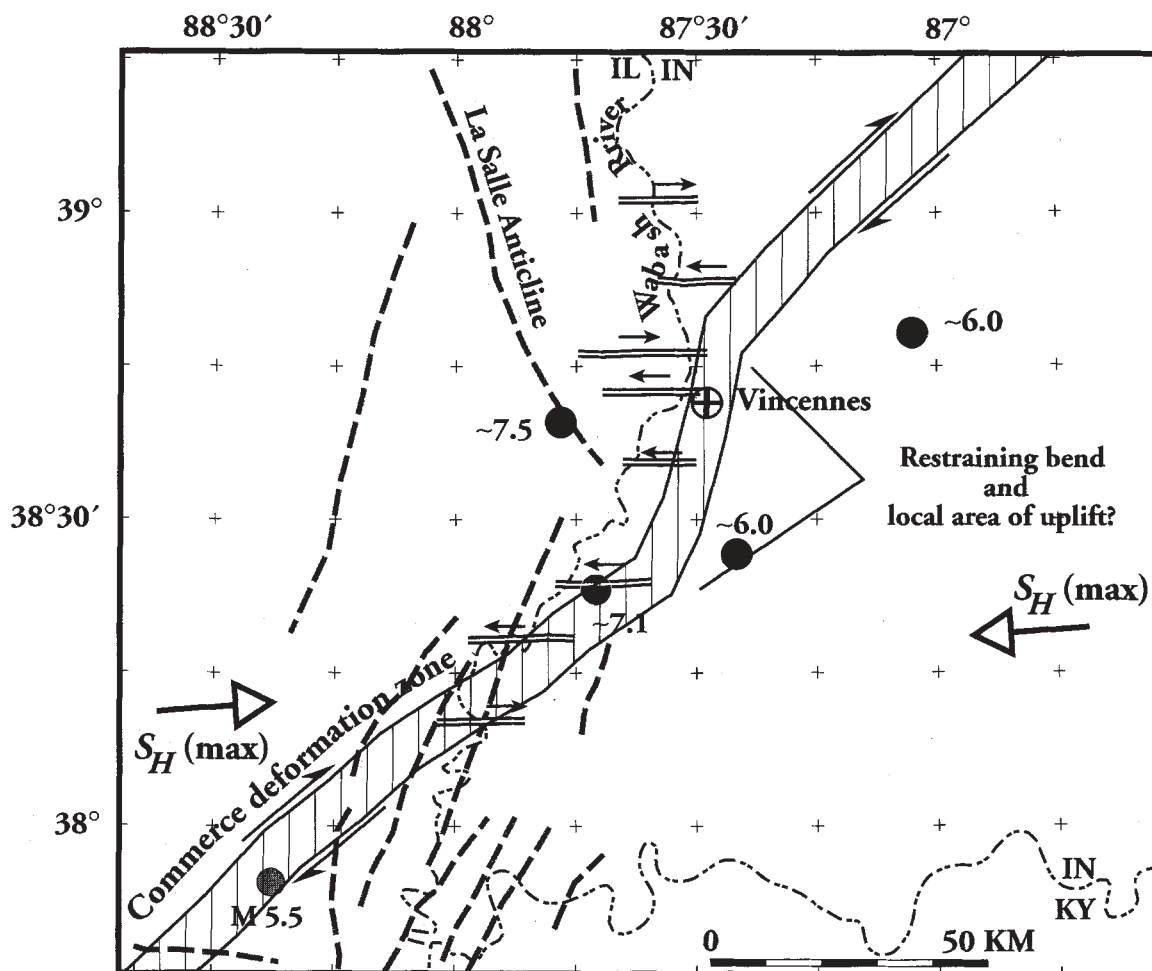
Seismic Hazards Report for the EGC ESP Site
**Earthquake Chronology for NMSZ from Dating and Correlation of
 Liquefaction Features at Sites Along NE-SW Transect Across Region**

Figure
2.1-26

Timing and Recurrence Intervals of New Madrid Events



From Tuttle et al. (2002)

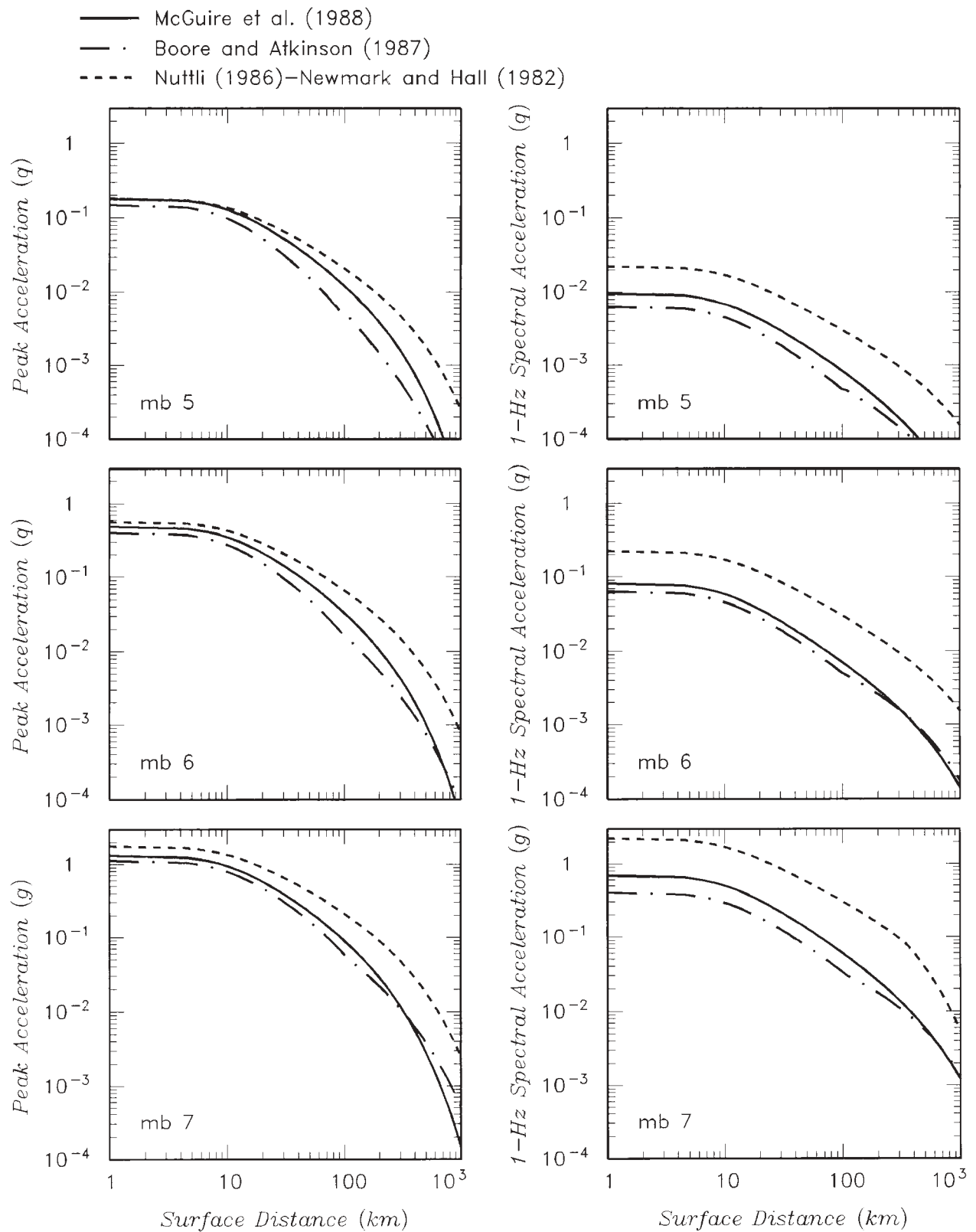


Wabash Valley region highlighting the proposed restraining bend or left step in the Commerce deformation zone (Commerce geophysical lineament). Along eight east-west profiles in the Wabash River region (shown by double black lines), Fraser et al. (1997) carried out detailed morphometric analysis of the land surface, detailed geologic mapping, and structural analysis of bedrock. Arrows on these profiles show the tilt of bedrock and indicate that bedrock generally tilts to the west at the left step and to the east outside the step. Dashed lines are mapped faults based on the structural map of Illinois by Nelson (1995) and structural maps of the Illinois basin (Nelson, 1991). The direction of maximum horizontal compressive stress is shown by arrows and $S_H(\max)$. Assuming right-lateral movement along the CDZ, thrust faults may have developed at the restraining bend, leading to a local uplifted block. The westward tilt of bedrock may suggest uplift in the vicinity of the proposed restraining bend. The four black circles are the approximate locations of epicenters of large prehistoric earthquakes (interpreted moment magnitudes of ~6, 7.1, and 7.5 and estimated radial location error of less than 20 km) discussed by McNulty and Obermeier (1999). Because these earthquakes occur near the proposed restraining bend, we suggest the possibility of a relationship between large earthquakes and stress build-up at the bend. Gray circle (M 5.5) identifies the epicenter of the November 1968 moment magnitude 5.5 earthquake in southern Illinois.

From Hildenbrand et al. (2002)

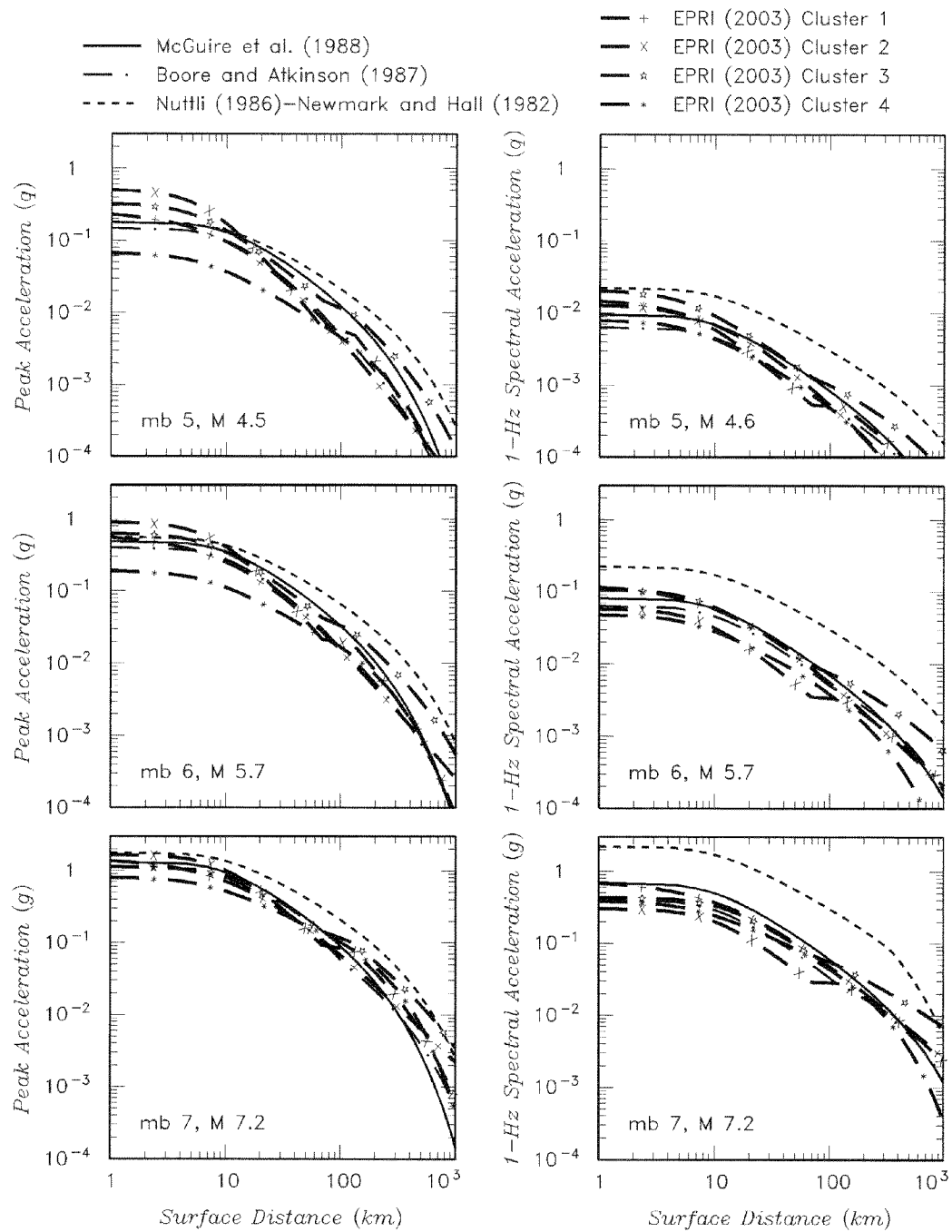
Seismic Hazards Report for the EGC ESP Site
Map Showing Restraining Bend In Commerce Geophysical Lineament

Figure
2.1-28



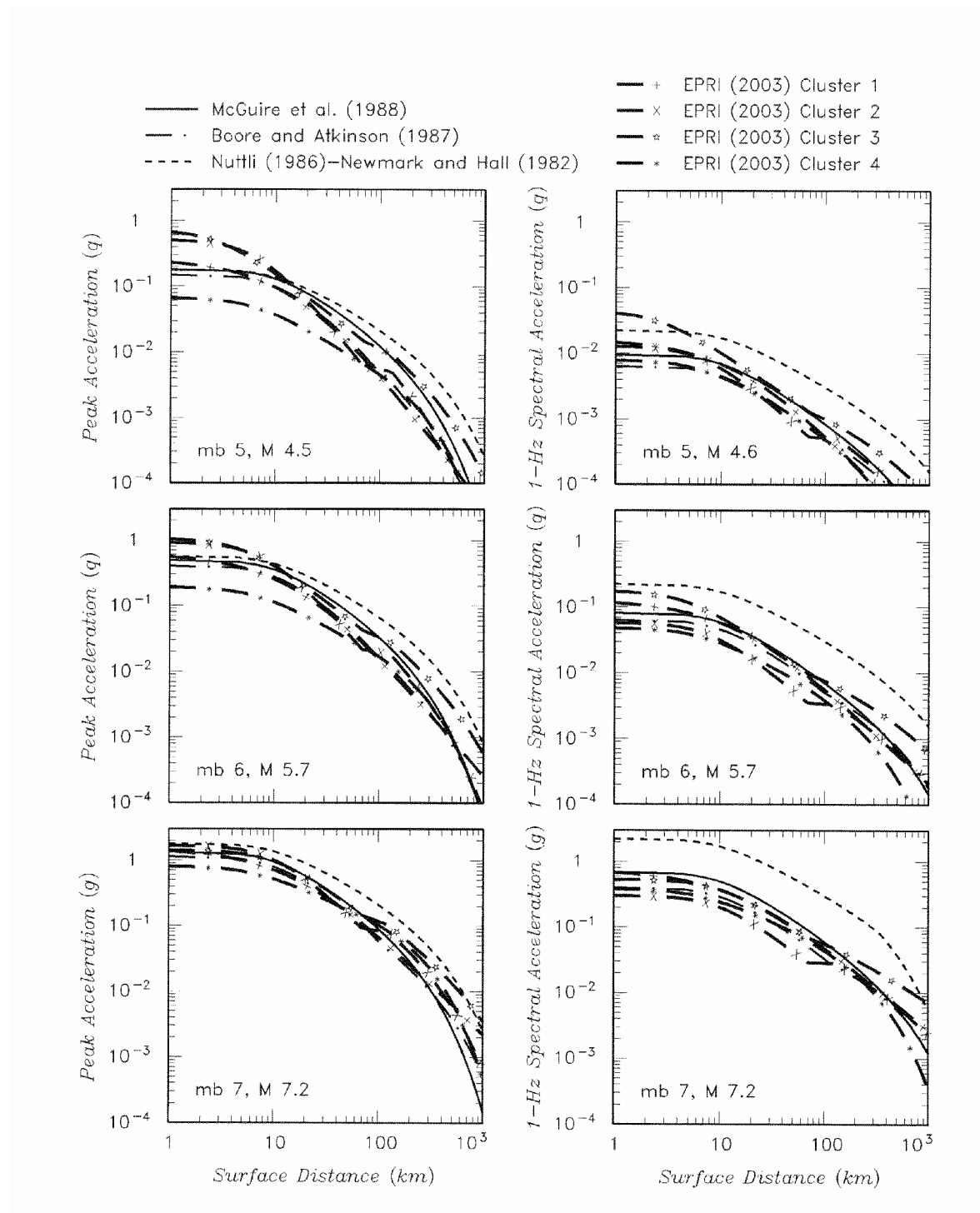
Seismic Hazards Report for the EGC ESP Site
 Median Ground Motion Relationships Used in EPRI-SOG Study

Figure
 2.2-1



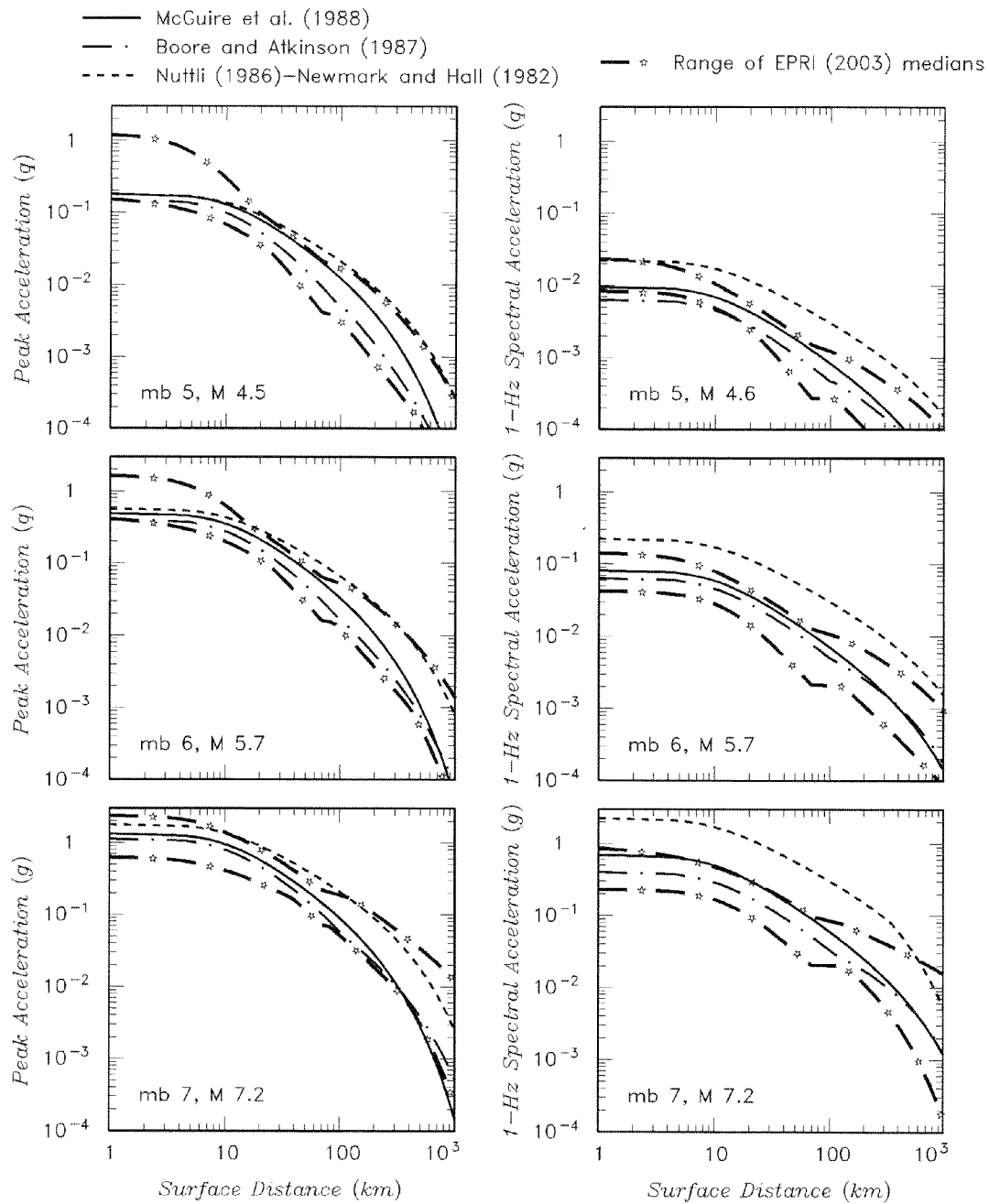
Seismic Hazards Report for the EGC ESP Site
**Comparison of Median Ground Motion Relationships Used in EPRI-SOG
 Study with Recently Developed Relationships**

Figure
2.2-2



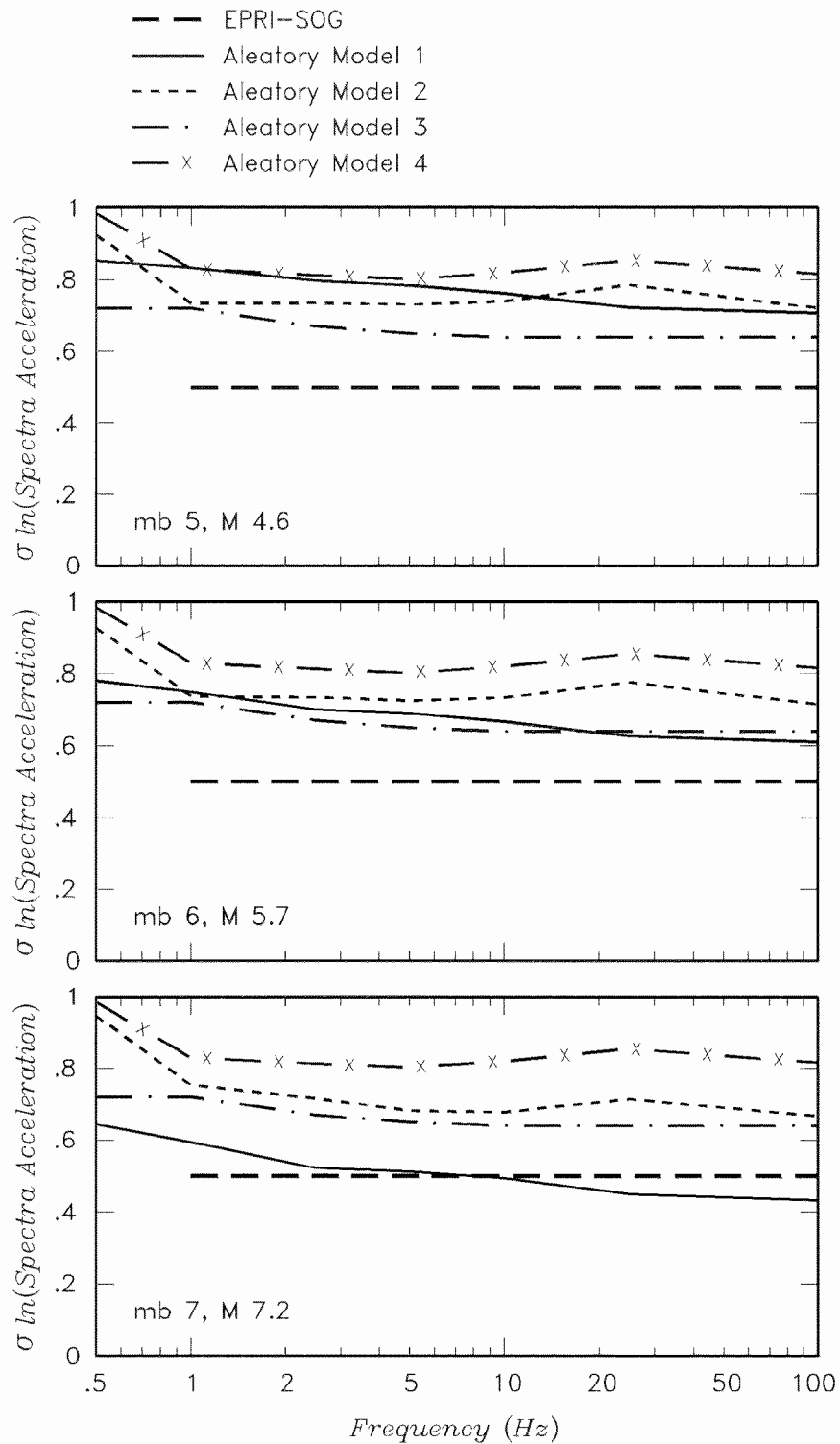
Seismic Hazards Report for the EGC ESP Site
Comparison of the EPRI (2003) Median Attenuation Relationships to the EPRI-SOG Attenuation Relationships

Figure
2.2-3



Seismic Hazards Report for the EGC ESP Site
 Uncertainty Range for EPRI (2003) Median Ground Attenuation Relationships
 Compared to the EPRI-SOG Attenuation Relationships

Figure
 2.2-4



Seismic Hazards Report for the EGC ESP Site
**Comparison of the EPRI (2003) Models for Aleatory Variability with the Value
 Used in the EPRI-SOG Study**

Figure
2.2-5

Evaluation of Recent Information

This chapter summarizes and evaluates the recently acquired data and information compiled and reviewed for Chapter 2 with the goal of examining the effects that the data and information have on the understanding of seismic hazard at the EGC ESP Site. Section 3.1 examines the ways recent information affects input to the site's PSHA in terms of:

- any newly identified seismic sources in the site region (Section 3.1.1);
- modifications to earthquake recurrence rates for the region (Section 3.1.2);
- estimated maximum magnitudes for the region (Section 3.1.3); and
- the ground motion attenuation appropriate for the site region (Section 3.1.4).

In Section 3.2, these parameters are adjusted based on new information, and the sensitivity of the PSHA to each of these parameters is analyzed, using both the EPRI-SOG model (Section 3.2.1) and a simplified model (Section 3.2.2). Incorporating information developed since the EPRI-SOG study produces changes in site hazard that may be considered significant. Therefore, a decision was made that ground motions for the SSE for the EGC ESP Site would be based on an updated PSHA based on the EPRI-SOG model as adjusted in the following chapter (Section 4.1).

3.1 Summary of New Information

Several factors may produce changes in the level of seismic hazard at the EGC ESP Site compared to what would be estimated based on the EPRI-SOG study. Data and information that could affect the predicted level of seismic hazard include:

- identification of a possible new seismic source in the site vicinity;
- changes in the characterization of the rate of earthquake occurrence for one or more seismic sources;
- changes in the characterization of the maximum magnitude for seismic sources; and/or
- differences in the characterization of earthquake ground motions.

The relevance of the data presented in Chapter 2 to these items is evaluated following Regulatory Guide 1.165 (Appendix E, Section E.3 – USNRC, 1997) discussed below.

3.1.1 Identification of Seismic Sources (RG 1.165, E.3 Step 1 Evaluation)

As discussed in Chapter 2 of this Appendix, much of the seismic hazard research conducted within 200 miles of the EGC ESP Site has focused on the region comprising the Wabash Valley/southern Illinois/southwestern Indiana. Investigators have found evidence for a number of moderate-to-large prehistoric earthquakes in the Wabash Valley region. The

faulting responsible for those earthquakes is presently unknown, and in the past several years investigators have proposed various source zone geometries (e.g., Toro and Silva, 2001; Wheeler and Cramer, 2002; Cramer et al., 2002). Some of these geometries are shown in the right-hand plot on Figure 3.1-1. The left-hand plot in that figure shows a composite of the source zones defined for the Wabash Valley/southern Illinois region by the EPRI-SOG expert teams. The EPRI-SOG sources encompass the recently proposed source zones.

The New Madrid seismic zone (NMSZ) is located just beyond the 200-mile radius around the EGC ESP Site. Dating of paleoliquefaction features has identified four prehistoric earthquake sequences in the region. Research continues to focus on correlating the 1811-1812 and prehistoric earthquakes with faults and lineaments of seismicity. Various investigators have proposed a range of actual and modeled-faults for use in PSHA (e.g., Cramer, 2001). These sources fall within the general outlines of the NMSZ defined by the EPRI-SOG expert teams (Figure 3.1-2). The EPRI-SOG experts' alternative interpretations of the New Madrid seismic source, therefore, adequately account for new information on possible fault sources within the New Madrid source zone.

In Figure 3.1-3, the spatial pattern of earthquakes recorded after completion of the EPRI-SOG study is compared to the pattern of earthquakes in the EPRI-SOG catalog. The earthquakes for the period 1985 to June 2002 show the same spatial pattern as those in the period 1777 to 1985. Events are concentrated in the New Madrid source zone and occur throughout the Wabash Valley/southern Illinois region. Activity in central and northern Illinois consists of only a few earthquakes larger than magnitude m_b 3. The EPRI-SOG experts' alternative configurations for the background earthquake at the EGC ESP Site are consistent with the updated seismicity patterns.

Based on the above evaluations, it is concluded that data obtained since the EPRI-SOG study suggest no additional specific seismic sources in the site region. The seismicity parameter values for these zones will be considered next.

3.1.2 Earthquake Recurrence Rates (RG 1.165, E.3 Step 1 Evaluation)

In the E.3 step 1 evaluation of the significance of new data regarding earthquake recurrence, a simplified zone model was used to represent the three most significant contributors to hazard at the EGC-ESP Site. The simplified source model consists of a New Madrid source zone, a Wabash Valley-southern Illinois source zone, and a central Illinois source zone (Figure 3.1-4).

Section 2.1.3 of this Appendix presents a discussion of an updated earthquake catalog for the study region. These data were used to compute earthquake recurrence rates for the sensitivity analyses. The method for calculating earthquake recurrence for the EPRI-SOG study computed earthquake frequencies over the entire time span of the catalog, accounting for incomplete recording periods by estimating the probability of detecting and recording earthquakes through time. It was judged that the probability of detecting $m_b \geq 3.3$ events is now 1.0 in the study region. The estimated probabilities of detection were then used to obtain an "equivalent period of completeness" for specific regions of the CEUS. The EPRI-SOG study demonstrated that the frequency of earthquakes could be estimated by dividing the total number of earthquakes in the catalog for a specific magnitude interval by the equivalent period of completeness. Using the EPRI-SOG catalog and the equivalent periods

of completeness obtained in the EPRI-SOG study, earthquake recurrence rates were obtained for the three source zones shown on Figure 3.1-4. Those rates are plotted as the open circles on Figure 3.1-5. The vertical error bars represent the 90-percent confidence intervals for earthquake frequency.

In computing earthquake frequencies for the updated catalog, it was assumed that the probability of detection for $m_b \geq 3.3$ events has remained 1.0 for the period 1985 to the present. Therefore, the period of completeness for the updated catalog is equivalent to the EPRI-SOG estimates plus the interval from January 1985 to June 2002. The earthquake frequencies computed using the updated catalog are shown by solid diamonds on Figure 3.1-5. For clarity the data points are plotted with a slight offset from those based on the EPRI-SOG catalog. The comparisons provided by the figure indicate that including an additional 17 years of earthquake data does not change significantly the earthquake frequencies computed from the catalog data.

The other source of information on earthquake recurrence is the paleoliquefaction data. Estimates for the rates of moderate-to-large events based on these data are shown on Figure 3.1-5. For New Madrid, the box indicates the \pm one-standard-deviation estimate on the mean frequency obtained by Cramer (2001). For the Wabash Valley, solid squares show the rates estimated for the counted number of large paleoearthquakes since 6,000 BC, the period for which the record of paleoearthquakes is likely complete. A similar calculation was performed for the central Illinois zone using the postulated Springfield paleoearthquake.

The comparisons shown on Figure 3.1-5 indicate that for central Illinois and the Wabash Valley, earthquake recurrence relationships fit to the recorded seismicity envelop the rates of larger earthquakes estimated from paleoliquefaction data. Such is not the case for the New Madrid zone, as illustrated on Figure 3.1-6. Added to this figure is the distribution of earthquake recurrence rates computed from the EPRI-SOG expert teams' recurrence assessments for the New Madrid source. These predicted rates are consistent with the rates calculated using the updated seismicity catalog. However, they under-predict the rate of large-magnitude earthquakes by about one order of magnitude.

The conclusion drawn from these comparisons is that, except for large earthquakes in the New Madrid seismic zone, the EPRI-SOG recurrence parameters should provide a good estimate of the current rate of seismicity in the study region and do not require updating.

3.1.3 Assessment of Maximum Magnitude (RG 1.165, E.3 Step 1 Evaluation)

Figures 3.1-7 through 3.1-9 show the composite maximum magnitude distributions for the three regions based on the EPRI-SOG experts' composite uncertainty assessment. The top plot on each figure shows the maximum magnitude distribution in terms of m_b magnitudes, the magnitude scale used in the EPRI-SOG study. The bottom plot shows the maximum magnitude distribution in terms of moment magnitude M . The m_b values were converted to moment magnitude using an equally weighted combination of the $m_b - M$ relationships given in EPRI (1993), Atkinson and Boore (1995), and Johnston (1996). The heavy arrows on the figures indicate the range in maximum magnitudes that have been published recently for the New Madrid seismic zone or are suggested by the estimated sizes of paleoearthquakes (for the Wabash Valley and central Illinois). These plots indicate that the recent maximum magnitude estimates for New Madrid seismic zone are consistent with the

EPRI-SOG experts' assessments. For the Wabash Valley, the largest identified paleoearthquake has an estimated magnitude of **M** 7.0 to 7.8. The estimated maximum magnitude for an earthquake nucleating in the basement in the southern Illinois basin in the vicinity of the DuQuoin monocline and Loudon anticline is **M** 6-7 (Su and McBride, 1999). These estimates lie near the upper end of the range of the EPRI-SOG experts' composite assessments for Wabash Valley-southern Illinois sources. The estimated magnitude for the postulated paleoearthquake in central Illinois is **M** 6.5 \pm 0.3, a value that lies near the upper tail of the EPRI-SOG composite maximum magnitude distribution for central Illinois sources.

The conclusion drawn from these comparisons is that the maximum magnitude uncertainty distributions for the central Illinois-background source zones and the Wabash Valley-southern Illinois sources developed by the EPRI-SOG expert teams do not adequately encompass magnitudes as large as those implied by the new paleoliquefaction data. Consequently, a Regulatory Guide 1.165, Position E.3, Step 2 sensitivity analysis is needed to determine the significance of these new data.

3.1.4 Assessment of Ground Motion Attenuation

The comparisons developed in Section 2.2 of this Appendix indicate that current ground motion models for the CEUS generally are consistent with the median models used in the EPRI-SOG study. The aleatory variability about the median ground motions used in the EPRI-SOG study, however, is significantly lower than current estimates. Given the extensive research on CEUS ground motions since the EPRI-SOG work, the effect of the newer models should be examined.

3.1.5 Summary

Based on the above assessments and consistent with the requirements of Regulatory Guide 1.165, Position E.3, the following source parameter adjustments are studied as part of PSHA sensitivity tests for the EGC ESP Site.

- Sensitivity to new data relative to the occurrence of large earthquakes in the New Madrid Seismic zone. Specifically, the interpretation that the data support the occurrence of characteristic, time-clustered earthquake sequences in the NMSZ with an average return period in the range of 500 to 1,000 years.
- Sensitivity to new data and interpretations relative to assessment of maximum magnitude for the Wabash Valley seismic source.
- Sensitivity to new data and interpretations of maximum magnitude for the central Illinois/background seismic source.
- Sensitivity to new ground motion models.

3.2 PSHA Sensitivity Studies

This section of Appendix B describes the sensitivity studies that were carried out to address changes in the PSHA model used by the EPRI-SOG. Results of these sensitivity studies led to an updated PSHA for the EGC ESP Site, as discussed in Section 4 of this Appendix.

3.2.1 Sensitivity of EPRI-SOG PSHA Results to New Data

The first step in the analysis was to translate the EPRI-SOG input evaluations into a format usable by Geomatrix PSHA software. Figure 3.2-1 compares the rock hazard curves obtained using the EPRI-SOG software and input files to the rock hazard curves computed using Geomatrix's software and the EPRI-SOG input. The comparison indicates that the EPRI-SOG results can be duplicated using Geomatrix software.

The first sensitivity analysis tests the effect of increasing the maximum magnitude distribution for central Illinois from that shown on Figure 3.1-9 to a uniform distribution in the range of m_b 6.4 to 6.8 (M 6.5 to 7). Figure 3.2-2 compares the resulting hazard curves to EPRI-SOG results. As shown, there is a noticeable increase in hazard (increase in the frequency of exceedance). (Note that the curves labeled EPRI-SOG (this study) are computed using Geomatrix software and the EPRI-SOG inputs.)

Figure 3.2-3 shows the results of two sensitivity analyses on the mean and median hazard. The curves labeled "local M_{max} " show the effect of changing the M_{max} distribution of the local source (the same sensitivity as shown on Figure 3.2-2). The curves labeled "Local M_{max} plus Characteristic New Madrid" show the effect on the mean and median hazard of adding a single source of New Madrid characteristic earthquakes with a return period of 500 to 1,000 years in addition to modifying the maximum magnitude distribution for the local sources. The addition of the characteristic New Madrid earthquakes has no effect on peak acceleration hazard beyond that caused by an increase in the local maximum magnitude distribution, but does produce an increase in the hazard for 1 Hz spectral acceleration.

Figure 3.2-4 shows the effect of replacing the three m_b -based ground motion attenuation models used in the EPRI-SOG study with two more recently published models, also defined in terms of m_b . The EPRI-SOG source parameters were not modified for this comparison. The newer models are those of Atkinson and Boore (1995) and Toro et al. (1997), and they were given equal weight in the calculations. The newer m_b attenuation models result in lower peak acceleration hazard, except at peak accelerations above approximately 0.3 g. Use of the newer m_b attenuation models results in an increase in the median hazard for the 1 Hz spectral acceleration, partly because of the greater aleatory variability in the newer models (the Toro et al. [1997] uncertainty model was applied to both relationships). The mean hazard for 1-Hz spectral acceleration decreases using the newer attenuation models because both newer models give 1-Hz spectral acceleration estimates well below those obtained from the Nuttli-Newmark-Hall model used in the EPRI-SOG study.

Figure 3.2-5 shows the effect of replacing the three m_b -based ground motion attenuation models used in the EPRI-SOG study with the new M -based ground motion attenuation models developed by EPRI (2003). The three m_b - M relationships described in Section 3.1.3 were used to convert m_b magnitudes into moment magnitude for calculation of the hazard using the EPRI (2003) ground motion models. The effect of the EPRI (2003) ground motion attenuation models on the hazard is similar to that shown on Figure 3.2-4 for the newer m_b -based attenuation models. For peak acceleration, the EPRI (2003) attenuation models produce lower hazard for peak accelerations below about 0.15g, and higher hazard for larger motions. Similar to the results shown on Figure 3.2-4, the EPRI (2003) attenuation models produce higher median hazard for 1-Hz spectral acceleration and lower mean hazard.

3.2.2 PSHA Sensitivity Using Simplified Source Model

To more efficiently explore the effects of other new data, the simplified seismic source model was used. The model consists of three sources (Figure 3.1-4) developed from EPRI-SOG sources: a New Madrid source, a Wabash Valley-southern Illinois source, and a central Illinois source. The sources were assumed to have spatially homogeneous seismicity. The seismicity parameters were developed from the earthquake catalog using the equivalent periods of completeness developed in the EPRI-SOG study. Figure 3.2-6 shows the fits to the seismicity data for each seismic source. As shown, the extrapolation of the seismicity rates obtained from the catalog encompasses the paleoearthquake rates for the Wabash Valley-southern Illinois and central Illinois sources. Figure 3.2-7 compares the median and mean hazard computed from the simplified model to that obtained using the full EPRI-SOG model. The simplified model produces slightly higher hazard, but the shape of the hazard curves and the relative locations of the median and mean are consistent between the two models. The higher hazard may be due, in part, to the use of spatially homogeneous seismicity within each source, allowing some of the higher earthquake activity rates in southern Illinois and southern Indiana to occur closer to the EGC ESP Site.

Figure 3.2-8 shows the effect of making all the modifications to the seismic sources described in Section 3.1: increasing the maximum magnitude for the central Illinois source, increasing the maximum magnitudes for the Wabash Valley-southern Illinois source, and adding characteristic New Madrid earthquakes with a return period about 500 years. As discussed in Section 2.1.5.2.1 of this Appendix, large earthquakes in the New Madrid source zone appear to be clustered in time. For this simplified analysis, the characteristic New Madrid earthquakes were modeled as a cluster of three earthquakes. Figure 3.2-9 shows the effect of using the newer m_b attenuation models on the hazard computed using the simplified source model. The effects of these modifications on the hazard computed using the simplified model are very similar to those found for the full EPRI-SOG model (Figures 3.2-3 and 3.2-4), indicating that the simplified model provides a good basis for examining hazard sensitivity.

Figure 3.2-10 shows the combined effect of the source modifications shown on Figure 3.2-8 and use of the newer m_b attenuation models (Figure 3.2-9) on the hazard computed using the simplified source model. The combined source and attenuation updates produce lower peak acceleration hazard for ground motions below about 0.15g and higher hazard for higher peak acceleration levels. For 1-Hz spectral acceleration, the combined effect is to produce higher hazard in general for both the mean and the median.

The more recent attenuation models for central-eastern North America are most often defined in terms of moment magnitude, M . Figure 3.2-11 compares the hazard results obtained using the updated source parameters and the Atkinson and Boore (1995) and Toro et al. (1997) attenuation models in terms of m_b to the hazard results obtained using the Atkinson and Boore (1995) and Toro et al. (1997) attenuation models in terms of M . The use of moment magnitude attenuation relationships produces slightly higher hazard than the use of m_b attenuation relationships.

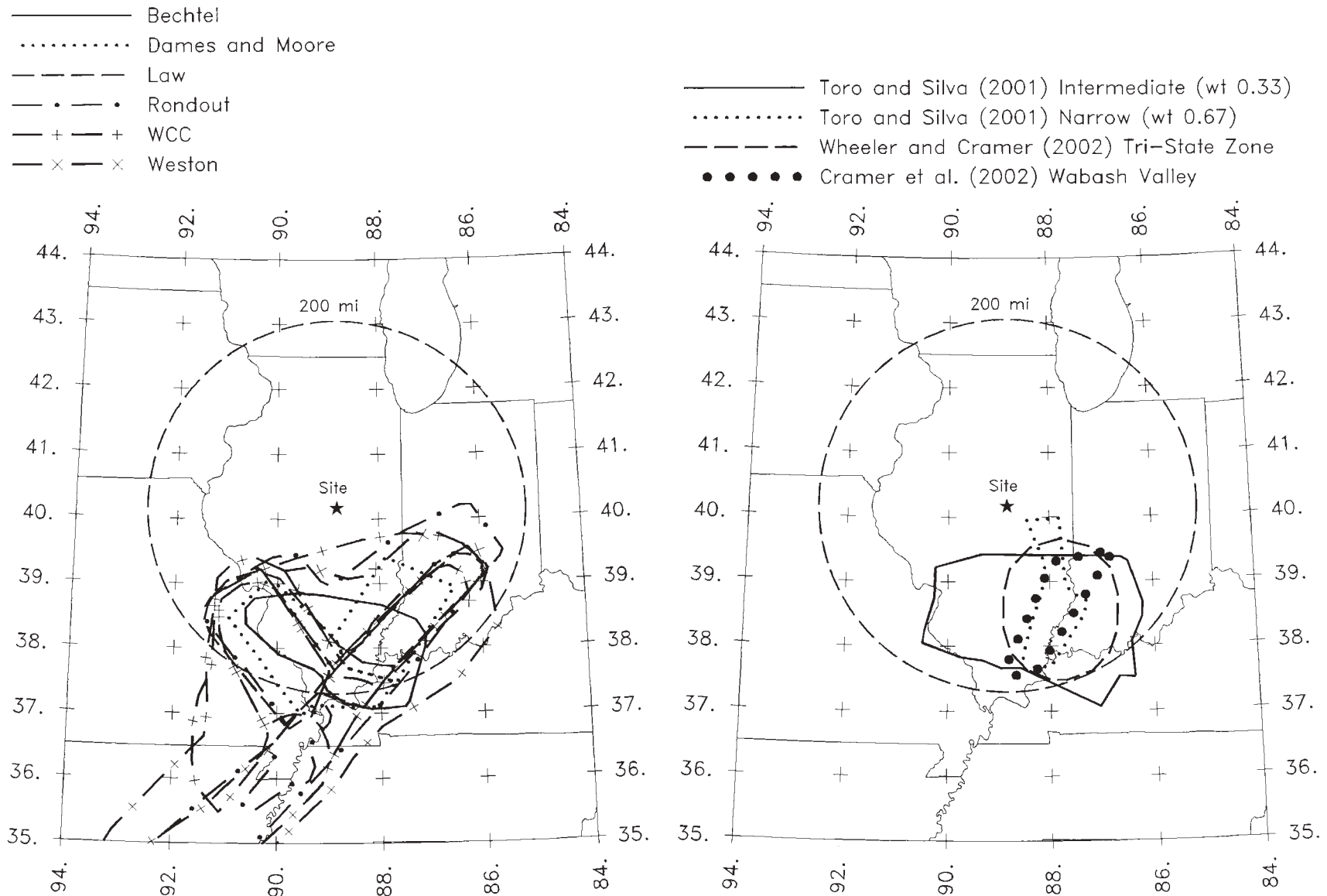
An additional issue regarding seismic sources concerns the configuration of the Wabash Valley-southern Illinois source. Figure 3.1-1 compares the EPRI-SOG Wabash Valley-southern Illinois sources to recently proposed sources for that region. The EPRI-SOG source

alternatives cover essentially the same region as the recently proposed source geometries. The effect of the newer sources on hazard is small. Figure 3.2-12 shows the hazard results obtained using the alternative source geometry that produces the largest increase, the Tri-State zone defined by Wheeler and Cramer (2002). Note that in both cases, uniform seismicity density was used in the calculation. Imposing spatial smoothing may produce a somewhat lower hazard and smaller differences between source models. The USGS incorporates the Tri-State zone into the spatial smoothing of seismicity. It is used only to define an area with a higher maximum magnitude than the surrounding region.

3.2.3 Conclusions

Incorporating information developed since the EPRI-SOG study produces changes in site hazard that may be considered significant. This result is illustrated on Figure 3.2-13, which shows, (using the simplified model) the combined effect of increasing the maximum magnitude distributions for the central Illinois and Wabash Valley sources, incorporating a clustered characteristic earthquake sequence having a mean return period of 500 to 1,000 years at New Madrid, and using recent attenuation relationships defined in terms of moment magnitude.

Based on the differences in seismic hazard shown by the sensitivity analysis, a decision was made that ground motions for the SSE for the EGC ESP Site will be based on an updated PSHA. The evaluations of new information presented above indicate that, for the most part, the EPRI-SOG seismic hazard model remains appropriate for assessing seismic hazards in central Illinois. The required updates to the EPRI-SOG model are very specific: adjustment of the maximum magnitude distribution for the central Illinois- background sources, adjustment of the maximum magnitude distribution for the Wabash Valley-southern Illinois sources, and the addition of characteristic New Madrid earthquakes. Recent studies in the EGC ESP Site region have identified possible centers for moderate magnitude earthquakes in southern and central Illinois. The results of these studies provide a longer seismic record than is provided by historical seismicity alone, which was the primary basis for the EPRI-SOG experts' assessments of maximum magnitude in the central Illinois-background source zones. An EPRI-sponsored study published in the mid-1990s provides a quantitative way to use this information to assess maximum magnitudes. A number of paleoseismicity studies in the Wabash Valley region provide information for assessing the size of the largest events that may be associated with those sources. The issues surrounding modeling of New Madrid earthquakes for hazard assessments have been discussed in recent literature and workshops. In addition, EPRI has sponsored a recent study to provide a comprehensive model of ground motion attenuation in the CEUS (EPRI, 2003). Consequently, there is sufficient information to develop the required updates of the EPRI-SOG model. These updates and the resulting updated PSHA are described in Section 4.1.



Seismic Hazards Report for the EGC ESP Site
**Alternative Southern Illinois-Wabash Valley Source Configurations Used in EPRI-SOG (Left)
 and Proposed in the Recent Literature (Right)**

Figure
3.1-1

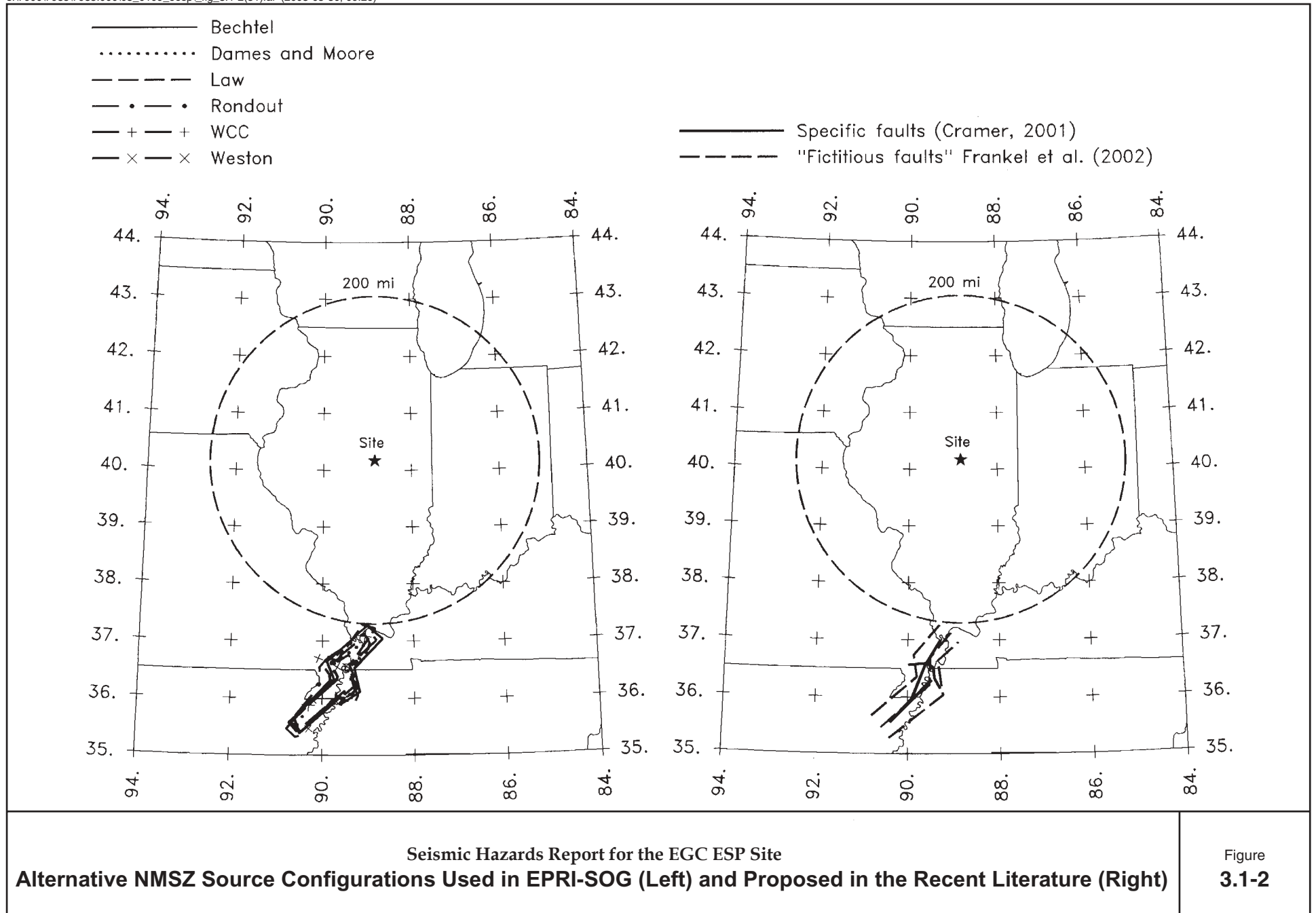
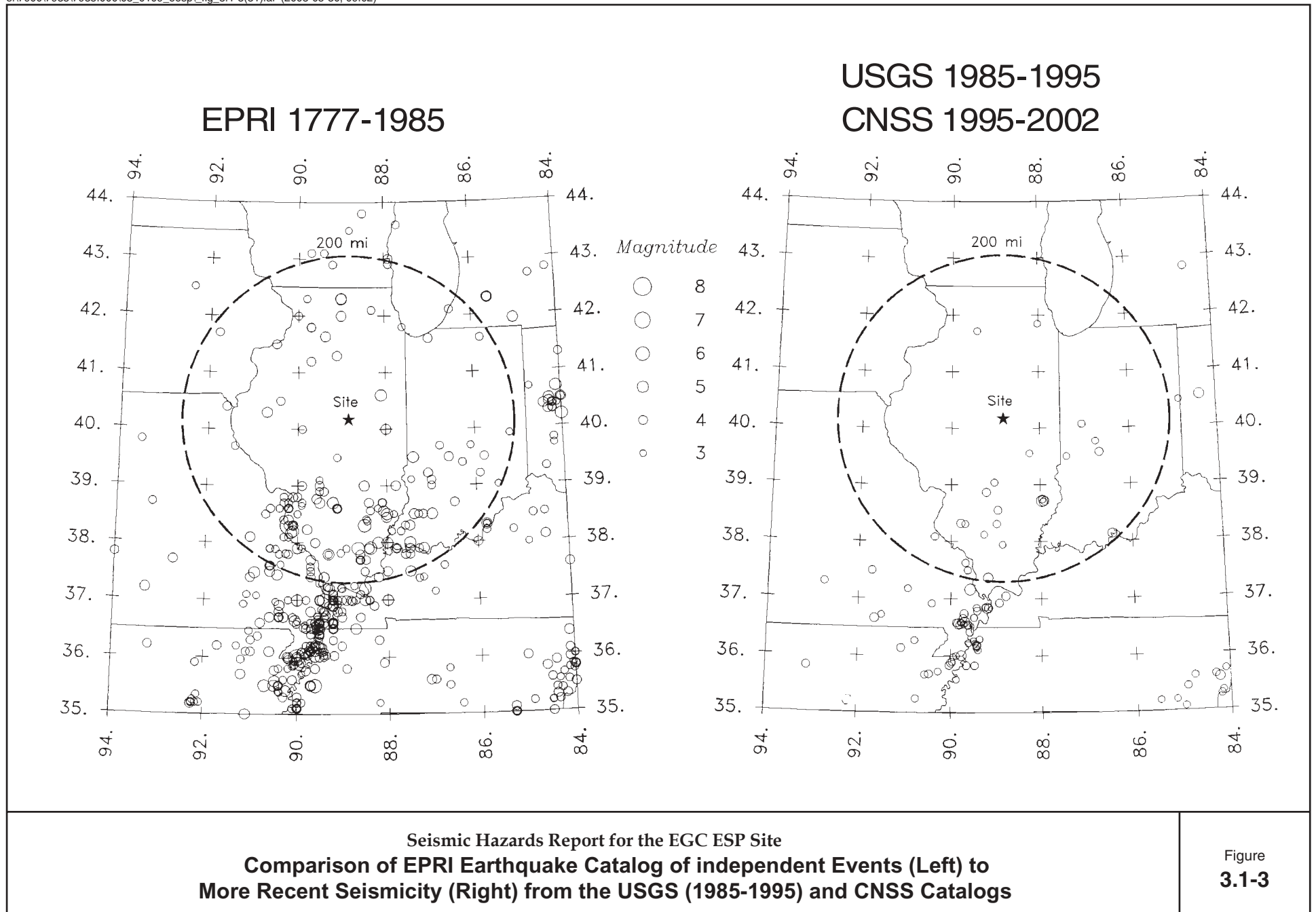
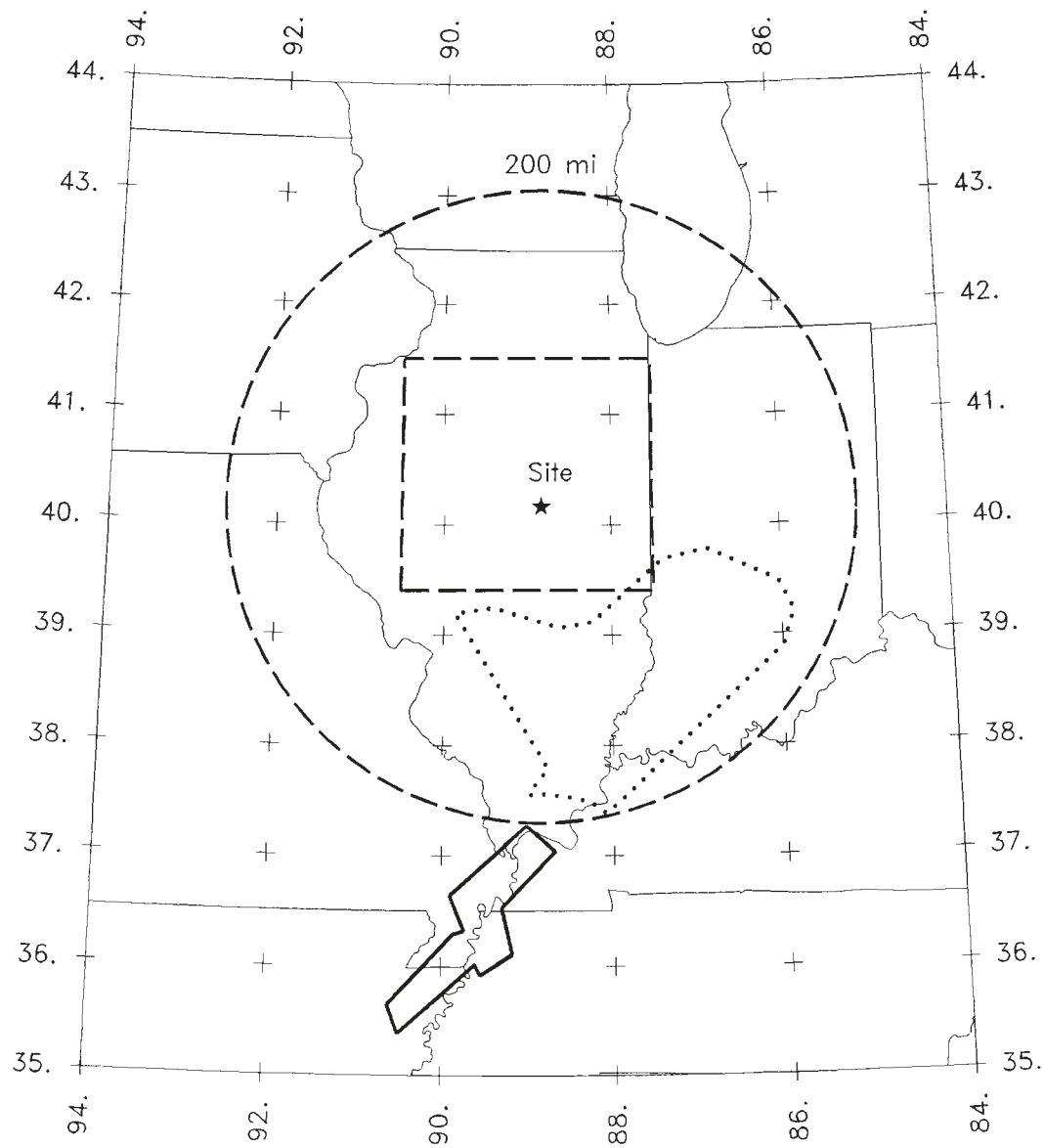


Figure
3.1-2

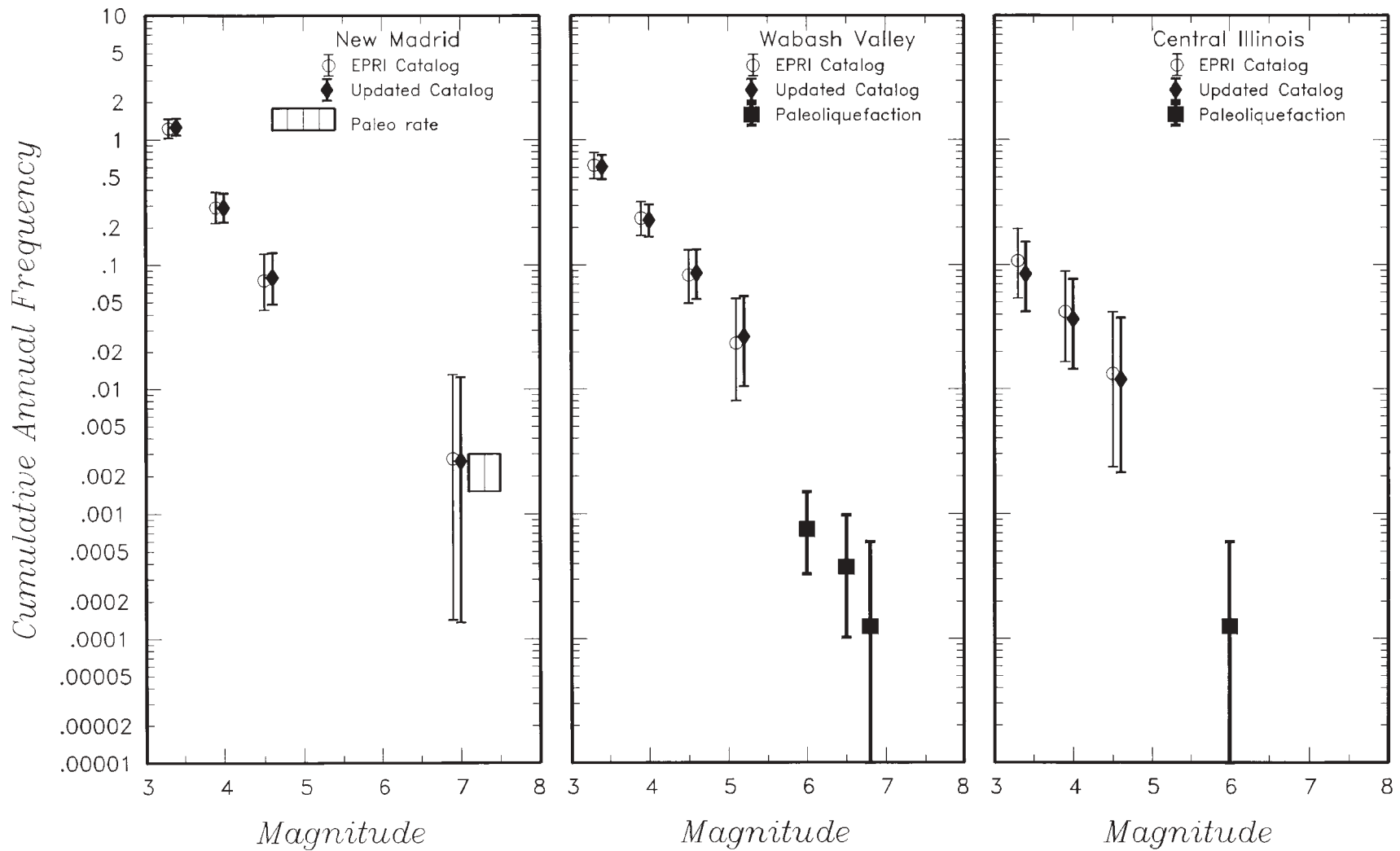


- New Madrid
- Wabash Valley - Southern Illinois
- - - - Central Illinois



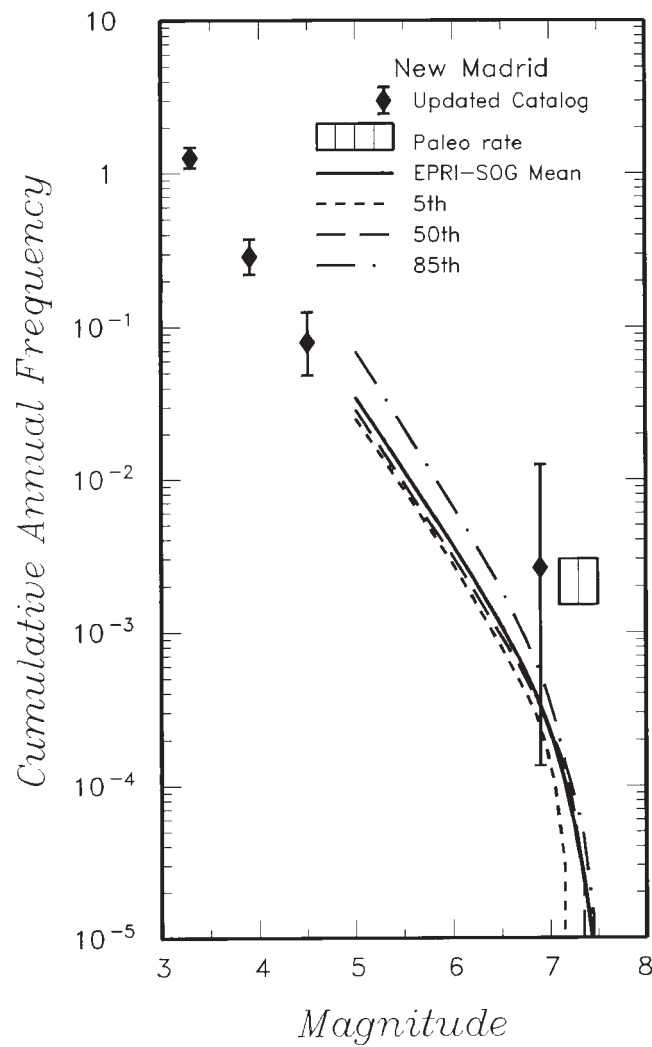
Seismic Hazards Report for the EGC ESP Site
Sources Used in Simplified Model

Figure
3.1-4



Seismic Hazards Report for the EGC ESP Site
Comparison of Seismicity Rates Based on the EPRI-SOG Catalog and m_b Magnitudes to those Computed from the Updated Catalog and Paleoseismic Data

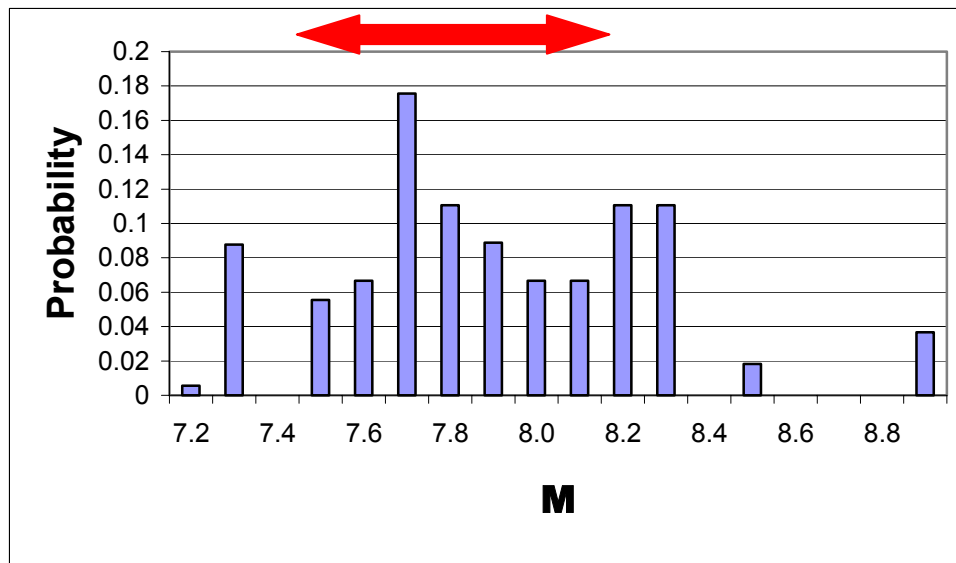
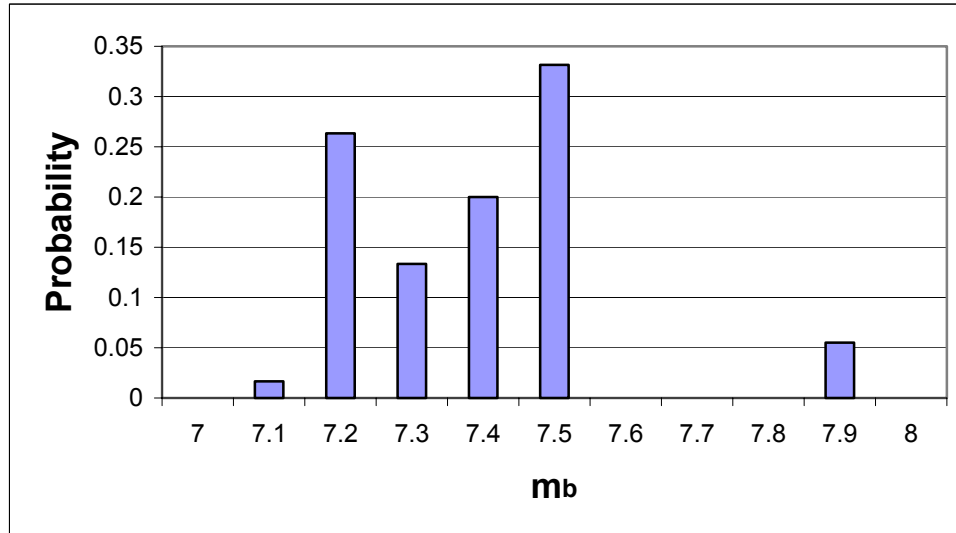
Figure
3.1-5

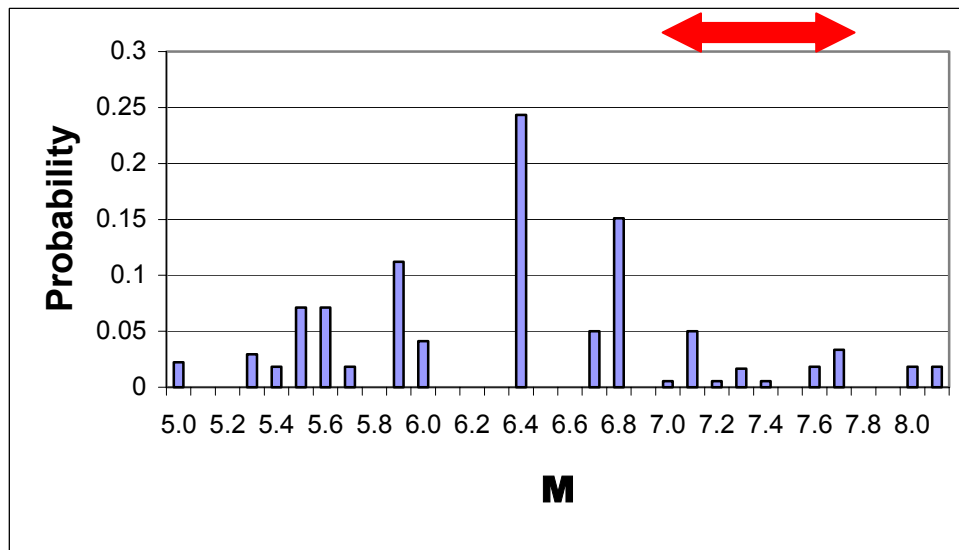
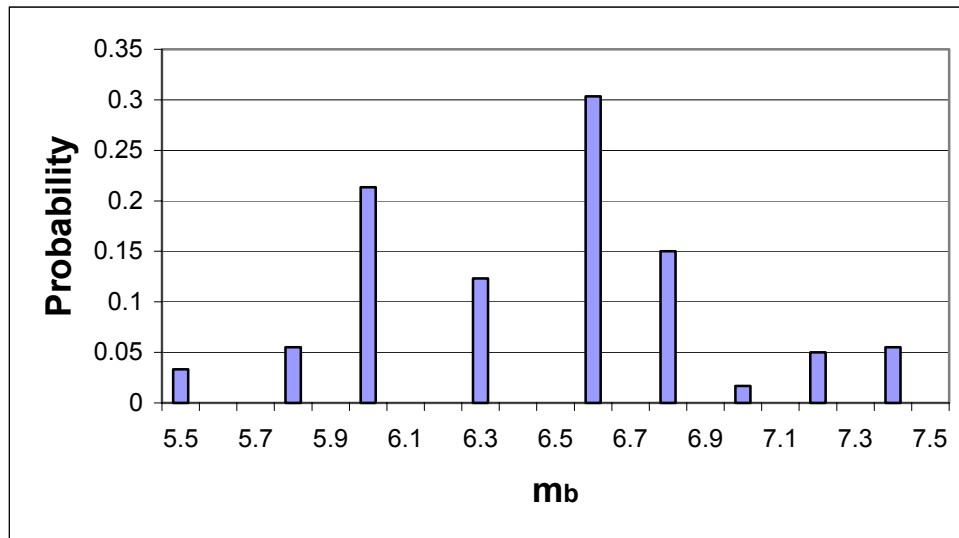


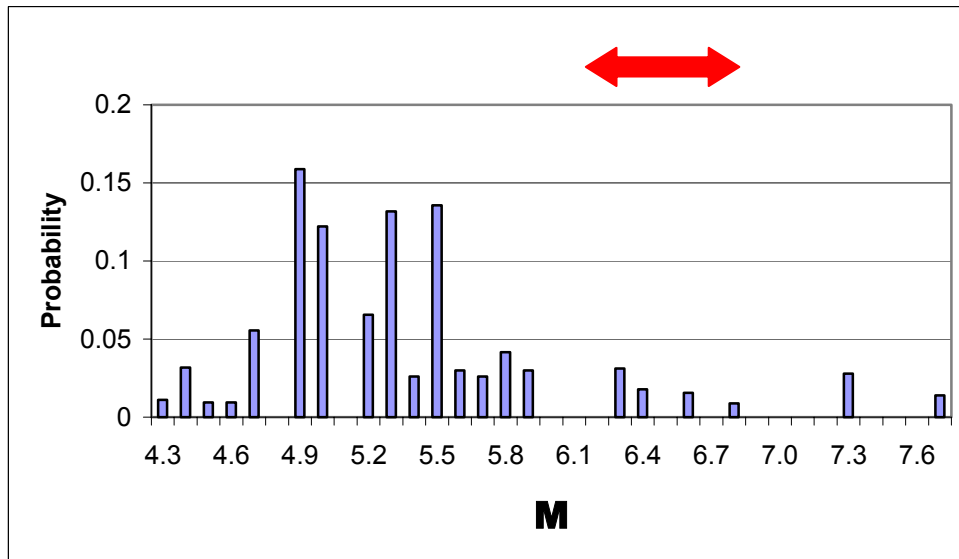
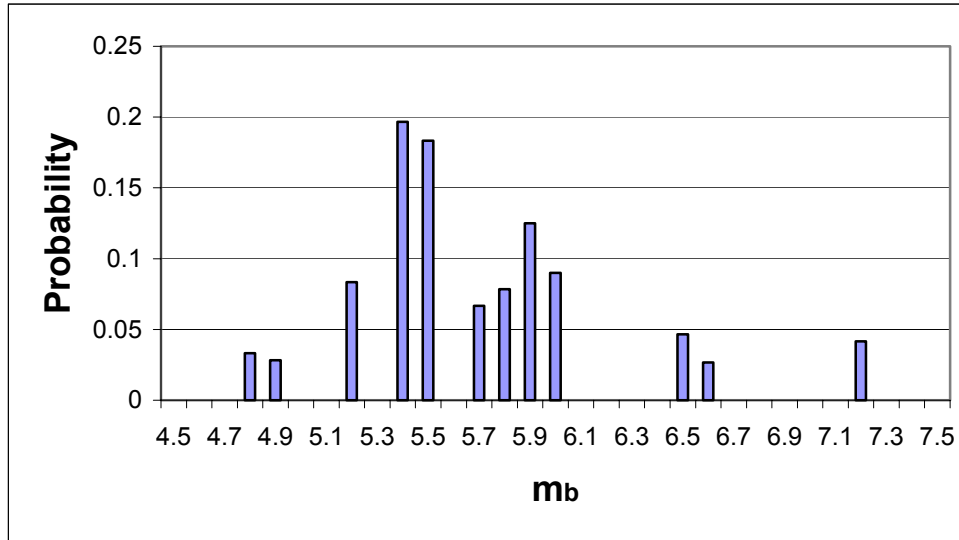
Seismic Hazards Report for the EGC ESP Site

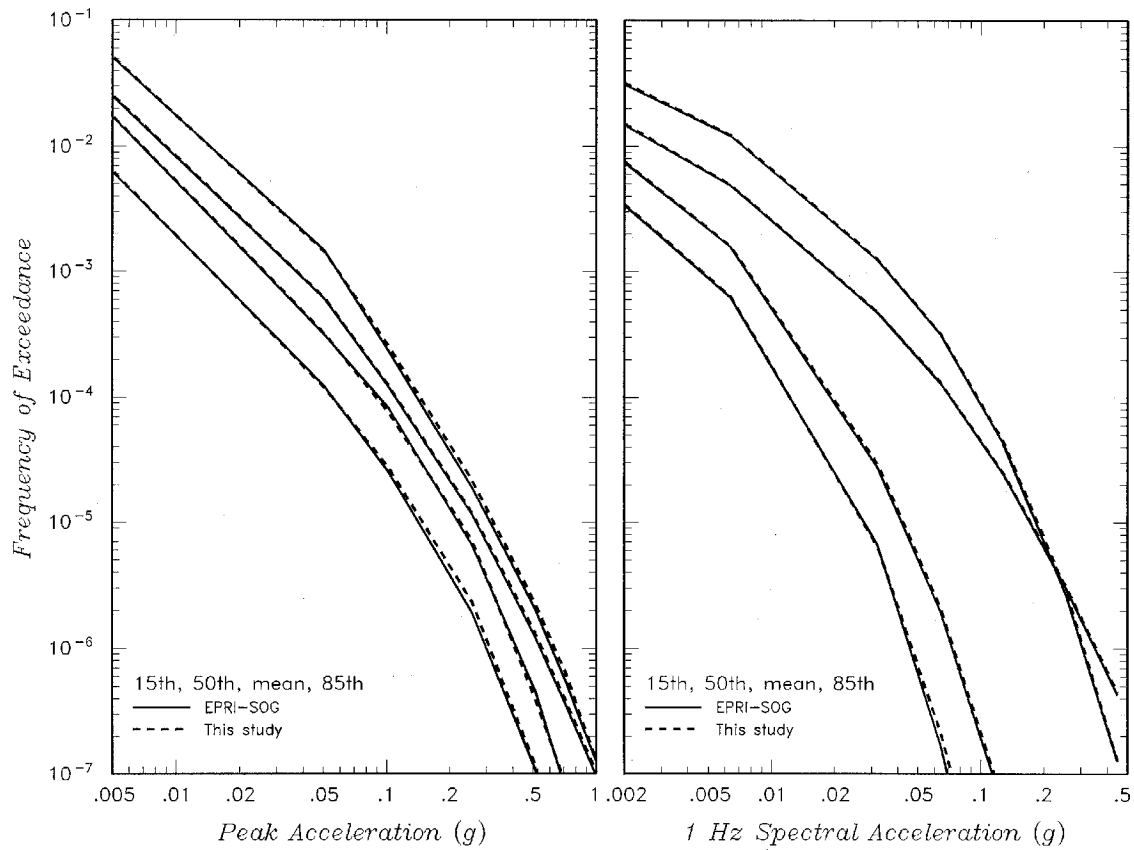
Comparison of Seismicity Rates for New Madrid Based on EPRI-SOG Model and m_b Magnitudes to those Computed from the Updated Catalog and Paleoseismic Data

Figure
3.1-6



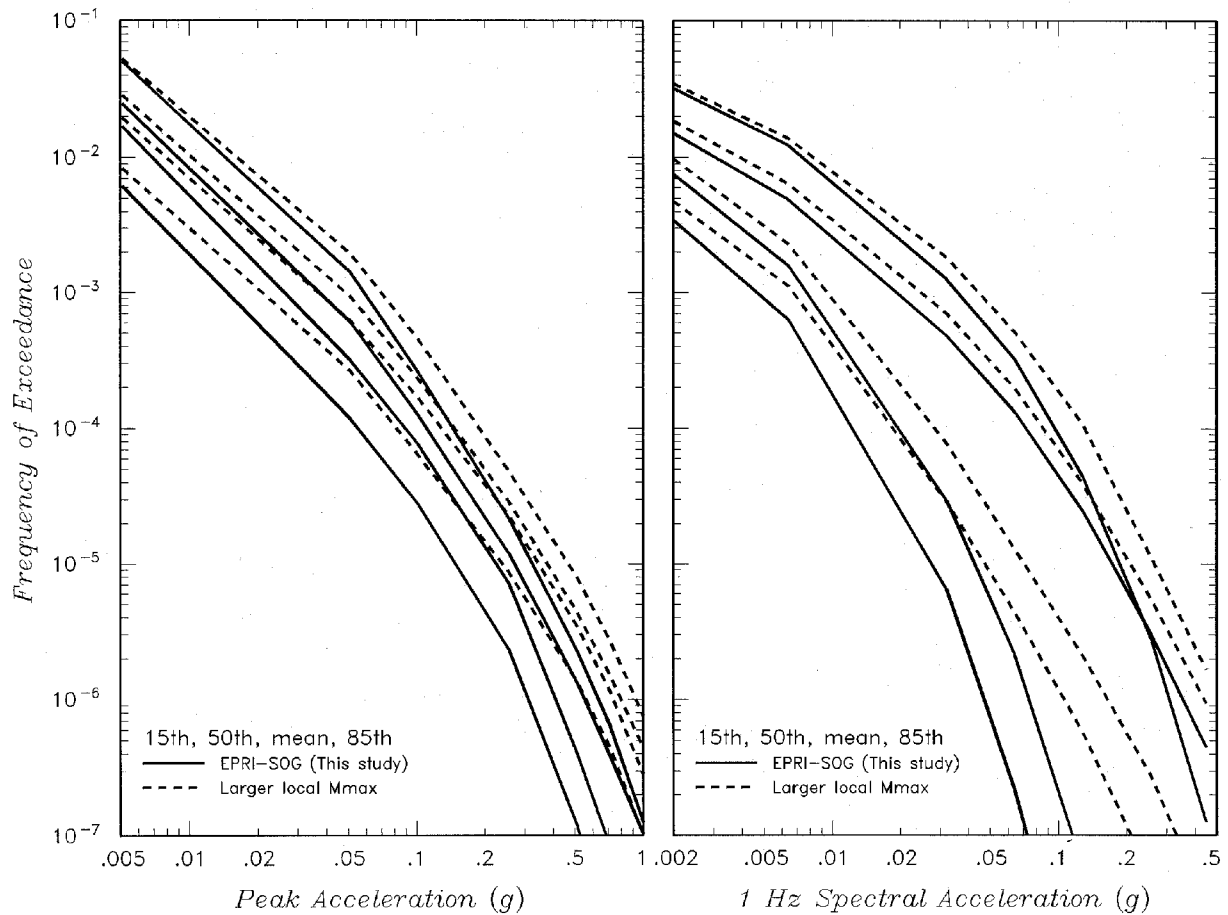






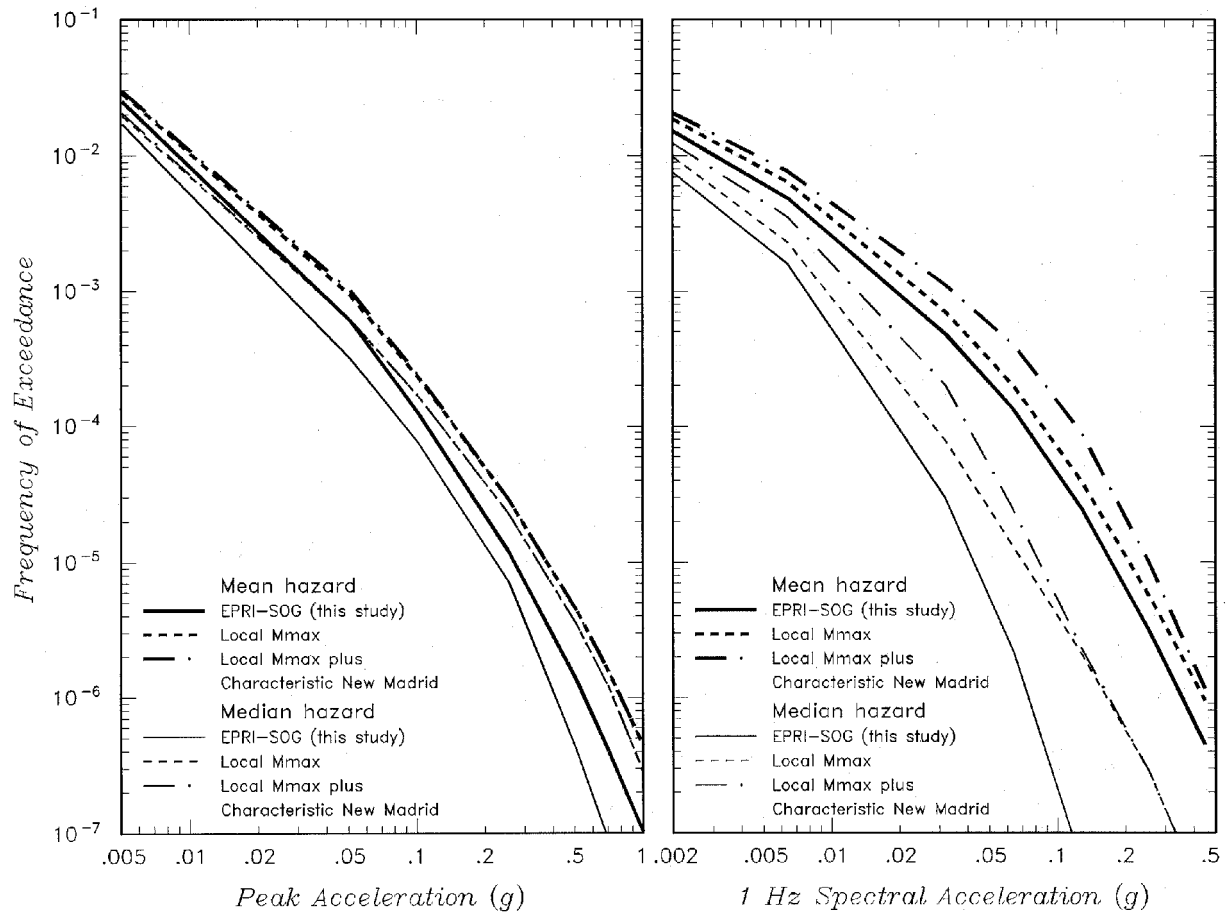
Seismic Hazards Report for the EGC ESP Site
Rock Hazard Results for the EGC ESP Site Computed Using EQHAZ and EQPOST Compared to Results Computed Using Geomatrix's PSHA Software

Figure
3.2-1



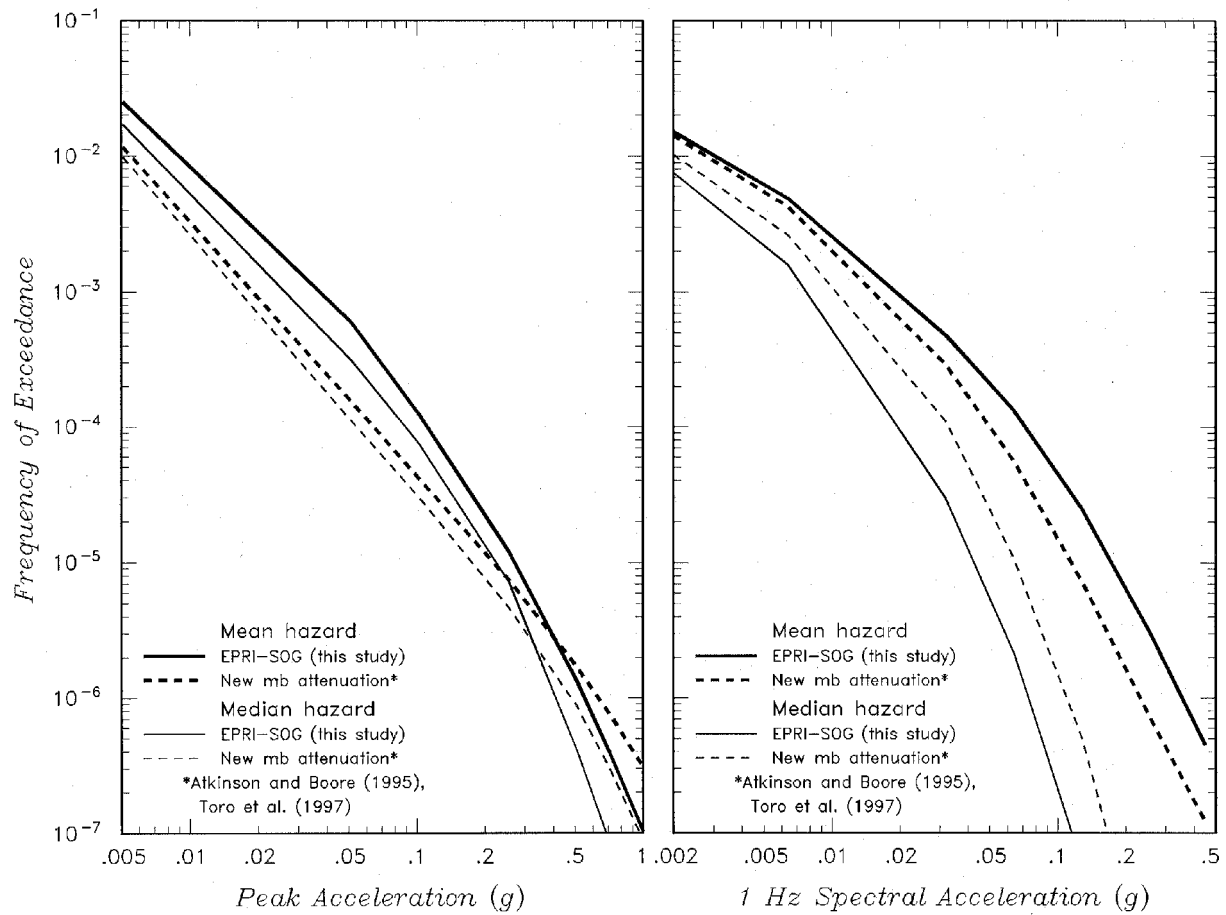
Seismic Hazards Report for the EGC ESP Site
Effect of Increasing the M_{\max} Distribution for Central Illinois Sources in EPRI-SOG Model on the Rock Hazard at the EGC ESP Site Computed Using the EPRI-SOG Attenuation Models and m_b Magnitudes

Figure
3.2-2



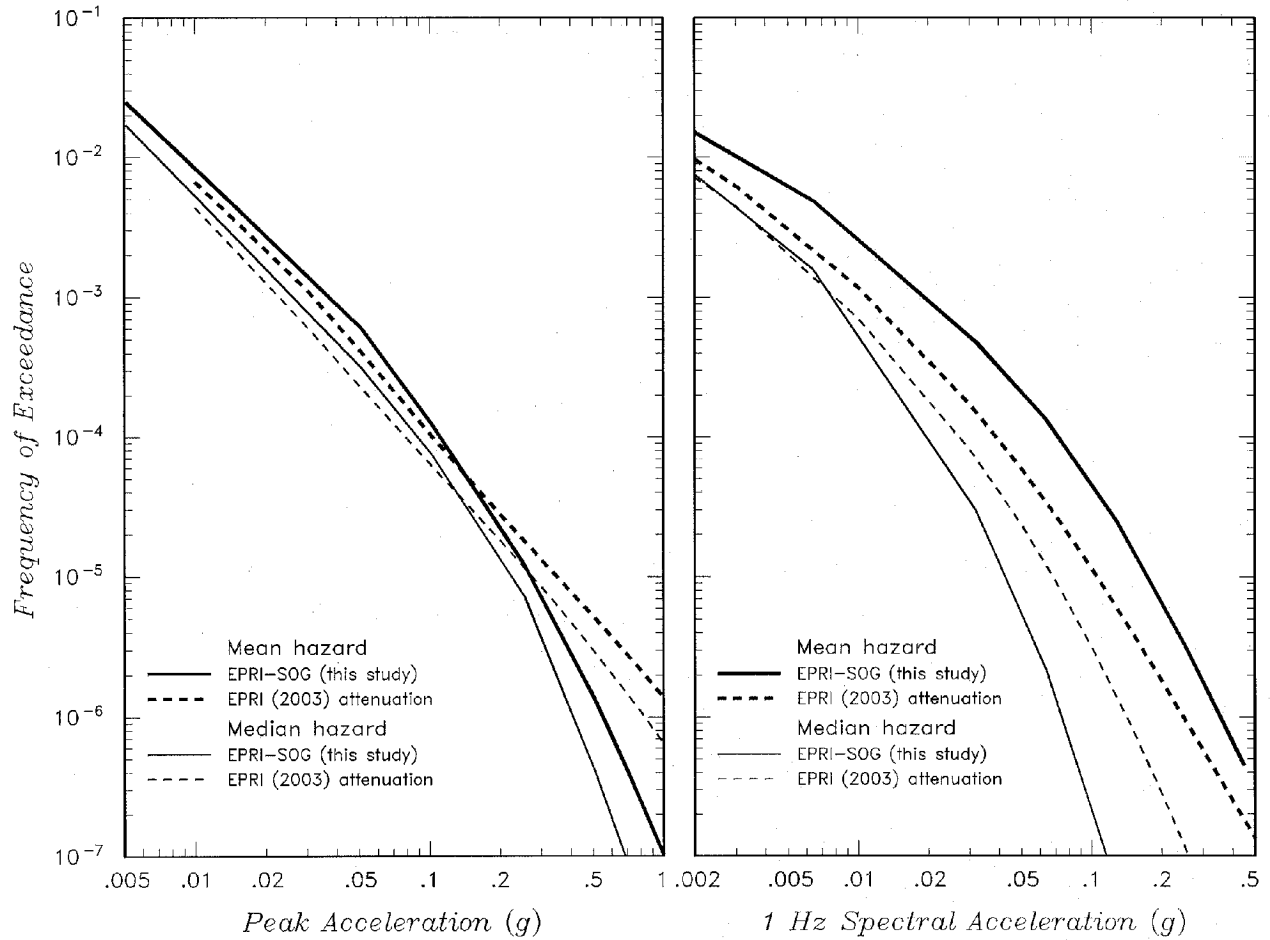
Seismic Hazards Report for the EGC ESP Site
Effect of Increasing the M_{\max} Distribution for Central Illinois Sources and Including Characteristic Earthquakes on the New Madrid Source on the Median and Mean Rock Hazard at the EGC ESP Site Computed Using the EPRI-SOG Attenuation Models and m_b Magnitudes

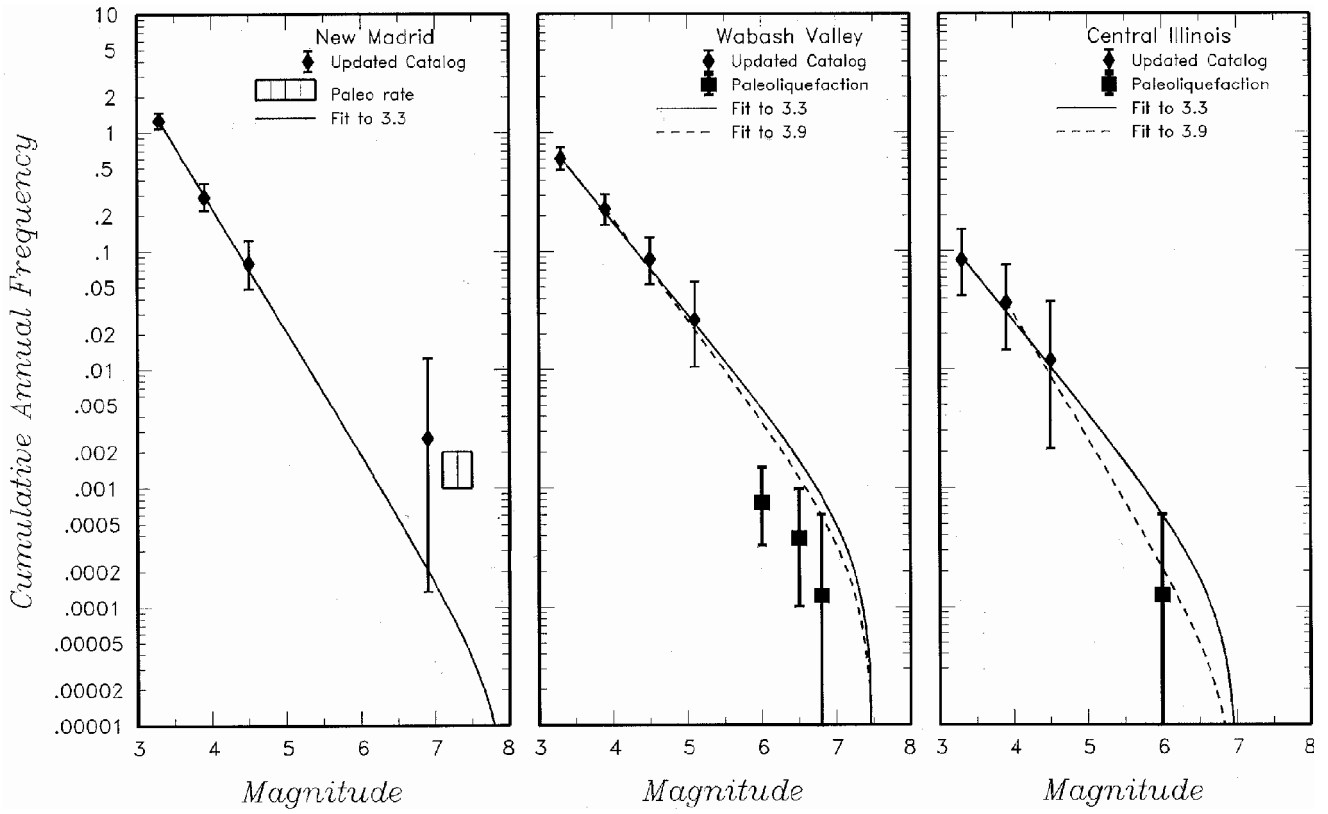
Figure
3.2-3



Seismic Hazards Report for the EGC ESP Site
Effect of Using Newer m_b Attenuation Models on Rock Site Hazard

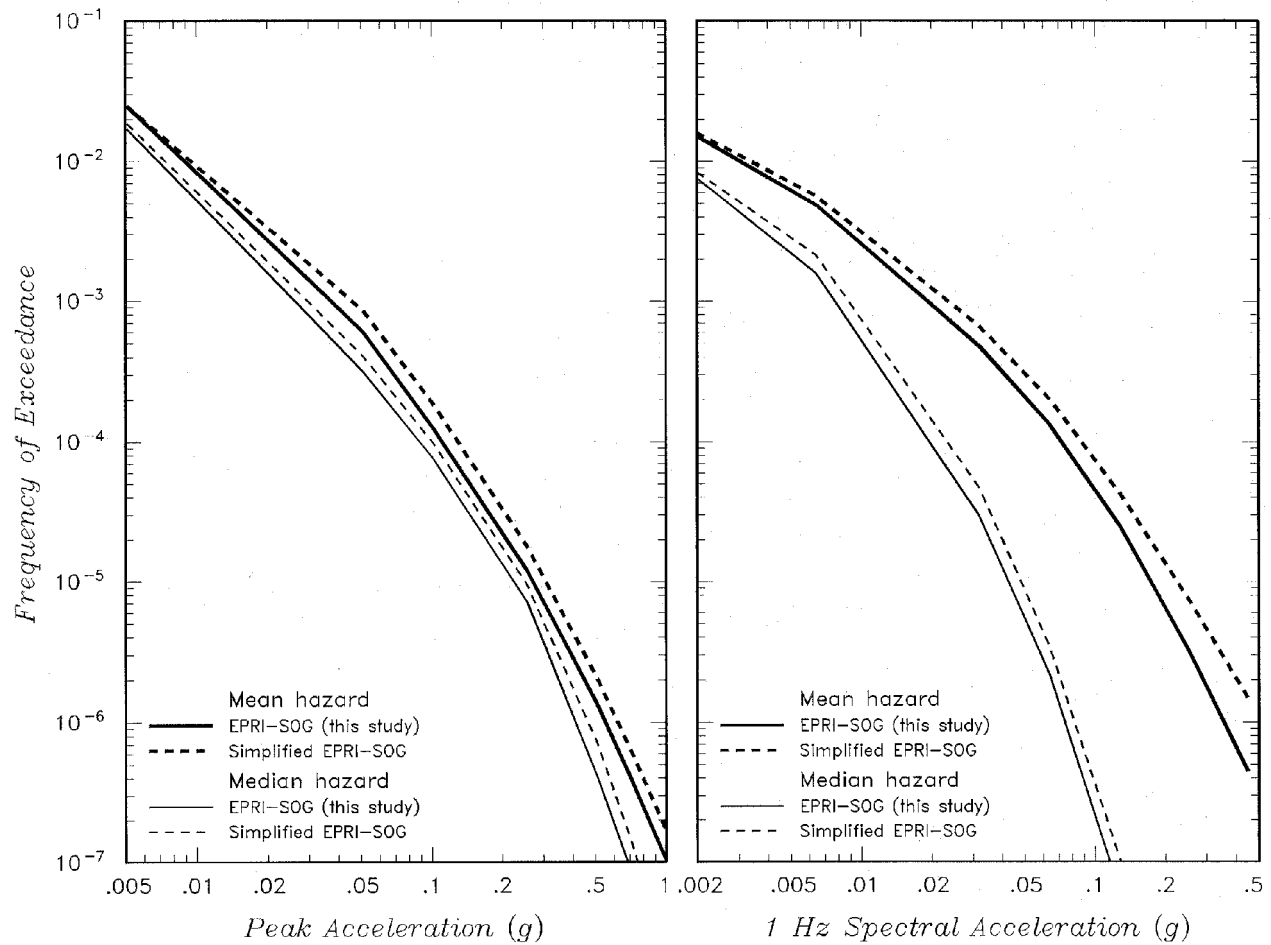
Figure
3.2-4





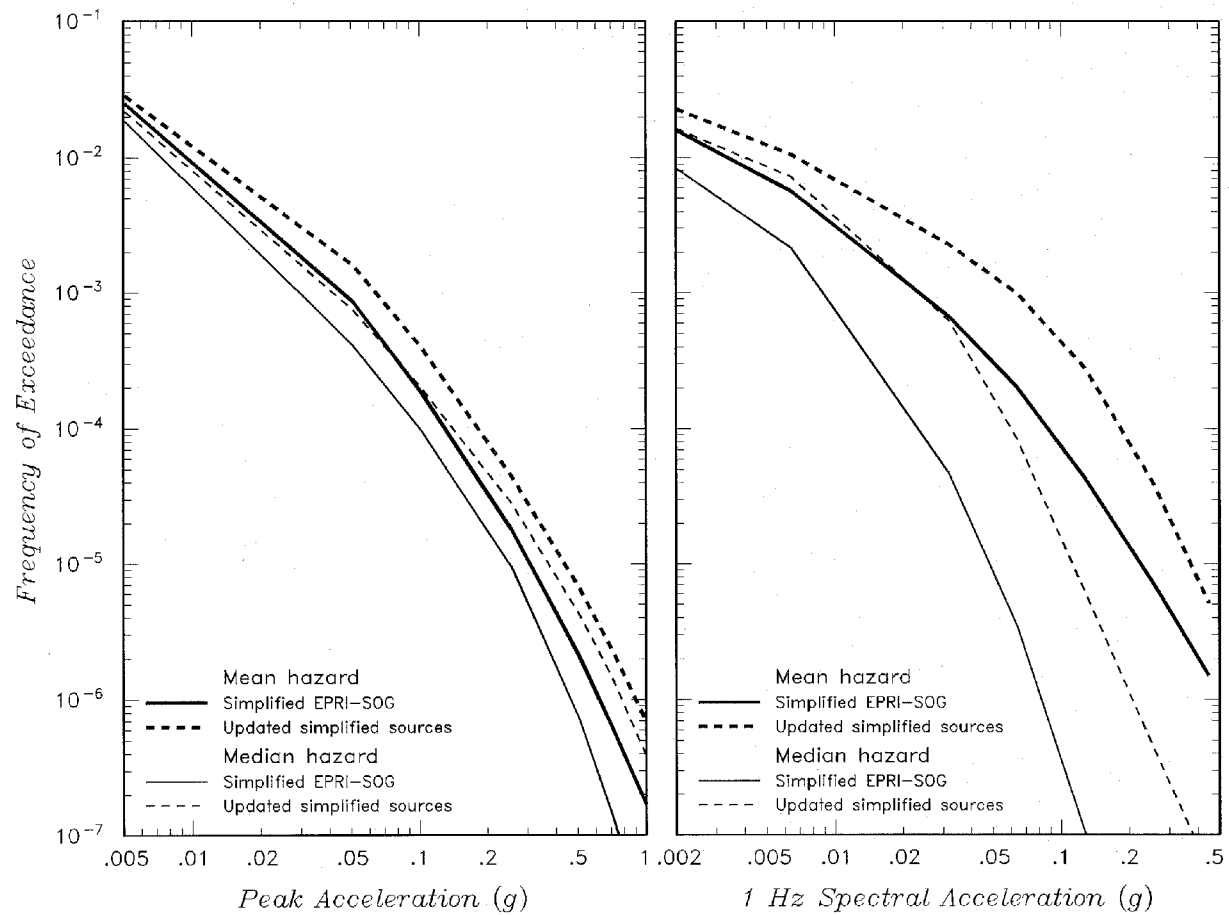
Seismic Hazards Report for the EGC ESP Site
Seismicity Rates and m_b Magnitudes Used in Simplified Source Models

Figure
3.2-6



Seismic Hazards Report for the EGC ESP Site
**Comparison of Hazard Computed from Simplified Source Model to EPRI-SOG
 Rock Site Results**

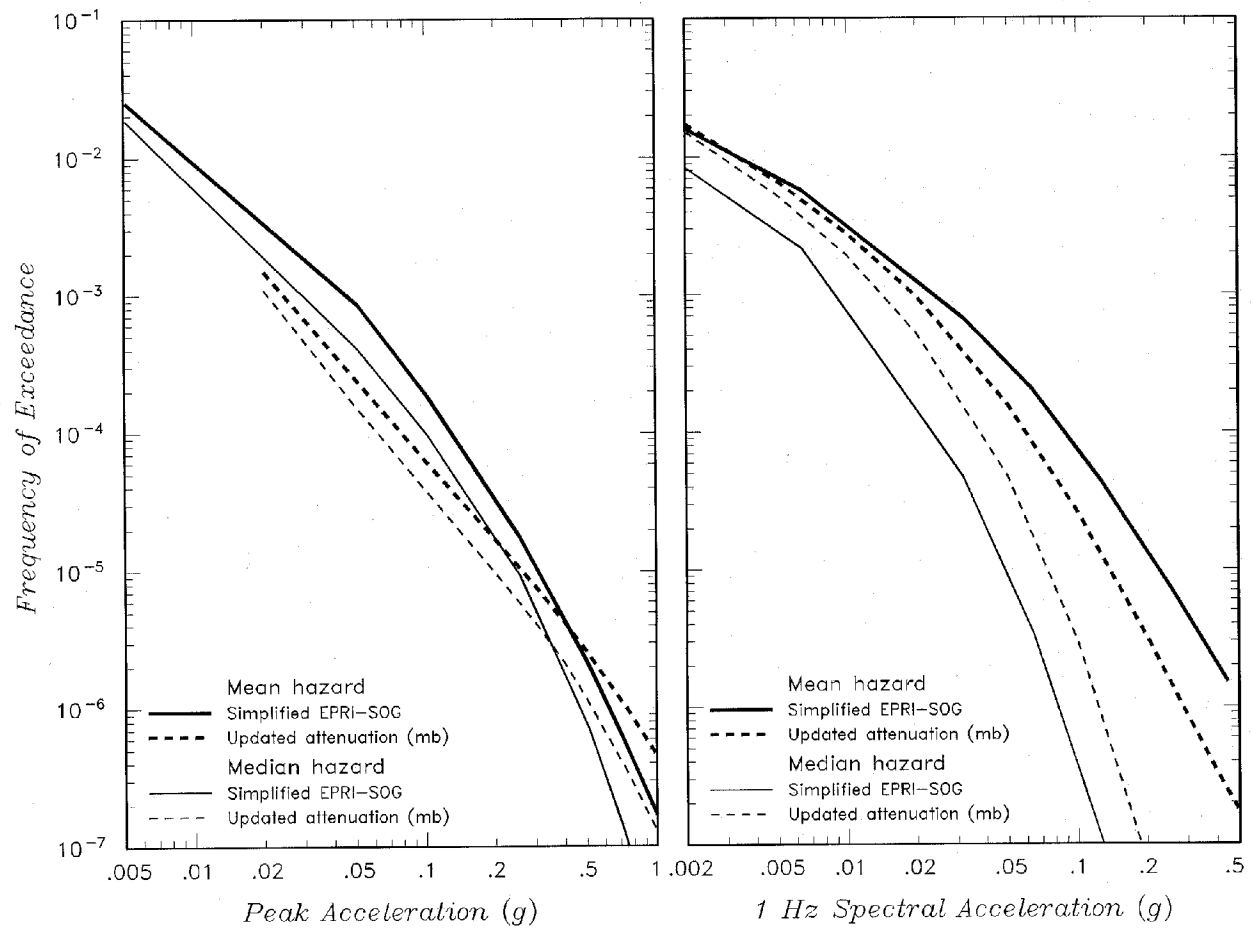
Figure
3.2-7



Seismic Hazards Report for the EGC ESP Site

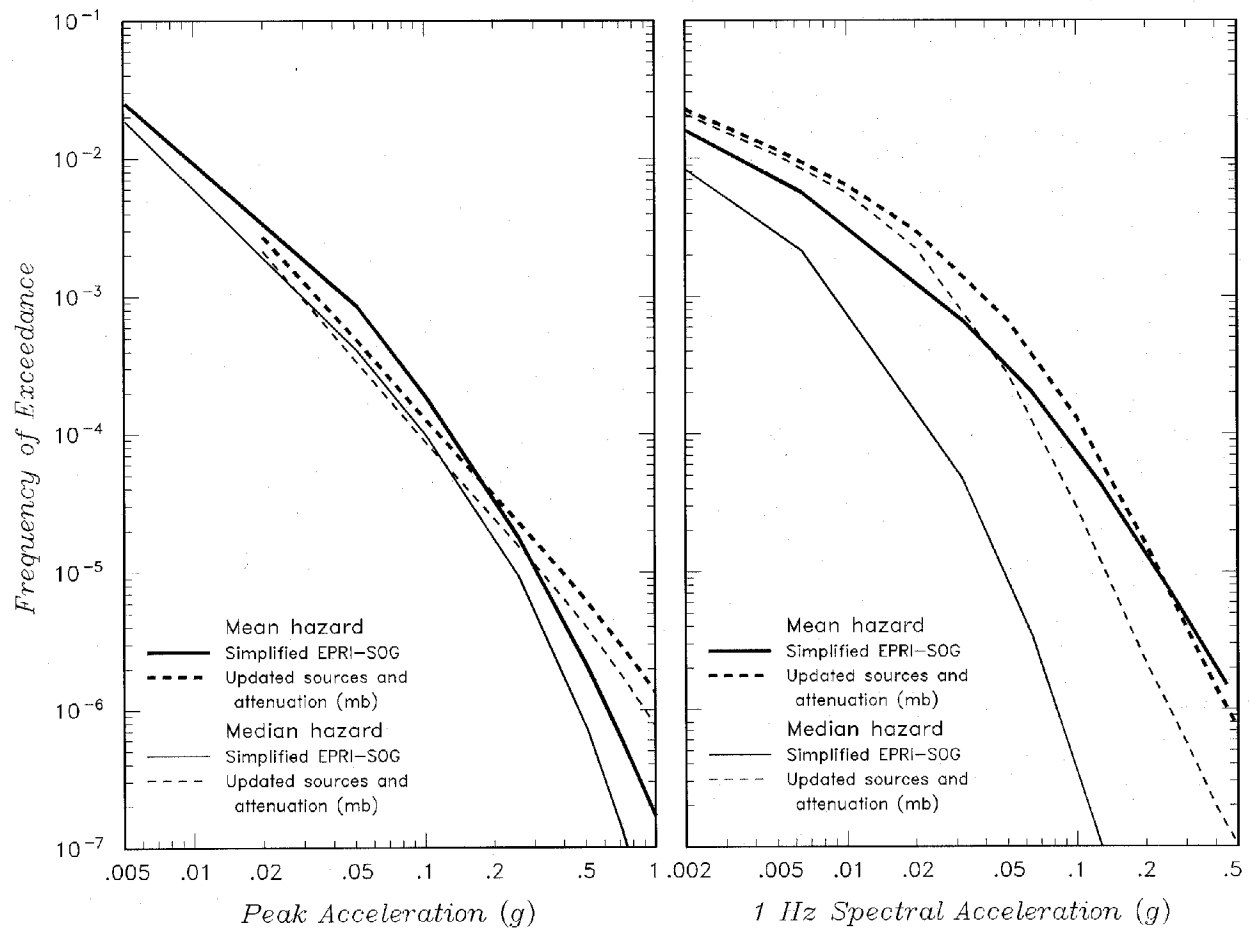
Effect of Increasing M_{\max} Distribution for Local and Wabash Sources and Adding a Clustered Characteristic New Madrid Sequence on Rock Site Hazard for Simplified Source Model and m_b Magnitudes

Figure
3.2-8



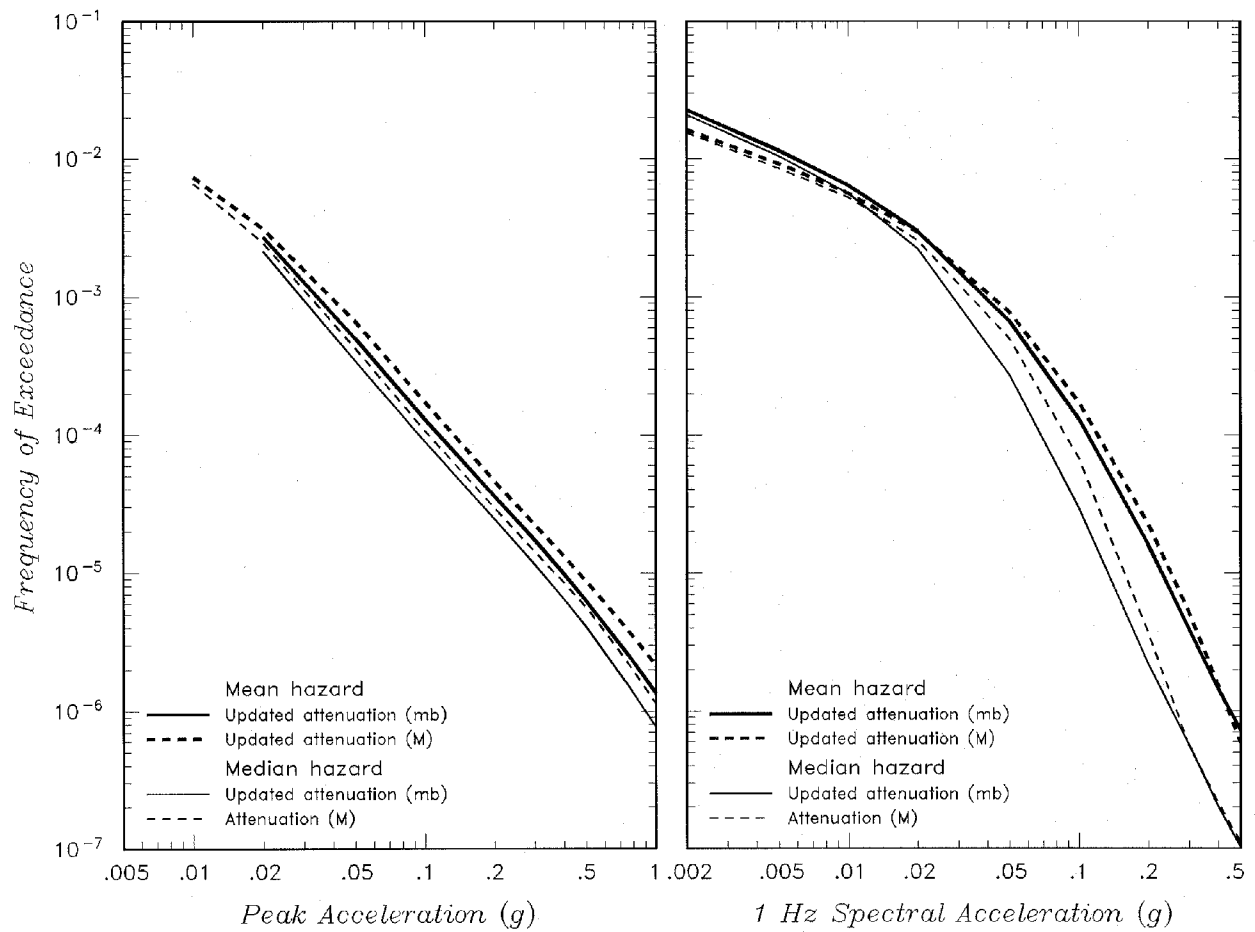
Seismic Hazards Report for the EGC ESP Site
 Use of Newer m_b Attenuation Relationships on Rock Site Hazard for
 Simplified Source Model

Figure
 3.2-9



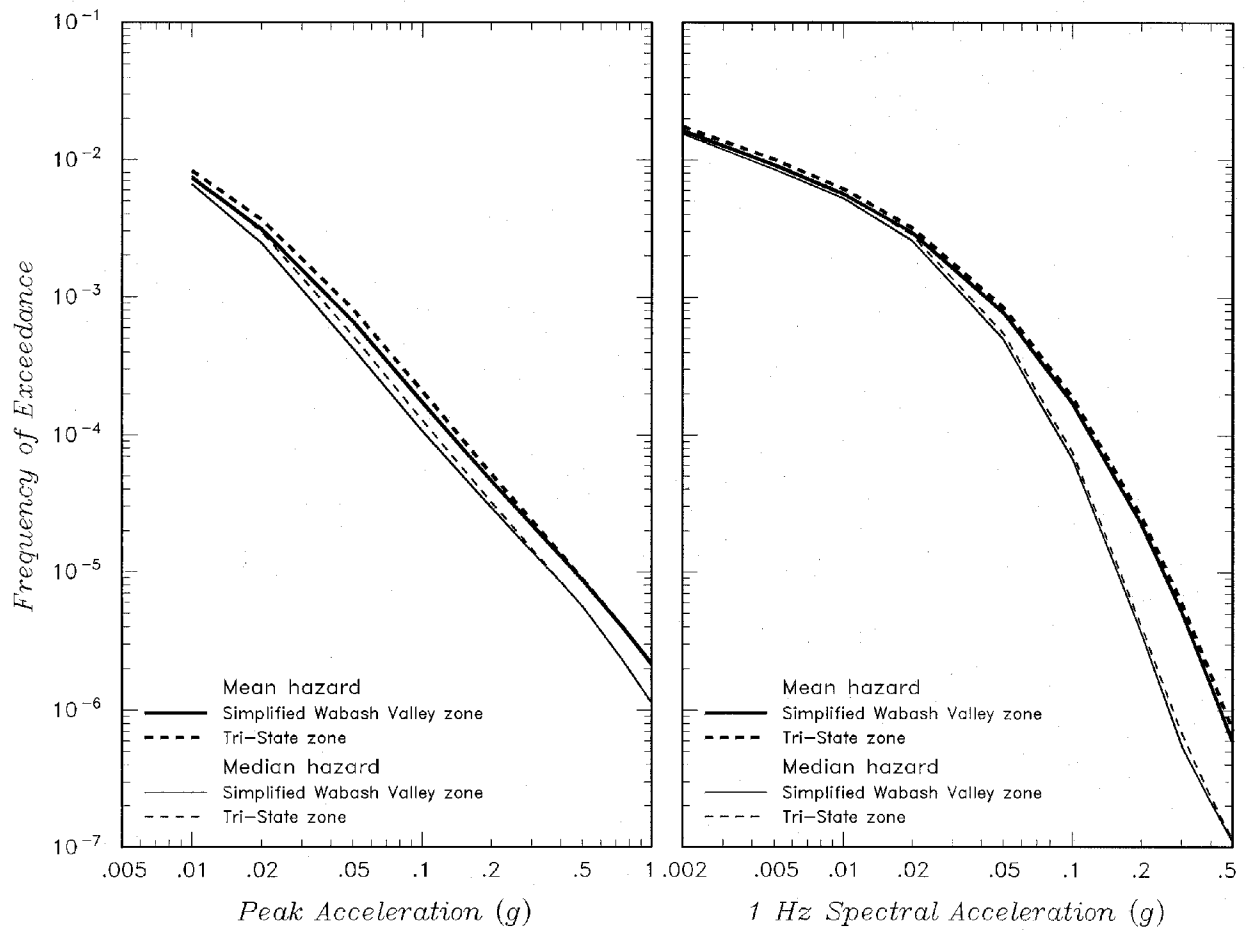
Seismic Hazards Report for the EGC ESP Site
Effect of Source Modifications and Use of Newer m_b Attenuation Relationships on Rock Site Hazard for Simplified Source Model

Figure
3.2-10



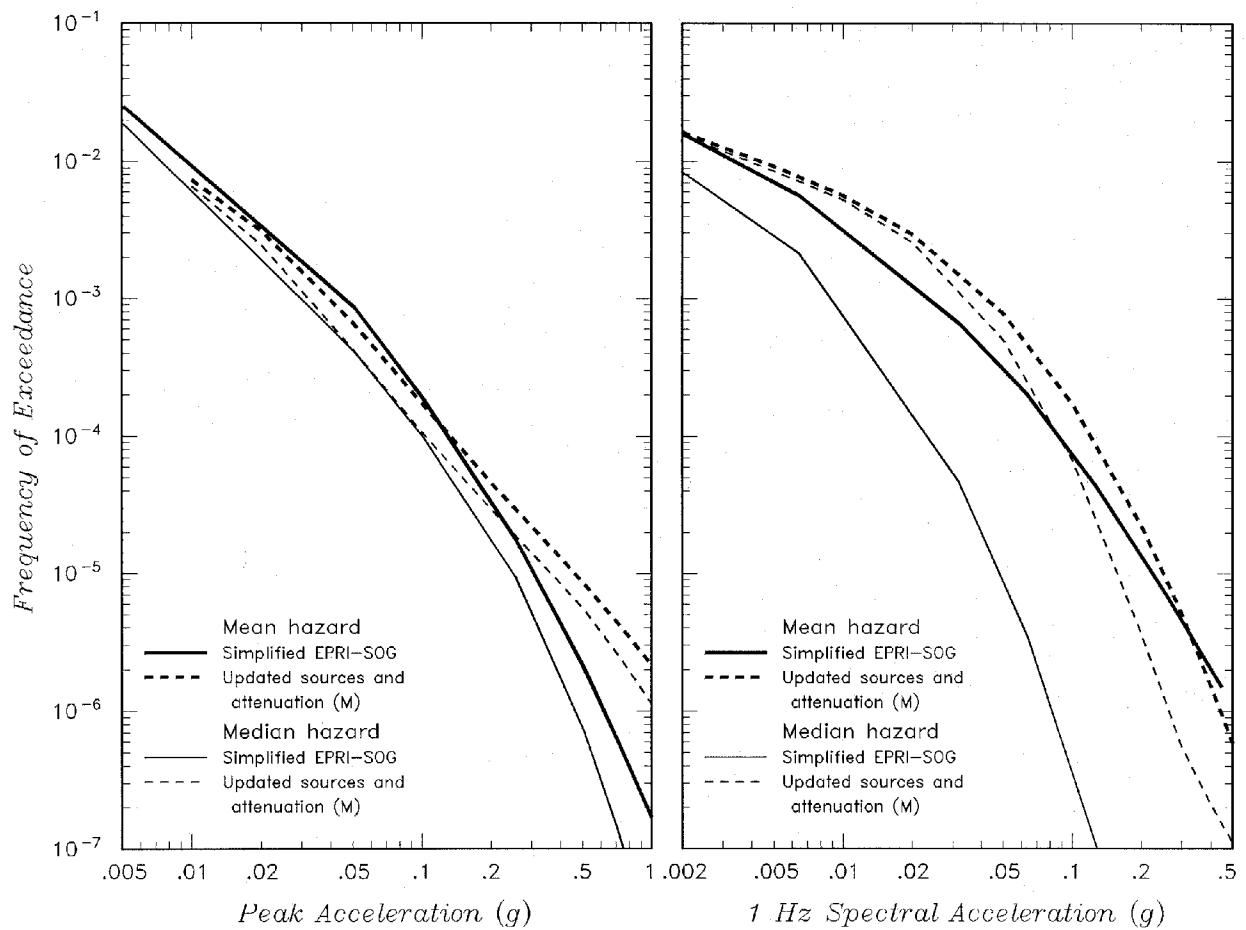
Seismic Hazards Report for the EGC ESP Site
**Comparison of Updated Hazard for Simplified Source Model Based on
 m_b and M Attenuation Relationships**

Figure
3.2-11



Seismic Hazards Report for the EGC ESP Site
Effect on Hazard for Simplified Source Model from Replacing Weston Wabash Valley Source with USGS Tri-State Zone

Figure
3.2-12



Seismic Hazards Report for the EGC ESP Site

Effect on Hazard of Source Modifications and Converting to Moment Magnitude Representation of Seismicity Parameters and Attenuation for Simplified Source Model

Figure
3.2-13

Development of SSE Ground Motions

This chapter presents the development of ground motions for the Safe Shutdown Earthquake (SSE) applicable to the EGC ESP Site. For a soil site, the SSE ground motions are developed through a three-step process. The first step is to compute the site hazard for a reference rock condition using an updated PSHA. Section 4.1 presents the updated PSHA. The updates to the EPRI-SOG parameters for the PSHA consist of the following:

- addition of fault sources for characteristic earthquakes in the New Madrid Seismic Zone (Section 4.1.1);
- revised maximum magnitude distribution for the Wabash Valley-Southern Illinois source zone(s) (Section 4.1.2);
- revised maximum magnitude distribution for the central Illinois basin/background source (Section 4.1.3); and
- updated ground motion attenuation models (Section 4.1.4).

The results of the PSHA are summarized in Section 4.1.5. The development of mean uniform hazard spectra and the identification of the controlling earthquakes are presented in Section 4.1.6.

The second step is to perform a soil amplification analysis to determine the appropriate response spectra at the free surface at the proposed ESP site. The site response analysis is described in Section 4.2, and incorporates:

- assessment of the dynamic properties of the site's subsurface materials (Section 4.2.1);
- representation of the uncertainty in dynamic properties in the analysis (Section 4.2.2); and
- development of time histories representative of the controlling earthquakes (Section 4.2.3).

The results of the site response analysis are presented in Section 4.2.4 in which smooth free surface response spectra are developed for the required probability levels.

The third step involves determination of the horizontal design response spectrum (DRS) using the risk-consistent approach presented in ASCE Standard XXX (ASCE, 2003). The DRS defines the horizontal SSE spectrum. The vertical SSE spectrum is developed from the horizontal SSE spectrum using appropriate vertical/horizontal spectral ratios. The development of the SSE ground motion spectra for the EGC ESP Site are described in Section 4.3.

The resulting SSE ground motion spectra are enveloped by the Regulatory Guide 1.60 response spectrum anchored to a PGA of 0.3 g except for some frequencies above 16 Hz. The maximum exceedance is 25 percent and occurs at a frequency of 33 Hz.

4.1 Updated PSHA

The sensitivity evaluations described in Section 3.2 identified four specific elements of the EPRI-SOG assessments that are impacted by the new information and data. The areas that require updating are: (1) the characterization of the size and rate of the more frequently occurring large-magnitude New Madrid events originating on the fault system that generated the 1811-1812 earthquake sequence; (2) the maximum magnitude distribution for the Wabash Valley-Southern Illinois sources; (3) the maximum magnitude distribution for the Central Illinois basin-local background sources; and (4) new ground motion attenuation models for the CEUS. The modifications to the EPRI-SOG parameters for these elements of the EPRI-SOG evaluations are discussed in the following sections. Note that, with the exception of the characteristic New Madrid earthquakes, the recurrence parameters defined for the EPRI-SOG seismic sources are unchanged by new data and are found, consistent with Regulatory Guide 1.165 (USNRC, 1997), to be appropriate for use in the updated PSHA for the EGC ESP Site.

4.1.1 New Madrid Seismic Zone — Characteristic Earthquake Sources

The principal seismic activity within the upper Mississippi embayment is interior to the Reelfoot rift along the New Madrid Seismic Zone (NMSZ). Recent seismologic, geologic, and geophysical studies have associated faults within the NMSZ with large-magnitude historical earthquakes that occurred during 1811 to 1812 (see Section 2.1.5.2.1 of this Appendix for a discussion of new data). Paleoliquefaction studies provide evidence that large-magnitude earthquakes have occurred on these faults more frequently than the seismicity rates specified in the EPRI-SOG source characterizations.

The EPRI-SOG source characterizations, as they stand, adequately address the uncertainty related to location, magnitude, and frequency of earthquakes that may occur on other potential seismic sources in the region of the NMSZ, such as recently identified active faults along the northern and southern rift margins (see Table 2.1-3 of this Appendix). Updating the EPRI-SOG seismic source evaluations for this study, therefore, focuses on the characterization of characteristic large-magnitude events along the central fault system. The key source parameters are discussed in the following sections. The logic tree used to represent the uncertainty in the seismic source characterization model for the NMSZ characteristic fault is shown on Figure 4.1-1.

4.1.1.1 Fault Source Geometry

Three fault sources are included in the updated characterization of the central fault system of the NMSZ: (1) the New Madrid South (NS) fault; (2) the New Madrid North fault (NN) and (3) the Reelfoot fault (RF). The first two levels of the logic tree for these sources address the uncertainty in the research community regarding the location and extent of the causative faults that ruptured during the 1811 to 1812 earthquake sequence. This uncertainty is represented by alternative geometries for the NN and NS faults. These alternative geometries affect the distance from characteristic earthquake ruptures to the EGC ESP Site.

The locations of the faults that make up the New Madrid characteristic earthquake sources are shown on Figure 4.1-2. For the New Madrid South fault source, two alternatives are considered, as described by Johnston and Schweig (1996): (1) the BA/BL (Blytheville arch/Bootheel lineament); and (2) the BA/BFZ (Blytheville arch/Blytheville fault zone) (also see Figure 2.1-22). Although modern seismicity is occurring primarily along the BFZ, Johnston and Schweig (1996) present arguments suggesting that the BA/BL is the most likely location for the main NM1(D1) event and that major NM1(D1) aftershocks occurred on the BFZ (the northeast extension of the Cottonwood Grove fault). (A description of the 1811-1812 earthquake sequence and its relationship to the identified faults is given in Section 2.1.5.2.1 of this Appendix). Therefore, slightly greater weight is given to BA/BL [0.6] (total length of 132 km [80 miles]) versus BA/BFZ [0.4] (total length of 115 km [69 miles]).

Two alternative total lengths are considered for the New Madrid North fault source. The first, which is given the highest weight [0.7], allows for rupture of the 60-km (36-mile) fault segment (NN, Figure 4.1-2) as defined by Johnston and Schweig (1996). Cramer (2001) uses a similar value (59 km) (35.4 mile) as the length of his northeast arm. Concentrated, first-order seismicity defines the segment as ~40 km (24 miles) long. Johnston (1996), in modeling the source fault for the NM2 (J1) earthquake, extends the fault to the epicentral region of the 1895 Charleston, Missouri, earthquake (**M** 6.0-6.6), for a total length of 65 km (39 miles). An alternative total length of 97 km (58 miles) allows for the fault to extend north to include second-order seismicity trends noted by Wheeler (1997) (Figure 2.1-24). Wheeler et al. (1997) and other researchers argue for a structural northern boundary to the rift in this region (Table 2.1-3). The northern extension (NNE, Figure 4.1-2) is not as well defined by seismicity as is the NN segment. Also the recurrence interval of large magnitude earthquakes in the northern Mississippi embayment appears significantly longer than the recurrence interval for NMSZ earthquakes based on paleoliquefaction studies. Van Arsdale and Johnston (1999) cite as evidence of a long recurrence interval (on the order of 10,000s of years) the sparse seismicity, the lack of Holocene fault offsets in the Fluorspar Area fault complex along trend to the north, the presence of only minor Quaternary faulting, and the lack of discernable offset of the margins of Sikeston Ridge where it meets the NN. Given these observations, the longer (97 km [58 miles]) fault length that includes the NN and NNE is given less weight [0.3].

Johnston and Schweig (1996) conclude from historical accounts that the NM3 (F1) event occurred on the Reelfoot fault (Figure 2.1-22). Johnston and Schweig (1996) identify three possible segments of the Reelfoot fault, a central 32-km (19 miles) long reverse fault defined by the Reelfoot fault scarp between the two northeast-trending strike-slip faults, a 35-km (21 miles) long segment (RS) that extends to the southeast, and a 40-km (24 miles) long segment west of the New Madrid north fault (Figure 2.1-22). Seismicity and geomorphic data indicate that the southeast segment is slightly shorter (25 to 28 km) (15 to 17 miles) than indicated by Johnston and Schweig (Van Arsdale et al., 1999; Mueller and Pujol, 2001). Cramer (2001) uses a total length of 60 km (36 miles) for the Reelfoot fault. The alternative fault rupture scenarios of Johnston and Schweig (1996) include rupture of a 40-km (24 miles)-long northwest fault segment. Cramer (2001) assigns a length of 33 km (20 miles) to this segment, which he refers to as the west arm. Mueller and Pujol (2001) note that this westerly arm is imaged as a vertical fault that terminates the Reelfoot blind thrust. They interpret the westerly arm as a left-lateral strike-slip fault kinematically linked to the

Reelfoot blind thrust. Bakun and Hopper (2003, in press) suggest an epicenter location at the northern end of the RS segment and note that displacements and estimates of **M** for the February 7, 1812, earthquake are consistent with rupture across the entire Reelfoot blind thrust (including segments NW, RF, and RS). These alternatives do not affect the closest distance from the Reelfoot thrust to the EGC ESP Site and thus are not included as alternatives in the seismic hazard model. The RF fault as modeled for this study includes the NW, RF, and RS segments as defined in Cramer (2001).

4.1.1.2 Characteristic Earthquake Magnitude

The next level of the logic tree addresses the magnitude for the characteristic earthquakes on the three New Madrid fault sources. Table 4.1-1 illustrates the significant differences in estimated magnitudes for the largest historical earthquakes (1811-12) in the NMSZ (see also discussion in Section 2.1.5.2.1 of this Appendix). Hough et al. (2000) and Bakun and Hopper (2003, in press) discuss factors that may contribute to the uncertainty in magnitude estimates. The factors generally are considered to be (1) the lack of instrumental data; (2) the paucity of intensity assignments, especially to the west, and the sparse, sometimes inconsistent, felt assignments to the east; (3) the subjective nature of interpretation of felt reports and contouring of MMI data, especially with sparse and/or old reports; (4) the lack of large recent earthquakes in the eastern United States to calibrate the intensity attenuation relation; and (5) the potential bias in intensity assignments introduced by site response.

For this study, probability distributions for characteristic earthquake magnitudes are assigned to each of the major faults within the central NMSZ. Magnitude estimates are weighted based on consideration of the published values estimated from intensity data (Table 4.1-1) and the magnitude-from-rupture-area estimates for individual fault segments as outlined by Cramer (2001) (Table 2.1-4). The probability distribution for the characteristic magnitude assigned to the New Madrid south (NS) fault is: **M** 7.3 (0.4), **M** 7.7 (0.5), and **M** 8.1 (0.1). The highest value (**M** 8.1) represents the preferred value of Johnston (1996) for the NM1 event based on isoseismal areas and a common attenuation relationship developed for a worldwide database of all stable continental regions. The lowest value (**M** 7.3) reflects the estimate of Hough et al. (2000) after adjusting intensities for site amplification. This value also agrees with the preferred **M** estimated for this event by Bakun and Hopper (2003, in press). The intermediate value of **M** 7.7 generally reflects the weighted average of the current range of opinion on the magnitude of the largest events of the 1811 to 1812 sequence (Frankel et al., 2002). Frankel et al. (2002) also note the general similarity in the isoseismals with distance between the 2001 Bhuj, India, earthquake (measured **M** 7.6 to 7.7) and those of the December 16, 1811, New Madrid event, although they caution that there may be differing rates of attenuation of intensities for the eastern United States and India.

The probability distribution for the characteristic magnitude assigned to the New Madrid North (NN) fault is primarily based on estimates of the magnitude of the NM2 event. The following values are used in this study: **M** 7.0 (0.45), **M** 7.4 (0.45), and **M** 7.8 (0.1). The high and low values reflect estimates of Johnston (1996) and of Hough et al. (2000), respectively. The location of the NM2 event is generally acknowledged to be the least well known of the three 1811 to 1812 earthquakes. The intermediate value captures the upper range estimated by Bakun and Hopper (2003, in press). The lower magnitude values are judged to be more consistent with the magnitude-from-rupture-area estimates based on the preferred total

fault length (60 km) and downdip width of ~15 to 20 km (9-12 miles) and, therefore, are given higher weight than the highest value estimated from intensity data.

The probability distribution for the characteristic magnitude assigned to the Reelfoot fault (RF) encompasses the range of published estimates for the NM3 event. In addition, consideration is given to estimates based on the constraints for the geometry and extent of the Reelfoot fault (i.e., Mueller and Pujol, 2001; Cramer, 2001). The following distribution is assigned to this fault: **M** 7.2 (0.2), **M** 7.4 (0.4), **M** 7.6 (0.3), and **M** 8.0 (0.1). The lowest value is based on the estimated moment and magnitude presented by Mueller and Pujol (2001) that uses fault geometry, slip rate, and displacement data from seismicity, geomorphic, and trench data. The **M** 7.4 and the **M** 8.0 values reflect magnitudes estimated from isoseismals of this event as given by Hough et al. (2000) and Johnston (1996), respectively. The **M** 7.4 value also represents the preferred value of Bakun and Hopper (2003, in press). The **M** 7.6 value is consistent with the higher value-estimated from the magnitude-from-rupture-area for the Reelfoot fault based on a length of 60 km (36 miles) and an intermediate estimate of 19 km (11.4 miles) for the thickness of seismogenic crust (Table 2.1-4 of this Appendix). The **M** 7.6 value is slightly less than the weighted average value assigned to the largest of the New Madrid 1811 to 1812 events by experts in the research community (Frankel et al., 2002). The **M** 7.4 and **M** 7.6 values, however, are more consistent with the magnitude-from-rupture-area (Table 2.1-4) and moment magnitude estimates based on paleoseismic trenching and geomorphic analysis (Mueller and Pujol, 2001). Therefore, these estimates have been given the higher weights in this study.

As discussed in the following section, the present interpretation of the paleoearthquake data is that the two prehistoric earthquake ruptures that occurred before the 1811 to 1812 sequence also consisted of multiple, large-magnitude earthquakes. Therefore, for this assessment, the “characteristic” event is considered to be rupture of multiple (two to three) of the fault sources shown on Figure 4.1.2. Furthermore, the arguments for the high versus low magnitude assessments for the individual faults are considered to be highly correlated. Therefore, five alternative sets of characteristic ruptures were produced from the distributions developed above for each fault, as shown in the logic tree on Figure 4.1-1 and given in Table 4.1-2.

The magnitudes listed in Table 4.1-2 are considered to represent the size of the expected characteristic earthquake rupture for each fault within the NMSZ. Following the development of the characteristic earthquake recurrence model by Youngs and Coppersmith (1985), as modified by Youngs et al. (1988), the size of the next characteristic earthquake is assumed to vary randomly about the expected value following a uniform distribution over the range of $\pm\frac{1}{4}$ magnitude unit. This range represents the aleatory variability in the size of individual characteristic earthquakes. For example, given that the expected magnitude for the characteristic earthquake on the NS fault source is **M** 7.8, the magnitude for the next characteristic earthquake is uniformly distributed between **M** 7.55 and **M** 8.05.

4.1.1.3 Characteristic Earthquake Recurrence

The best constraints on recurrence of characteristic NMSZ events derive from paleoliquefaction studies throughout the New Madrid region and paleoseismic investigations of the Reelfoot fault scarp and associated fold (see Section 2.1.5.2.1). Age

constraints for these events are given in Table 2.1-5 of this Appendix. Based on studies of hundreds of earthquake-induced paleoliquefaction features at more than 250 sites, Tuttle et al. (2002) conclude that: (1) the fault system responsible New Madrid seismicity generated temporally clustered, very large earthquakes in AD 900±100 and AD 1450±150 years as well as in 1811 to 1812; (2) given uncertainties in dating liquefaction features, the time between the past three events may be as short as 200 years or as long as 800 years, with an average of 500 years; and (3) prehistoric sand blows probably are compound structures, resulting from multiple earthquakes closely clustered in time (i.e., earthquake sequences).

Cramer (2001) obtained a 498-year mean recurrence interval for New Madrid characteristic earthquakes based on a Monte Carlo sampling of 1,000 recurrence intervals and using the Tuttle and Schweig (2000) uncertainties as a range of permissible dates (\pm two standard deviations) (i.e., AD 900±100 and AD 1450±135). The resulting 68-percent confidence interval for the mean recurrence interval was 267 to 725 years, and the 95-percent confidence interval was 162 to 1196 years (ranges for one and two standard deviations, respectively).

The uncertainty estimates from Tuttle and Schweig (2000) used by Cramer (2001) represent nominal uncertainties for the date of each earthquake. These estimates are based in a general way on the constraints imposed by dates of individual samples (wood, charcoal, etc.) taken from the soil deposits above or below individual liquefaction features. For this study, we have used the data in Table 2.1-5 of this Appendix to develop a more quantitative assessment of the uncertainty in the dates for prehistoric New Madrid earthquakes.

Attachment 2 to this Appendix presents an analysis in which the individual sample age date uncertainties are used in a Monte Carlo simulation of constraints on the possible dates for the prehistoric earthquakes. The time intervals between these simulated dates were then fit with two recurrence models, a Poissonian model and a renewal model in which the time between earthquakes was fit with a lognormal distribution. For the lognormal distribution, the standard deviation was constrained to values obtained for larger data sets by the Working Group on California Earthquake Probabilities (Working Group, 2003). Figure 4.1-3 shows the resulting distributions for the average time between earthquakes. Also shown on Figure 4.1-3 is a distribution for the average time between earthquakes obtained by repeating the analysis performed by Cramer (2001). The results obtained in this study for a lognormal distribution with a standard deviation of 0.5 are very similar to those obtained repeating the analysis performed by Cramer (2001).

Table B-2-2 in Attachment 2 of this Appendix lists the discrete distribution for equivalent annual frequency for characteristic New Madrid earthquakes obtained using the various recurrence models analyzed. As described in Attachment 2, these equivalent rates produce the appropriate probability of occurrence for the next 50-year time period. These rates are used in the PSHA formulation to allow direct addition of the hazard from the New Madrid characteristic earthquakes to the hazard from all of the other sources. The distributions for the equivalent annual frequency of New Madrid characteristic earthquake sequences are also shown on the far right set of branches of the New Madrid source logic (Figure 4.1-1).

Two alternative recurrence models are used to represent the occurrence of characteristic New Madrid earthquakes, the Poissonian model and a renewal model. The Poissonian model is the standard assumption used for earthquake occurrence in PSHA, whereas a renewal time model is more representative of the physics of stress buildup and release on a

fault with repeating characteristic earthquakes. For this study the two modeling approaches are given equal weight. The renewal model is considered more appropriate on a physical basis, but has not been used to any significant extent in PHSA in the CEUS. Equal weights represent maximum uncertainty as to which is the more appropriate model. In applying the renewal model, the three-point discrete distribution for the standard deviation developed by the Working Group (2003) was used (see Attachment 2 to this Appendix).

The paleoliquefaction data gathered in the New Madrid region indicates that the prehistoric earthquakes have occurred in sequences closely spaced in time that are similar to the 1811-1812 sequence. Figure 4.1-4, taken from Tuttle et al. (2002), shows the estimated earthquake sizes and event locations for the 1811-1812 sequence and the two previous sequences. These data indicate that the RF has ruptured in all three sequences, but the NN and NS sources may not have produced large earthquakes in all three sequences. These observations were used to set the relative frequency of event sequences on the central New Madrid fault sources. The model used consists of: ruptures of all three sources NN, RF, and NS one third of the time, rupture of NN and RF one third of the time, and rupture of NS and RF one third of the time. The computation of the hazard from the earthquake sequence uses the formulation outlined in Toro and Silva (2001). The frequency of exceedance, $v(z)$, from the characteristic earthquake sequence is given by the expression:

$$v(z)_{characteristic} = \lambda_{sequence} \left[1 - \prod_i \{1 - P_i(Z > z)\} \right] \quad (\text{Eq. 4-1})$$

where $\lambda_{characteristic}$ is the equivalent annual frequency of event clusters and $P_i(Z > z)$ is the probability that earthquake i in the sequence produces ground motions in excess of level z .

4.1.2 Maximum Magnitude Probability Distribution for the Wabash Valley-Southern Illinois Source Zones

The updated maximum magnitude distribution for the Wabash Valley-Southern Illinois source zone is based on recent analysis of paleoliquefaction features in the vicinity of the lower Wabash Valley of southern Illinois and Indiana (see Attachment 1 to this Appendix). The magnitude of the largest paleoearthquake in the lower Wabash Valley (the Vincennes-Bridgeport earthquake), which occurred $6,011 \pm 200$ yr BP, was estimated to be $\geq \mathbf{M} 7.5$ using the magnitude-bound method (Obermeier, 1998). Use of a more recently developed magnitude-bound curve for the CEUS based on a value of $\mathbf{M} \sim 7.6-7.7$ for the largest of the 1811-1812 New Madrid earthquakes (reduced from the higher $\mathbf{M} 8$ used in the older curve) (Olson et al., 2003) and a distance of 89 km (Obermeier et al., 1993) gives a lower estimate of $\mathbf{M} 7.2$ to 7.3 . Estimates based on a suite of approaches (magnitude-bound, cyclic stress, and energy-stress methods) range from $\mathbf{M} 7.5$ to 7.8 (summarized in Obermeier et al., 1993). The highest value of $\mathbf{M} 7.8$ is based on geotechnical studies using the energy-acceleration method (Pond and Martin, 1997). A re-analysis of this earthquake has been done by R. Green, S. Olson, and S. Obermeier using more recent ground motion attenuation relationships for the central United States (Somerville et al., 2001; Campbell, 2001; Atkinson and Boore, 1995; and Toro et al., 1997); review of approximately 50 boring logs presented by Pond to select appropriate SPT values for the re-analysis; and using the most recent magnitude scaling factors, suggested by Youd and Idriss (S. Obermeier, written communication, 10 January 2003). Using the cyclic stress method, the best estimate of the

magnitude for the Vincennes-Bridgeport earthquake based on all these solutions ranges from **M** 7+ to 7.5. The energy-based solution developed by Green (2001) that circumvents the use of the magnitude scaling factor, which is a large questionable factor in the use of the cyclic stress method in the central United States, gives a value of **M**~7.5 for each of the four newer ground motion attenuation relationships.

The next largest earthquake occurred $12,000 \pm 1,000$ yr BP (Hajic et al., 1995; Munson et al., 1997; and Obermeier, 1998). This earthquake is estimated to be an **M** 7.1 to 7.2 by Munson et al., (1997) or **M** 7.3 by Pond and Martin (1997). Both of these earthquakes were in proximity to one another and took place in the general vicinity of the most numerous and strongest historic earthquakes (**M** 4 to 5.5) in the lower Wabash Valley of Indiana-Illinois (Obermeier, 1998).

Based on these interpretations of the size of the prehistoric earthquakes, the following maximum magnitude probability distribution is used in the updated PSHA to capture the range in uncertainty in the magnitude of the largest prehistoric earthquakes in the lower Wabash Valley region: **M** 7.0 (0.1), **M** 7.3 (0.4); **M** 7.5 (0.4); **M** 7.8 (0.1). The highest weight is given to the range from **M** 7.3 to 7.5 where most of the magnitude estimates lie.

4.1.3 Maximum Magnitude Probability Distribution for Central Illinois Basin-Background Source

Evidence from recent paleoliquefaction studies and seismic-reflection data suggests that significant earthquakes may occur in parts of the Illinois basin where there are no obvious surface faults or folds. As described in Section 2.1.5.2.3 and Attachment 1 to this Appendix, paleoliquefaction evidence suggests that moderate-magnitude events may have occurred in central Illinois (e.g., the postulated **M** 6.2 to 6.8 Springfield earthquake) that are significantly larger than the historical earthquakes of the region. The location, size, and recurrence of such events are not well constrained by available data. Field reconnaissance conducted for this study (Attachment 1 to this Appendix) also identified latest Pleistocene to Holocene paleoliquefaction features within 11.5 to 29 miles of the EGC ESP Site.

The study of earthquakes in stable continental regions conducted by EPRI (Johnston et al., 1994) specifically addresses the problem of defining a maximum magnitude for regions that are characterized by the rare occurrence of maximum earthquakes and the lack of recognized surface expression or well-defined seismicity patterns associated with seismic sources, typical conditions over much of the CEUS. The 1994 EPRI study (Johnston et al., 1994) developed worldwide databases that could be used to develop scientifically supportable assessments of maximum earthquake magnitude for seismic sources in the CEUS.

Johnston et al. (1994) recommend a Bayesian approach to assessing maximum magnitude that is based on a prior distribution of maximum magnitude derived from the statistical analysis of the global database. The prior distribution is updated with information (the sample likelihood function for maximum magnitude) specific to the seismic source of interest. The final product is a probabilistic distribution of maximum magnitude that incorporates uncertainties in the assessment.

Based on general crustal type, Johnston et al. (1994) developed two prior distributions of maximum magnitude, one for extended crust and one for non-extended crust. Because the central Illinois basin and surrounding background sources lie in the stable craton of North America, the non-extended crust prior distribution is used for this assessment. For non-extended crust, the bias-adjusted estimate for the mean maximum magnitude is **M** 6.3, with a standard error of 0.5. This prior distribution (normal with mean 6.3 and σ 0.5) is shown at the top of Figure 4.1-5.

The likelihood function is based on the observed number of earthquakes larger than **M** 4.5. Paleoliquefaction evidence suggests that one or more moderate-size events may have occurred in the central Illinois basin, but there is considerable uncertainty in the size and location of these prehistoric earthquakes. The paleoliquefaction evidence suggests two events in the Springfield region and possibly another as well as in the Farmer City area (Attachment 1 to this Appendix). An additional event may be recorded along the Mackinaw River to the north. The limited data that constrain the location, timing, and tectonic origin of these events (particularly the latter event) allow for the possibility of two to as many as five earthquakes in central Illinois in latest Pleistocene to Holocene time. As discussed in Attachment 1 of this Appendix, some of the features may be related to nontectonic processes (glaciotectonic) and all the paleoliquefaction features observed in central Illinois could be related to more distant earthquakes originating in the Wabash Valley-southern Illinois source zone(s).

The following distribution is used to represent the uncertainty in the number and size of large earthquakes known to have occurred in the central Illinois basin: one small prehistoric event (0.05) (the Springfield liquefaction features represent the effects of a distant earthquake and to combined liquefaction evidence suggests only a small-to-moderate sized earthquake), only the larger Springfield event has occurred (0.1), the Springfield and one other prehistoric event have occurred (0.4), the Springfield and two other prehistoric events have occurred (0.3), the Springfield and three other prehistoric events have occurred (0.1), and the Springfield and four other prehistoric events have occurred (0.05). If the Springfield liquefaction features are considered to be the effects of a distant earthquake (0.05 weight), then the largest prehistoric earthquake is assumed to be on the order of **M** 5.5 because of the very limited extent of the liquefaction features associated with other prehistoric events. If the Springfield liquefaction features are considered to be the result of a local prehistoric earthquake (0.95 weight), then it would represent the largest event known to have occurred in the region. McNulty and Obermeier (1999) estimate the magnitude of the second event in the Springfield area to have been a minimum of **M** 5.5. The magnitude of an earthquake that could have caused liquefaction features near Farmer City is more uncertain; the size of the older event is not well constrained because of the limited extent of deposits of sufficient age to record the event. The younger event recorded near Farmer City may be related to the Springfield events or to more distant Wabash Valley events, or alternatively may be related to a more local, smaller-magnitude event at or above the threshold for paleoliquefaction in moderately susceptible deposits (\sim **M** 5.2 to 5.5). Therefore, the Springfield event is considered to be the largest event for which there is evidence in central Illinois. Given the uncertainty in the size of this event, a range of values for the maximum observed magnitude is considered: **M** 6.2 (0.4), **M** 6.4 (0.3), **M** 6.6 (0.2), and **M** 6.8 (0.1). Based on the observation of McNulty and Obermeier (1999) that the water table may have been higher during this event and that the deposits would therefore have been more susceptible to liquefaction at

lower levels of ground shaking, the lower magnitude values are given more weight. In addition, there has been one historic earthquake of magnitude $\geq M$ 4.5 adding to the total number of events. Sample likelihood functions were computed for each assessment of the number of earthquakes of magnitude $\geq M$ 4.5 and the magnitude of the largest event. The weighted combination of these likelihood functions is shown in the second panel from the top of Figure 4.1-5.

The posterior distribution for maximum magnitude is obtained by multiplying the prior distribution with the weighted sample likelihood function. The resulting posterior distribution is shown in the second panel from the bottom of Figure 4.1-5. The continuous posterior distribution is discretized for input into the PSHA, as shown at the bottom panel of Figure 4.1-5.

4.1.4 Ground Motion Assessment

The updated PSHA was conducted using the representation of CEUS ground motions developed by EPRI (2003). Figure 4.1-6 shows the logic tree structure defined by EPRI (2003) to represent the uncertainty in the median ground motion relationship and in the aleatory variability about the median (standard deviation in the log of ground motion amplitude). As described in Section 2.2.2 of this Appendix, the EPRI (2003) ground motion model defines four alternative sets of median ground motion models (termed model clusters) to represent the alternative modeling approaches. Three of these ground motion clusters are appropriate for use in assessing the hazard from moderate-sized local earthquakes occurring randomly in source zones and all four are to be used for assessing the hazard from large-magnitude distant earthquakes. The first level of the logic tree shown on Figure 4.1-6 shows the weights assigned to the three median cluster models appropriate for local sources. The second level addresses the appropriate ground motion cluster median model to use for distant, large magnitude earthquake sources. For the EGC ESP Site, these sources are the Wabash Valley-southern Illinois sources and the New Madrid sources (both those defined in the EPRI-SOG model and the characteristic New Madrid sources added for this analysis). Two alternatives are given, either use of the cluster model used for the local sources or use of the Cluster 4 model. The effect of this logic structure on the PSHA is as follows. Following the branch for Cluster 1 at the first node, two options are available. The first is to also use the Cluster 1 model for the distant, large magnitude sources. The second option is to use Cluster 1 for only the local sources and use Cluster 4 for the distant, large magnitude sources. This same logic is repeated for the branches for Clusters 2 and 3. The non-rift Cluster 4 model was used for the Wabash Valley-southern Illinois sources and the rift Cluster 4 model was used for the New Madrid sources.

The third level of the logic tree addresses the uncertainty in the median attenuation relationship for each ground motion cluster. This uncertainty is modeled by a three-point discrete distribution with ground motion relationships for the 5th, 50th, and 95th percentiles of the epistemic uncertainty in the median attenuation relationship for each ground motion cluster, as illustrated on Figure 4.1-6.

The fourth level of the ground motion logic tree addresses the uncertainty in the model for the aleatory variability in ground motions about the median attenuation relationship. EPRI (1993) represented the uncertainty in the aleatory variability by four alternative models with the weights shown on Figure 4.1-6.

The last level of the ground motion logic tree addresses the relationship between body wave magnitude, m_b , and moment magnitude, \mathbf{M} . This conversion is required because the ground motion models are defined in terms of \mathbf{M} , whereas the EPRI-SOG recurrence rates are defined in terms of m_b . Conversion between m_b and \mathbf{M} was handled in the following manner.

The PSHA formulation used in this study for computing the frequency of exceeding a specified ground motion level, $v(z)$, can be written as:

$$v(z) = \lambda(m_0) \int_{m_0}^{m^u} f(m) \left\{ \int_0^{\infty} f(r|m) \cdot P(Z > z|m, r) dr \right\} dm \quad (\text{Eq. 4-2})$$

where $\lambda(m_0)$ is the frequency of earthquakes above a minimum magnitude of interest, m_0 ; $f(m)$ is the probability density for earthquake magnitude between m_0 and the maximum magnitude that can occur, m^u ; $f(m|r)$ is the probability density function for distance between the site and the earthquake, which may depend on the earthquake magnitude; and $P(Z > z|m, r)$ is the conditional probability of exceeding ground motion level z given the occurrence of an earthquake of magnitude m , at a distance r from the site. Equation 4-2 is applied source by source and the results summed over all sources to produce the total hazard.

The frequency of earthquakes, $\lambda(m_0)$ and the probability density function $f(m)$ are obtained from the EPRI-SOG source parameters defined in terms of m_b . The conditional probability of exceedance, $P(Z > z|m, r)$, for a specified value of m_b is obtained by first converting the m_b into moment magnitude, \mathbf{M} , then using one of the EPRI (2003) ground motion models to obtain the median and standard deviation of the ground motion measure Z . In order to incorporate the uncertainty in the m_b - \mathbf{M} conversion, three alternative relationships between m_b and \mathbf{M} were used in the PSHA. These relationships are compared on Figure 4.1-7. These three relationships are commonly used in converting between m_b and \mathbf{M} for ground motion estimation. The three relationships were given equal weight in the PSHA. In addition, the maximum-magnitude distributions defined above in terms of \mathbf{M} were converted to m_b for use in Equation 4-2 as the upper bound magnitude m^u . This conversion also was performed using the relationships shown on Figure 4.1-7. The two conversions were assumed to be perfectly correlated – that is, when the Atkinson and Boore (1995) relationship is used to convert m_b to \mathbf{M} for obtaining the median and standard deviation of the ground motion measure, its inverse is used to convert maximum magnitudes defined in terms of \mathbf{M} into m_b .

The ground motion attenuation relationships presented in EPRI (2003) define distance to the earthquake source in terms of either closest distance to the rupture plane or closest distance to the surface projection of the rupture plane (Joyner-Boore distance). In contrast, the EPRI-SOG seismic source models treat the earthquake ruptures as points in performing the integration over distance in Equation 4-2. However, EPRI (2003) provides a set of relationships to convert point-source distance to equivalent Joyner-Boore or rupture distance under the assumption that the orientation of the earthquake rupture (the strike of the fault) is uniformly distributed in azimuth between 0 and 360 degrees. These distance

adjustments were used in the updated PSHA for the EPRI-SOG sources. The EPRI (2003) adjustment factors for the random placement of the rupture on the point source location were used because this model imposes the minimum additional information on the EPRI-SOG source interpretations. The EPRI (2003) point-source adjustments include both an adjustment from point-source distance to expected closest or Joyner-Boore distance and an additional component of aleatory variability to account for the variability in rupture (or Joyner-Boore) distance for a given point-source distance.

4.1.5 PSHA Results

The PSHA update was conducted by combining the hazard from EPRI-SOG seismic sources (with updated maximum magnitude distributions as described above) with the hazard from the New Madrid characteristic earthquake sources. As discussed in Section 4.1.4, the hazard calculations were performed in terms of m_b magnitudes. Accordingly, the size of the characteristic New Madrid earthquakes was converted from moment magnitude M into m_b using the alternative three m_b - M relationships shown on Figure 4.1-7 in the same fashion as the updated maximum magnitudes for EPRI-SOG sources. In addition, the aleatory variability of ± 0.25 magnitude unit (moment magnitude) in the size of the individual characteristic events was transformed into ± 0.2 magnitude unit in terms of m_b . Earthquakes occurring within the EPRI-SOG sources were treated as point sources, consistent with the EPRI-SOG analysis, and the distance adjustment and additional aleatory variability factors discussed in Section 4.1.4 were applied. Characteristic earthquakes on the central New Madrid faults were assumed to rupture the entire fault, and the closest approach of the fault to the EGC ESP Site was used as the distance to rupture. The distance adjustment factors of the EPRI (2003) models were not applied in calculating the hazard from the characteristic earthquake New Madrid sources because the fault ruptures were specifically defined for these sources. As discussed in Section 4.1.1.3, characteristic earthquakes occurring on the central New Madrid faults were treated as clustered events using Equation 4-1.

Figure 4.1-8 shows the hazard results for peak acceleration and 5-Hz and 1-Hz spectral acceleration. Shown are the mean hazard curves and the 5th, 15th, 50th-(median), 85th-, and 95th fractile hazard curves. For peak ground acceleration, the width of the uncertainty distribution for the high frequency hazard is comparable to that obtained in the EPRI-SOG study (Figure 3.2-1). For 1-Hz spectral acceleration, the uncertainty distribution from the updated PSHA is narrower than that obtained in the EPRI-SOG study, primarily because of the change in the ground motion attenuation models.

Figures 4.1-9a and 4.1-9b show the relative contributions of the main sources to the median and mean hazard, respectively. At low ground motion levels, the distant Wabash Valley and New Madrid characteristic earthquakes produce the highest hazard. As ground motion level increases, the local central Illinois source becomes the dominant contributor to hazard for high-frequency ground motions. For low-frequency ground motions, the characteristic New Madrid earthquakes and the Wabash Valley sources are the main contributors to hazard at nearly all ground motion levels.

Figures 4.1-10a and 4.1-10b show the effect of using the alternative m_b to M conversion relationships (Figure 4.1-7) on the computed median and mean hazard, respectively. Similar estimates of seismic hazard are obtained using each of the relationships.

Figures 4.1-11a through 4.1-13b show the effects of the alternative components of the EPRI (2003) CEUS ground motion model on the hazard. Figures 4.1-11a and 4.1-11b show the effect of the alternative ground motion cluster models on the median and mean hazard, respectively. (Note that the results labeled Cluster 4 were computed using the Cluster 4 model for all sources for the purpose of this sensitivity test only. This causes the high-frequency hazard results for Cluster 4 to fall below the 5th-fractile hazard curves, which was computed without using the Cluster 4 model for local sources.) In general, use of the Cluster 3 ground motion model produces the highest hazard. Figures 4.1-12a and 4.1-12b show the effect of the epistemic uncertainty in the median ground motion models for each cluster on the median and mean hazard, respectively. The uncertainty in the hazard is somewhat greater for low-frequency motions than for high frequency motions, reflecting greater uncertainty in the median low-frequency ground motion models. Figures 4.1-13a and 4.1-13b show the effect of the alternative models for aleatory variability on the median and mean hazard, respectively. Aleatory model 1 produces the lowest hazard and aleatory model 4 the highest. Aleatory model 1 is the closest to the aleatory model used in the EPRI-SOG study.

Figures 4.1-14a through 4.1-16b show the effects of alternative models of New Madrid characteristic earthquakes on the hazard from just that source. Figures 4.1-14a and 4.1-14b show the effects of alternative fault end points and geometries for the fault sources on the median and mean hazard, respectively. The alternative geometries have only a slight effect on hazard because they produce only minor changes in the distance from the faults to the EGC ESP Site. Figures 4.1-15a and 4.1-15b show the effect of alternative estimates of the size of the characteristic earthquakes on the median and mean hazard, respectively. The alternative estimates lead to significant differences in the hazard from the characteristic New Madrid earthquakes because of the significant increase in ground motion amplitude produced by the $\sim 3/4$ unit increase in the magnitude of the characteristic earthquakes. Figures 4.1-16a and 4.1-16b show the effect of the alternative recurrence models on the median and mean hazard, respectively. The Poisson model produces slightly higher hazard because it leads to a slightly higher estimate of the equivalent annual frequency of characteristic earthquake sequences.

Figures 4.1-17a and 4.1-17b show the effect of the range in assessed maximum magnitude for the Wabash Valley–southern Illinois sources on the median and mean hazard, respectively, from just those sources. The uncertainty in maximum magnitude is a significant contributor to the uncertainty in the hazard from these sources.

Figures 4.1-18a and 4.1-18b show the effect of the range in assessed maximum magnitude for the central Illinois basin-background sources on the median and mean hazard, respectively, from just those sources. The uncertainty in maximum magnitude is a significant contributor to the uncertainty in the hazard for high frequency ground motions from these sources and a major contributor to the uncertainty in the hazard for low frequency ground motions.

4.1.6 Uniform Hazard Spectra for Rock and Identification of Controlling Earthquakes

PSHA calculations were performed for peak ground acceleration and spectral acceleration at frequencies of 25, 10, 5, 2.5, 1, and 0.5 Hz (spectral periods of 0.04, 0.1, 0.2, 0.4, 1.0, and 2.0

seconds, respectively). Figure 4.1-19 shows the uniform hazard spectra for rock site conditions developed from these results using the ground motion levels for each spectral frequency corresponding to the mean 10^{-4} and 10^{-5} annual frequency of exceedance. Peak ground acceleration is plotted at a frequency of 100 Hz (a period of 0.01 second).

The magnitude and distance for earthquakes controlling the hazard were identified following the procedure outlined in Appendix C of Regulatory Guide 1.165 (USNRC, 1997). Figure 4.1-20 shows the deaggregation of the mean 10^{-4} hazard. The top plot shows the averaged results for spectral frequencies of 5 and 10 Hz and the bottom plot shows the averaged results for frequencies of 1 and 2.5 Hz. For the high-frequency (HF) (5 and 10 Hz) mean 10^{-4} hazard, three sources can be identified: nearby earthquakes in the magnitude range of m_b 5 to 6+, corresponding to earthquakes occurring within the local central Illinois sources; magnitude m_b 6.5 to 7+ earthquakes occurring at distances of approximately 100 to 200+ km from the site, corresponding to earthquakes occurring in the Wabash Valley-southern Illinois sources; and magnitude m_b 7 to 7.5+ earthquakes occurring between 300 and 400 km from the site, corresponding to characteristic New Madrid earthquakes. For the low-frequency (LF) (1 and 2.5 Hz) mean 10^{-4} hazard, the characteristic New Madrid earthquakes become the largest contributors with the nearby earthquakes contributing only a small amount to the hazard.

Figure 4.1-21 shows the deaggregation of the mean 10^{-5} hazard. For the high-frequency (HF) (5 and 10 Hz) mean 10^{-5} hazard, the nearby m_b 5 to 6+ earthquakes have become the major contributor to the hazard with small contributions from the Wabash Valley-southern Illinois sources and characteristic New Madrid earthquakes. For the low-frequency (LF) (1 and 2.5 Hz) mean 10^{-5} hazard, the characteristic New Madrid earthquakes remain the largest contributors to the hazard, but the nearby earthquakes have an increased contribution compared to the mean 10^{-4} hazard (Figure 4.2-20).

Table 4.1-3 lists the magnitudes and distances for the controlling earthquakes computed for the mean 10^{-4} and mean 10^{-5} hazard. The values for the low-frequency hazard are listed considering all earthquakes and considering only those earthquakes occurring at distances greater than 100 km, consistent with the procedure outlined in Appendix C of Regulatory Guide 1.165.

The general approach for computing the amplification effects of the site soils uses as input ground motions appropriate for the HF and LF controlling earthquakes. Approach 2B for site response analyses described in NUREG/CR-6728 (McGuire et al., 2001) further refines this by using a range of magnitudes to reflect the distribution of earthquakes contribution to the HF and LF hazard. For the EGC-ESP Site, this distribution is defined based on the three distinct sets of sources identified in the deaggregation results. These “deaggregation earthquakes” (DEs) are listed in the right-hand side of Table 4.1-3. The magnitude and distance for each DE was computed by averaging the relative contributions among the appropriate magnitude-distance bins shown on Figures 4.1-20 and 4.1-21. The weights assigned to each DE represent the relative contribution of the sum of the appropriate magnitude-distance bins to the total hazard.

4.2 Site Response Analysis and Development of Soil Surface Spectra

Site response analyses were conducted to evaluate the response of local soils following approach 2B outlined in NUREG/CR-6728 (McGuire et al., 2001). The steps involved in this approach are:

1. Characterize the dynamic properties of the subsurface materials
2. Randomize these properties to represent their uncertainty and variability across the site.
3. Based on the deaggregation of the rock hazard, define the distribution of magnitudes contributing to the controlling earthquakes for high-frequency (HF) and low-frequency (LF) ground motions, (these are termed deaggregation earthquakes in McGuire et al., 2001) and define the response spectra appropriate for each of the deaggregation earthquakes.
4. Obtain appropriate rock site time histories to match the response spectra for the deaggregation earthquakes.
5. Compute the mean site amplification function for the HF and LF controlling earthquakes based on the weighted average of the amplification functions for the deaggregation earthquakes.
6. Scale the response spectra for the controlling earthquakes by the mean amplification function to obtain soil surface motions.
7. Envelop these scaled spectra to obtain the soil motions consistent with the rock hazard level.

4.2.1 Dynamic Properties of Subsurface Materials

The soil profile at the EGC ESP Site is described in detail in the EGC ESP Geotechnical Report (SSAR, Appendix A). Surface soils consist of a thin layer of loess. Underlying this soil are interbedded glacial tills and lacustrine deposits of Quaternary age to a depth of approximately 300 ft. These soils are classified primarily as silty clays and clayey silts. The rock encountered at a depth of approximately 300 ft consists of limestone, shale, and siltstone of Pennsylvanian age.

Figure 4.2-1 shows the shear-wave velocity data obtained at the EGC ESP Site. The data consist of one downhole velocity profile to a depth of 310 ft, and two seismic-cone velocity profiles to depths of 55 and 76 ft. The data from the two seismic-cone tests are consistent with the downhole velocity data. Also shown by the dashed line on Figure 4.2-1 is the shear-wave velocity profile defined in the CPS Updated Safety Analysis Report (USAR). These results are also consistent with the velocity data from the EGC ESP Site.

The solid line on Figure 4.2-1 shows the median shear-wave velocity profile developed to represent the EGC ESP site's Quaternary soils. The velocity profile was configured to capture the major trends in the measured velocity with depth. The median velocity profile was drawn smoothly through small-scale variations in velocity measurements.

A set of shear modulus reduction and damping tests were performed on samples taken from borings at the EGC ESP Site, as described in the EGC ESP Geotechnical Report (SSAR Appendix A). Figures 4.2-2 through 4.2-6 show the test results compared to the generic modulus reduction (G/G_{\max}) and damping relationships developed by EPRI (1993). (Note that one test sample produced what are considered to be erroneous values of modulus reduction and high damping values, as discussed in Appendix A to the SSAR. The test data from that sample were not included in developing the site dynamic properties and are not shown here.) In general, the site data are consistent with the EPRI (1993) relationships, except that the site data tend to show higher damping levels at very low shear strains. The EPRI (1993) curves are shown together on Figure 4.2-7, illustrating the effect of increasing confining pressure (increasing depth) on the nonlinear behavior of soils.

The CEUS ground motion relationships are defined for hard rock conditions corresponding to a shear-wave velocity of at least 2.83 km/sec (9,300 ft/sec) (EPRI, 2003). The shear-wave velocity of the rock encountered at a depth of 310 ft at the EGC ESP Site is approximately 4,000 ft/sec. This material is part of a Pennsylvanian sequence of shale, sandstone, coal, limestone, and siltstone that represents the bedrock surface in central Illinois. As described in the CPS USAR, the stratigraphic sequence in central Illinois consists of several hundred ft of the Pennsylvanian sequence underlain by 500 to 600 ft of Mississippian limestone, approximately 200 ft of Devonian shale and limestone, and approximately 400 ft of Silurian carbonate rocks. Below these rocks lie approximately 1,500 ft of Ordovician dolomite and sandstone and approximately 3,000 ft of Cambrian sedimentary rocks. Below the Cambrian rocks lie Precambrian igneous rocks.

Nine compression-wave velocity profiles have been obtained in deep borings drilled within about 10 miles of the EGC ESP Site. Figure 4.2-8 summarizes velocity data from these borings plotted against elevation above sea level. The measured compression-wave velocities (V_P) have been smoothed by eye over 50-ft intervals and converted into shear-wave velocities (V_S) using two values of the ratio V_P/V_S . A V_P/V_S ratio of 2 (corresponding to a Poisson's ratio of 0.33) was obtained in rock from the downhole velocity survey conducted at the EGC ESP site. This V_P/V_S ratio was used to convert the measured compression wave velocities to shear wave velocities for elevations above -1,200 ft. At the shallowest depths, the resulting shear wave velocities are consistent with the shear wave velocity measured at the EGC ESP site. At an elevation of approximately -1,200 ft (depth of approximately 1,900 ft), the rocks become Ordovician dolomite and sandstone, and there is a marked increase in the measured compression wave velocities. It is expected that Poisson's ratio decreases as the rock becomes more competent, approaching a value of 0.25 typically assumed for crustal rocks (e.g., EPRI, 1993). The estimated shear wave velocities for elevations below -1,200 ft are plotted on Figure 4.2-8 using V_P/V_S ratios of 2.0 and 1.73. If $V_P/V_S = 1.73$ is the correct value for the Ordovician and deeper rocks, then the rock velocity reaches "hard rock" values within the Ordovician sequence, and the appropriate sedimentary soil and rock profile depth for evaluating site response effects is approximately 1,900 ft. If $V_P/V_S = 2$ is the correct value for the deeper rocks, then the rock velocity does not reach "hard rock" values within the Ordovician sequence or in the underlying Cambrian rocks encountered at an elevation of approximately -2,300 ft (depth of approximately 3,000 ft). For this case, the appropriate depth of sedimentary soil and rock profile depth is approximately 6,000 ft, the depth to Precambrian igneous rocks.

The solid line on Figure 4.2-8 indicates the median shear wave velocity developed for the sedimentary sequence (soil and rock) beneath the EGC ESP Site. The shallow portion is taken from Figure 4.2-1 and the deeper portion is based on the converted compression wave velocity data shown on Figure 4.2-8. The dashed lines at the base of the profile represent the uncertainty in the depth to hard rock, which ranges between 2,000 and 6,000 ft.

For the site response analyses, the sedimentary rocks below a depth of 310 ft are assumed to behave linearly during earthquake shaking. The damping within these materials was established using the following procedure. The energy lost in shear-wave propagation is measured by the parameter Q_s , which can be equated to two other representations of energy loss in wave-propagation analysis. If linear viscoelastic wave-propagation modeling is used (such as in the site response analyses performed for this study using the program SHAKE – Schnabel et al., 1972), then the material damping is equivalent to $1/2Q_s$. Thus, Q_s values in the range of 10 to 25 correspond to damping ratios of 2 to 5 percent. Q_s can also be related to the high-frequency attenuation parameter κ developed by Anderson and Hough (1984) by the relationship $\kappa = H/Q_s V_s$, where H is the thickness of the crust over which the energy loss occurs, typically taken to be 1 to 2 km (Silva and Darragh, 1995). Silva and Darragh (1995) find that Q_s is proportional to shear-wave velocity ($Q_s = \tau V_s$). Using this assumption, the amount of high-frequency attenuation in the i^{th} layer of a velocity profile, κ_i , is given by the relationship $\kappa_i = H_i/\tau V_s^2$. Given the total value of κ appropriate to site conditions and velocity profiles, one can solve for the value of τ that will produce the appropriate damping values.

Silva and Darragh (1995) and Silva et al. (1996) give values of total κ appropriate to CEUS rocks. Their suggested value for CEUS sedimentary rocks with a shear wave velocity of 4,000 ft/sec is 0.019 second. The attenuation models for CEUS hard rock are developed assuming a shallow crustal κ of approximately 0.006 second (EPRI, 2003). Therefore, the damping values for sedimentary rocks underlying the EGC ESP Site were set at values that produce an equivalent κ value of 0.013 second (0.019 – 0.006). The resulting values of damping ratio obtained for the median velocity profile are given in Table 4.2-1.

4.2.2 Randomization of Dynamic Properties

Site response analyses were conducted using randomized shear-wave velocity profiles to account for variations in shear-wave velocity across the EGC ESP Site. The randomized profiles were generated using the shear-wave velocity correlation model developed by Toro (1996). In this model, the shear-wave velocity in a soil layer is modeled as lognormally distributed. The expression for the correlation coefficient between the velocity in two adjacent layers, ρ , is given by:

$$\rho(h,t) = (1 - \rho_d(h))\rho_t(t) + \rho_d(h) \quad (\text{Eq. 4-3})$$

where ρ_d represents the depth-dependent correlation (generally increasing with increasing depth), and ρ_t is the thickness-dependent correlation (generally decreasing with increasing layer thickness). The factors ρ_d and ρ_t are obtained from the expressions:

$$\rho_d(h) = \begin{cases} \rho_{200} \left[\frac{h + h_0}{200 + h_0} \right]^b & \text{for } h \leq 200 \text{ m} \\ \rho_{200} & \text{for } h > 200 \text{ m} \end{cases} \quad (\text{Eq. 4-4})$$

and

$$\rho_t(t) = \rho_0 \exp \left[- \left(\frac{t}{\Delta} \right)^\alpha \right] \quad (\text{Eq. 4-5})$$

where h is the average of the midpoint depths of layers i and $i-1$, and t is the difference between those midpoint depths. The correlation model parameters developed by Toro (1996) for stiff soil sites were used in the simulations. The parameters for this model are as follows: $\rho_0 = 0.99$, $\rho_{200} = 0.98$, $\Delta = 3.9$, $h_0 = 0.0$, and $b = 0.344$.

Completion of the model requires the standard deviation of $\ln(V_s)$ for individual soil layers. The data from the EGC ESP Site are too limited to provide a reliable estimate of $\sigma_{\ln(V_s)}$. Toro (1996) reports standard deviations for a number of sites where many shear-wave velocity profiles were obtained. These results suggest a value of $\sigma_{\ln(V_s)}$ on the order of 0.2 is appropriate to represent the variability in shear wave velocity across a site. The limited EGC ESP Site soil data give a value of 0.13. On the basis of the data presented in Toro (1996), a standard deviation of 0.2 is judged appropriate to represent the variability in shear wave velocity in the site soils.

The converted compression wave velocity data shown on Figure 4.2-8 were used to compute the standard deviation about the median velocity profile. The resulting value of $\sigma_{\ln(V_s)}$ is approximately 0.15, and this value was used to represent the variability of the shear wave velocity in the sedimentary rocks. The variability in the shear wave velocity typically decreases with increasing depth. Therefore $\sigma_{\ln(V_s)}$ was reduced to 0.1 for depths below 1,900 ft. This variability was also applied to the velocity at the base of the site response analysis profile (the half-space velocity).

Sixty randomized shear wave velocity profiles were generated to represent the uncertainty and variability in site velocity. The thicker layers in the median soil velocity profile (Figure 4.2-1) were subdivided into layers with thickness comparable to the velocity variation observed in the downhole velocity data. The thickness of individual layers was also randomized assuming a uniform distribution over the range of approximately ± 20 percent variation in thickness. The depth to the hard rock half-space was randomized assuming a uniform distribution over the depth range of 2,000 to 6,000 ft.

Figures 4.2-9a and 4.2-9b show the upper 500 ft of the 60 randomized velocity profiles. Figure 4.2-10 compares the statistics computed from the randomized profiles to the target values. Figures 4.2-11a and 4.2-11b show the full randomized velocity profiles, and Figure 4.2-12 compares the statistics computed from the randomized profiles to the target values to a depth of 4,000 ft.

The shear modulus reduction and damping relationships (Figure 4.2-7) were also randomized to account for the uncertainty and variability in these properties. Silva et al. (1996, Appendix D) present data on the variability in modulus reduction and damping ratio

based on testing of rock and soil samples. Figure 4.2-13 summarizes the data presented for soils. The top plot shows the data presented for sands in terms of the standard deviation of $\ln(G/G_{\max})$ plotted against G/G_{\max} . These data can be represented by the relationship:

$$\sigma_{\ln(G/G_{\max})} = 0.15 \left[1 - (G/G_{\max})^3 \right] \quad (\text{Eq. 4-6})$$

The bottom plot summarizes the data presented for sands and alluvial soils from the Savannah River Site (SRS) in terms of the standard deviation of $\ln(\text{damping ratio})$ plotted against the damping ratio in percent. These data can be represented by the relationship:

$$\sigma_{\ln(\text{damping ratio})} = 0.35 / \cosh[0.09 \times (\text{damping ratio, in \%})] \quad (\text{Eq. 4-7})$$

Equations 4-6 and 4-7 were used to define the variability of G/G_{\max} and damping ratio about the average curves presented on Figure 4.2-7. Figures 4.2-14 through 4.2-18 show the 60 sets of simulated G/G_{\max} and damping ratio curves.

The damping in the sedimentary rocks beneath the soil profile was also randomized in the analysis. As discussed in the previous section, the damping in the sedimentary rock layers is set so as to produce a site κ value of 0.013 sec (Table 4.2-1). However, the randomized velocity profiles will introduce an additional level of damping due to scattering off of the velocity interfaces. The average level of “scattering kappa” was estimated by comparing the response of the median profile to the average response of the randomized profiles for very low levels of motion. It was found that equivalent low-strain response at high frequencies could be obtained by reducing the site κ value by 0.002 sec to 0.011 sec. The value of κ assigned to an individual randomized profile was then drawn from a lognormal distribution with a median κ of 0.011 sec. The standard deviation of $\ln(\kappa)$ was set equal to 0.3, consistent with the variability in κ used in McGuire et al. (2001). The appropriate damping ratio in the sedimentary rock layers was then computed using the randomized sedimentary rock layer velocities and thicknesses and the randomly selected value of κ .

4.2.3 Time Histories for Site Response Analysis

Table 4.1-3 lists the controlling earthquakes for high frequencies (HF), defined as 5 to 10 Hz based on Regulatory Guide 1.165 (USNRC, 1997), and low frequencies (LF), defined as 1 to 2.5 Hz based on Regulatory Guide 1.165. These are denoted as reference earthquakes (REs) in McGuire et al. (2001). Appropriate rock site response spectra for these earthquakes were developed by computing the average spectral shape predicted by the EPRI (2003) ground motion models and then scaling this spectral shape to match the rock uniform hazard spectrum. The HF spectral shapes were scaled to match on-average the spectral acceleration at 5 and 10 Hz, and the LF spectral shapes were scaled to match on-average the spectral acceleration at 1 and 2.5 Hz.

The HF and LF controlling earthquakes listed in Table 4.1-3 are defined in terms of body wave magnitude and epicentral distance. These were converted to moment magnitude and the appropriate distance measure following the procedure used in the PSHA (Section 4.1.4). The spectra were extended beyond the range of frequencies defined in the EPRI (2003) ground motions models using the spectral shape relationships for CEUS earthquakes given in McGuire et al. (2001). The resulting rock RE spectra are shown on Figure 4.2-19. The HF

and LF spectra provide very good coverage of the rock uniform hazard spectra for all frequencies except below 1 Hz.

Table 4.1-3 also lists the distribution of deaggregation earthquakes for each HF and LF controlling or reference earthquake (RE). A response spectrum for each deaggregation earthquake (DE) was developed using the approach described above for the REs. These DE spectra represent the range of earthquakes contributing to the HF and LF hazard. The designation DEL refers to the earthquake at the low end of the magnitude range, DEM refers to the earthquake in the middle of the deaggregation magnitude range, and DEH refers to the earthquake at the upper end of the magnitude range. As discussed in Section 4.1.6, these earthquakes also correspond to different sources that contribute to the hazard. The DEL earthquake is a local earthquake occurring in central Illinois, the DEM earthquake is an earthquake occurring in the Wabash Valley-southern Illinois region, and the DEH earthquake is a characteristic New Madrid earthquake. Figures 4.2-20 and 4.2-21 show the DE spectra for the 10^{-4} and 10^{-5} mean rock hazard, respectively.

Time histories for the site response analyses were obtained from the CEUS time history library provided with NUREG/CR-6728 (McGuire et al., 2001). This library contains recordings divided into magnitude and distance ranges, each containing 30 time histories (15 recordings with two horizontal components each). The selected sets of records used for each DE are listed in Table 4.2-2. The selected time histories were scaled to the target DE spectrum using a limited number of iterations of the program RASCALS⁵. Figure 4.2-22 shows an example of the response spectra for the 30 time histories scaled to match the DEM spectrum for the mean 10^{-4} HF RE. As part of the scaling process, the time histories were high-pass filtered with a filter corner at 0.2 Hz to remove spurious long period motions. This filter corner frequency is less than or equal to the corner frequencies for the filters used to process the original time histories. This frequency is also well below the frequencies of interest in the site amplification studies.

4.2.4 Site Response Transfer Functions

Sixty response analyses were performed with program SHAKE⁶ to compute the site amplification function for each deaggregation earthquake. The 60 randomized velocity profiles were paired with the 60 sets of randomized modulus reduction and damping curves (one profile with one set of modulus reduction and damping curves). Each of the 30 scaled time histories was used to compute the response of two profile-soil property curves sets. For each analysis, the response spectrum for the computed surface motion was divided by the response spectrum for the input motion to obtain a site amplification function. The arithmetic mean of these 60 individual response spectral ratios was then computed to define the mean site amplification function for each DE. Figures 4.2-23 and 4.2-24 show the computed average site amplification functions for the mean 10^{-4} and mean 10^{-5} hazard levels DEs, respectively. The site amplification at 100 Hz was computed by averaging the ratios of

⁵ RASCALS is a frequency domain program for modeling earthquake ground motions and site response developed by Silva and Lee (1987). It was used extensively in the analyses presented in NUREG/CR-6728 (McGuire et al., 2001). The RASCALS option for frequency-domain modification of time histories to match a target response spectrum was used in this study.

⁶ SHAKE is an industry-standard program for site response analysis originally developed by Schnabel et al. (1972). Geomatrix's in house version of SHAKE was used for these analyses. This version has been benchmarked against the published versions of SHAKE and has been documented in accordance with project quality assurance requirements.

the peak ground acceleration for the surface motion divided by the peak acceleration for the input time history.

The final site amplification function for each RE is computed as the weighted average of the amplification functions for the associated DEs. The weights, listed in Tables 4.1-3 and 4.2-2, represent the relative contribution of earthquakes represented by the DEs to the hazard at the appropriate spectral frequency and hazard level. The weighted average site amplification functions are shown on Figures 4.2-23 and 4.2-24.

The peak site amplification of about 3.3 occurs at a frequency of approximately 1.7 Hz. This amplification is due primarily to the 310-ft soil column at the EGC ESP site. The peak amplification is not sensitive to the level of input motion, indicating that much of the soil profile is undergoing only low levels of strain. Deamplification of motions occurs at high frequencies, generally above 10 Hz. The degree of deamplification is sensitivity to the level of motion, indicating that the shallow soils are experiencing nonlinear behavior as the level of the input motion increases. The maximum deamplification occurs at frequencies near 30 Hz and reaches a minimum value of 0.45 for the 10⁻⁵ HF RE.

4.2.5 Soil Surface Spectra

The soil surface spectra for the EGC ESP site are obtained by scaling the rock reference earthquake (RE) spectra by the site amplification functions. As shown on Figure 4.2-19, the RE spectra provide good coverage of the rock uniform hazard spectra except for frequencies below 1 Hz. In order to develop soil surface spectra for the full frequency range, the low frequency (LF) RE spectra were shifted upward below a frequency of 1 Hz to match the uniform hazard rock spectra. These adjusted RE spectra are shown on Figure 4.2-25. This low frequency adjustment should not impact the results of the site response analyses because the site amplification at frequencies below 1 Hz is insensitive to the level of input motion.

The adjusted RE spectra on Figure 4.2-25 were multiplied by the appropriate weighted average site amplification functions from Figures 4.2-23 and 4.2-24. The resulting soil spectra are shown on Figure 4.2-26. Smooth envelope spectra were then constructed to define the 10⁻⁴ and 10⁻⁵ mean hazard horizontal spectra for the surface soil conditions. These envelope spectra are shown on Figure 4.2-26.

4.3 SSE Ground Motion Spectra

This section presents the development of the risk-consistent SSE motions (called design response spectra -- DRS) for the EGC ESP Site following the approach outlined in ASCE Standard XXX (ASCE, 2003).

4.3.1 Horizontal SSE Spectrum

The ASCE Standard XXX approach defines the risk-consistent DRS in terms of the site-specific Uniform Hazard Response Spectrum (UHRS) as:

$$\text{DRS} = \text{DF} * \text{UHRS}, \quad (\text{Eq. 4-8})$$

where UHRS is the site-specific UHRS, defined for Seismic Design Category (SDC)-5 at the mean 10^{-4} annual frequency of exceedance, and DF is the Design Factor (called a scale factor (SF) in the terminology of NUREG/CR-6728 (McGuire et al., 2001)) defined based on the slope of the mean hazard curve. When used to scale the UHRS, the derived DRS is a uniform risk spectrum, which used with the USNRC's seismic design criteria provides a consistent risk against failure across the facility structures, systems, and components (SSCs). Note that the SFs given in NUREG/CR-6728, Chapter 7 are more liberal than DFs given in the ASCE Standard XXX because the analysis in NUREG/CR-6728 starts with a more liberal assumption about the conservatism achieved by the NUREG-0800 seismic design requirements. The procedure for computing the DRS is as follows.

For each spectral frequency at which the UHRS is defined, a slope factor A_R is determined from:

$$A_R = \frac{SA_{0.1H_D}}{SA_{H_D}} \quad (\text{Eq. 4-9})$$

where SA_{H_D} is the spectral acceleration at the target mean UHRS exceedance frequency H_D (i.e., $10^{-4}/\text{yr}$) and $SA_{0.1H_D}$ is the spectral acceleration at $0.1H_D$ (i.e., $10^{-5}/\text{yr}$). Then the Design Factor (DF) at this spectral frequency is given by:

$$DF = \text{Maximum}(DF_1, DF_2) \quad (\text{Eq. 4-10})$$

For Seismic Design Category SDC-5, ASCE Standard XXX gives:

$$DF_1 = 1.0 \quad (\text{Eq. 4-11})$$

and

$$DF_2 = 0.6(A_R)^{0.80}. \quad (\text{Eq. 4-12})$$

The derivation of DF is described in detail in Commentary to the ASCE Standard XXX (ASCE, 2003).

The starting point for this calculation is the soil surface spectra for 10^{-4} and 10^{-5} mean hazard. These are shown on Figure 4.2-26 and listed in Table 4.3-1. The computation of the horizontal DRS is summarized in Table 4.3-1. The resulting horizontal DRS spectrum for the SSE motions is shown on Figure 4.3-1. Also shown for comparison on Figure 4.3-1 is the Regulatory Guide 1.60 spectrum scaled to a peak acceleration of 0.3 g.

4.3.2 Vertical SSE Spectrum

The vertical SSE spectrum is constructed from the horizontal DRS spectrum using vertical to horizontal (V/H) response spectral ratios appropriate for the EGC ESP Site following the approach described in NUREG/CR-6728 (McGuire et al., 2001).

The EGC ESP Site-specific horizontal DRS shown in Figure 4.3-1 is based on the mean 10^{-4} hazard on rock scaled to the site-specific soil conditions using two reference earthquake (RE) rock spectra. Figure 4.3-2 shows V/H ratios recommended by McGuire et al. (2001) for CEUS rock sites as a function of spectral frequency and the level of peak ground acceleration (PGA) for the horizontal component. Figure 4.3-3 shows the weighted average of these V/H ratios based on the PGA for the DEs that make up the high-frequency (HF) and low-frequency (LF) mean 10^{-4} REs. The weights assigned to the DEs are listed in Table 4.3-1. The resulting V/H ratios are essentially the same for the HF and LF DEs.

The rock V/H ratios plotted on Figure 4.3-3 require adjustment to ratios appropriate for soil sites. This adjustment is based on a comparison of the V/H ratios for rock and soil obtained from the empirical western United States (WUS) attenuation models discussed in NUREG/CR-6728 (McGuire et al., 2001). Two of these models (Abrahamson and Silva, 1997; and Campbell, 1997) provide vertical motions for both soil and rock conditions. Figure 4.3-4 shows the average of the V/H spectral ratios for these two attenuation models. The spectral ratios were computed for a magnitude **M** 6.4 earthquake at a source-to-site distance of 15 km. A magnitude **M** 6.4 earthquake was chosen to correspond to the magnitude for the HF RE (m_b 6.5) converted moment magnitude using the relationships shown on Figure 4.1-7. The distance of 15 km was chosen so that the WUS attenuation relationships produce a horizontal PGA on rock comparable to that for the mean 10^{-4} hazard at the EGC ESP Site. The resulting V/H ratios for soil sites are greater than those for rock sites at high frequencies and lower at low frequencies. Also the soil V/H ratios peak in about the same frequency range as the rock V/H ratios. The peak in the V/H ratios for WUS ground motions occurs at a lower frequency than for CEUS ground motions (Figure 4.3-2). The difference in the frequency range for peak V/H ratios is attributed to the difference in the shallow crustal damping factor κ (McGuire et al., 2001). Taking the ratio of the soil and rock V/H ratios from Figure 4.3-4 and shifting the peak response to conform to the peak of the CEUS rock V/H ratios (Figure 4.3-3) produces the scaled CEUS soil V/H ratio shown on Figure 4.3-5.

The vertical SSE spectrum is obtained by scaling the horizontal DRS spectrum by the soil V/H ratios shown on Figure 4.3-5. The resulting vertical SSE is shown on Figure 4.3-6 and is tabulated in Table 4.3-2 along with the horizontal SSE spectrum. The resulting SSE ground motion spectra are enveloped by the Regulatory Guide 1.60 response spectrum anchored to a peak ground acceleration of 0.3 g except for some frequencies above 16 Hz. The maximum exceedance is 25 percent and occurs at a frequency of 33 Hz.

TABLE 4.1-1
MAGNITUDE COMPARISONS FOR NEW MADRID
1811-1812 EARTHQUAKE SEQUENCE
Seismic Hazards Report for the EGC ESP Site

Study	NM1	NM2	NM3
Johnston (1996)	M 8.1 ± 0.3	M 7.8 ± 0.3	M 8.0 ± 0.3
Hough et al. (2000)	M 7.2 to 7.3	M ~7.0	M 7.4 to 7.5
Mueller and Pujol (2001)	-	-	M 7.2 to 7.4 (preferred M 7.2 to 7.3)
Bakun and Hopper (in press 2003)	M_I 7.2 (M 6.8 to 7.5)	M_I 7.1 (M 6.7 to 7.4)	M_I 7.4 (M 7.0 to 7.7)

TABLE 4.1-2
MAGNITUDE DISTRIBUTIONS FOR CHARACTERISTIC
NEW MADRID EARTHQUAKES

Seismic Hazards Report for the EGC ESP Site

Characteristic Rupture Set	Characteristic Magnitudes for Individual Faults (moment magnitude [M])			Weight
	New Madrid South	Reelfoot Thrust	New Madrid North	
1	7.3	7.2	7.0	0.2
2	7.3	7.4	7.0	0.2
3	7.7	7.4	7.4	0.2
4	7.7	7.6	7.4	0.3
5	8.1	8.0	7.8	0.1

TABLE 4.1-3
ROCK HAZARD CONTROLLING EARTHQUAKES
 Seismic Hazards Report for the EGC ESP Site

Hazard	Controlling Earthquake		Deaggregation Earthquakes		
	Magnitude (m_b)	Distance (km)	Magnitude (m_b)	Distance (km)	Weight
Mean 10^{-4} 5 and 10 Hz	6.5	83	5.7	15	0.377
			6.7	153	0.322
			7.2	375	0.301
Mean 10^{-4} 1 and 2.5Hz	7.0	223	5.9	15	0.093
	7.2*	320*	6.8	166	0.240
			7.3	379	0.667
Mean 10^{-5} 5 and 10 Hz	6.2	24	5.8	11	0.733
			6.8	140	0.149
			7.4	380	0.118
Mean 10^{-5} 1 and 2.5Hz	7.0	134	6.0	12	0.212
	7.3*	320*	6.9	155	0.220
			7.4	381	0.568

*computed using earthquakes with distances > 100 km

TABLE 4.2-1
NOMINAL DAMPING RATIOS FOR SEDIMENTARY ROCK
CORRESPONDING TO $\kappa = 0.013$ SEC
 Seismic Hazards Report for the EGC ESP Site

Depth Range¹ (ft)	Average Shear Wave Velocity (fps)	Shear Wave Quality Factor Q_s	Equivalent Damping Ratio (%)
310 - 400	4,000	15.2	3.30
400 – 450	4,275	16.2	3.08
450 – 650	4,650	17.6	2.84
650 – 1,200	5,500	20.9	2.40
1,200 – 1,900	7,200	27.3	1.83

¹ Depth range is depth below ground surface.

TABLE 4.2-2
TIME HISTORY DATA SETS FROM NUREG/CR-6728 USED FOR EACH
DEAGGREGATION EARTHQUAKE
Seismic Hazards Report for the EGC ESP Site

Hazard	Controlling Earthquake (RE)		Deaggregation Earthquakes (DE)				
	Magnitude (m _b)	Distance (km)	Designation	Magnitude (m _b)	Distance (km)	Weight	NUREG/CR-6728 CEUS Data Set
Mean 10 ⁻⁴ 5 and 10 Hz	6.5	83	HF DEL	5.7	15	0.377	M 4.5-6, D 0-50 km
			HF DEM	6.7	153	0.322	M 6-7, D 100-200 km
			HF DEH	7.2	375	0.301	M >7, D 100-200 km
Mean 10 ⁻⁴ 1 and 2.5Hz	7.0 7.2*	223 320*	LF DEL	5.9	15	0.093	M 4.5-6, D 0-50 km
			LF DEM	6.8	166	0.240	M 6-7, D 100-200 km
			LF DEH	7.3	379	0.667	M >7, D 100-200 km
Mean 10 ⁻⁵ 5 and 10 Hz	6.2	24	HF DEL	5.8	11	0.733	M 4.5-6, D 0-50 km
			HF DEM	6.8	140	0.149	M 6-7, D 100-200 km
			HF DEH	7.4	380	0.118	M >7, D 100-200 km
Mean 10 ⁻⁵ 1 and 2.5Hz	7.0 7.3*	134 320*	LF DEL	6.0	12	0.212	M 4.5-6, D 0-50 km
			LF DEM	6.9	155	0.220	M 6-7, D 100-200 km
			LF DEH	7.4	381	0.568	M >7, D 100-200 km

TABLE 4.3-1
COMPUTATION OF HORIZONTAL DRS SPECTRUM
FOR THE EGC ESP SITE

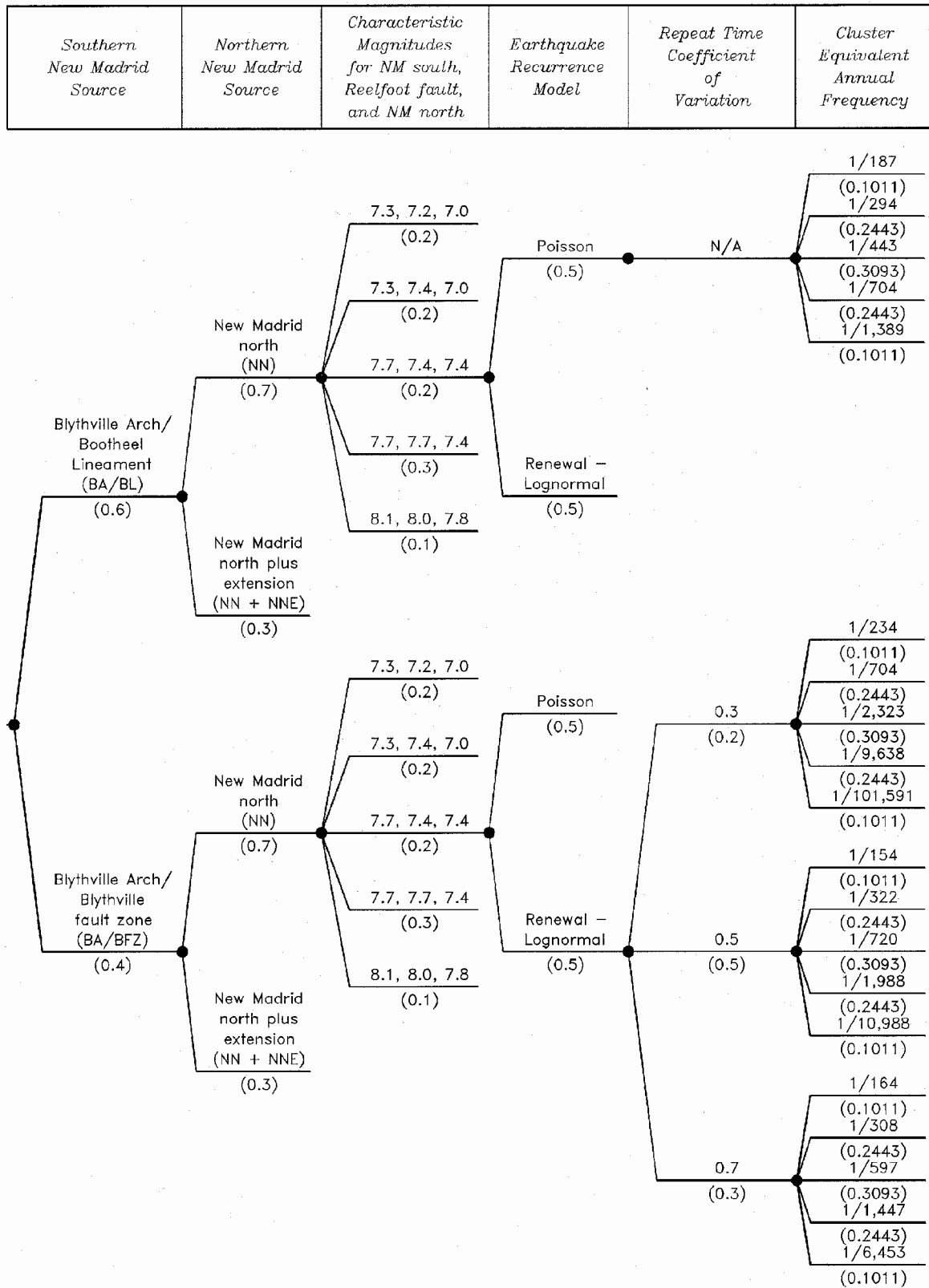
Seismic Hazards Report for the EGC ESP Site

Spectral Frequency (Hz)	10⁻⁴ Mean Hazard Spectral Acceleration (g)	10⁻⁵ Mean Hazard Spectral Acceleration (g)	DF₂	Horizontal DRS Spectral Acceleration (g)
100	0.2502	0.5031	1.049	0.2625
50	0.3177	0.5957	0.992	0.3177
30.3	0.3743	0.6821	0.970	0.3743
25	0.3986	0.7185	0.961	0.3986
20	0.4385	0.8002	0.971	0.4385
16.67	0.4741	0.8737	0.978	0.4741
13.33	0.5114	0.9730	1.004	0.5133
11.11	0.5247	1.0486	1.044	0.5478
10	0.5326	1.1089	1.079	0.5746
9.0	0.5405	1.1248	1.078	0.5829
6.67	0.5640	1.1718	1.077	0.6074
5	0.5874	1.1720	1.043	0.6125
4	0.6062	1.1722	1.017	0.6164
3.33	0.6220	1.1515	0.982	0.6220
2.5	0.5491	1.1110	1.054	0.5790
2	0.4985	1.0805	1.114	0.5554
1.67	0.4606	1.0315	1.144	0.5267
1.33	0.3612	0.8777	1.221	0.4409
1.18	0.3151	0.8017	1.266	0.3991
1	0.2640	0.6955	1.302	0.3438
0.67	0.1697	0.4880	1.397	0.2370
0.5	0.1240	0.3668	1.429	0.1772
0.33	0.0633	0.1826	1.401	0.0886
0.25	0.0392	0.1114	1.382	0.0542
0.2	0.0296	0.0852	1.399	0.0414
0.13	0.0177	0.0524	1.429	0.0253
0.1	0.0123	0.0371	1.450	0.0179

TABLE 4.3-2
SSE GROUND MOTION SPECTRA FOR THE EGC ESP SITE
(5 PECENT DAMPING)

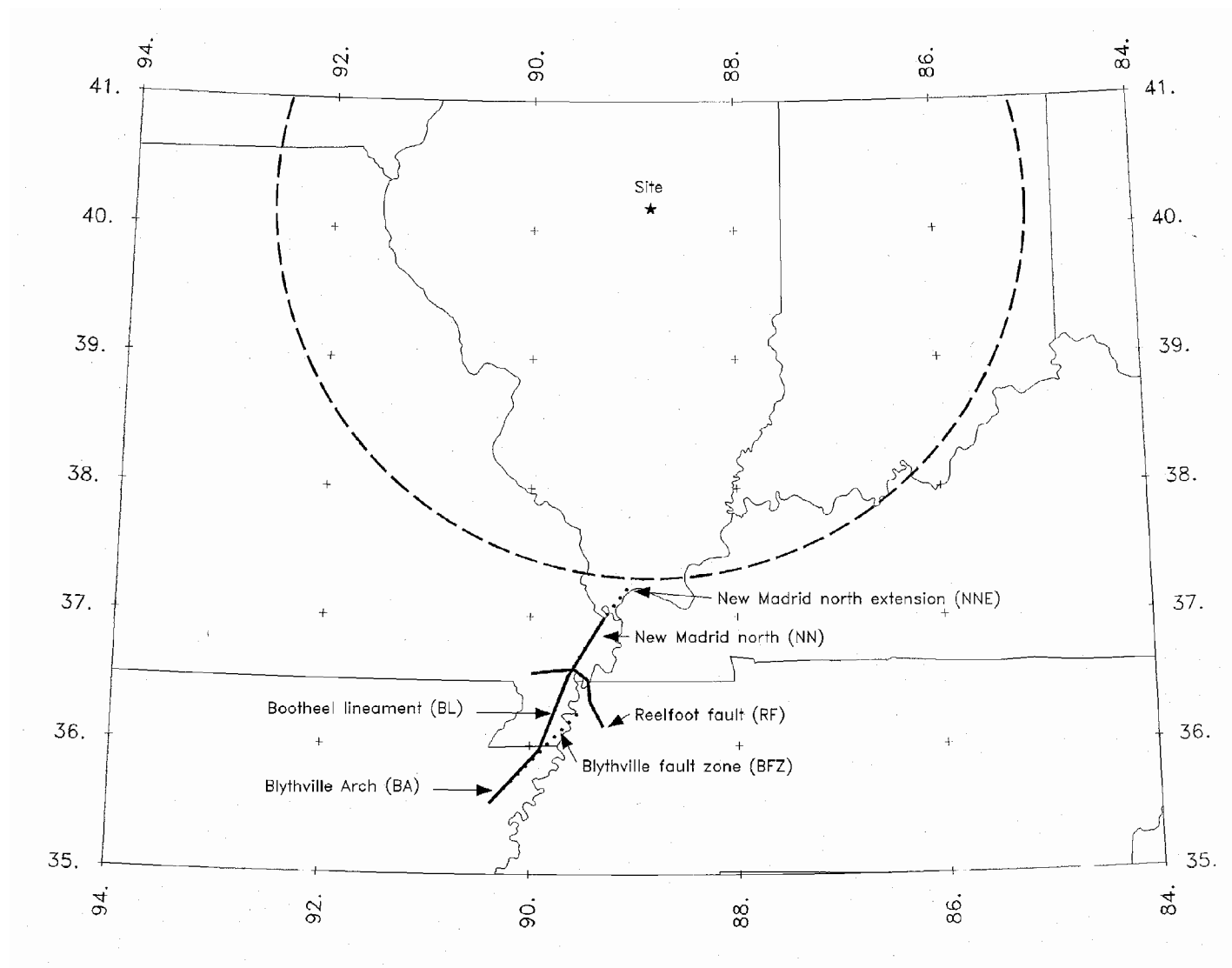
Seismic Hazards Report for the EGC ESP Site

Spectral Frequency (Hz)	Horizontal SSE Spectral Acceleration (g)	Vertical SSE Spectral Acceleration (g)
100	0.2625	0.2428
66.67	0.2935	0.3405
50	0.3177	0.3527
30.3	0.3743	0.3700
25	0.3986	0.3755
20	0.4385	0.3894
16.67	0.4741	0.4000
13.33	0.5133	0.4054
11.11	0.5478	0.4084
10	0.5746	0.4137
9.0	0.5829	0.4181
6.67	0.6074	0.4309
5	0.6125	0.4299
4	0.6164	0.4291
3.33	0.6220	0.4300
2.5	0.5790	0.3959
2	0.5554	0.3766
1.67	0.5267	0.3547
1.33	0.4409	0.2943
1.18	0.3991	0.2651
1	0.3438	0.2269
0.67	0.2370	0.1539
0.5	0.1772	0.1137
0.33	0.0886	0.0560
0.25	0.0542	0.0338
0.2	0.0414	0.0256
0.13	0.0253	0.0154
0.1	0.0179	0.0107



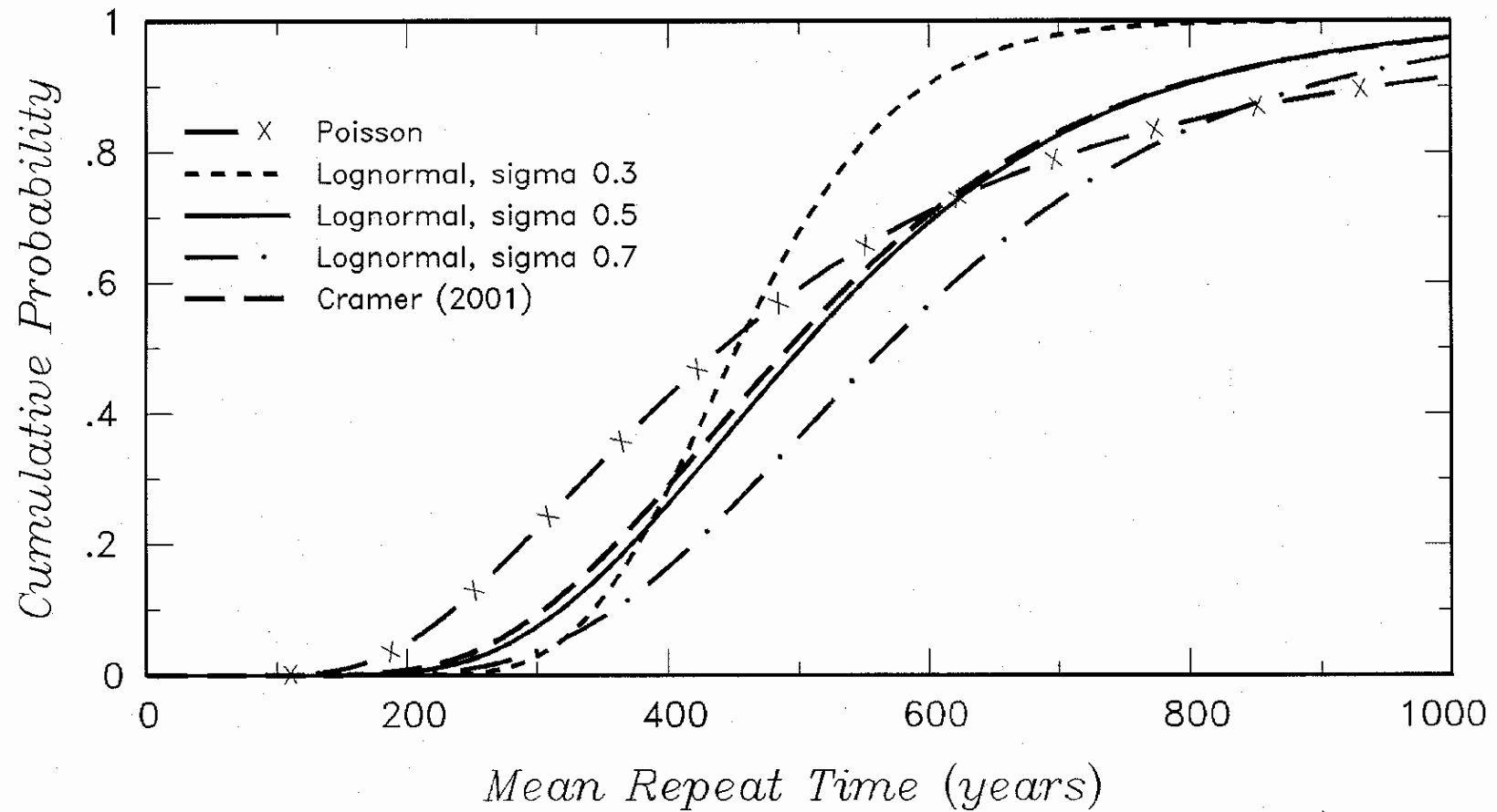
Seismic Hazards Report for the EGC ESP Site
Source Characterization Logic Tree for Characteristic New Madrid Earthquakes

Figure
4.1-1



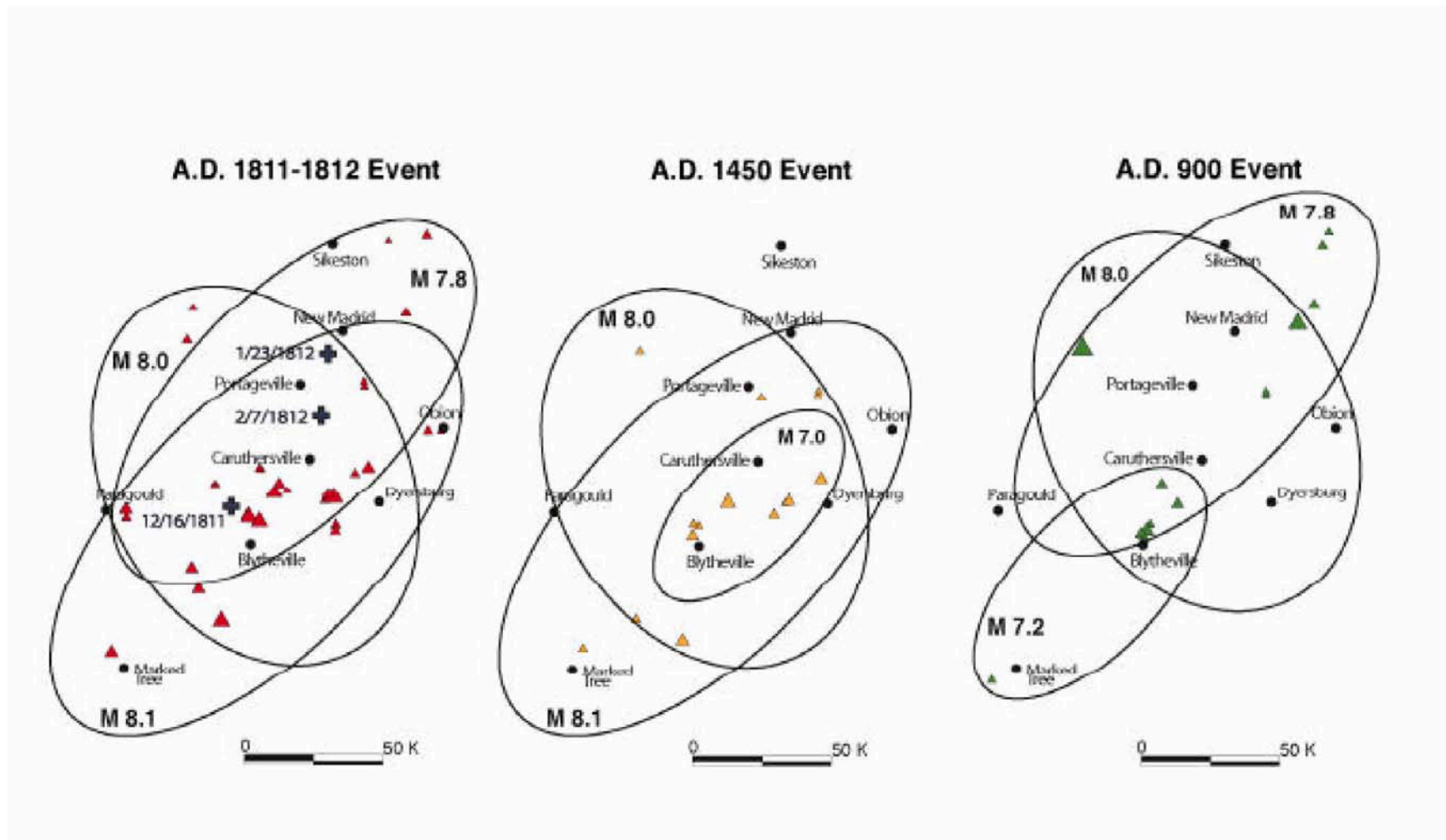
Seismic Hazards Report for the EGC ESP Site
Locations of Fault Sources for Characteristic New Madrid Earthquakes

Figure
4.1-2

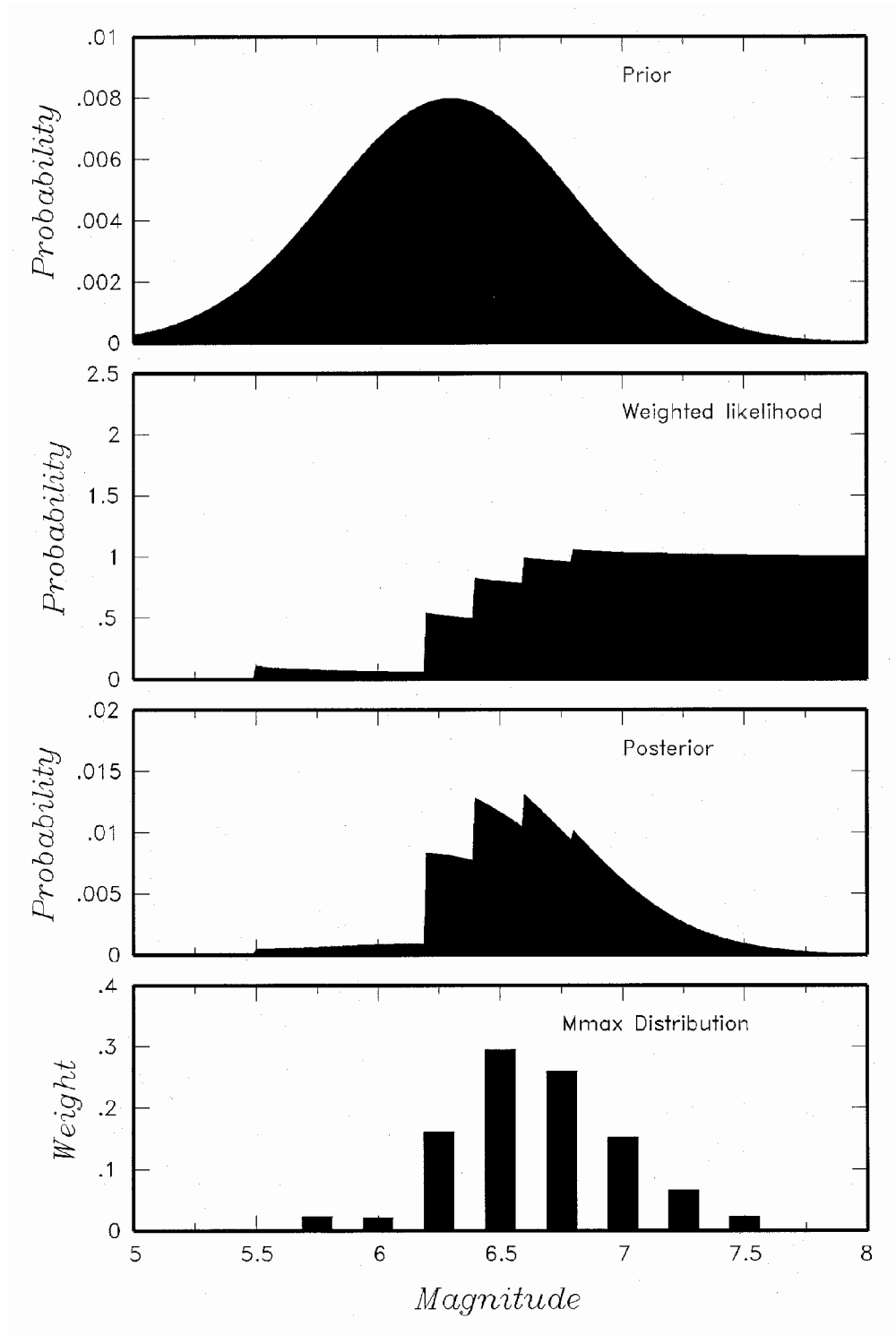


Seismic Hazards Report for the EGC ESP Site
Distributions of Mean Repeat Time for Characteristic New Madrid Earthquakes

Figure
4.1-3



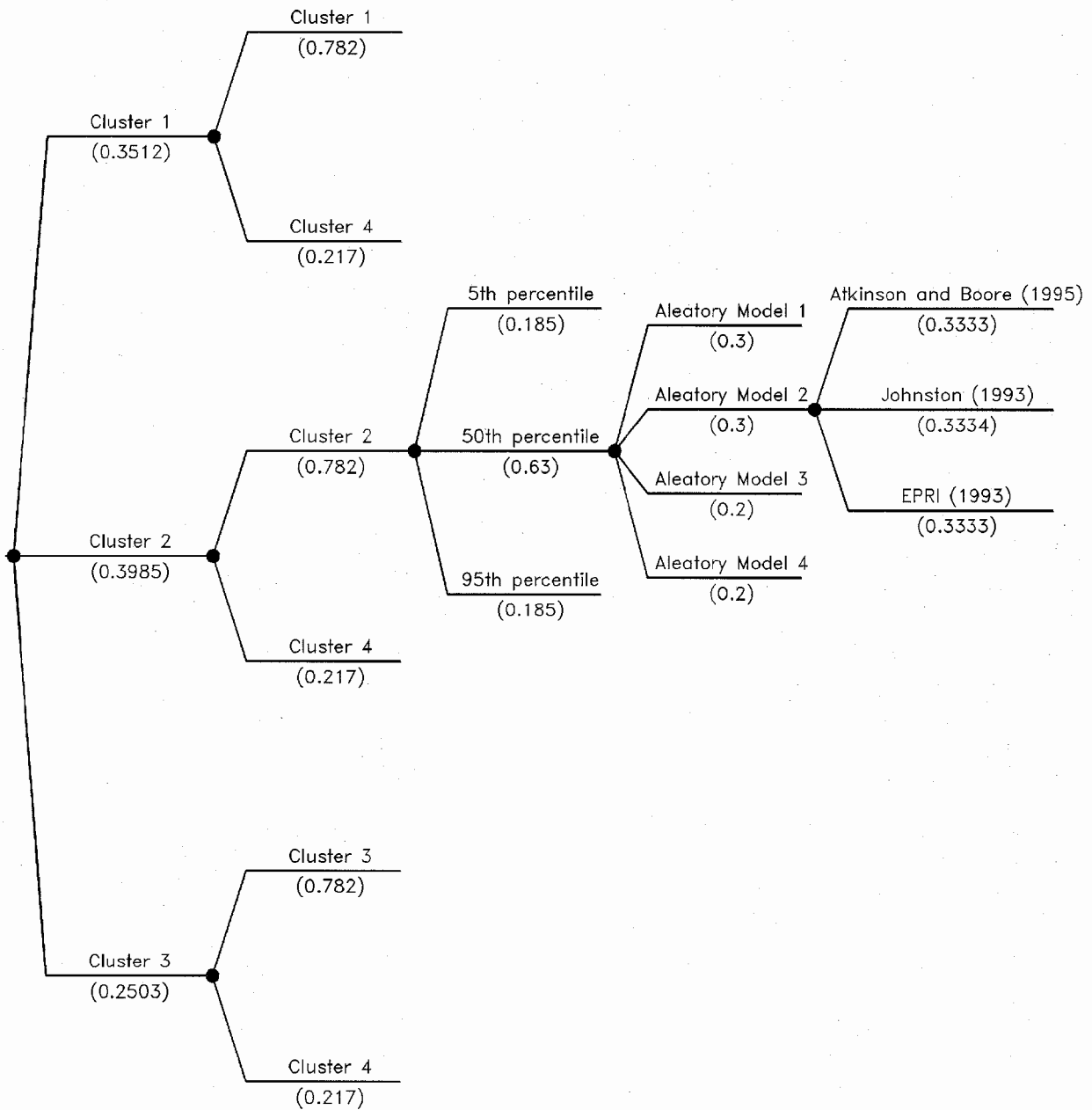
from Tuttle et al. (2002)

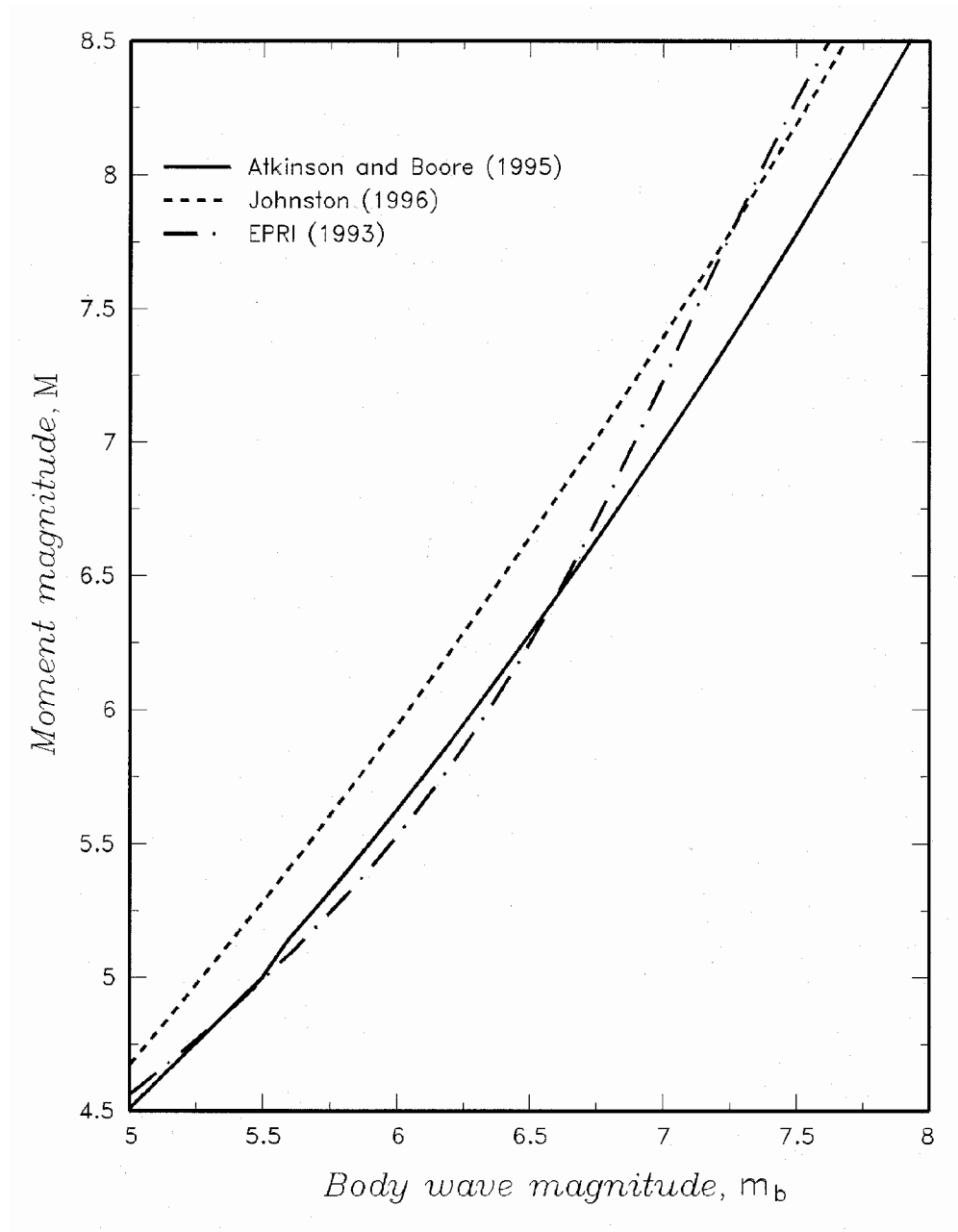


Seismic Hazards Report for the EGC ESP Site
Maximum Magnitude Distribution for Central Illinois Seismic Sources

Figure
4.1-5

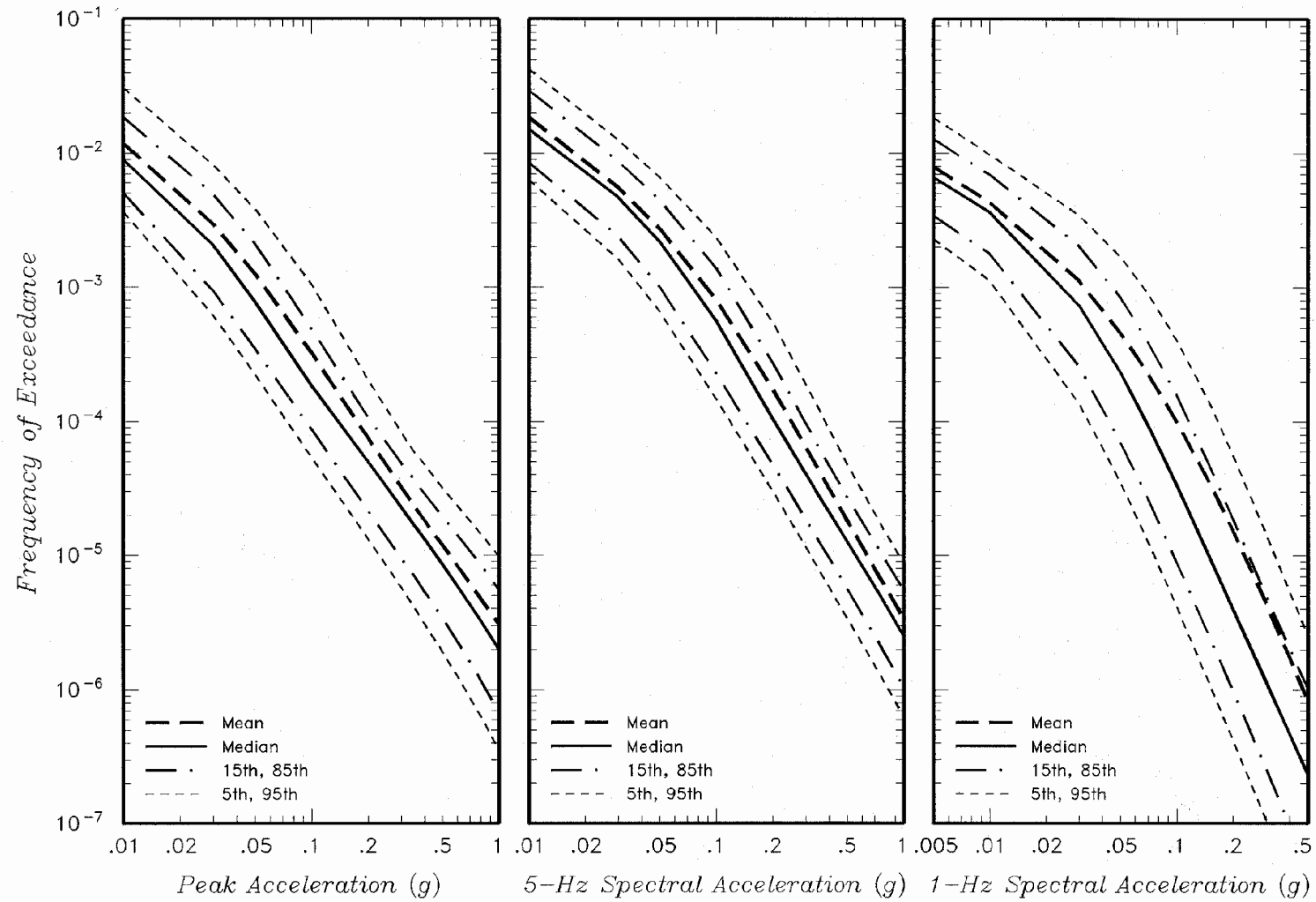
<i>Ground Motion Cluster for Local Sources</i>	<i>Ground Motion Cluster for Distant Sources</i>	<i>Epistemic Uncertainty in Cluster Median</i>	<i>Aleatory Variability Model</i>	<i>mb to M Conversion Relationship</i>
--	--	--	-----------------------------------	--





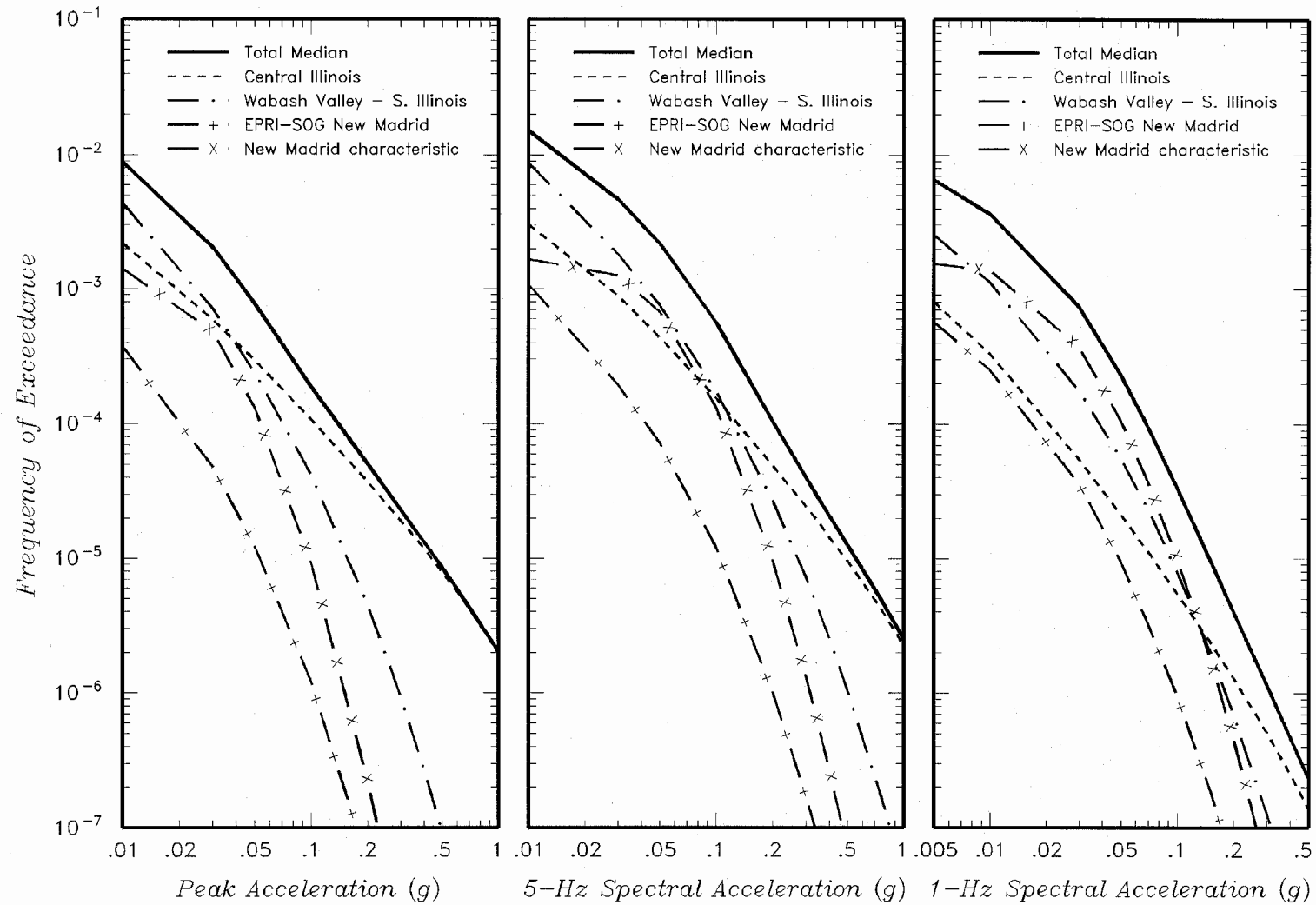
Seismic Hazards Report for the EGC ESP Site
Alternative m_b Versus M Relationships

Figure
4.1-7



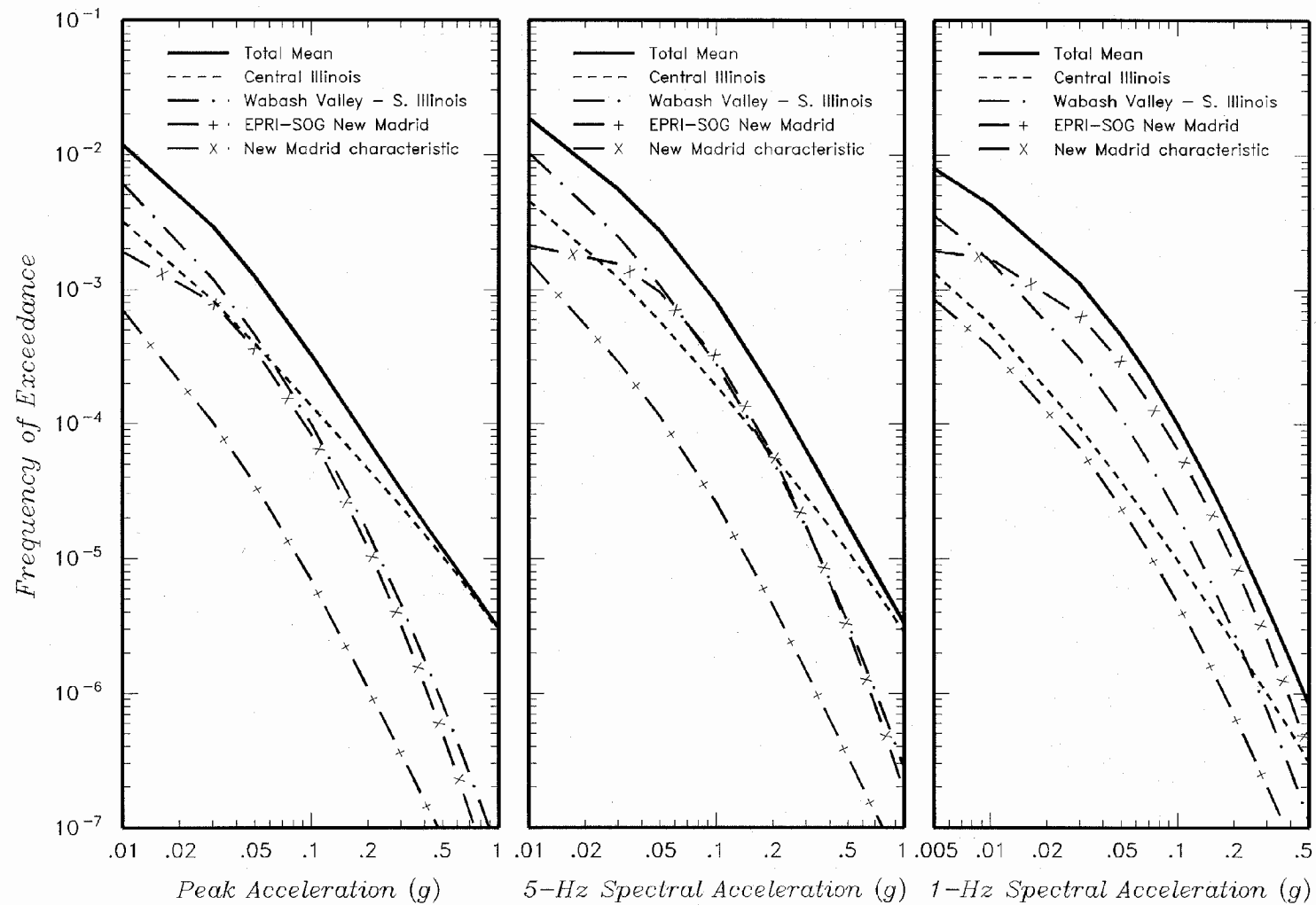
Seismic Hazards Report for the EGC ESP Site
Mean and Fractile Hazard Curves from Updated PSHA

Figure
4.1-8



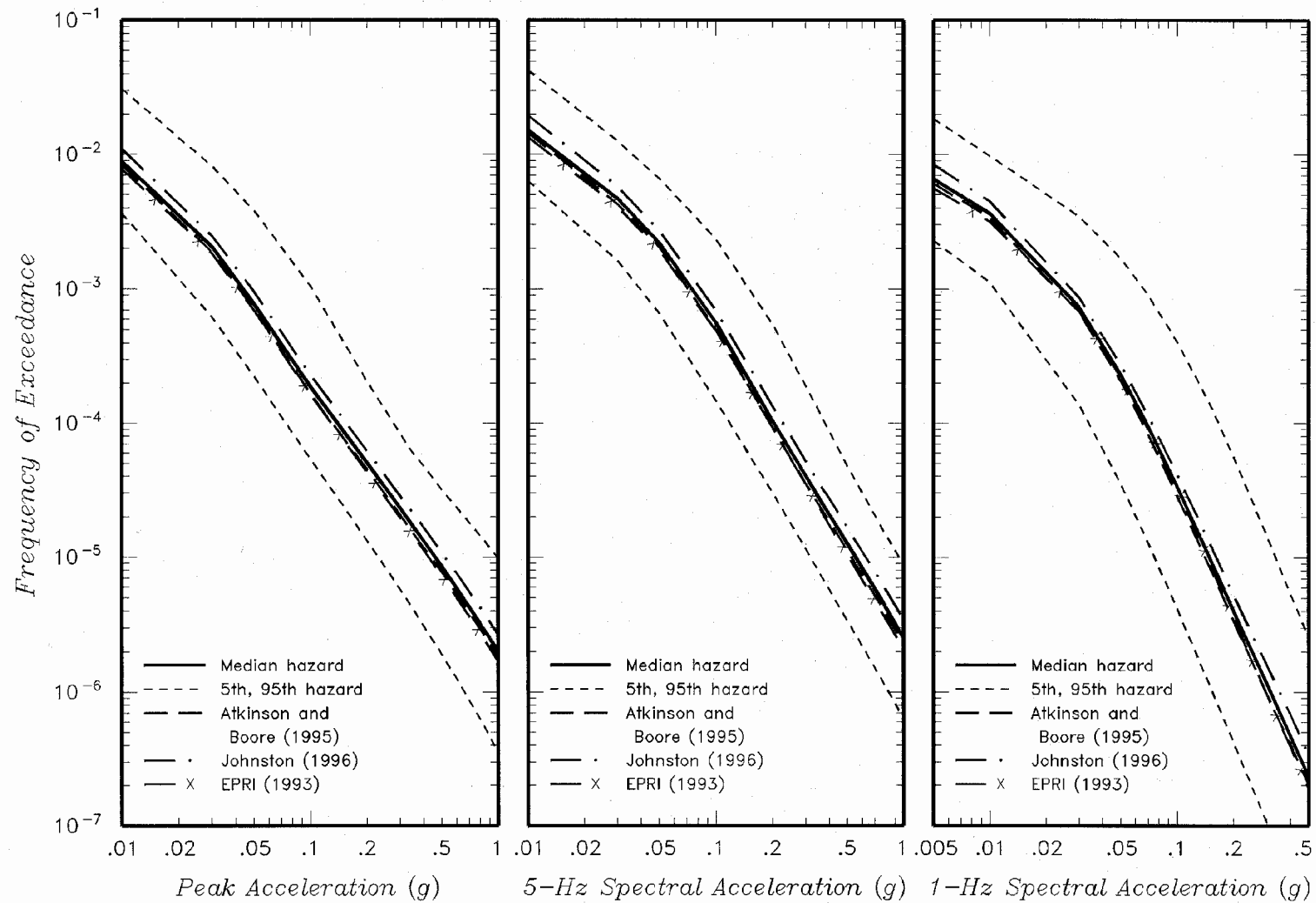
Seismic Hazards Report for the EGC ESP Site
Contribution of Individual Sources to Median Hazard

Figure
4.1-9a



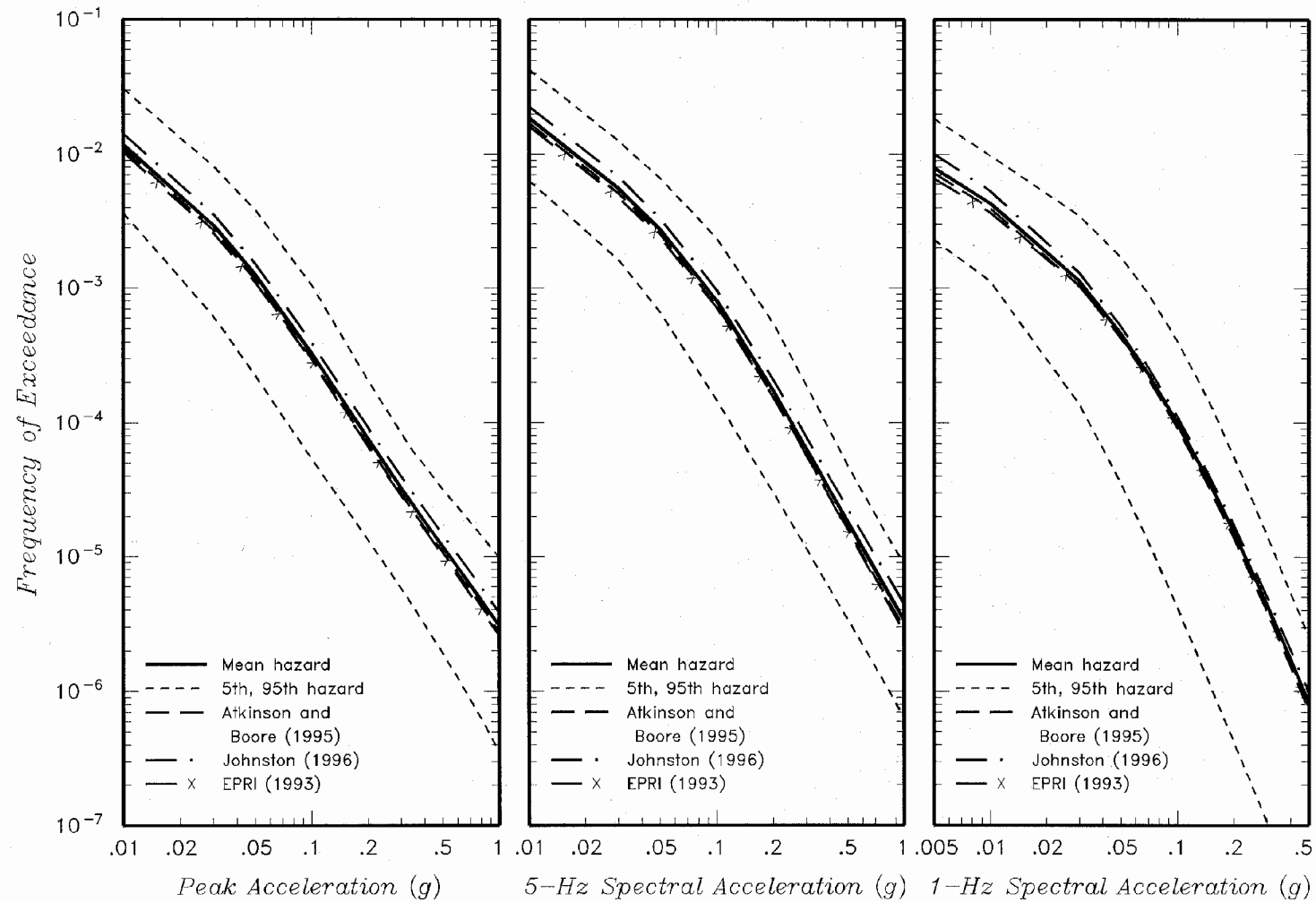
Seismic Hazards Report for the EGC ESP Site
 Contribution of Individual Sources to Mean Hazard

Figure
 4.1-9b



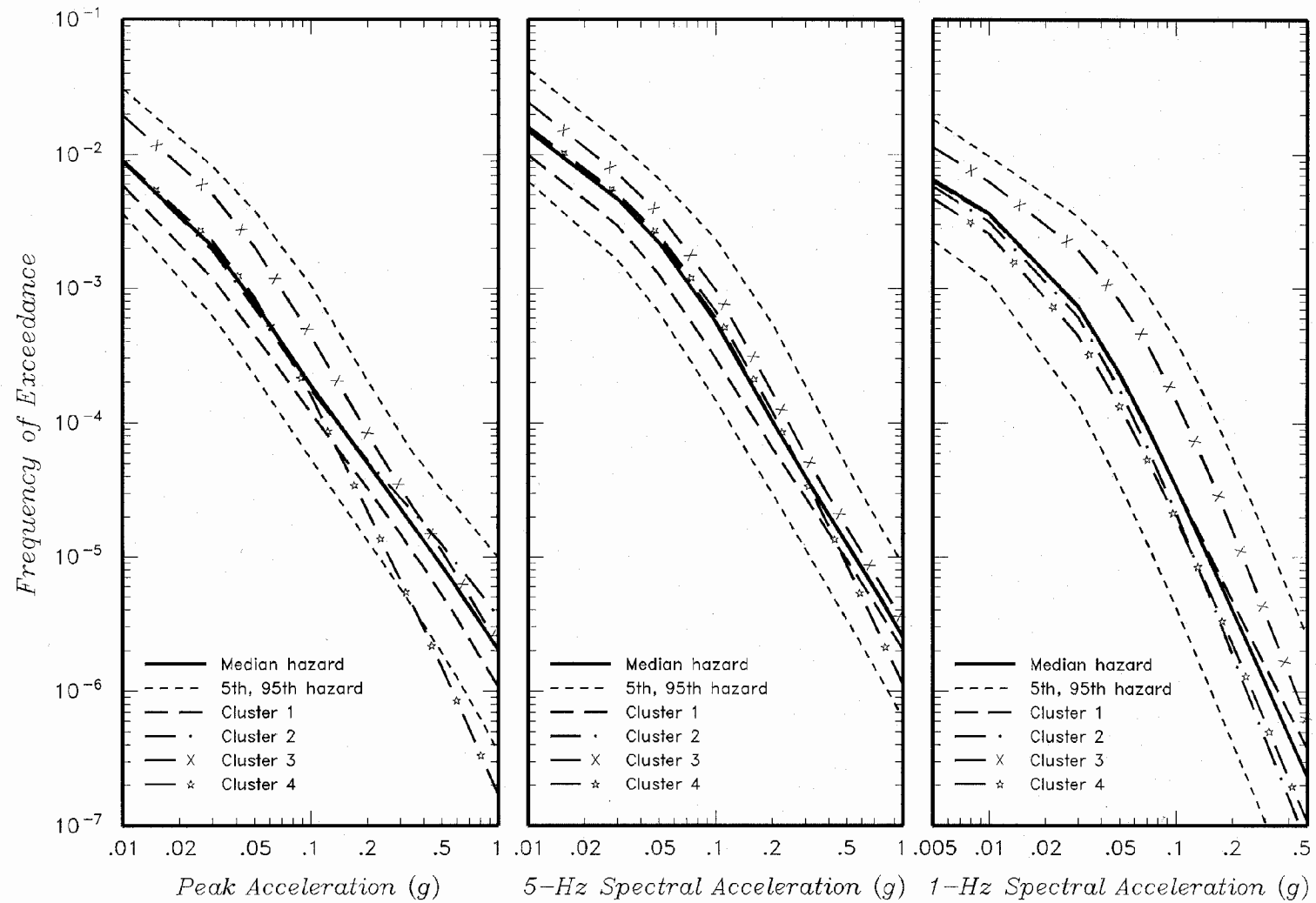
Seismic Hazards Report for the EGC ESP Site
 Effect of Alternative m_b -M Relationships on Median Hazard

Figure
 4.1-10a



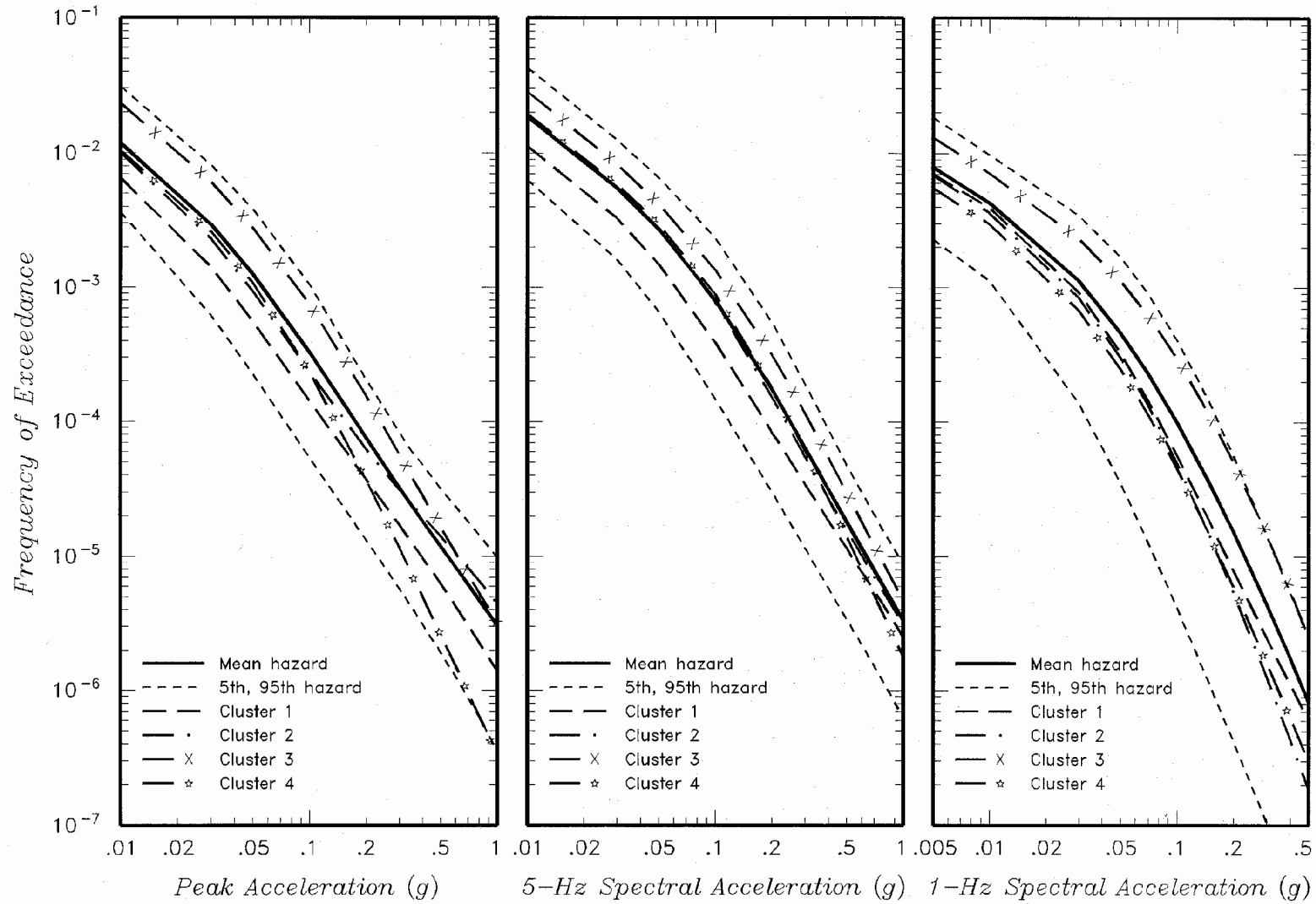
Seismic Hazards Report for the EGC ESP Site
Effect of Alternative m_b - M Relationships on Mean Hazard

Figure
4.1-10b



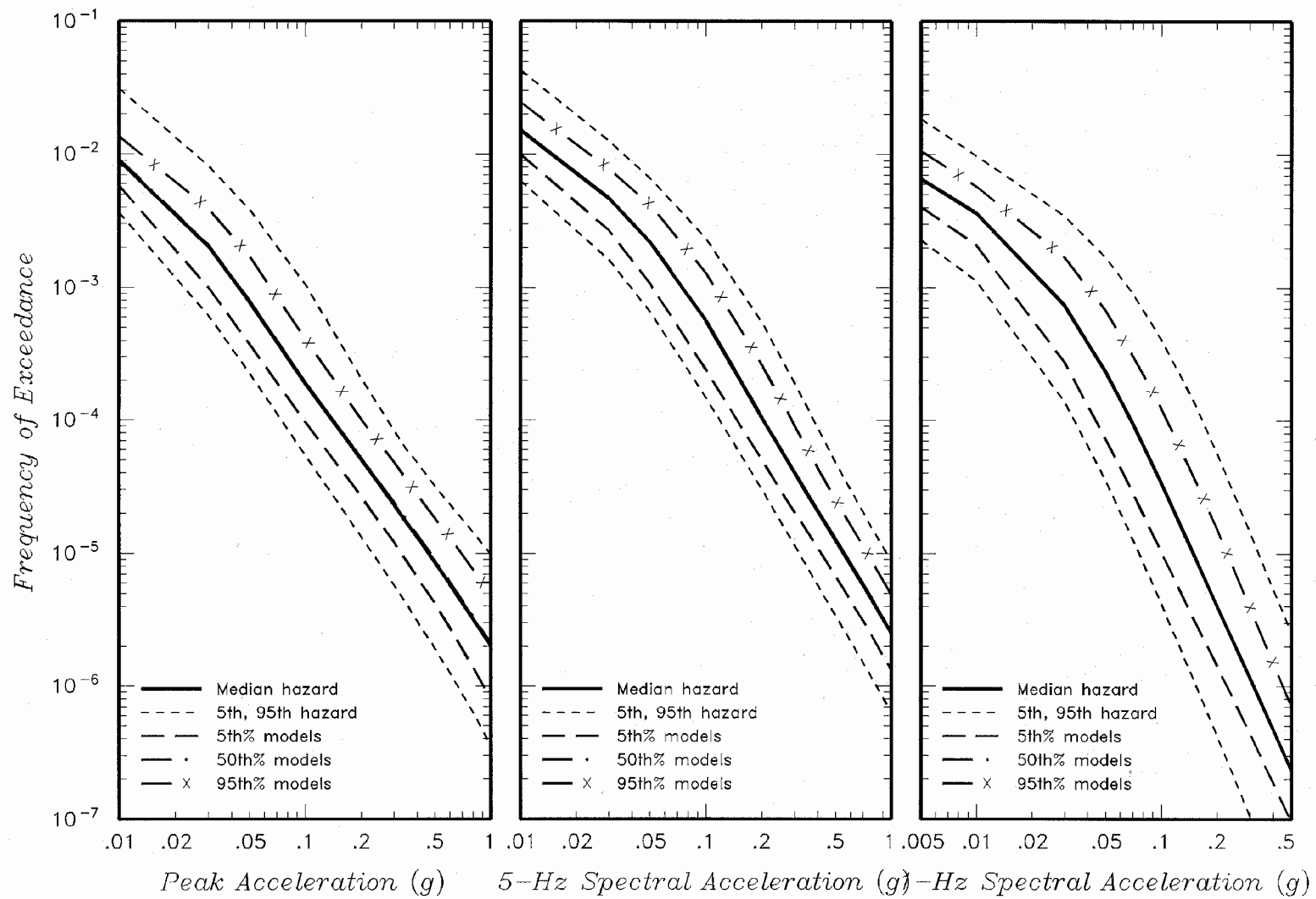
Seismic Hazards Report for the EGC ESP Site
Effect of Alternative Median Ground Motion Models on Median Hazard

Figure
4.1-11a



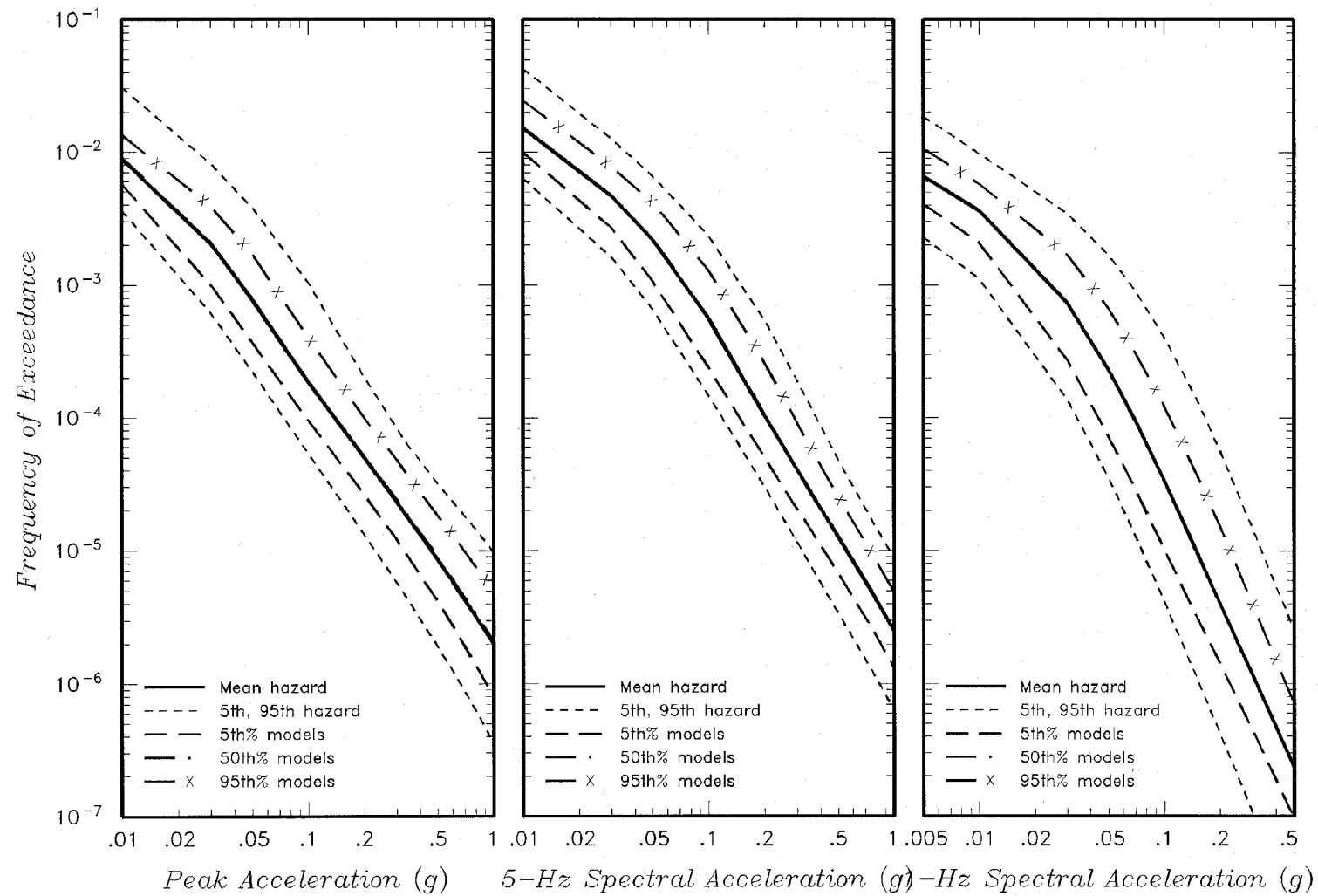
Seismic Hazards Report for the EGC ESP Site
Effect of Alternative Median Ground Motion Models on Mean Hazard

Figure
4.1-11b



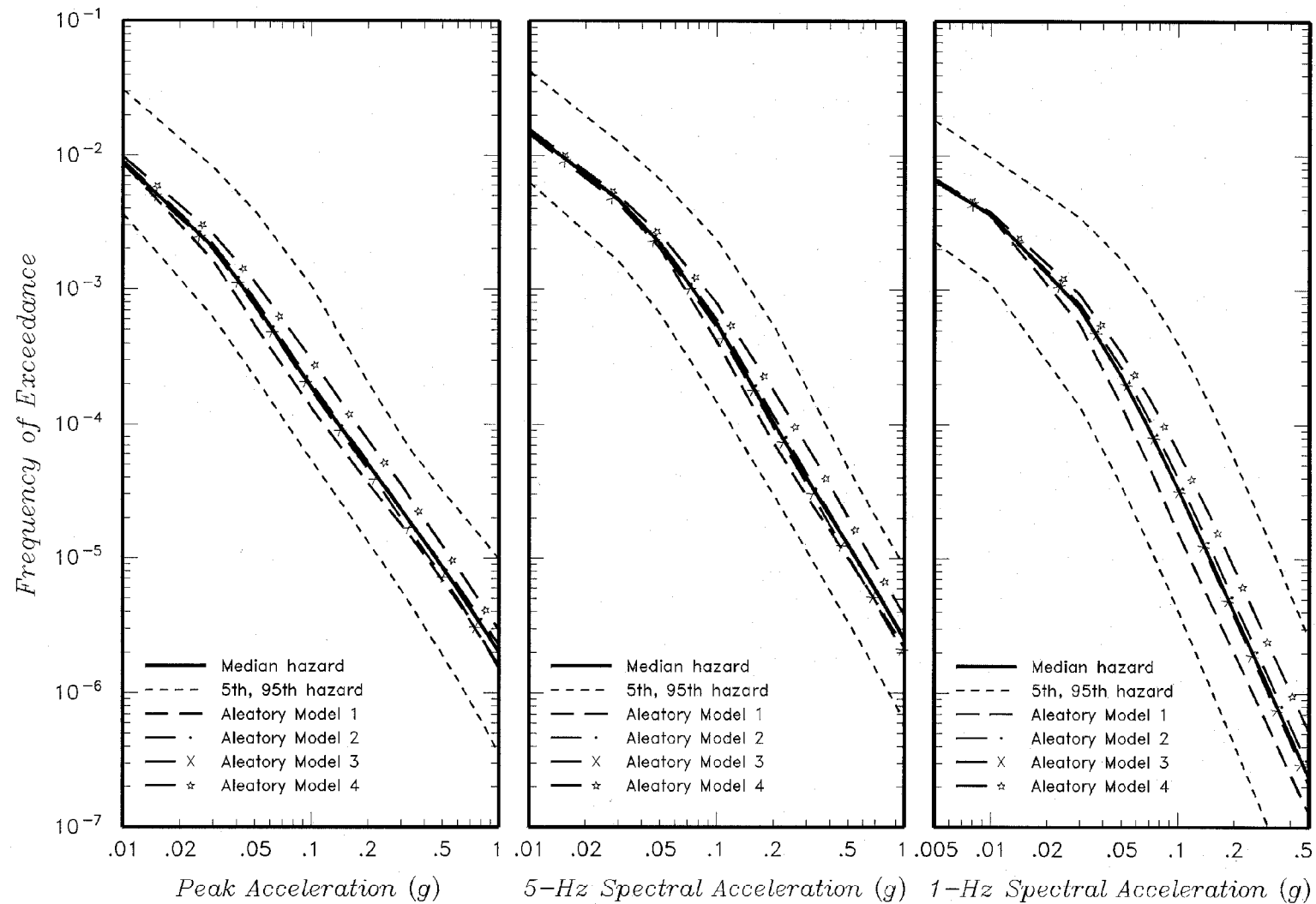
Seismic Hazards Report for the EGC ESP Site
 Effect of Epistemic Uncertainty in Median Ground Motion on Median Hazard

Figure
 4.1-12a



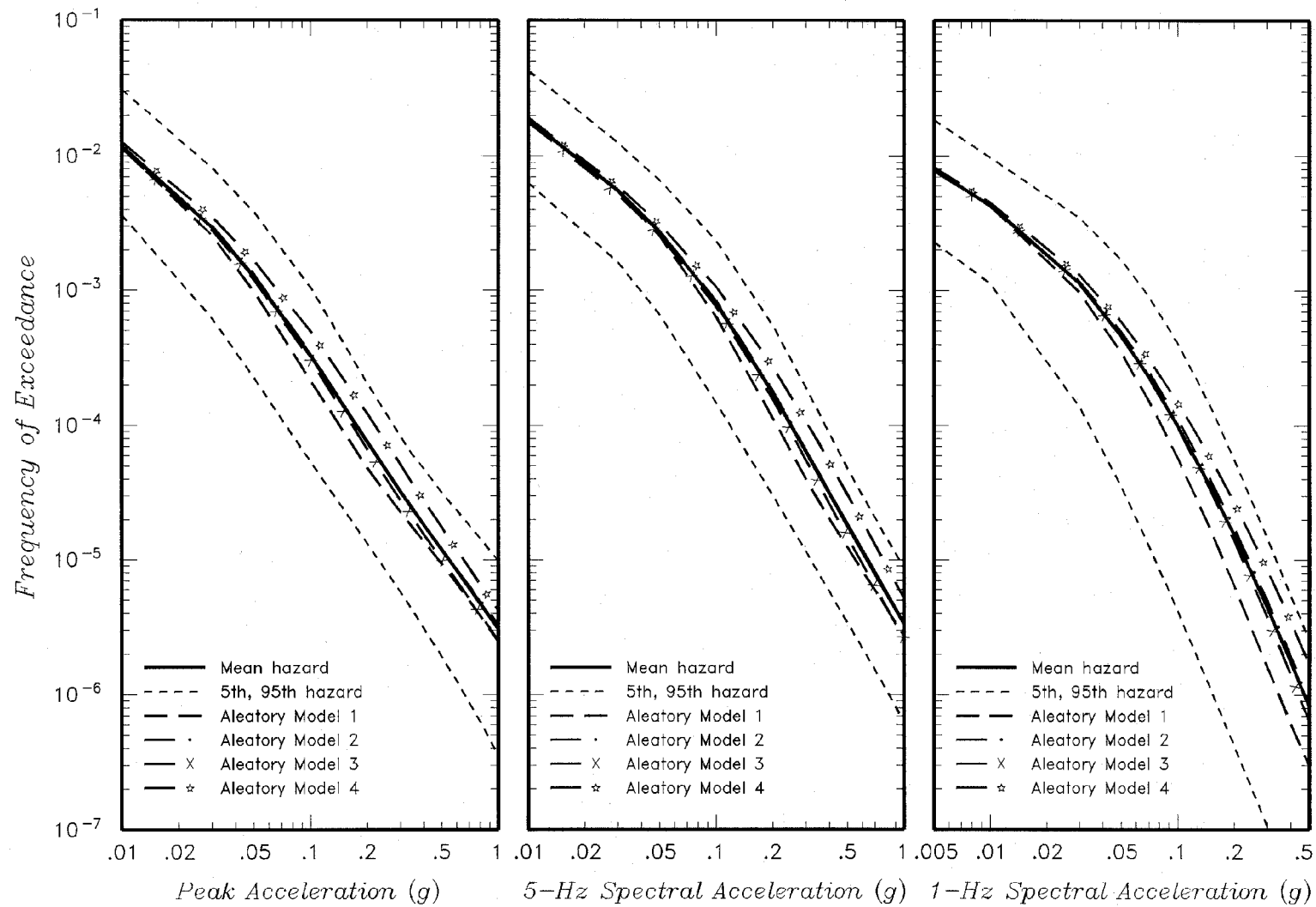
Seismic Hazards Report for the EGC ESP Site
Effect of Epistemic Uncertainty in Median Ground Motion on Mean Hazard

Figure
4.1-12b



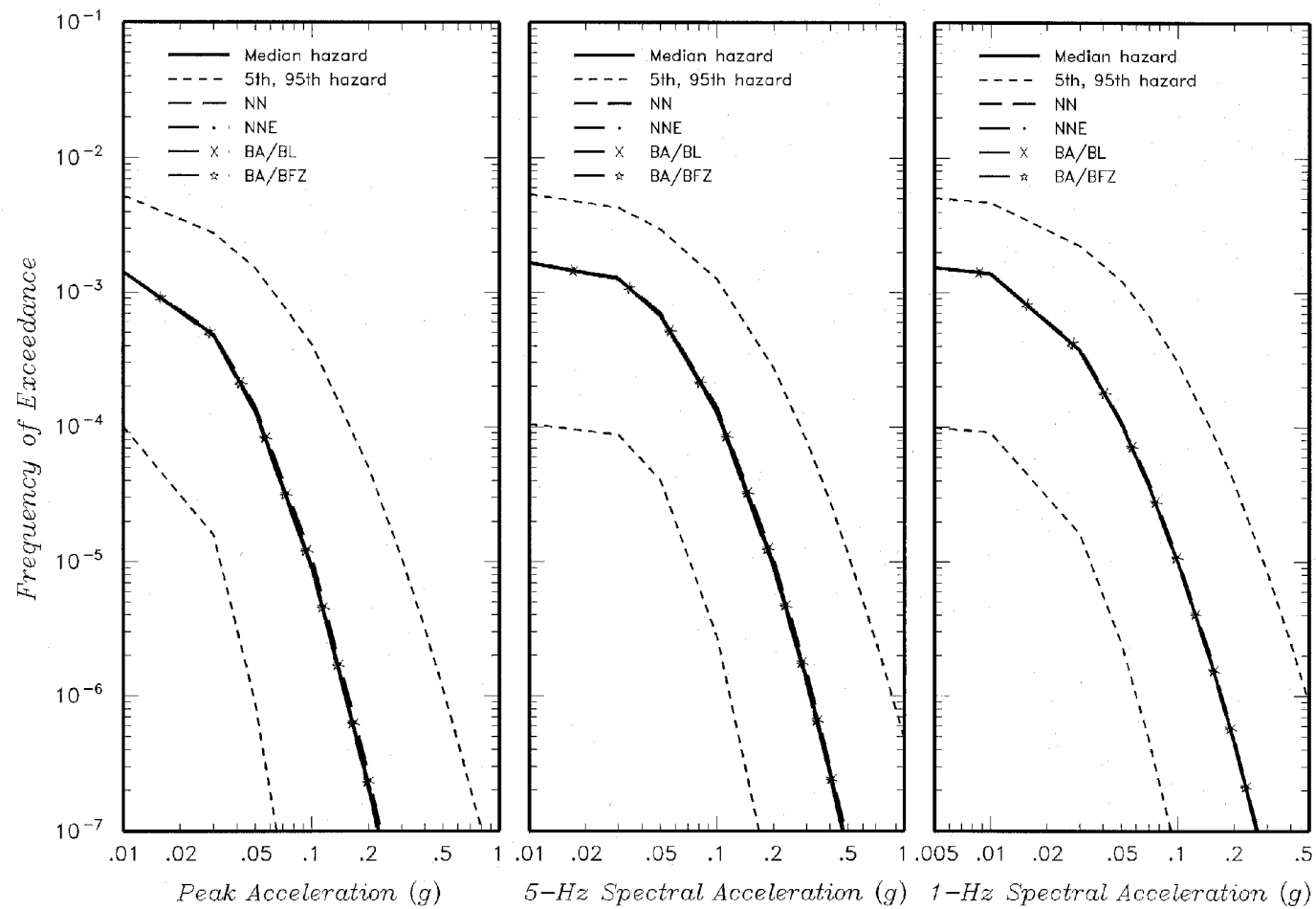
Seismic Hazards Report for the EGC ESP Site
Effect of Alternative Aleatory Variability Models on Median Hazard

Figure
4.1-13a



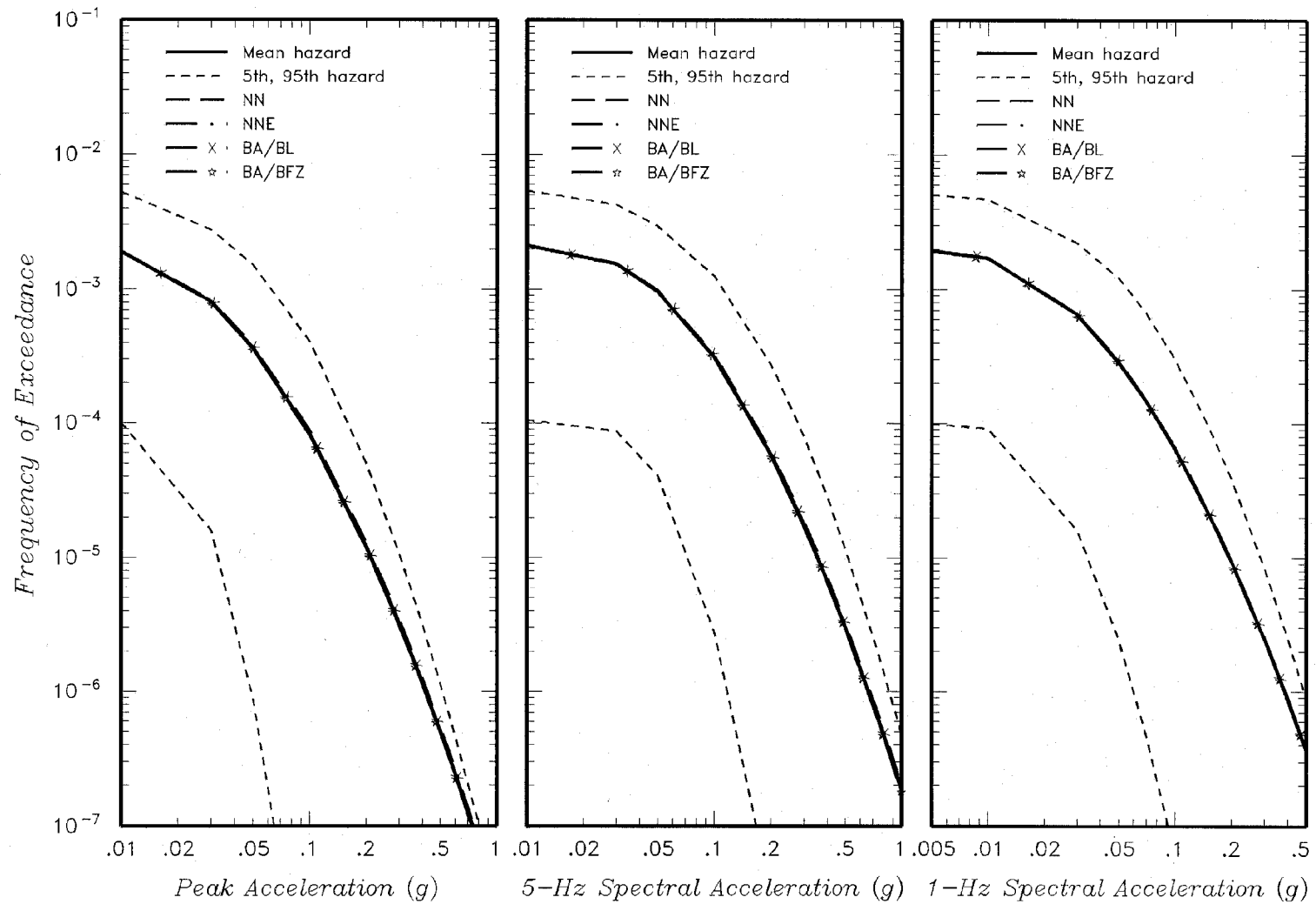
Seismic Hazards Report for the EGC ESP Site
Effect of Alternative Aleatory Variability Models on Mean Hazard

Figure
4.1-13b



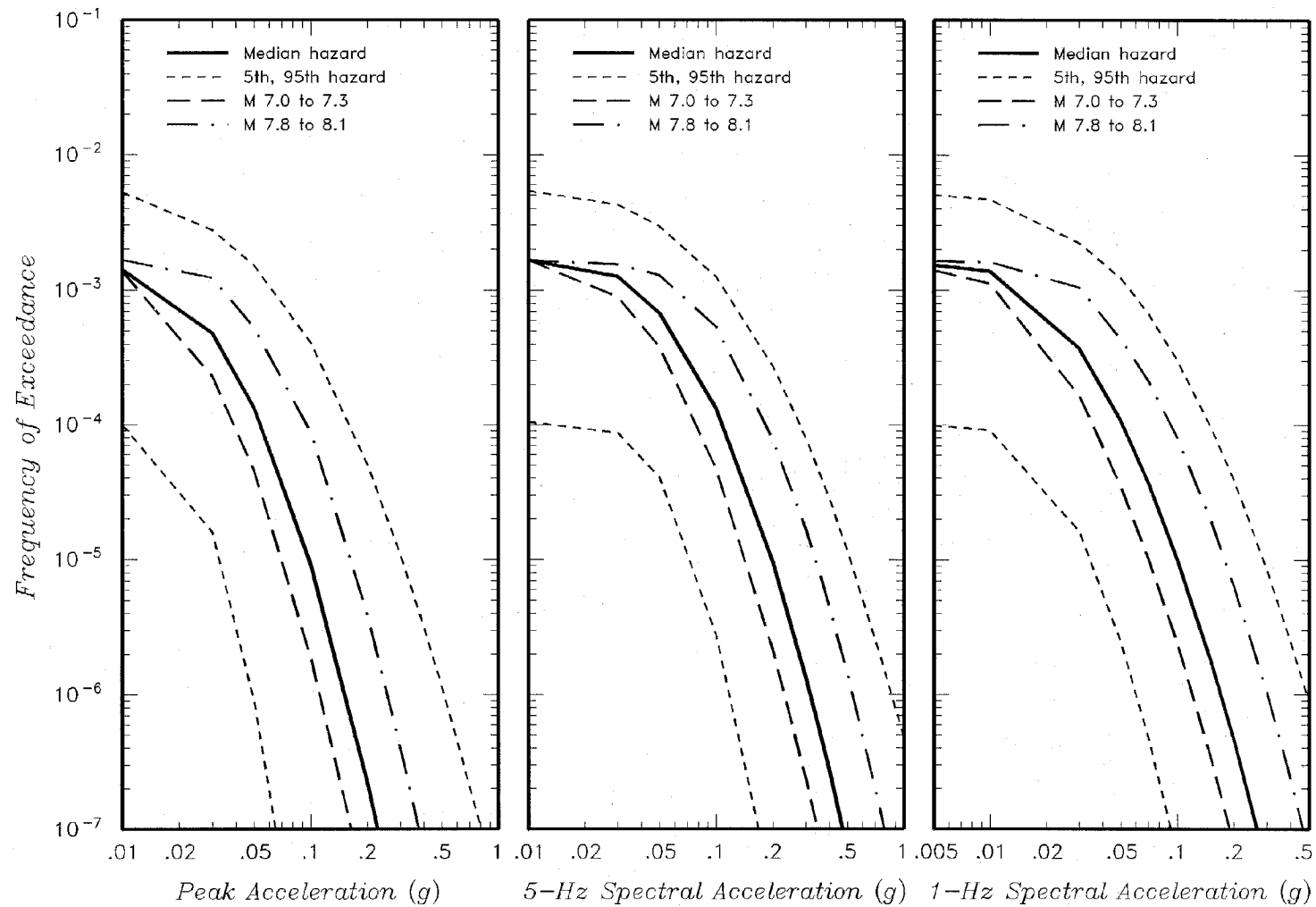
Seismic Hazards Report for the EGC ESP Site
Effect of Alternative End Points of New Madrid North on Median Hazard from
Only New Madrid Characteristic Earthquakes

Figure
4.1-14a



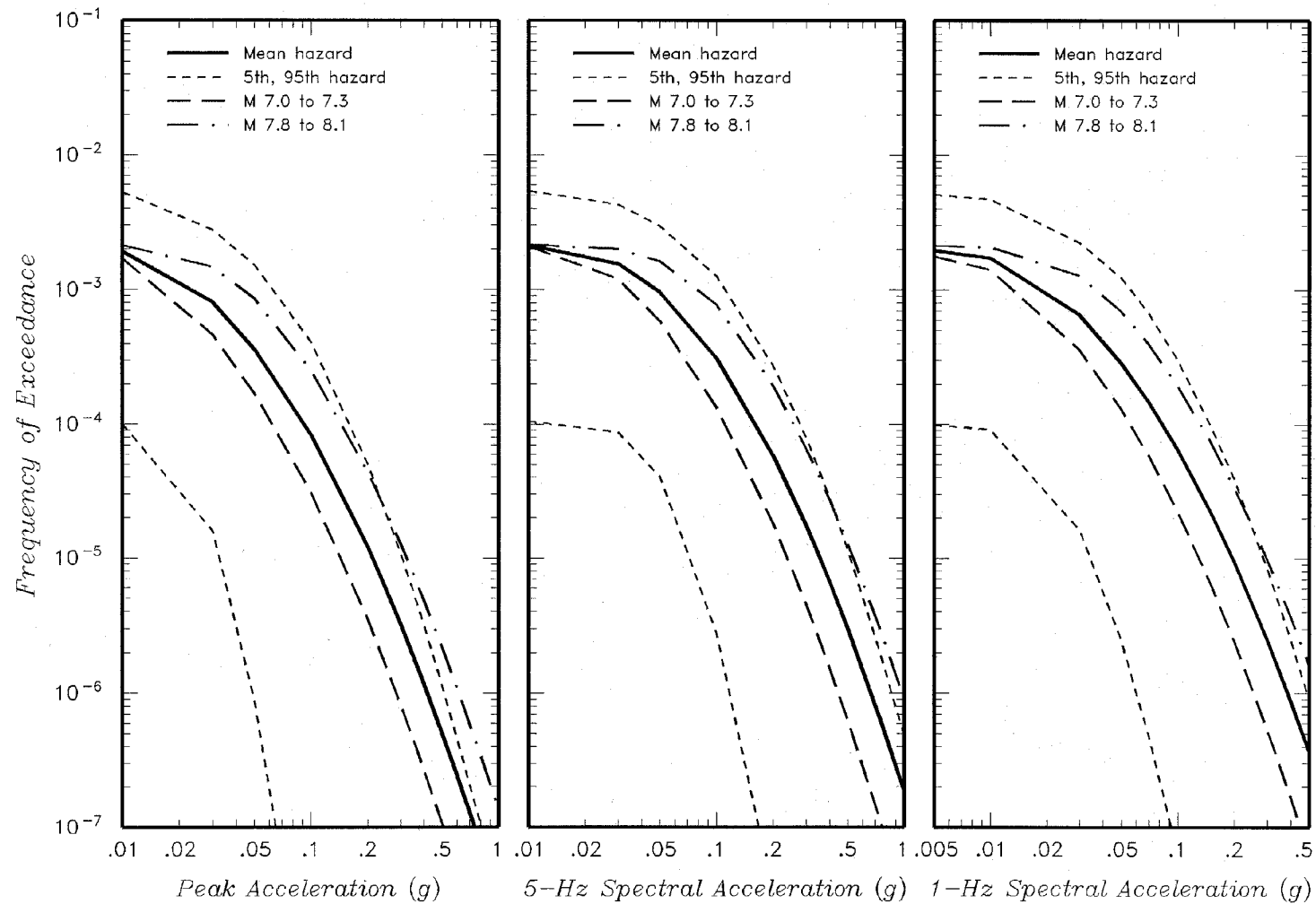
Seismic Hazards Report for the EGC ESP Site
 Effect of Alternative End Points of New Madrid North on Mean Hazard from
 Only New Madrid Characteristic Earthquakes

Figure
 4.1-14b



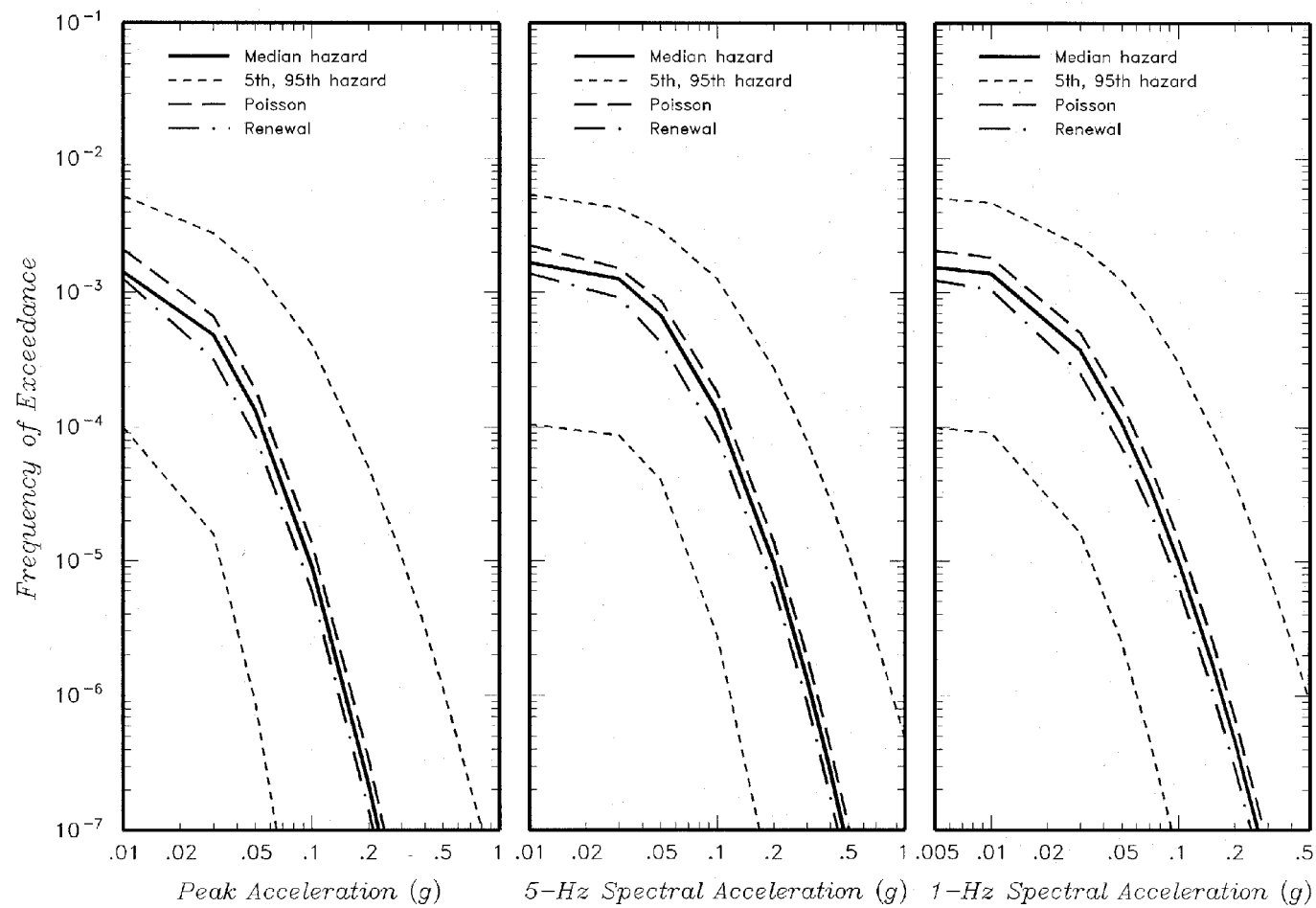
Seismic Hazards Report for the EGC ESP Site
**Effect of Alternative Geometries for New Madrid South on Median Hazard from
 Only New Madrid Characteristic Earthquakes**

Figure
4.1-15a



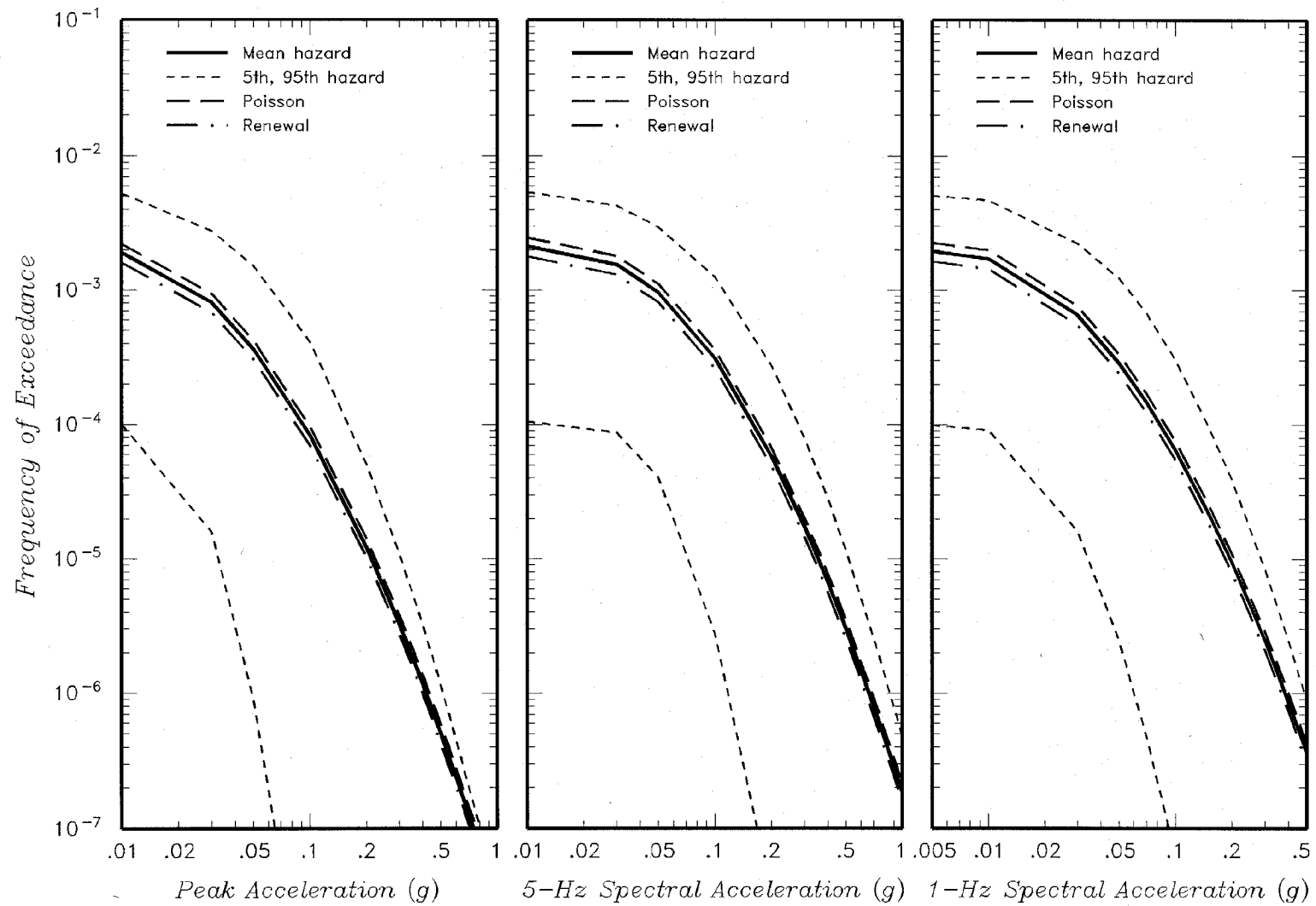
Seismic Hazards Report for the EGC ESP Site
 Effect of Alternative Geometries for New Madrid South on Mean Hazard from
 Only New Madrid Characteristic Earthquakes

Figure
 4.1-15b



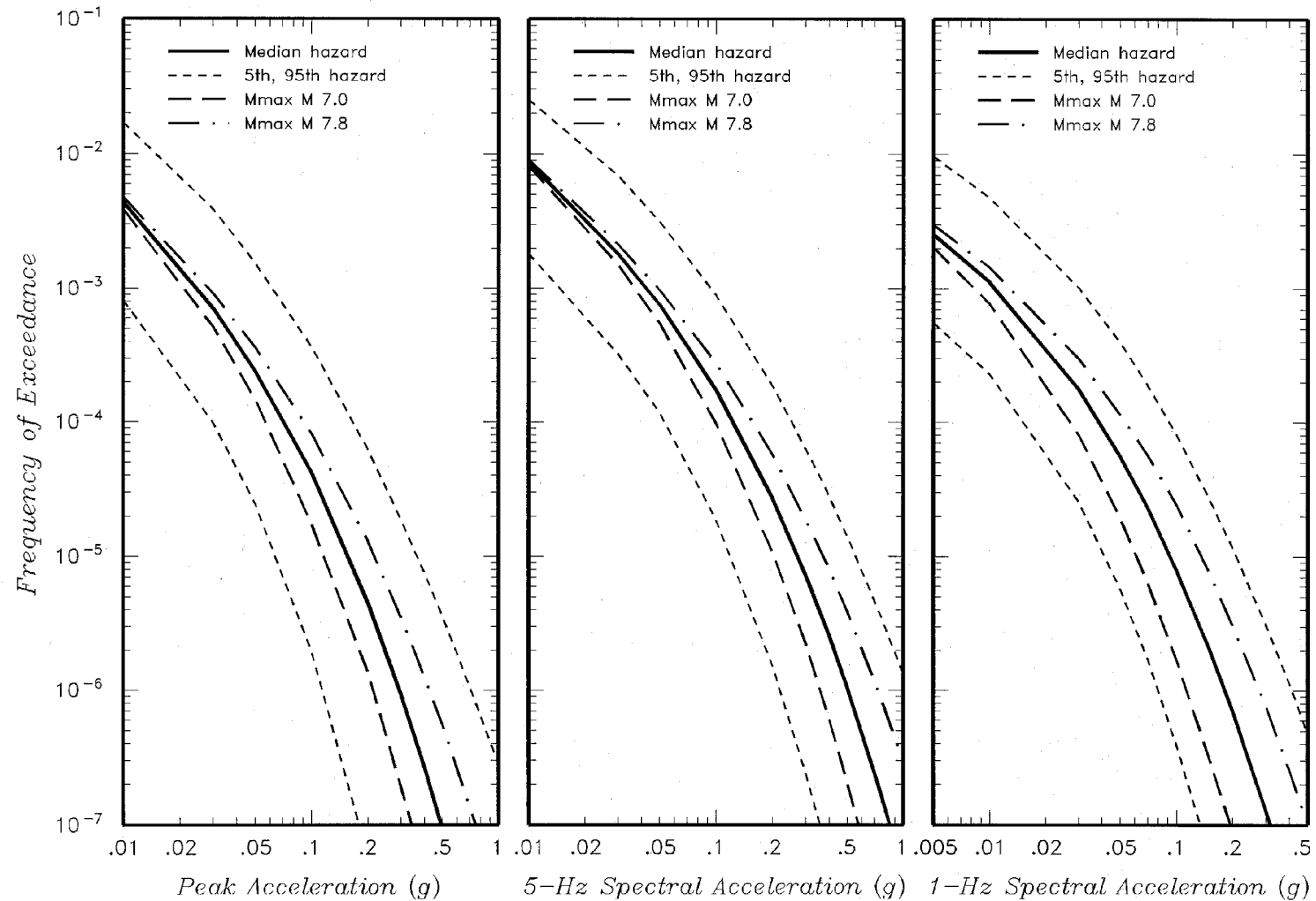
Seismic Hazards Report for the EGC ESP Site
Effect of Alternative Recurrence Models for New Madrid Characteristic Earthquakes on Median Hazard from Only New Madrid Characteristic Earthquakes

Figure
4.1-16a



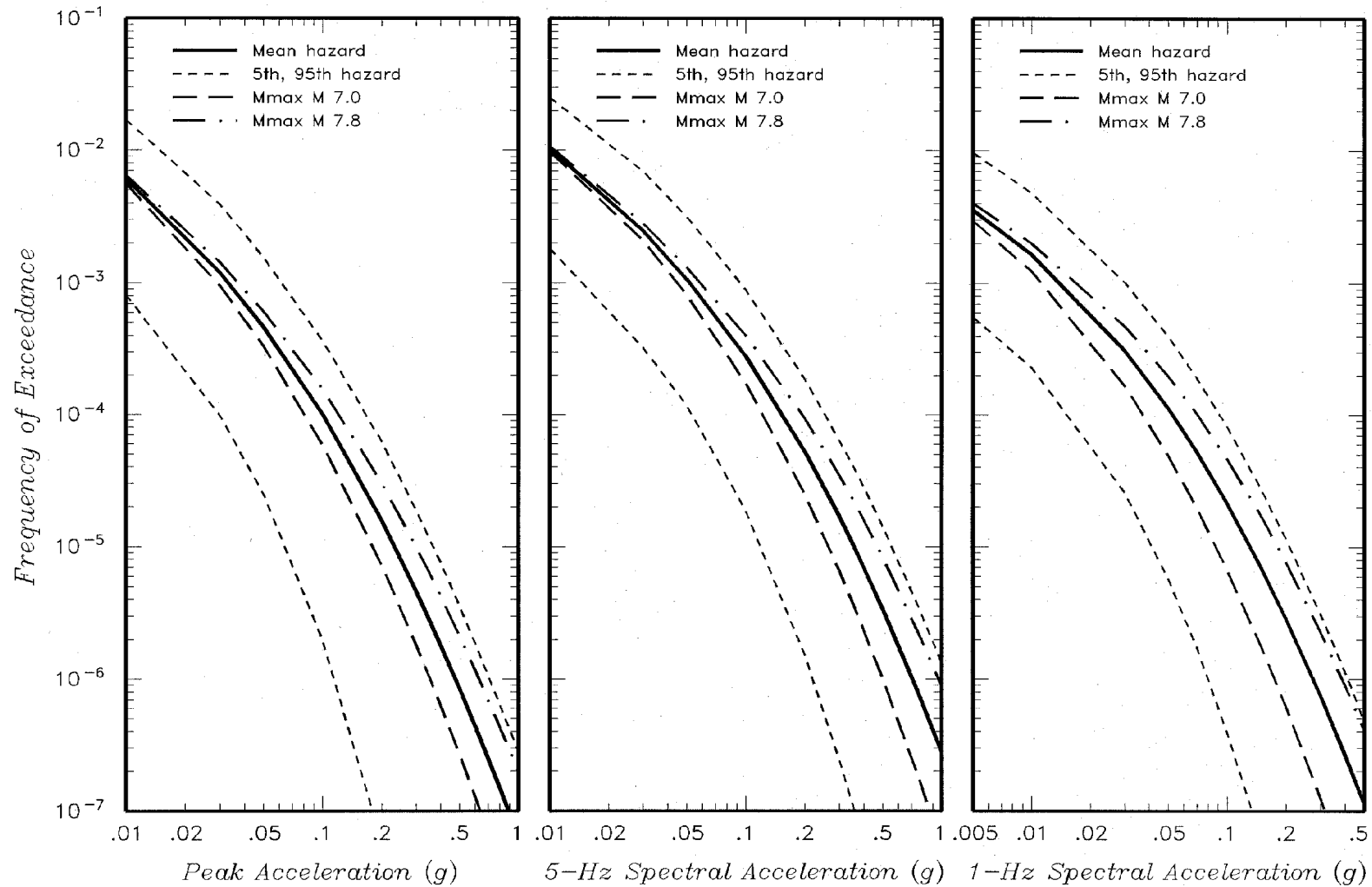
Seismic Hazards Report for the EGC ESP Site
Effect of Alternative Recurrence Models for New Madrid Characteristic Earthquakes on Mean Hazard from Only New Madrid Characteristic Earthquakes

Figure
4.1-16b



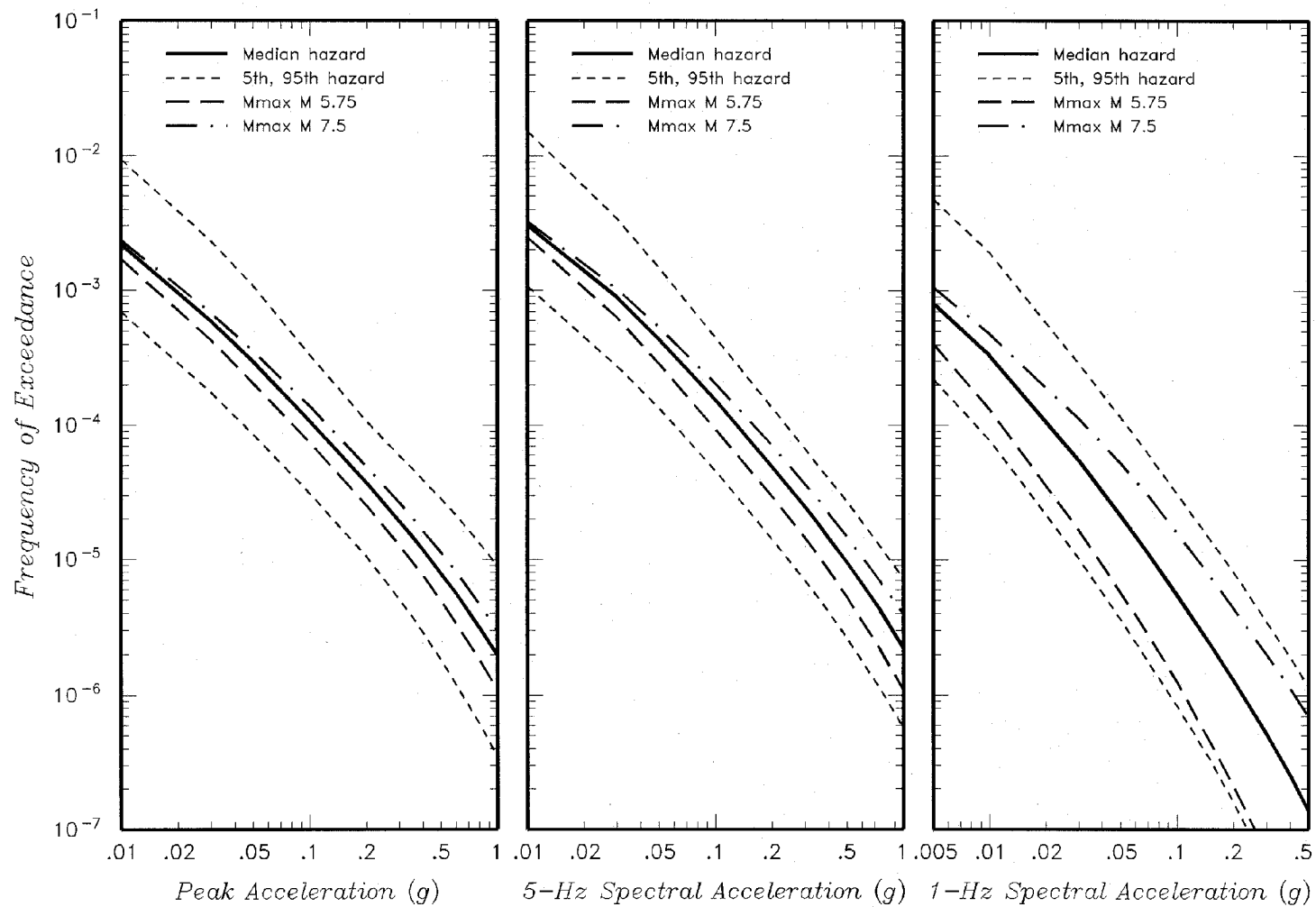
Seismic Hazards Report for the EGC ESP Site
Effect of Alternative Maximum Magnitude Estimates on Median Hazard from Only Wabash Valley-Southern Illinois Sources

Figure
4.1-17a



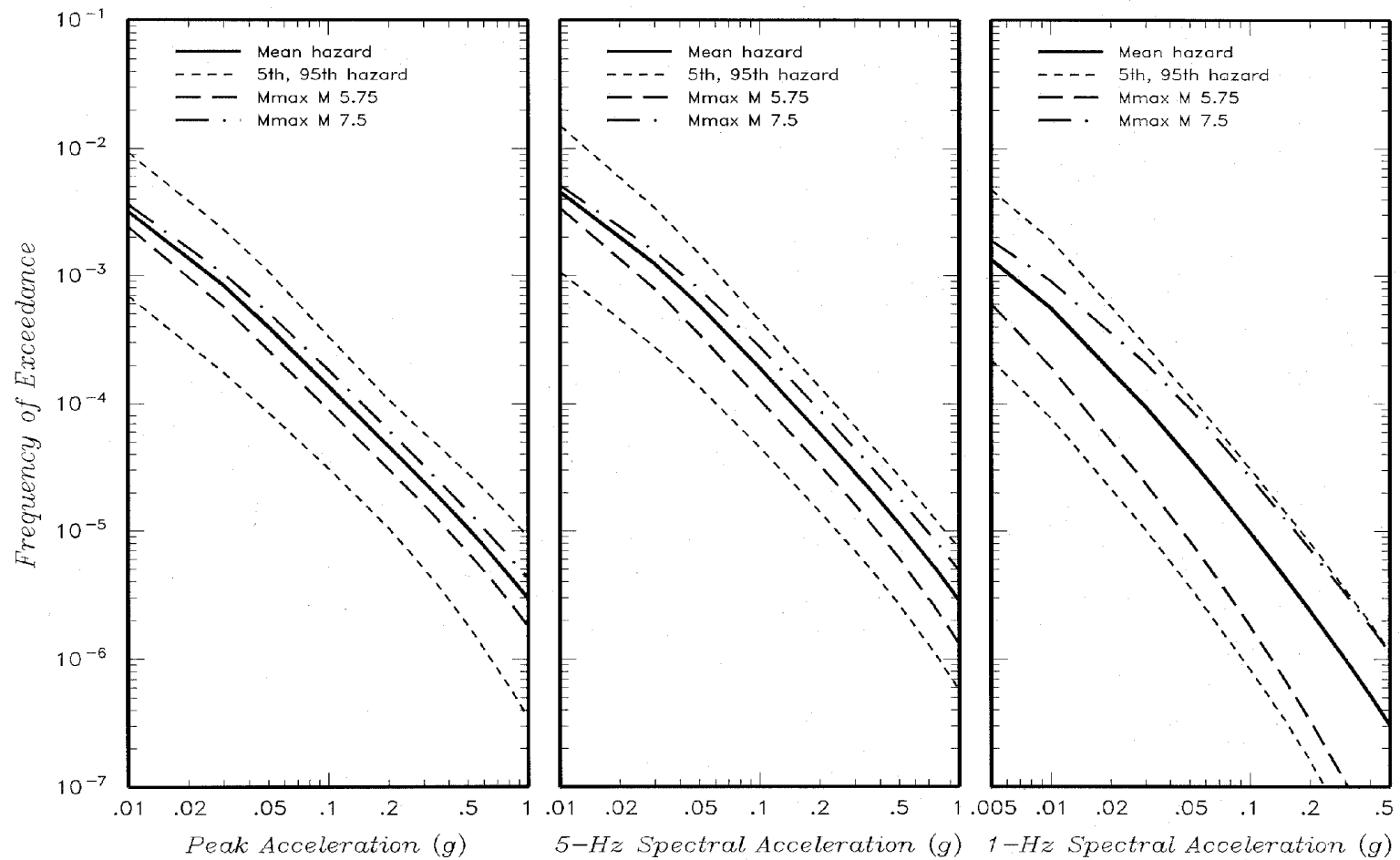
Seismic Hazards Report for the EGC ESP Site
Effect of Alternative Maximum Magnitude Estimates on Mean Hazard from Only Wabash Valley-Southern Illinois Sources

Figure
4.1-17b



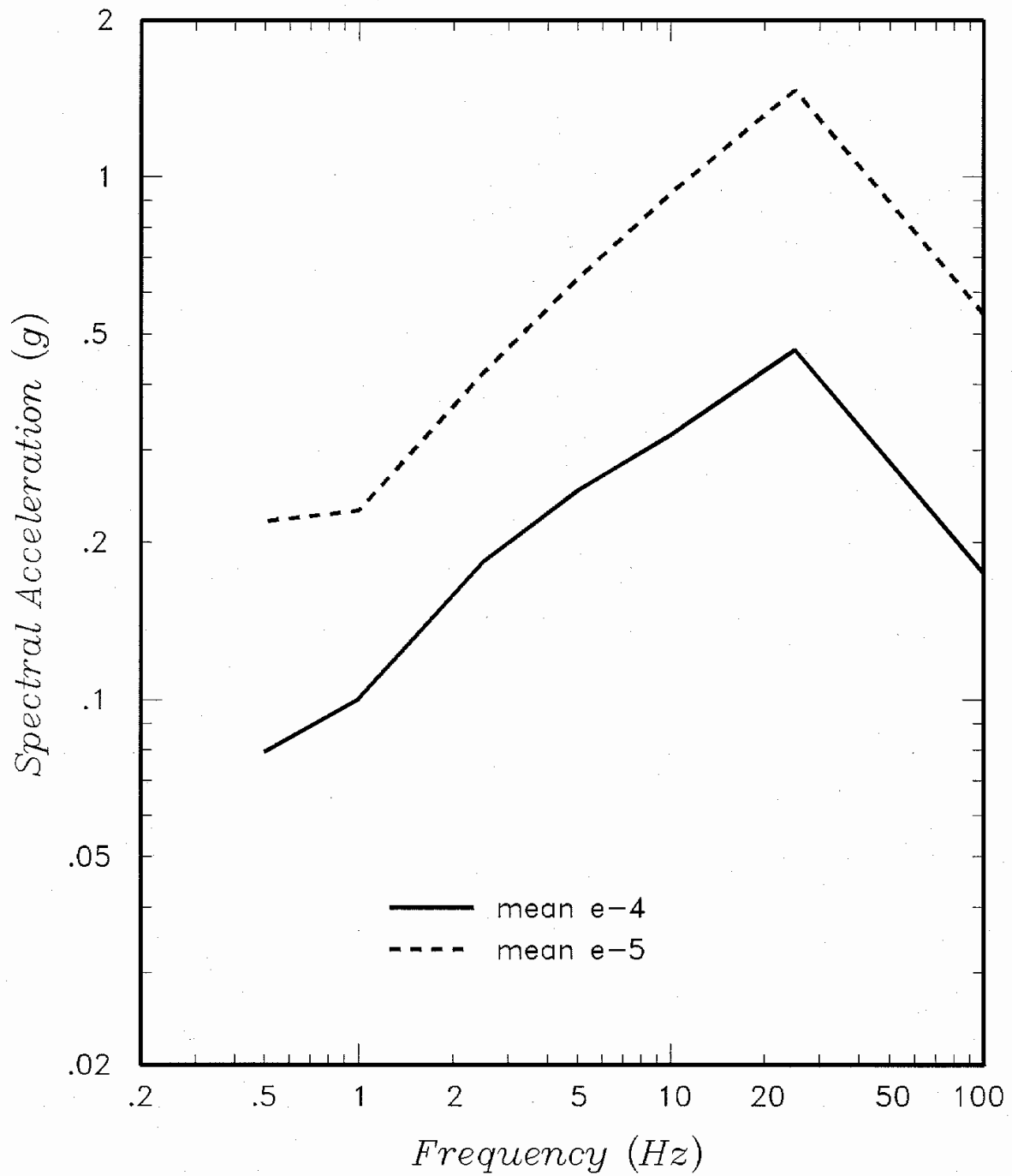
Seismic Hazards Report for the EGC ESP Site
Effect of Alternative Maximum Magnitude Estimates on Median Hazard from Only Central Illinois Sources

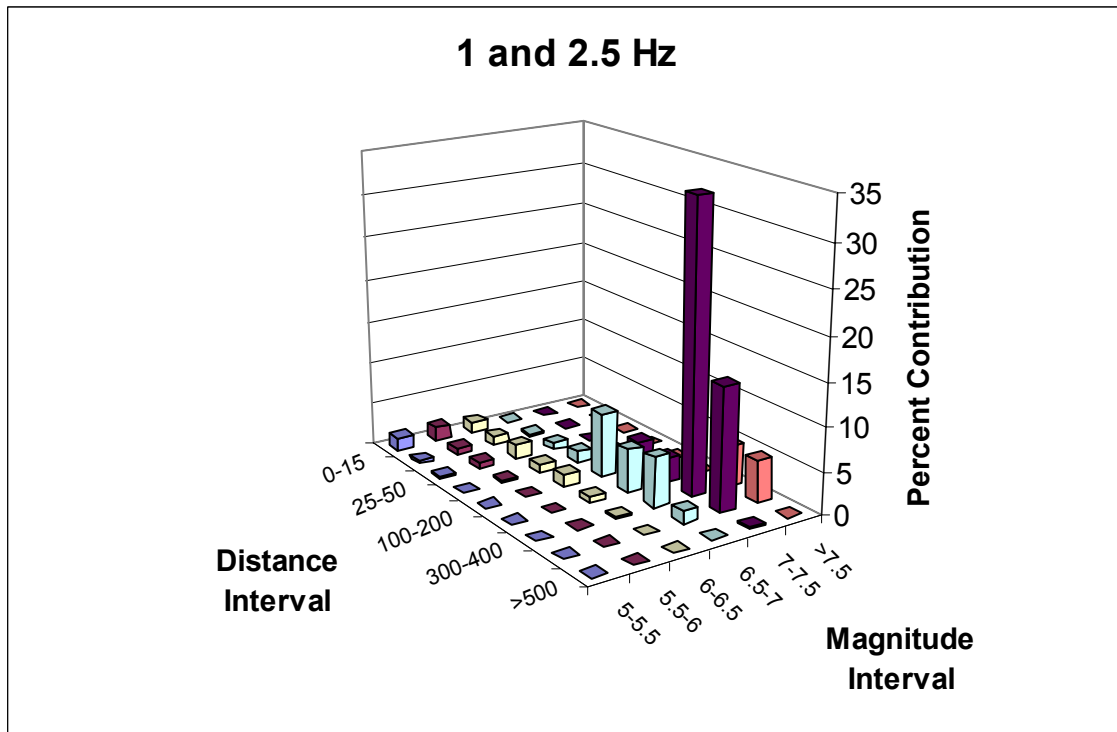
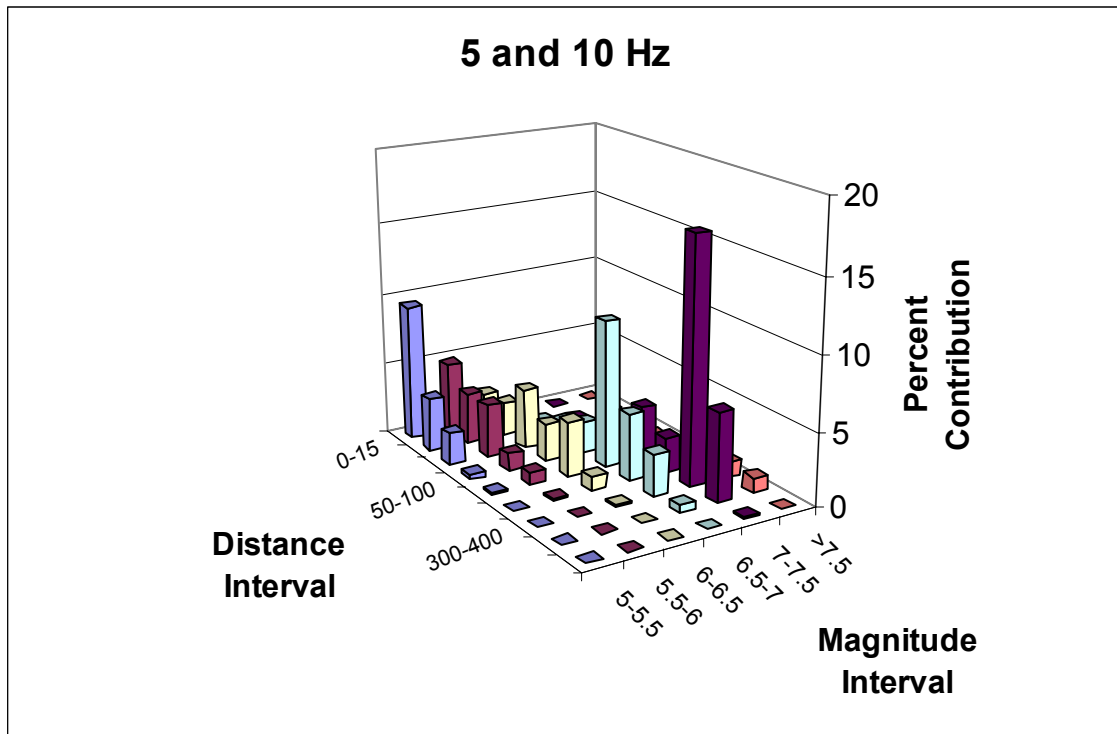
Figure
4.1-18a

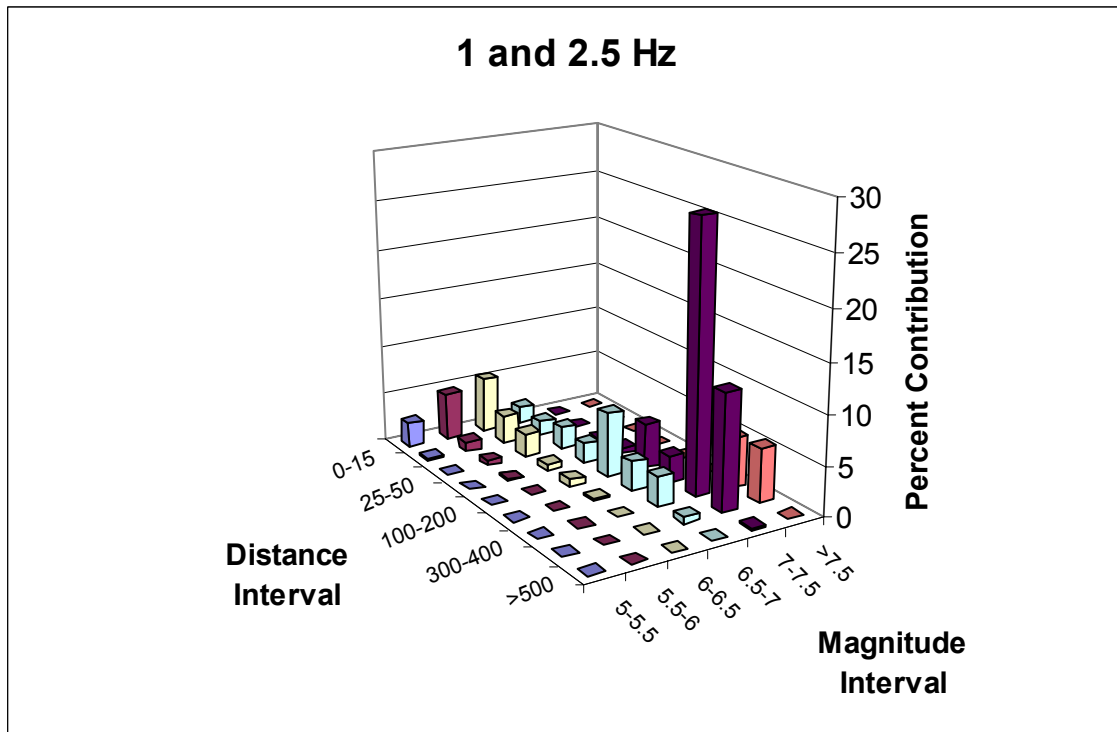
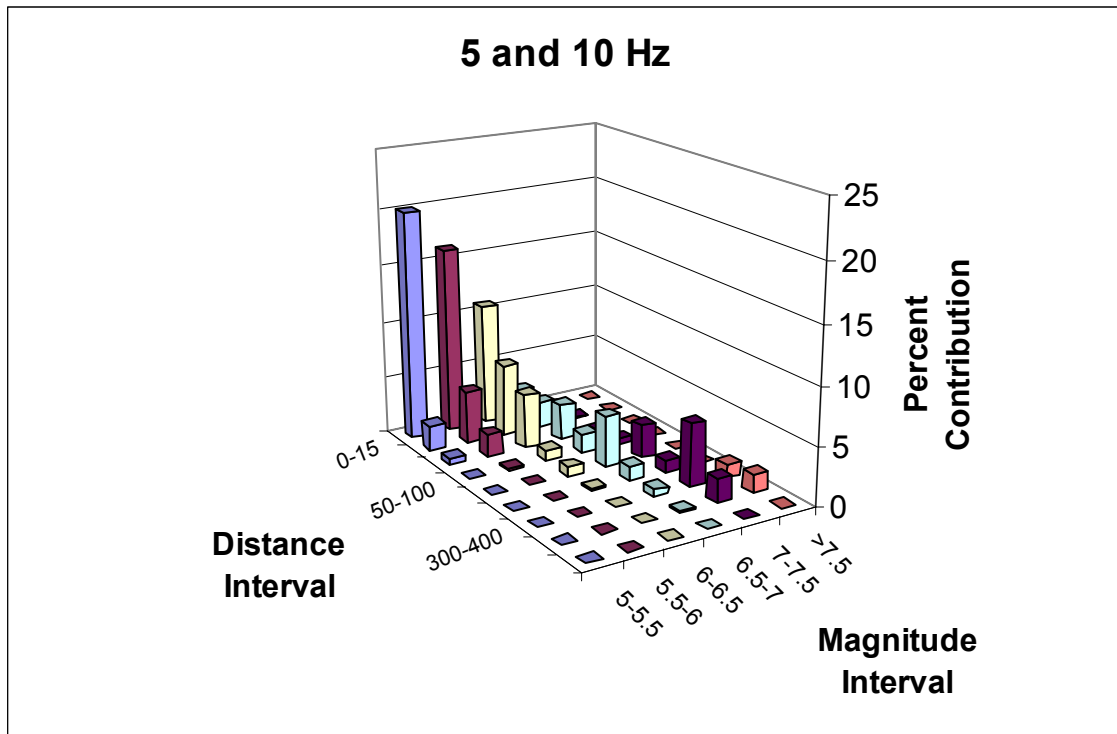


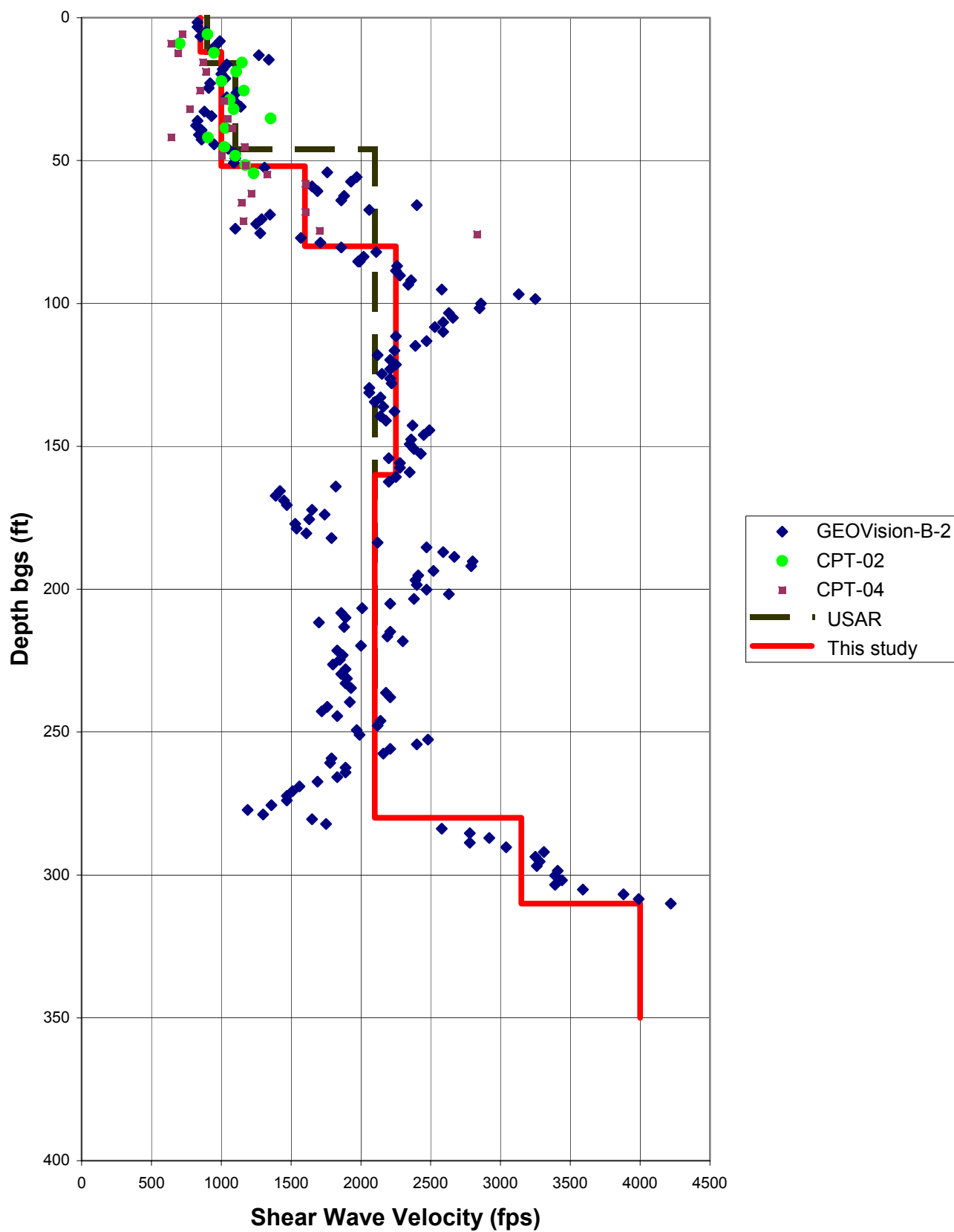
Seismic Hazards Report for the EGC ESP Site
 Effect of Alternative Maximum Magnitude Estimates on Mean Hazard from Only Central Illinois Sources

Figure
 4.1-18b





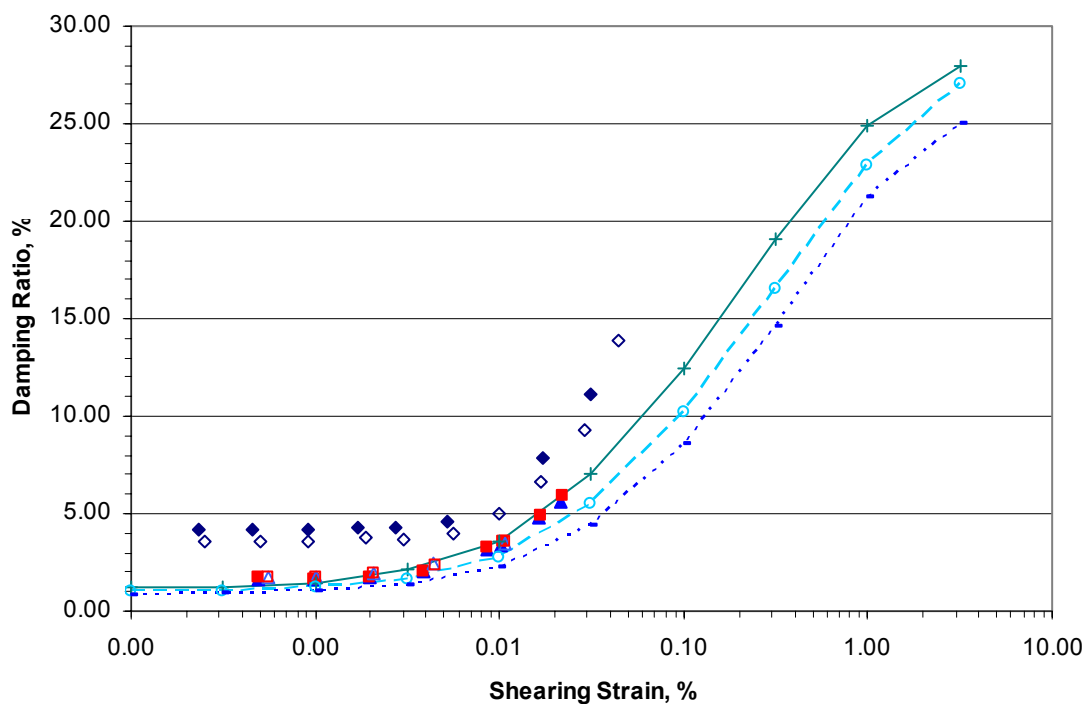
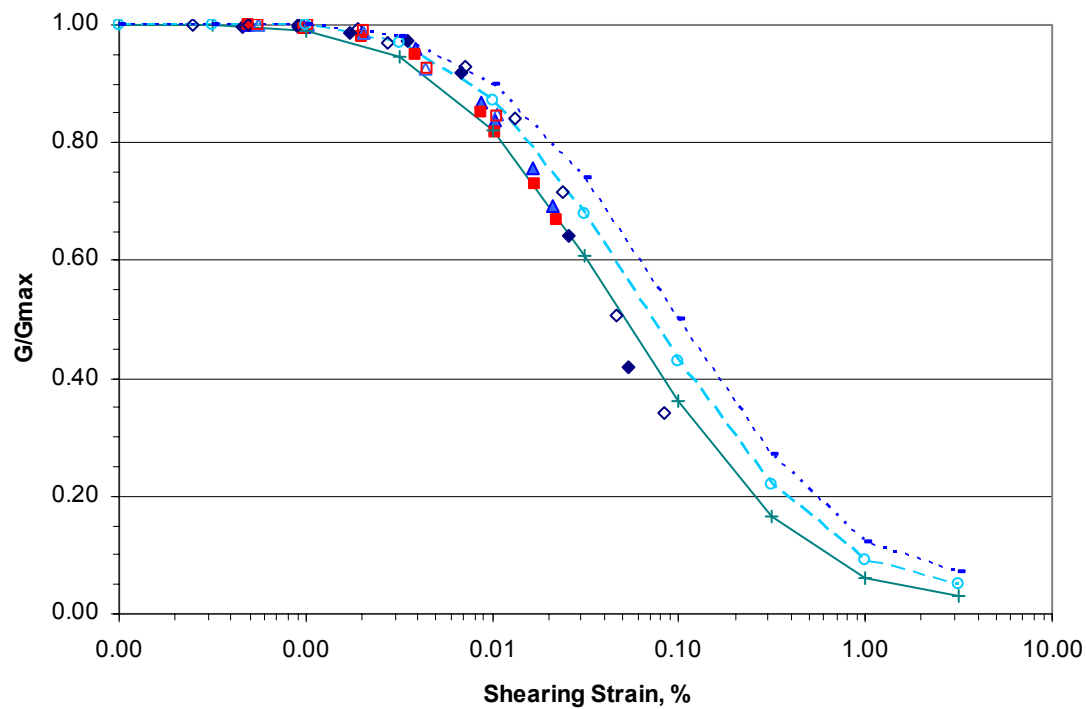




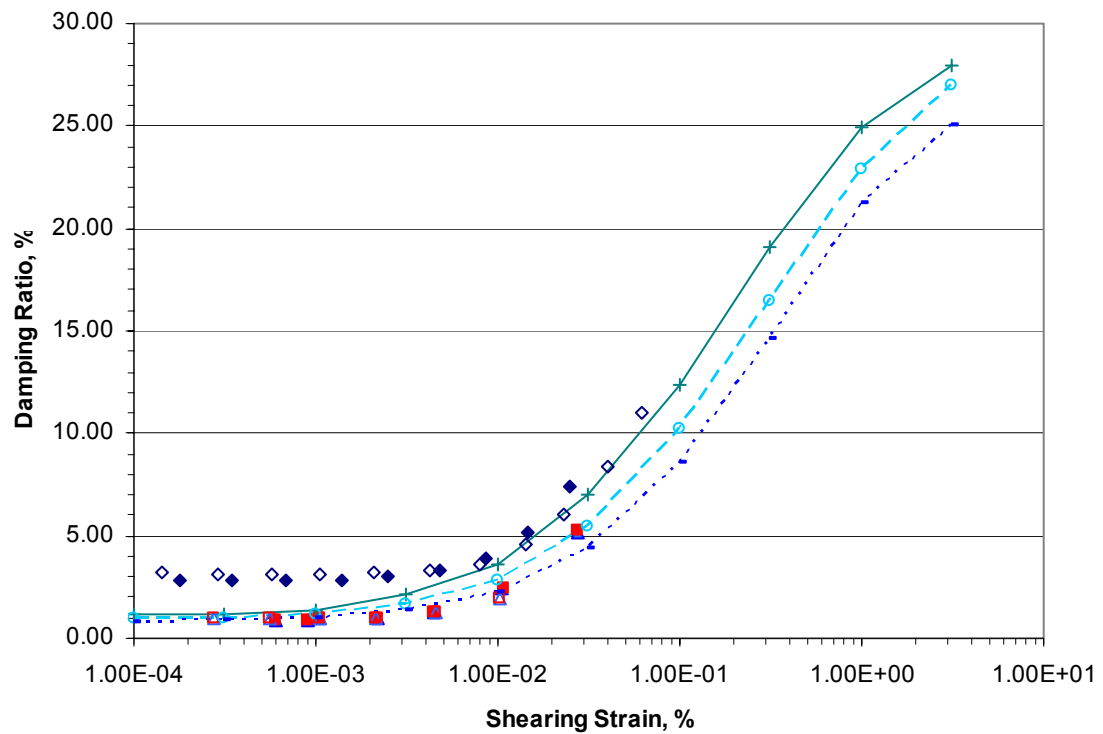
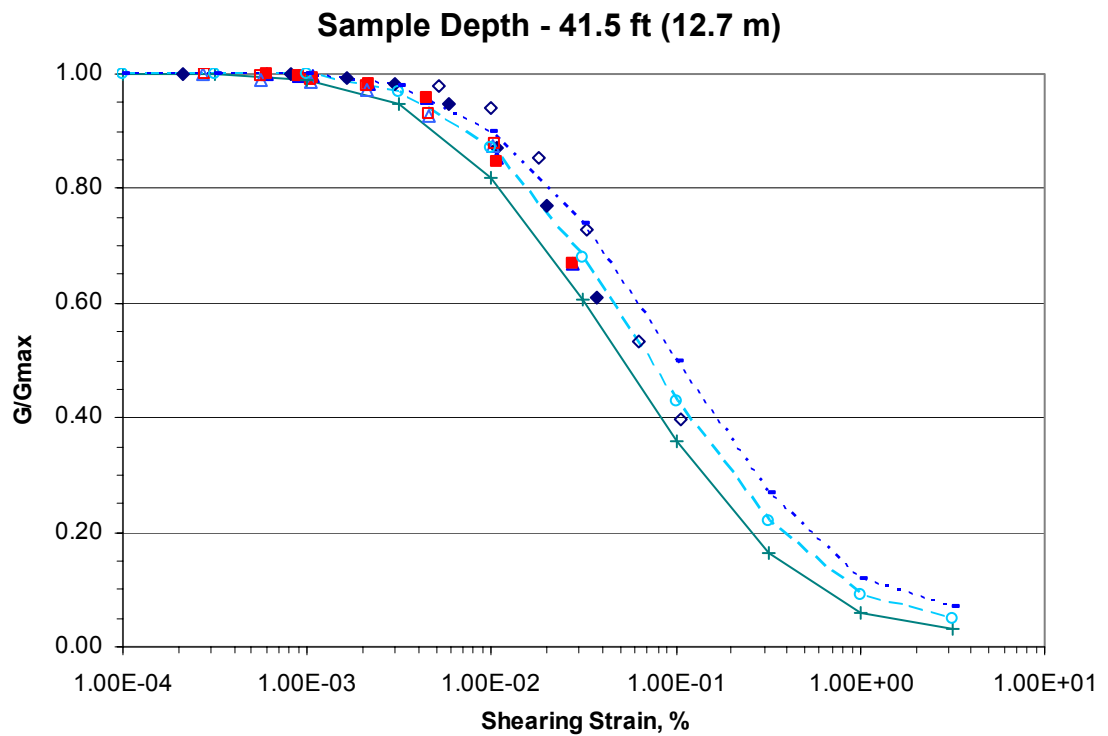
Seismic Hazards Report for the EGC ESP Site
Shear Wave Velocity Data Median Profile for Soils

Figure
4.2-1

Sample Depth - 33 ft (10.1 m)



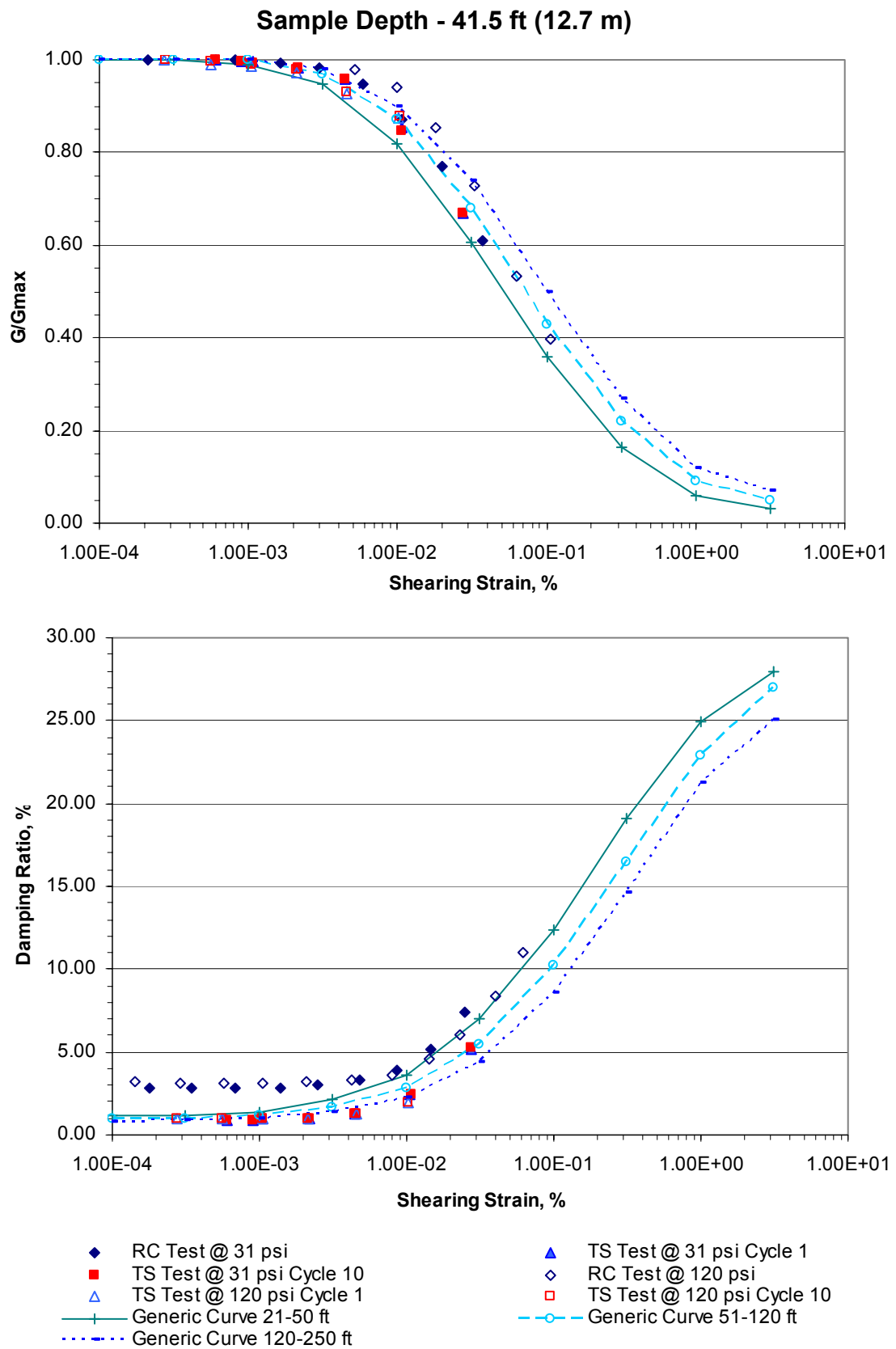
- ◆ RC Test @ 27 psi
- TS Test @ 27 psi Cycle 10
- △ TS Test @ 108 psi Cycle 1
- +— Generic Curve 21-50 ft
- Generic Curve 120-250 ft
- ▲ TS Test @ 27 psi Cycle 1
- ◇ RC Test @ 108 psi
- TS Test @ 108 psi Cycle 10
- Generic Curve 51-120 ft



- | | |
|--------------------------------|------------------------------|
| ◆ RC Test @ 31 psi | ▲ TS Test @ 31 psi Cycle 1 |
| ■ TS Test @ 31 psi Cycle 10 | ◇ RC Test @ 120 psi |
| △ TS Test @ 120 psi Cycle 1 | □ TS Test @ 120 psi Cycle 10 |
| —+— Generic Curve 21-50 ft | —○— Generic Curve 51-120 ft |
| ····· Generic Curve 120-250 ft | |

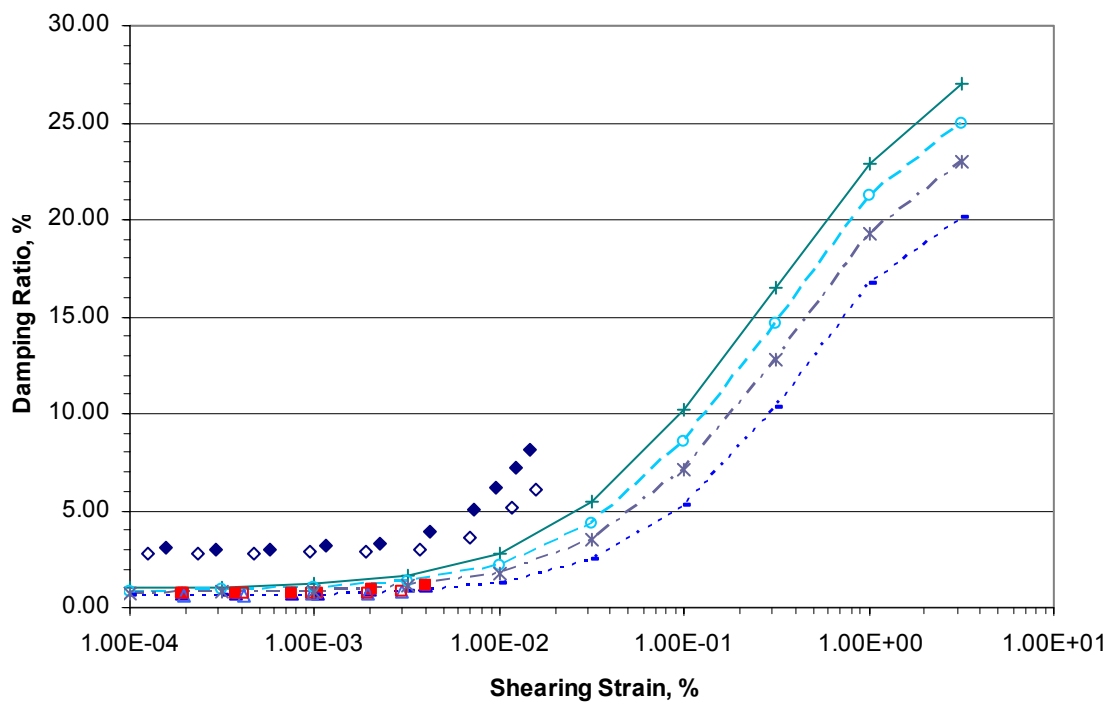
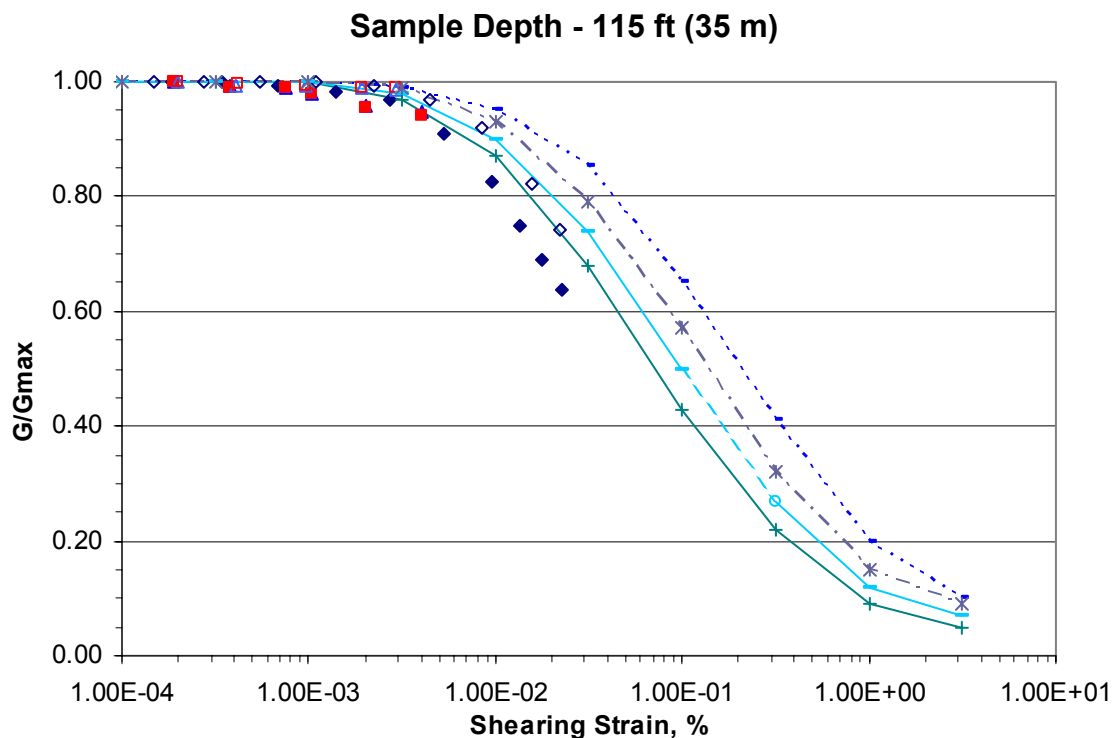
Seismic Hazards Report for the EGC ESP Site
Modulus Reduction and Damping Test Results Compared to EPRI (1993) Soil
Property Curves for Test UTA-34-B

Figure
4.2-3

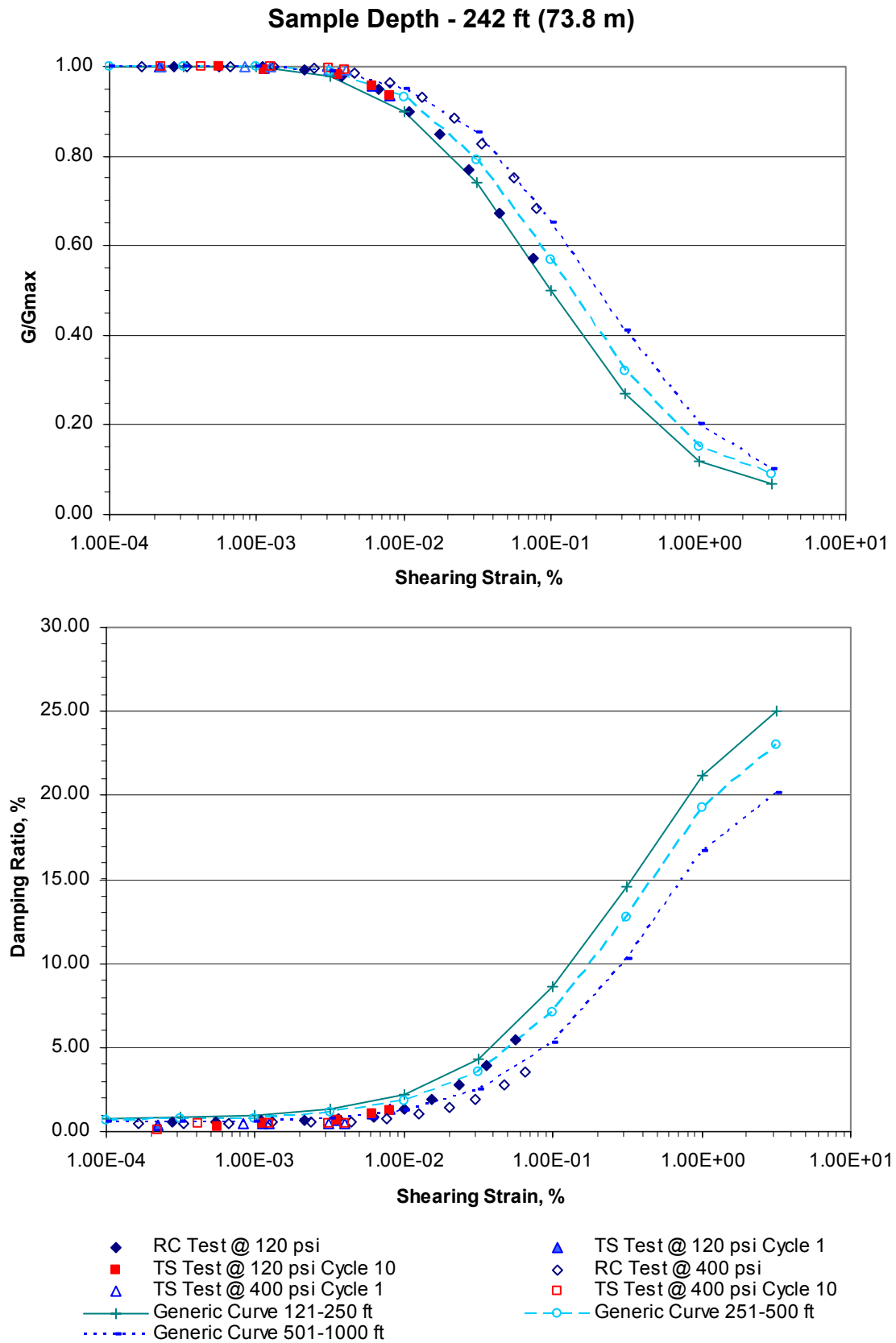


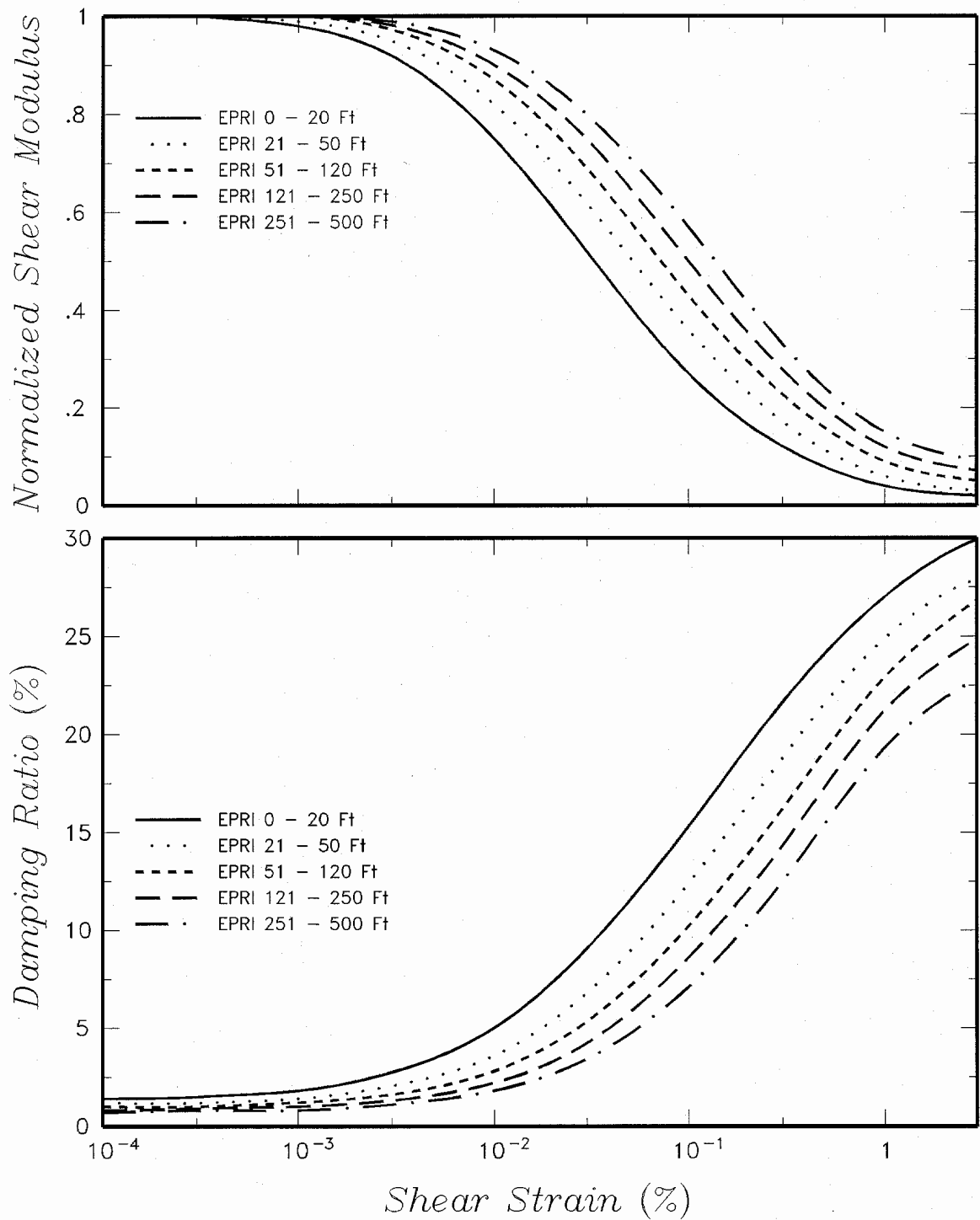
Seismic Hazards Report for the EGC ESP Site
**Modulus Reduction and Damping Test Results Compared to EPRI (1993) Soil
 Property Curves for Test UTA-34-C**

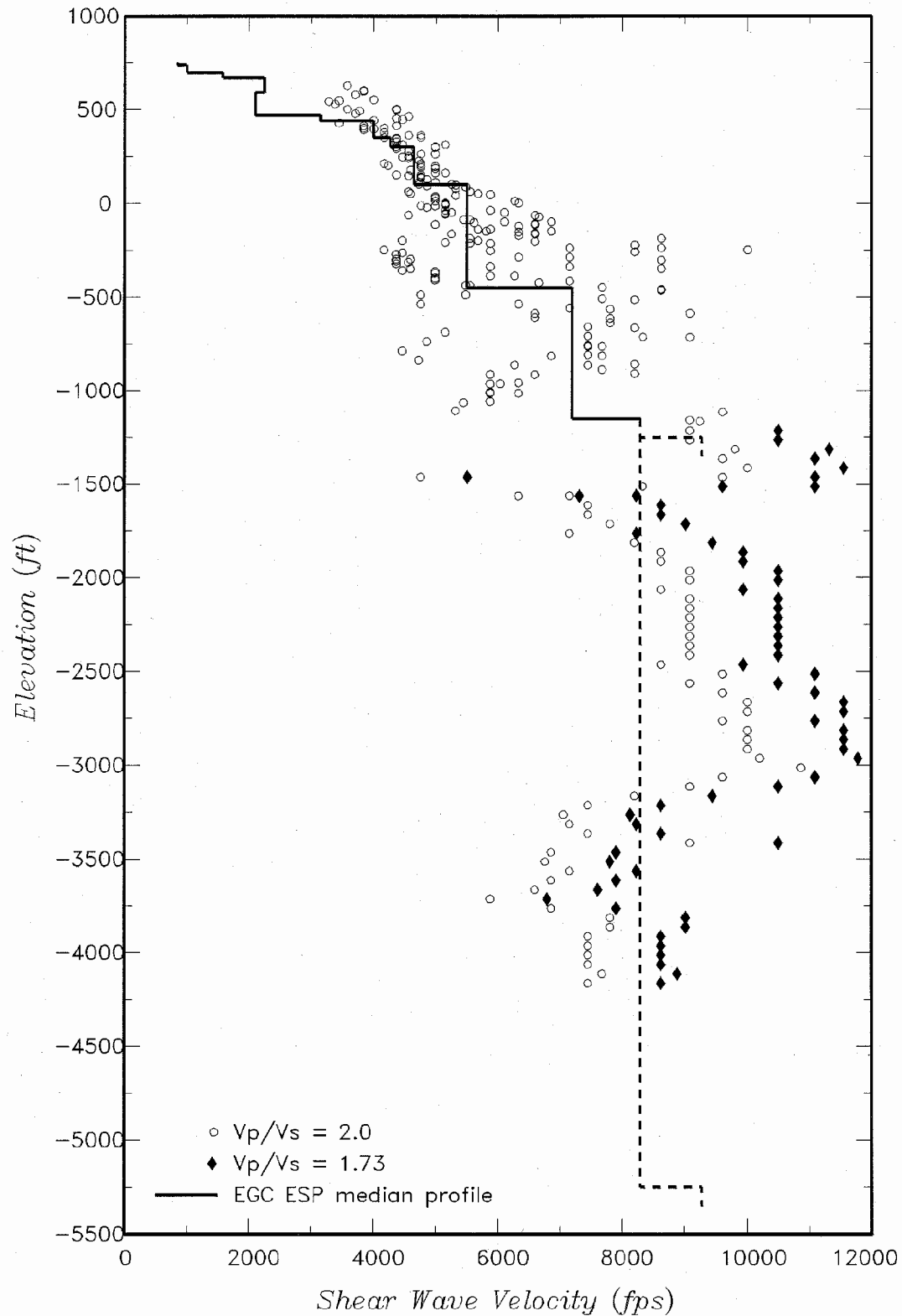
Figure
4.2-4



- | | |
|---------------------------------|------------------------------|
| ◆ RC Test @ 60 psi | ▲ TS Test @ 60 psi Cycle 1 |
| ■ TS Test @ 60 psi Cycle 10 | ◇ RC Test @ 240 psi |
| △ TS Test @ 240 psi Cycle 1 | □ TS Test @ 240 psi Cycle 10 |
| —+— Generic Curve 51-120 ft | —○— Generic Curve 121-250 ft |
| ····· Generic Curve 501-1000 ft | —*— Generic Curve 251-500 ft |

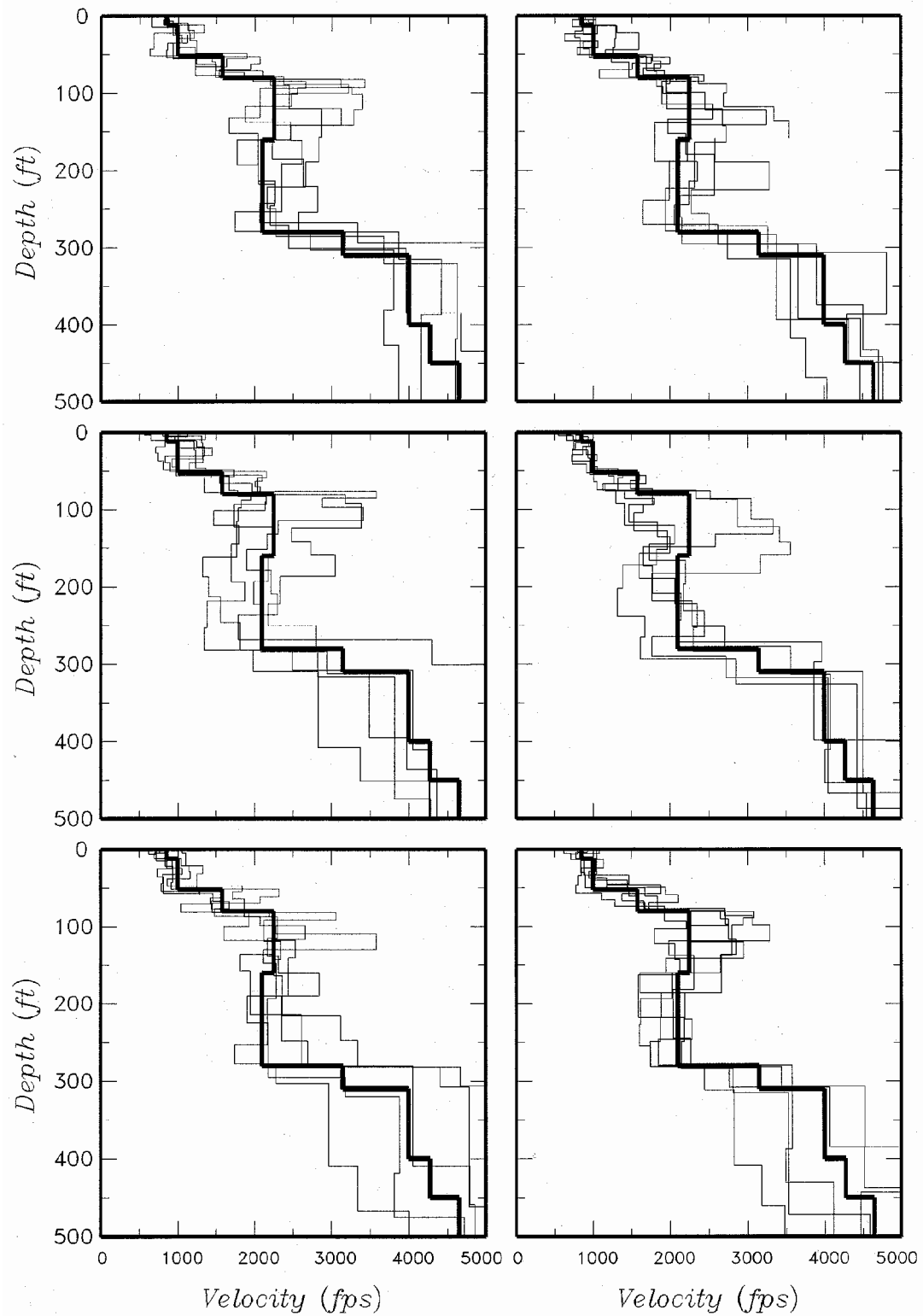






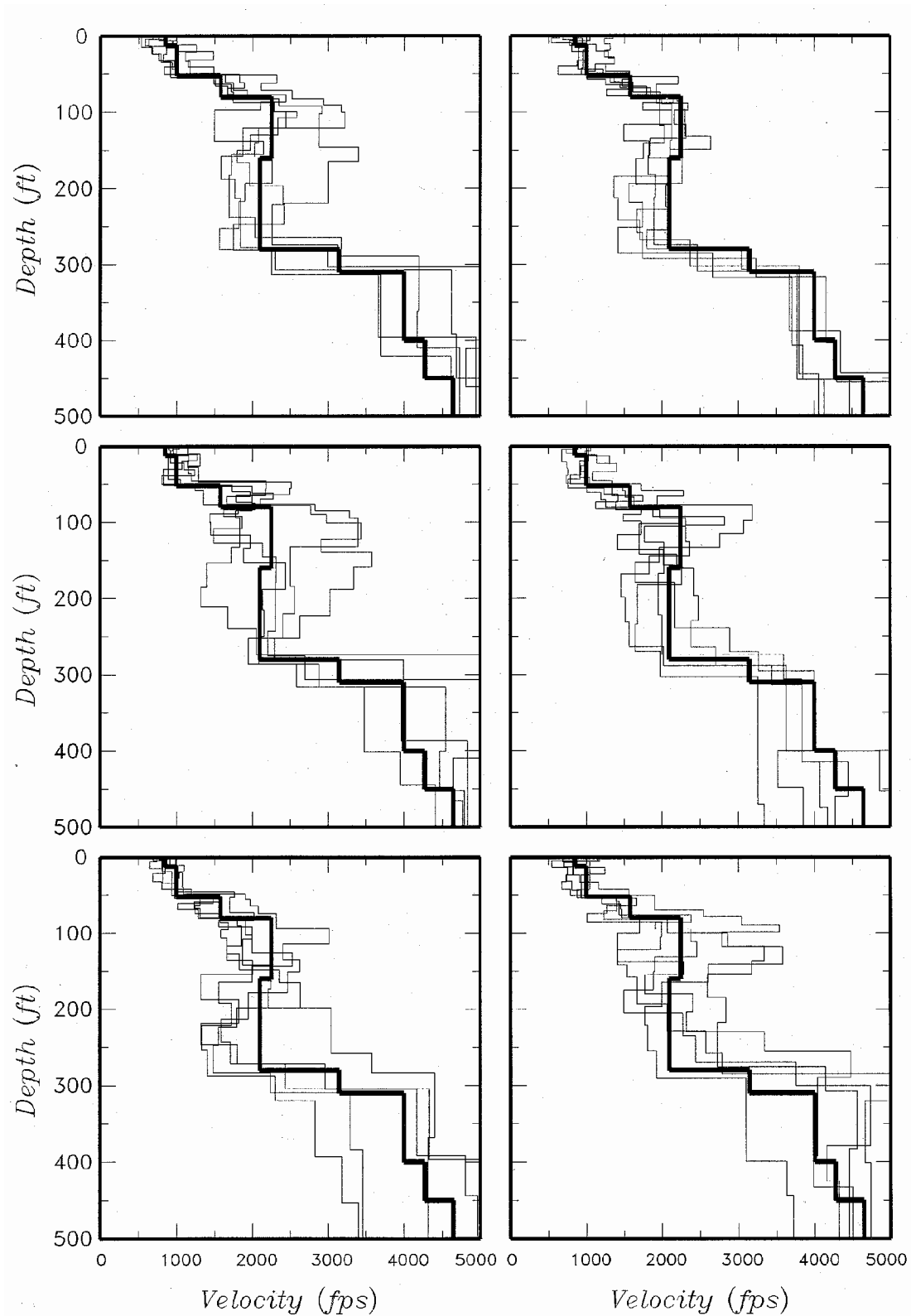
Seismic Hazards Report for the EGC ESP Site
**Shear Wave Velocity Data for Sedimentary Rocks and Median Velocity Profile
 for the EGC ESP Site**

Figure
4.2-8



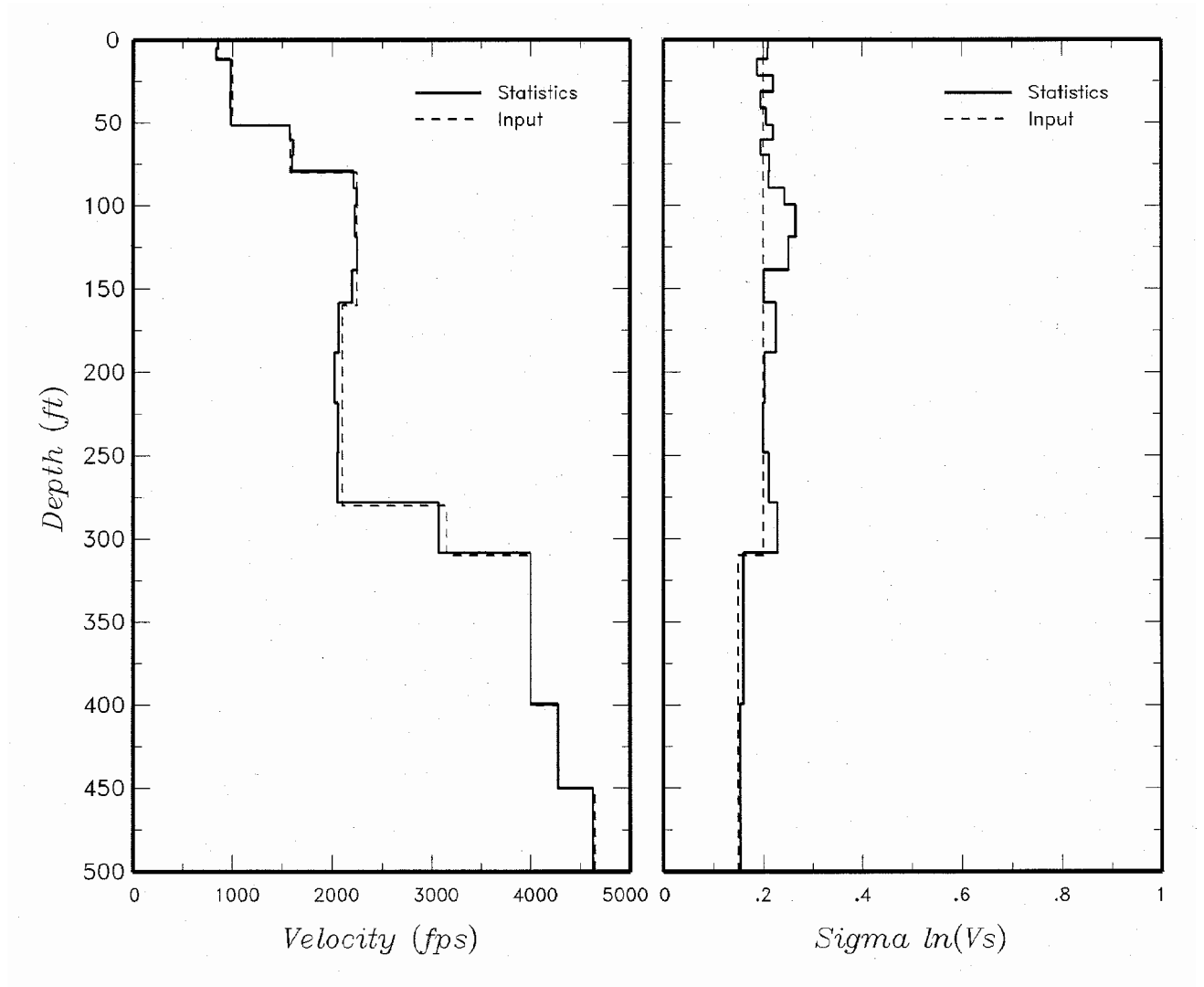
Seismic Hazards Report for the EGC ESP Site
**Upper 500 Feet of First Thirty Randomized Shear Wave Velocity Profiles for
the EGC ESP Site**

Figure
4.2-9a



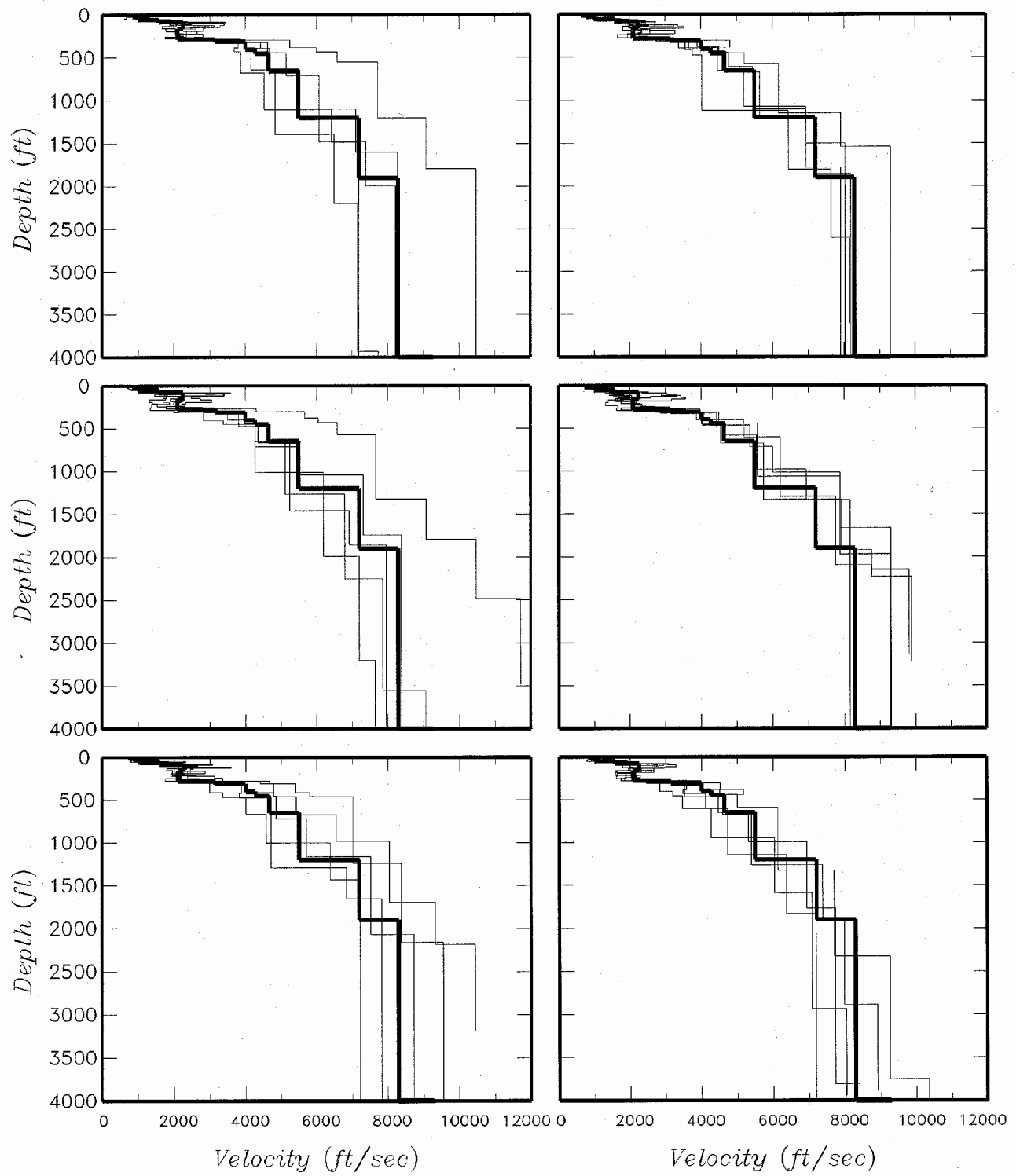
Seismic Hazards Report for the EGC ESP Site
**Upper 500 Feet of Second Thirty Randomized Shear Wave Velocity Profiles
 for the EGC ESP Site**

Figure
4.2-9b



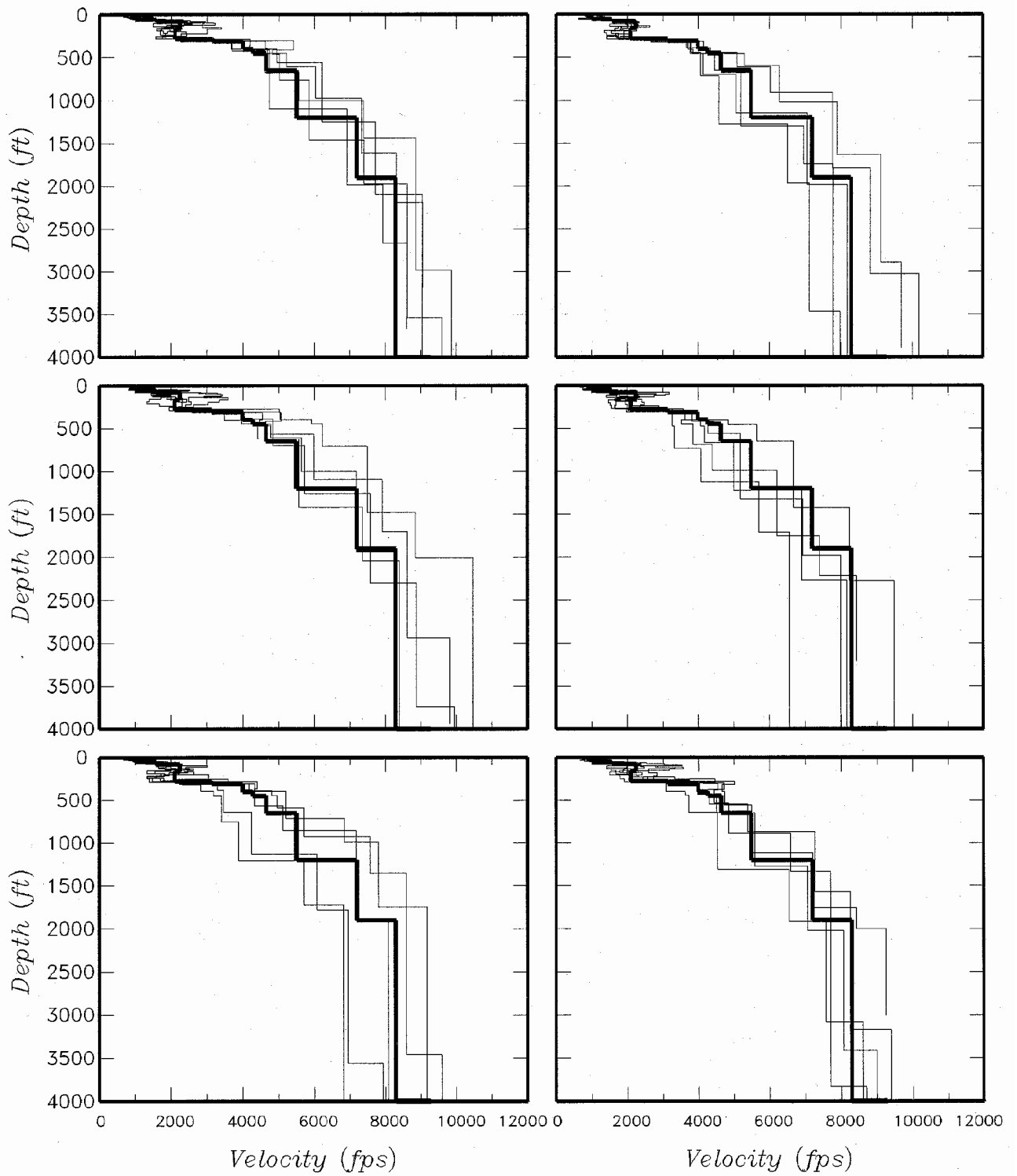
Seismic Hazards Report for the EGC ESP Site
Statistics of the Randomized Shear Wave Velocity Profiles (0 to 500-ft Depth)

Figure
4.2-10



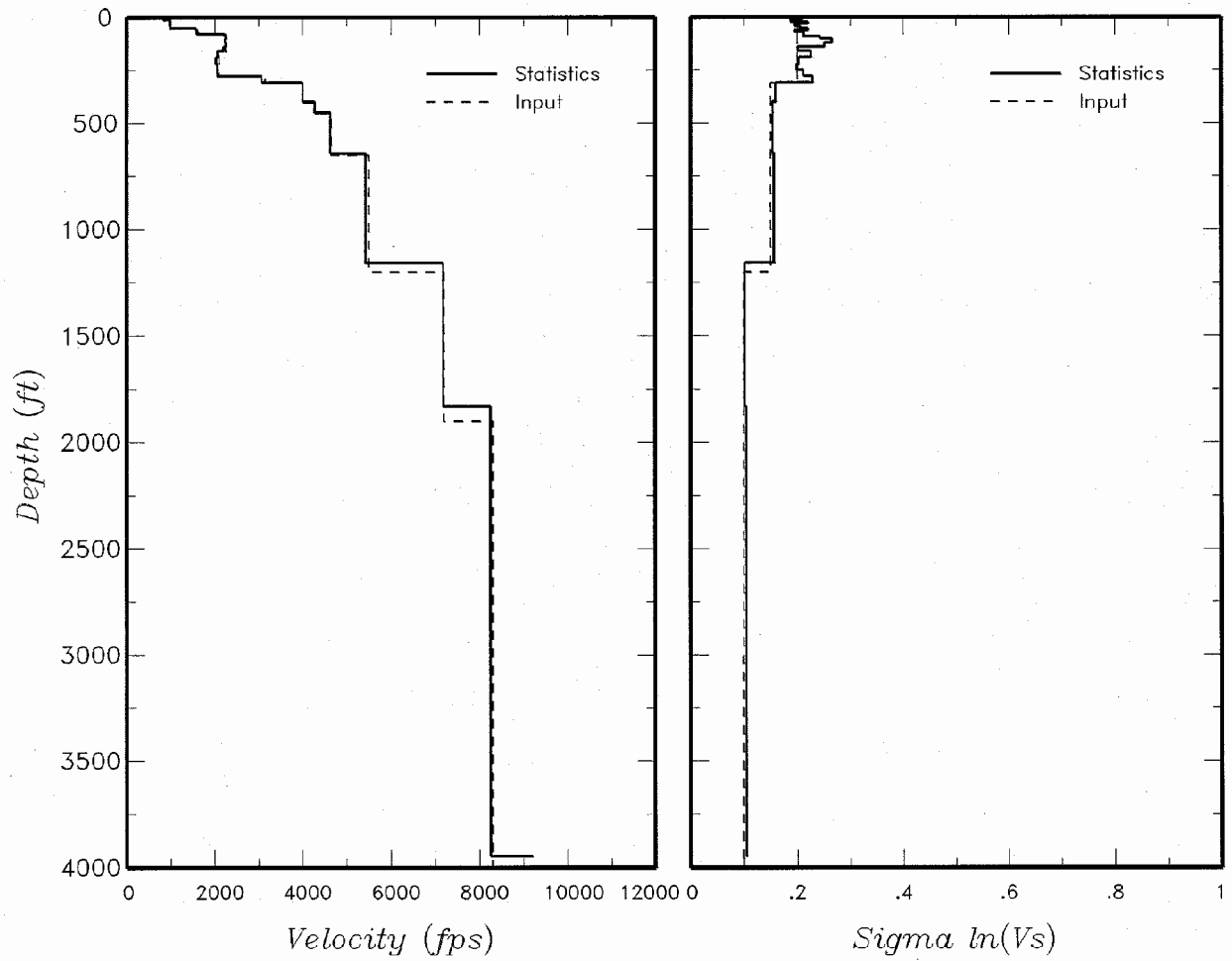
Seismic Hazards Report for the EGC ESP Site
First Thirty Randomized Shear Wave Velocity Profiles for the EGC ESP Site

Figure
4.2-11a



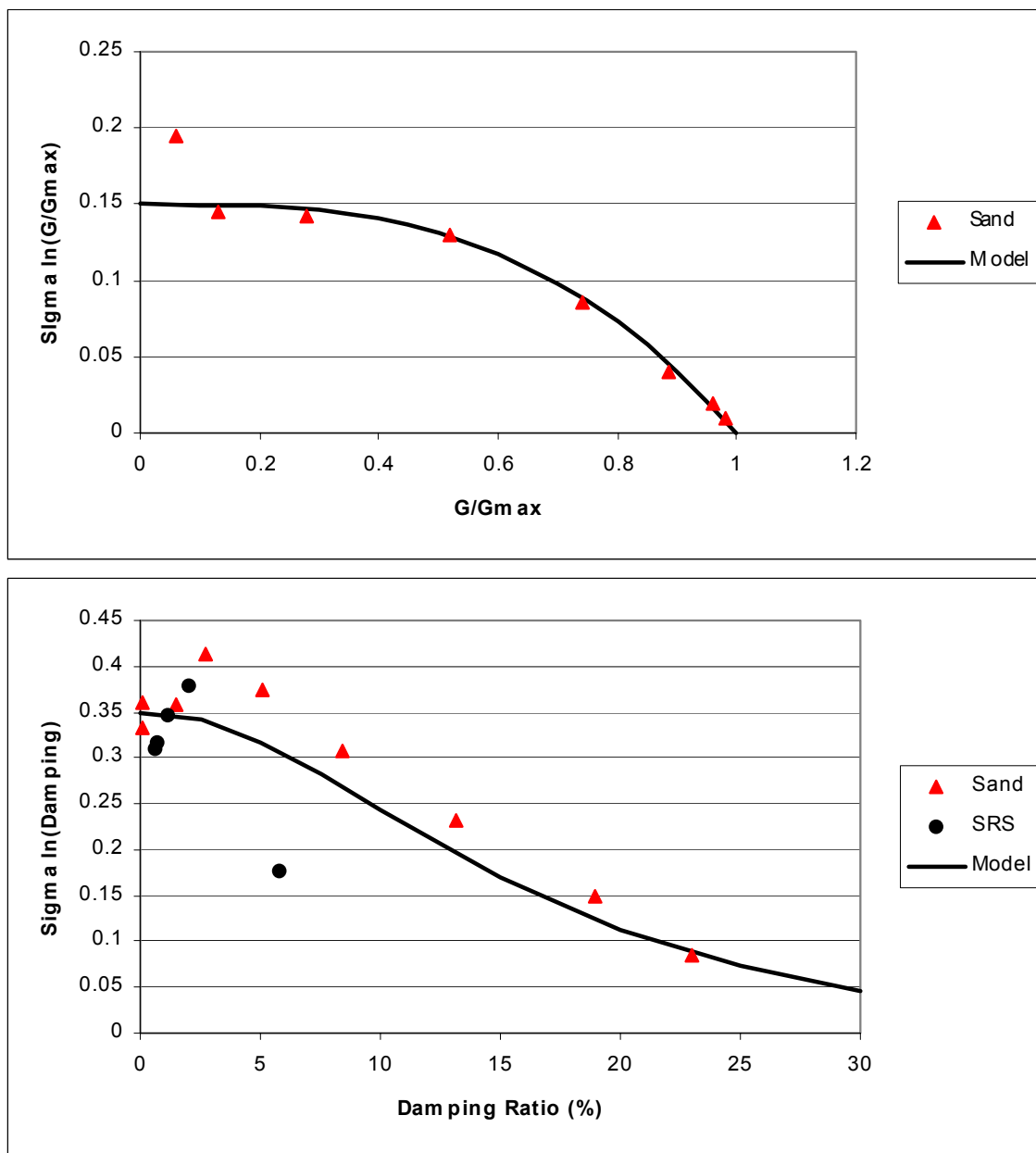
Seismic Hazards Report for the EGC ESP Site
Second Thirty Randomized Shear Wave Velocity Profiles for the EGC ESP Site

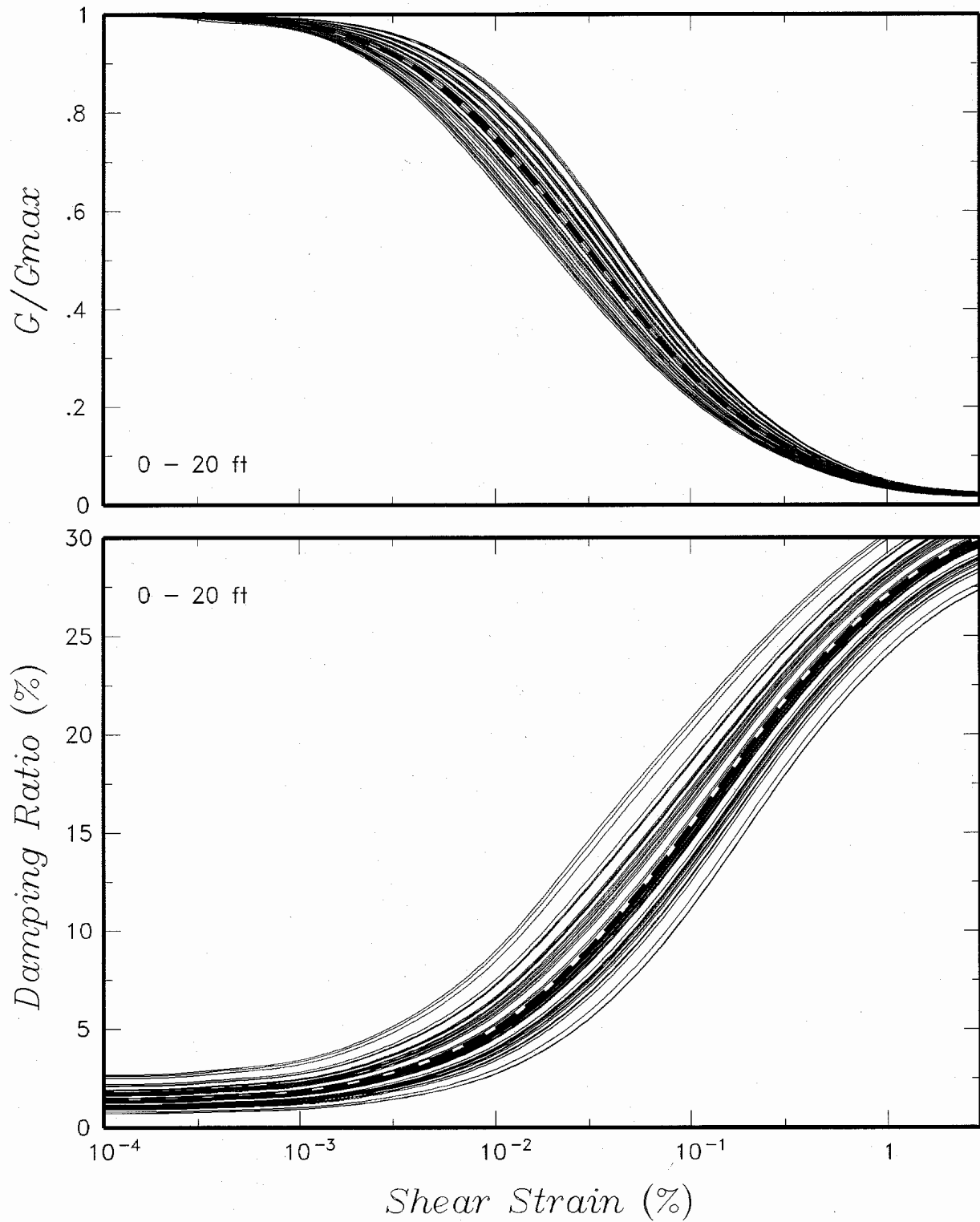
Figure
4.2-11b



Seismic Hazards Report for the EGC ESP Site
Statistics of the Randomized Shear Wave Velocity Profiles (0 to 4,000-ft Depth)

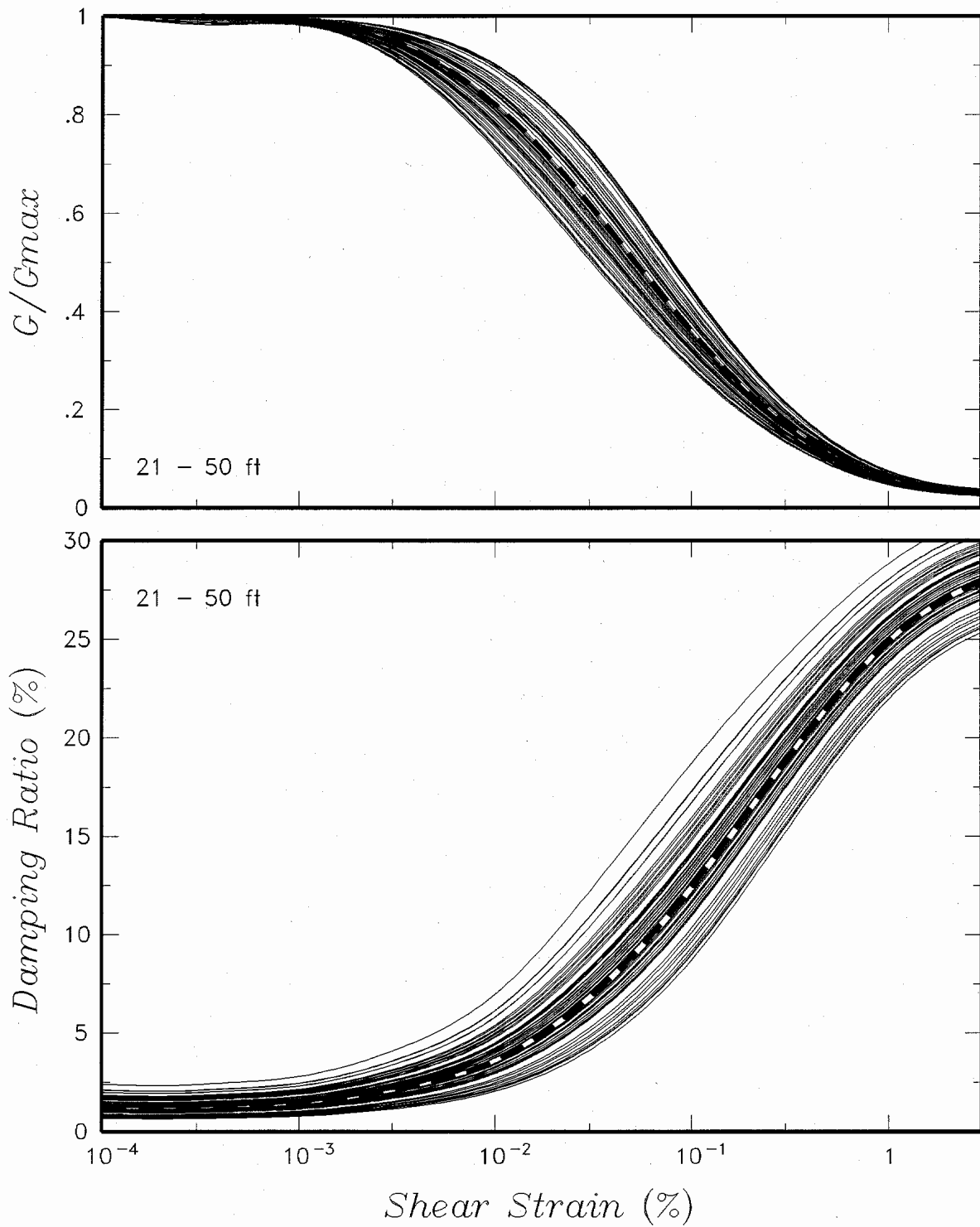
Figure
4.2-12





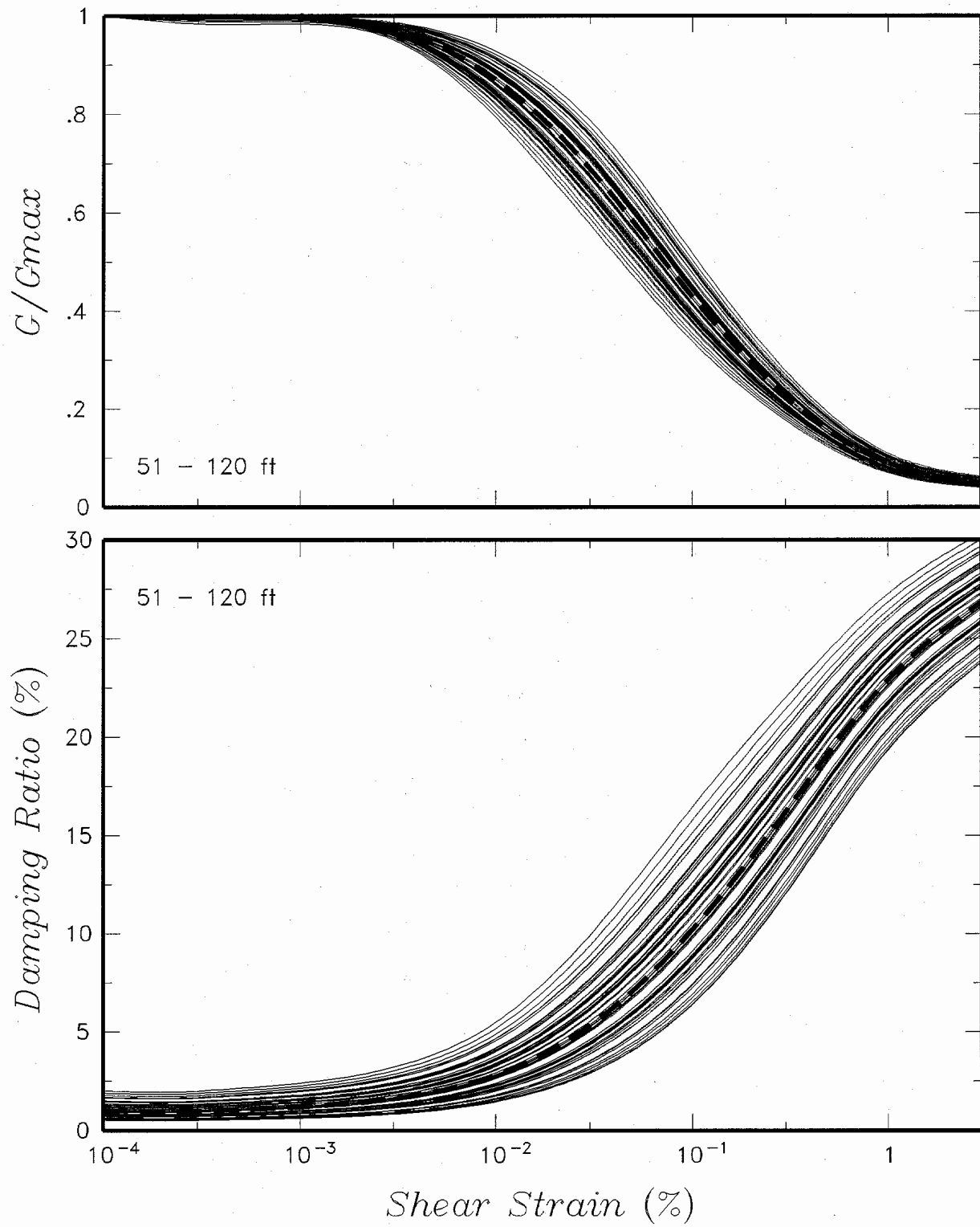
Seismic Hazards Report for the EGC ESP Site
**Randomized Modulus Reduction and Damping Relationships
for the Depth Range of 0 to 20 ft**

Figure
4.2-14



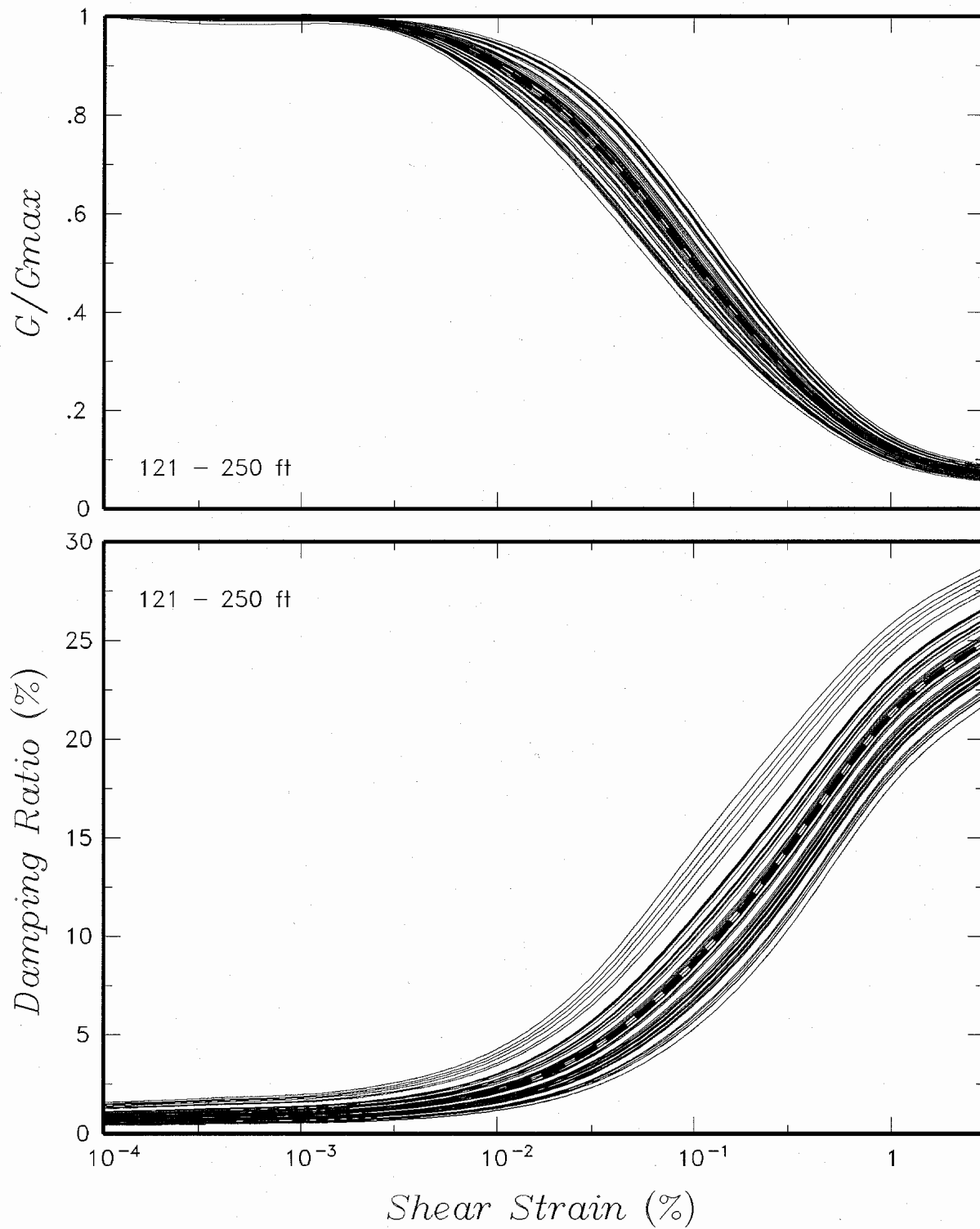
Seismic Hazards Report for the EGC ESP Site
**Randomized Modulus Reduction and Damping Relationships
for the Depth Range of 21 to 50 ft**

Figure
4.2-15



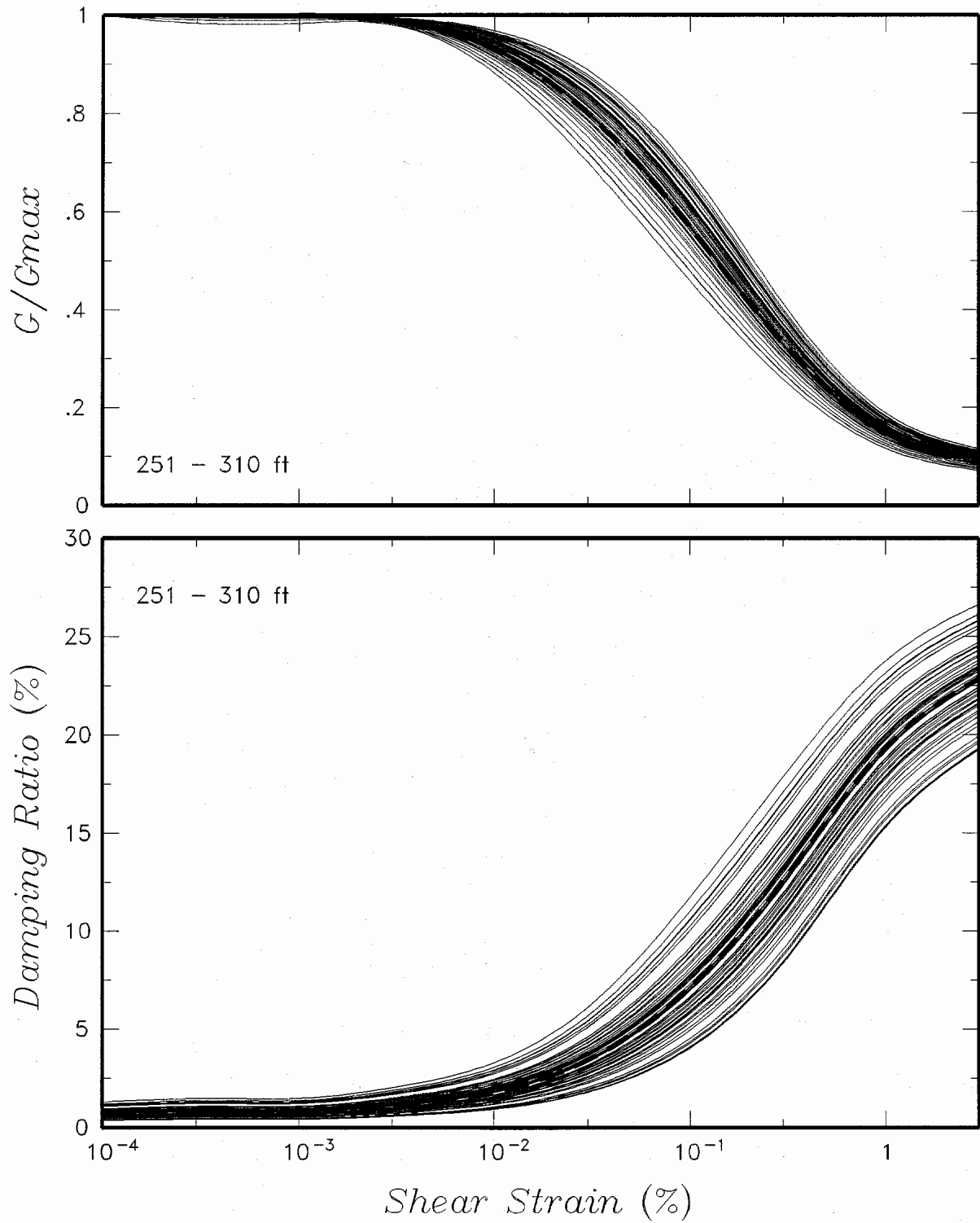
Seismic Hazards Report for the EGC ESP Site
**Randomized Modulus Reduction and Damping Relationships
for the Depth Range of 51 to 120 ft**

Figure
4.2-16



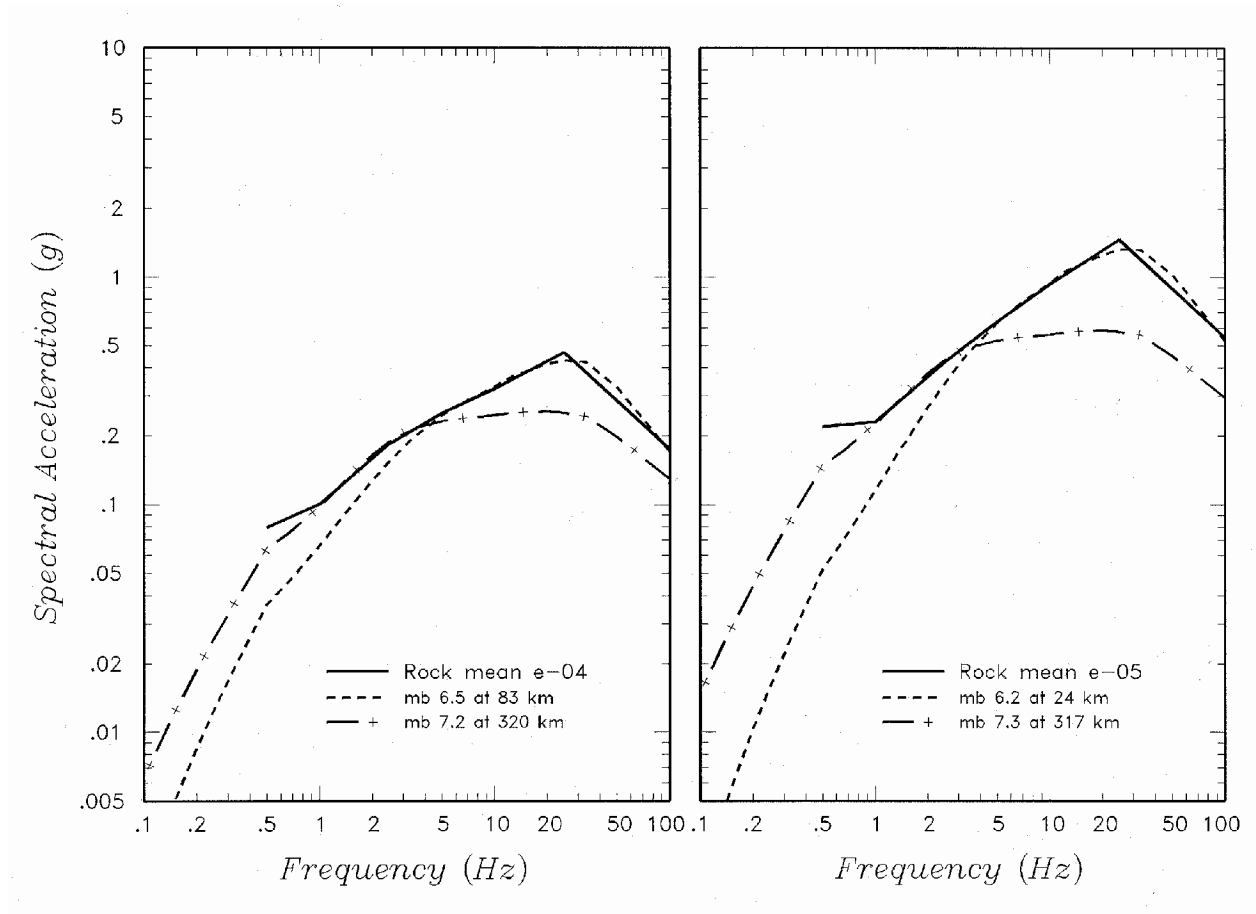
Seismic Hazards Report for the EGC ESP Site
**Randomized Modulus Reduction and Damping Relationships
for the Depth Range of 121 to 250 ft**

Figure
4.2-17



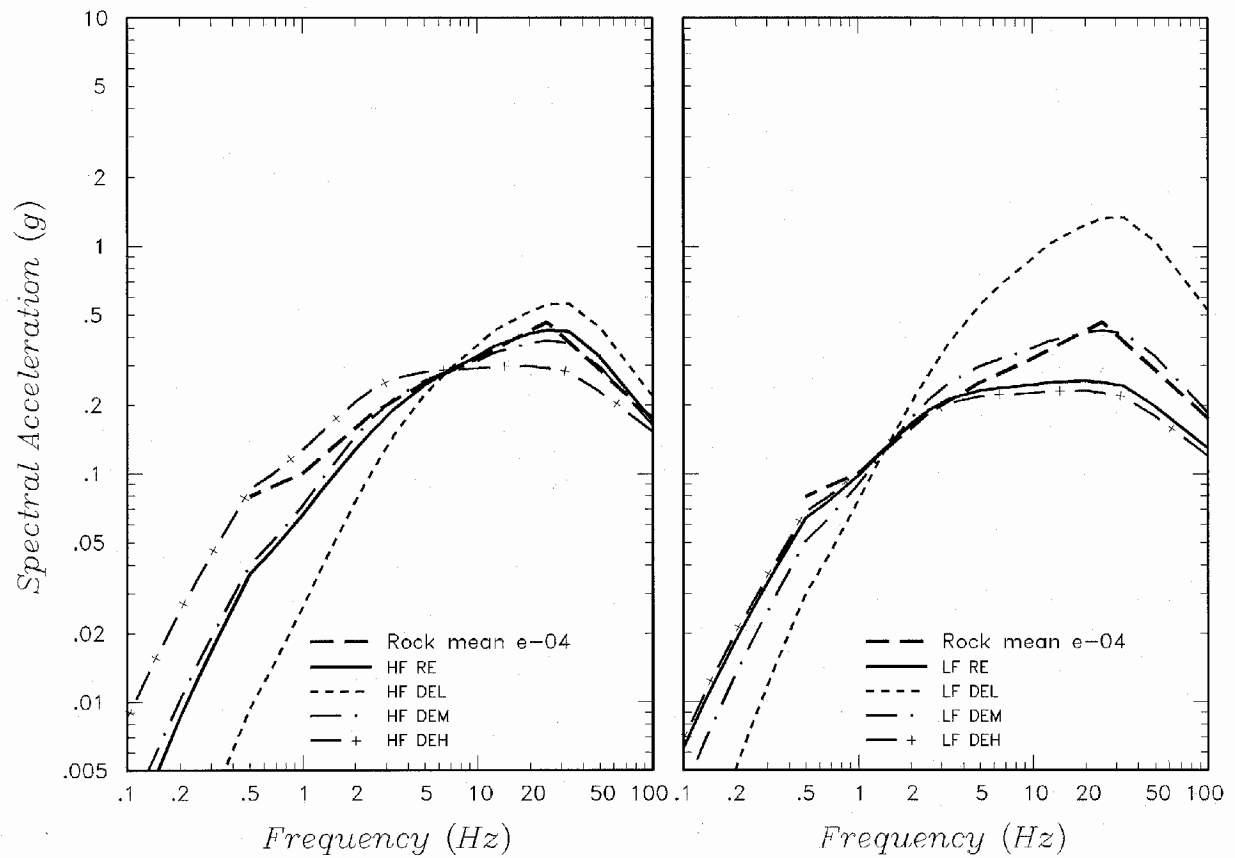
Seismic Hazards Report for the EGC ESP Site
**Randomized Modulus Reduction and Damping Relationships
 for the Depth Range of 251 to 310 ft**

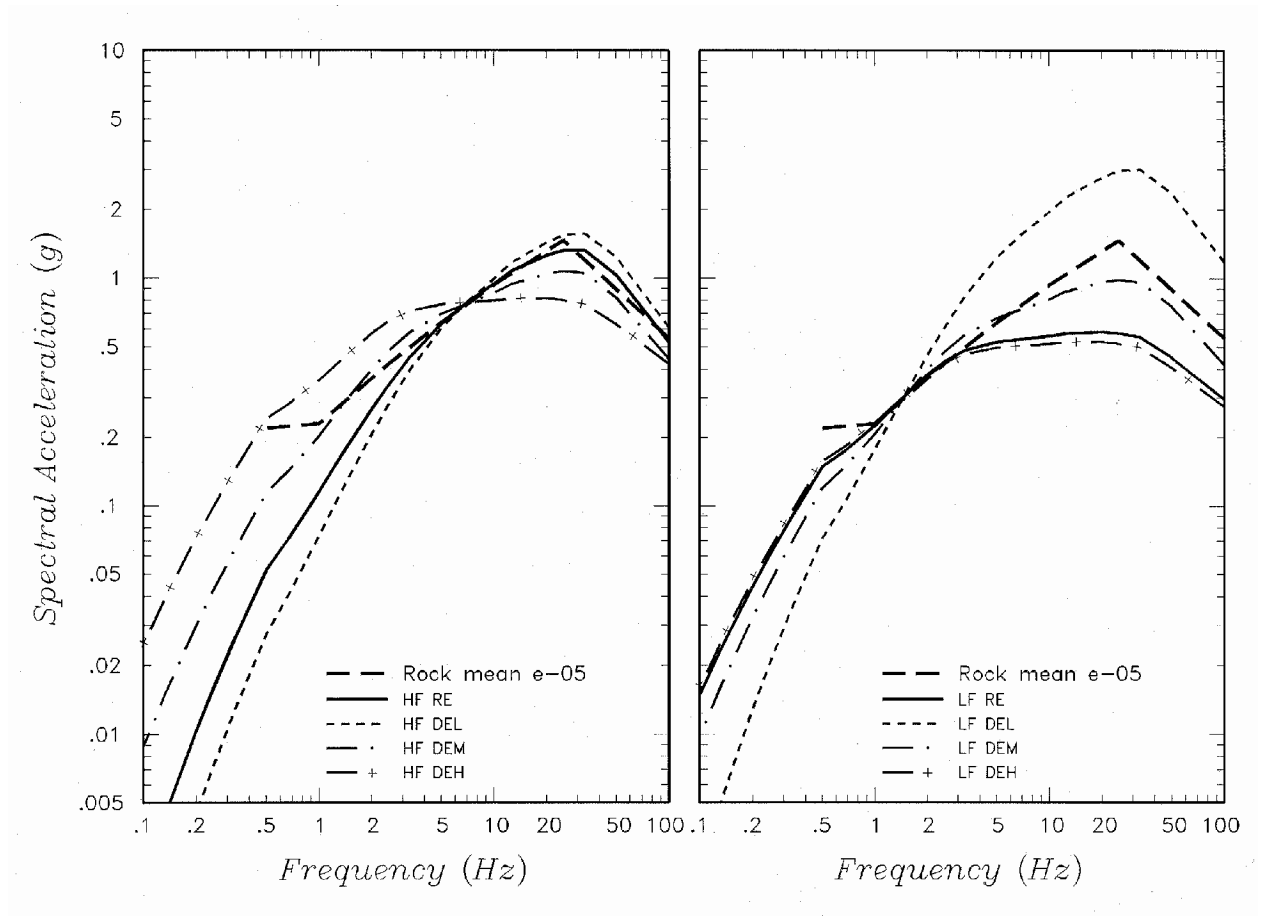
Figure
4.2-18

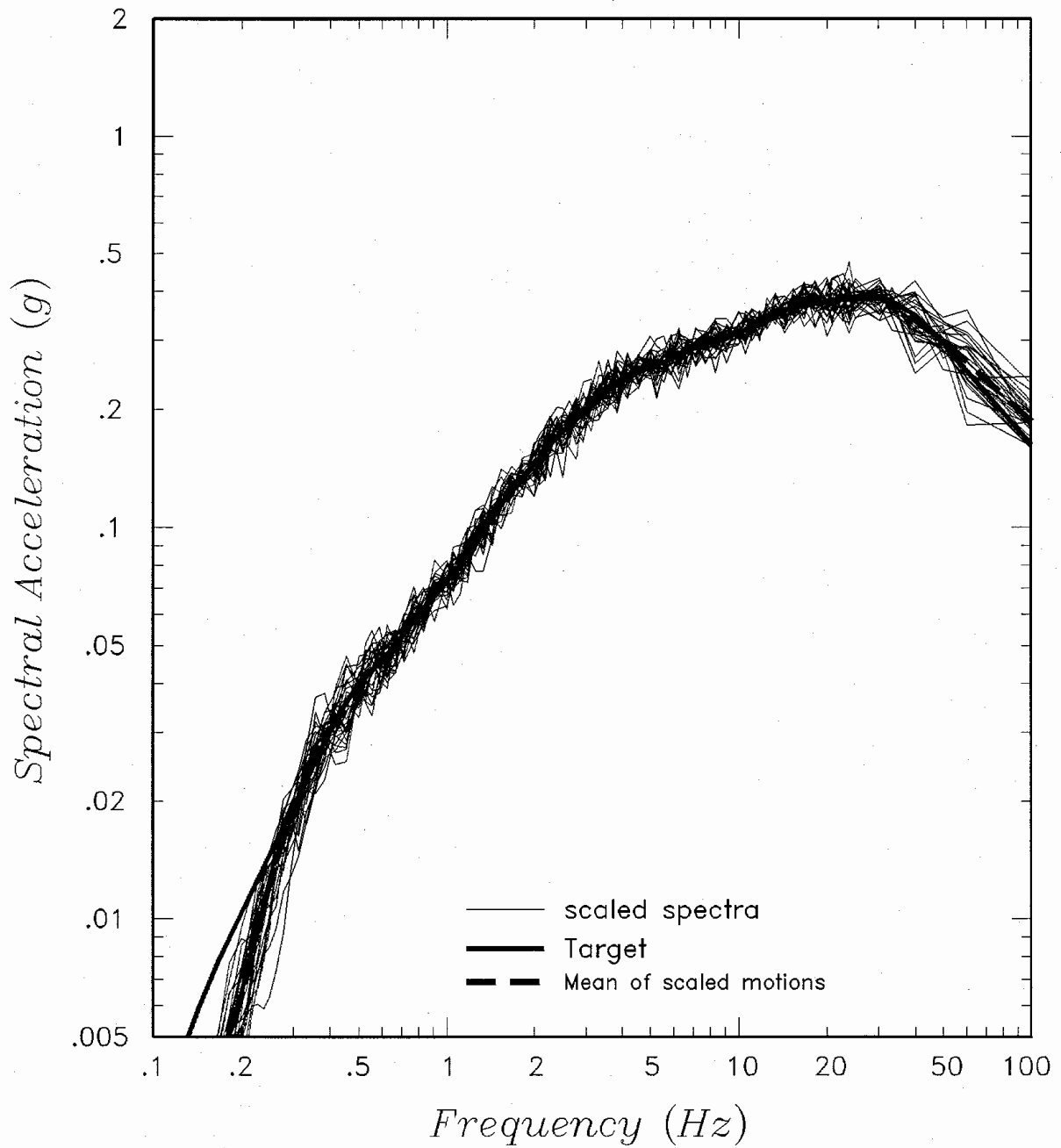


Seismic Hazards Report for the EGC ESP Site
**Reference Earthquake (RE) Response Spectra for Mean 10^{-4}
 and Mean 10^{-5} Hazard**

Figure
4.2-19

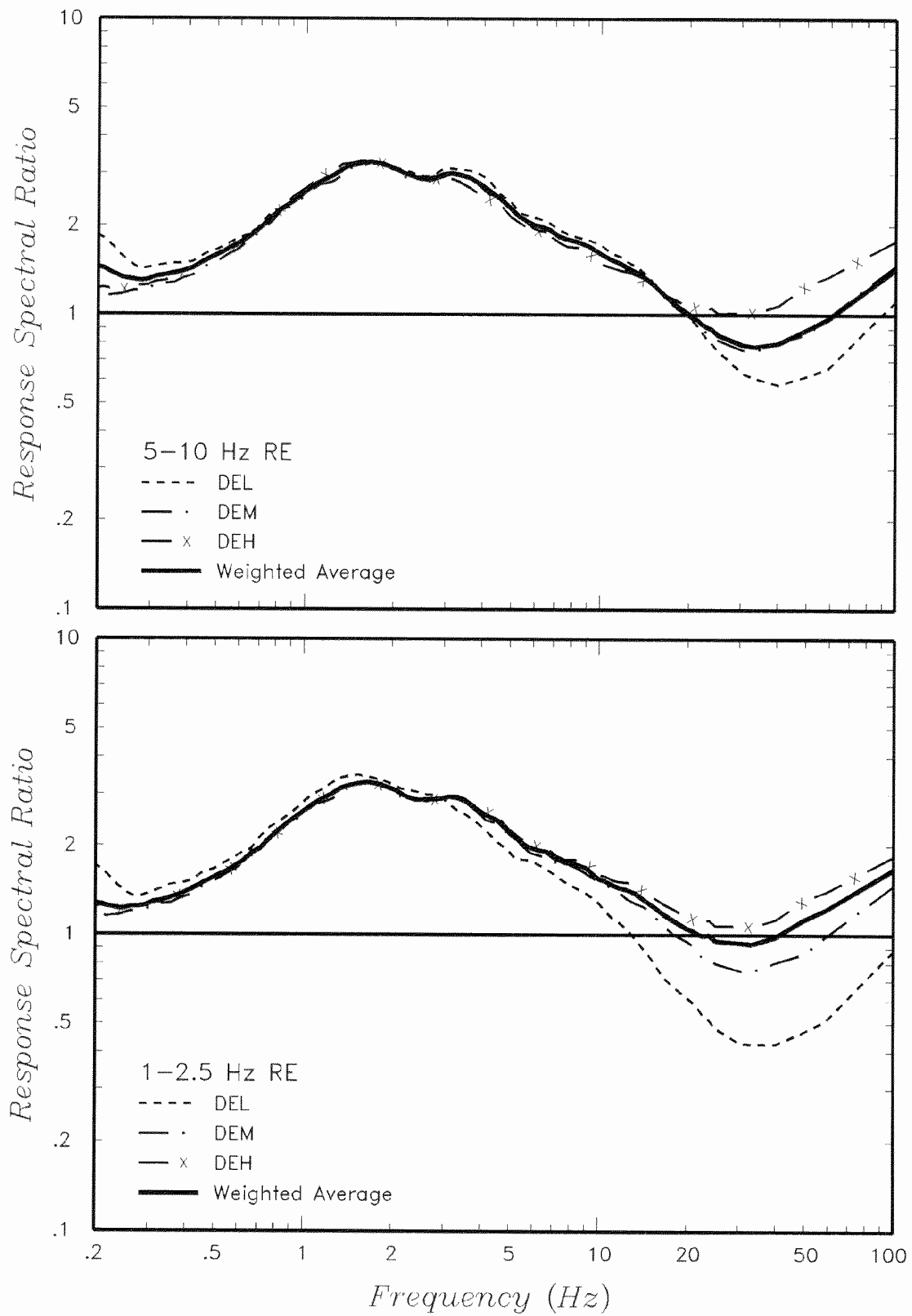






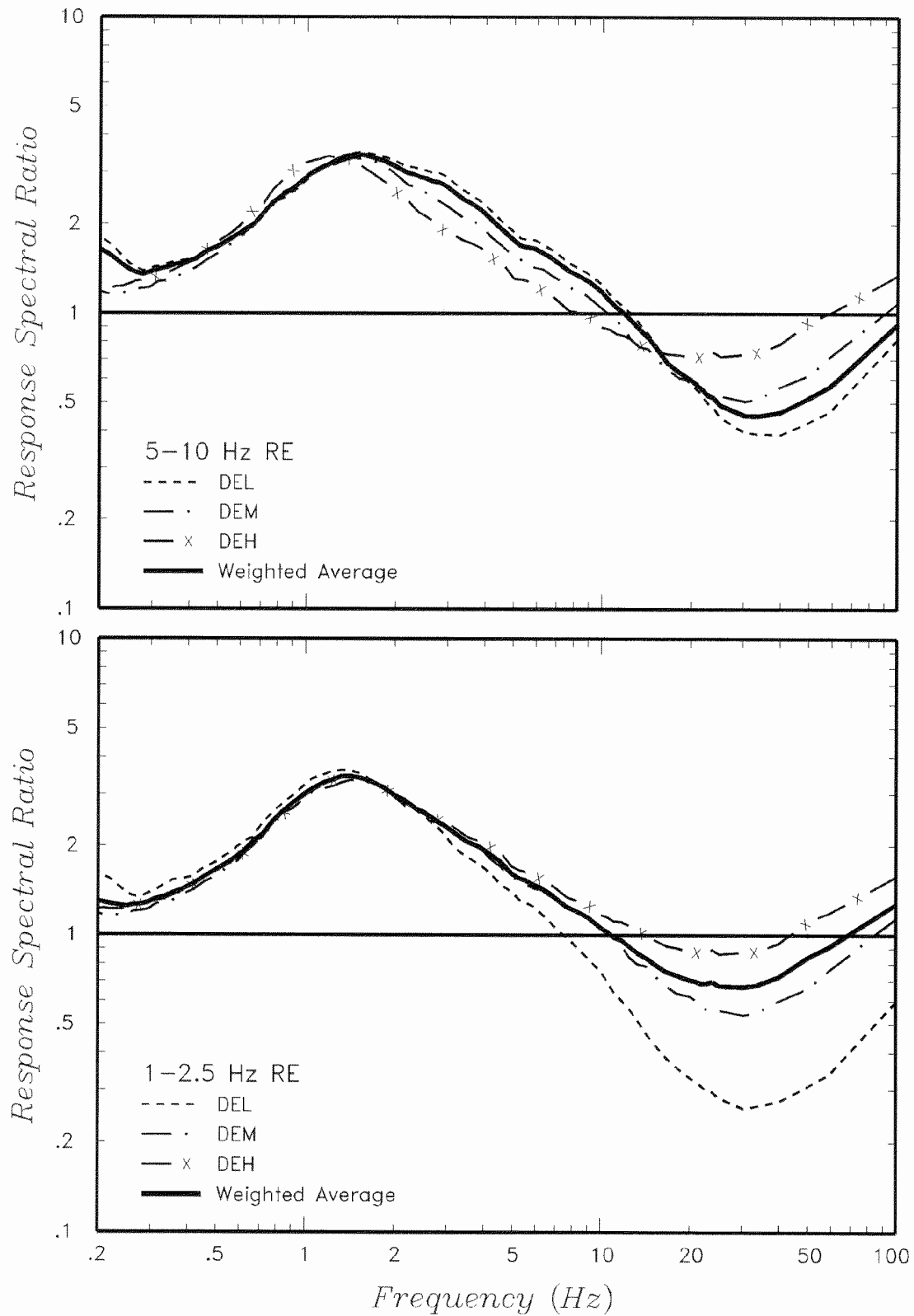
Seismic Hazards Report for the EGC ESP Site
Example of 30 Response Spectra Scaled to Deaggregation Earthquake Spectrum

Figure
4.2-22



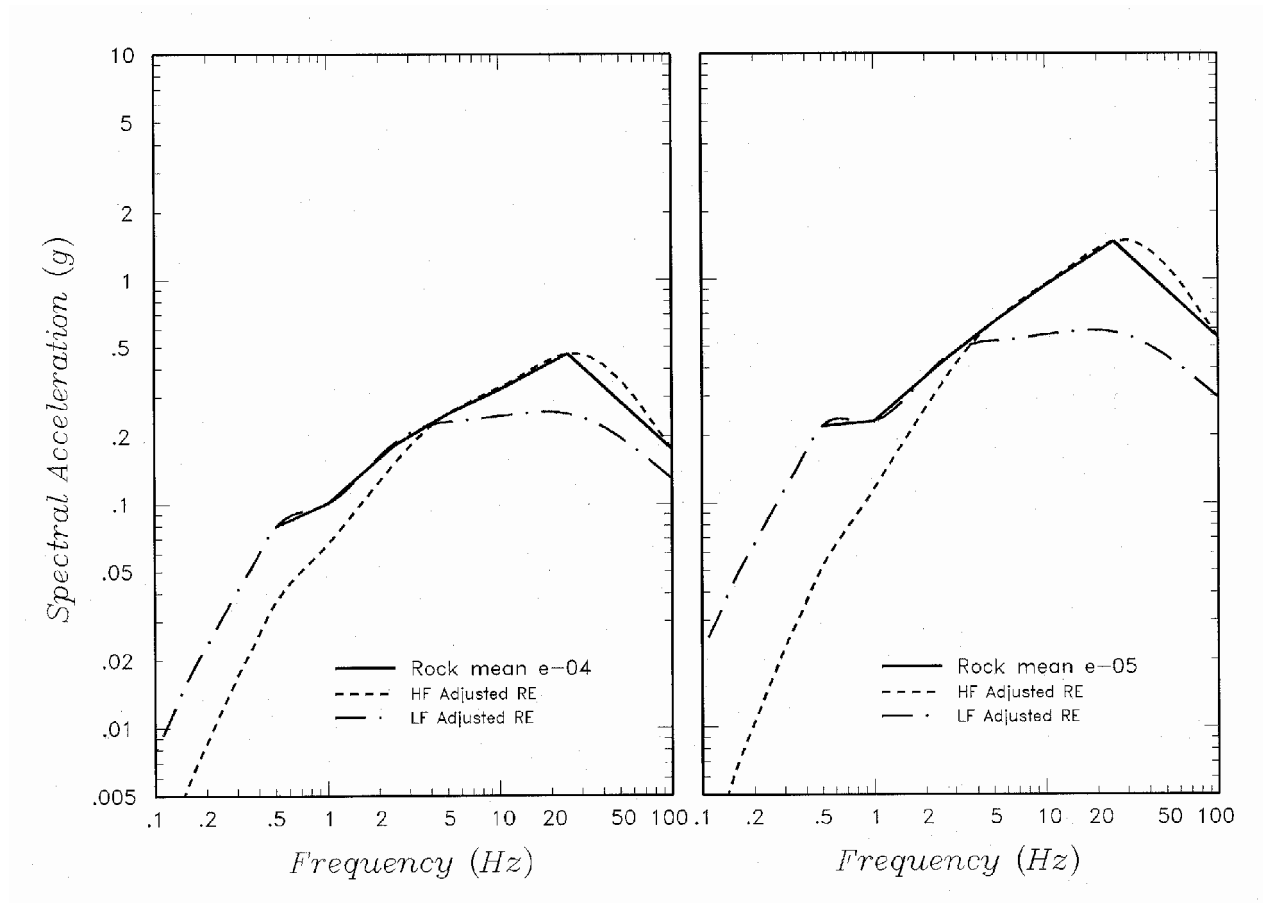
Seismic Hazards Report for the EGC ESP Site
Mean Site Amplification Functions for Deaggregation Earthquakes and Weighted Average Site Amplification Functions for Reference Earthquakes for Mean 10^{-4} Hazard

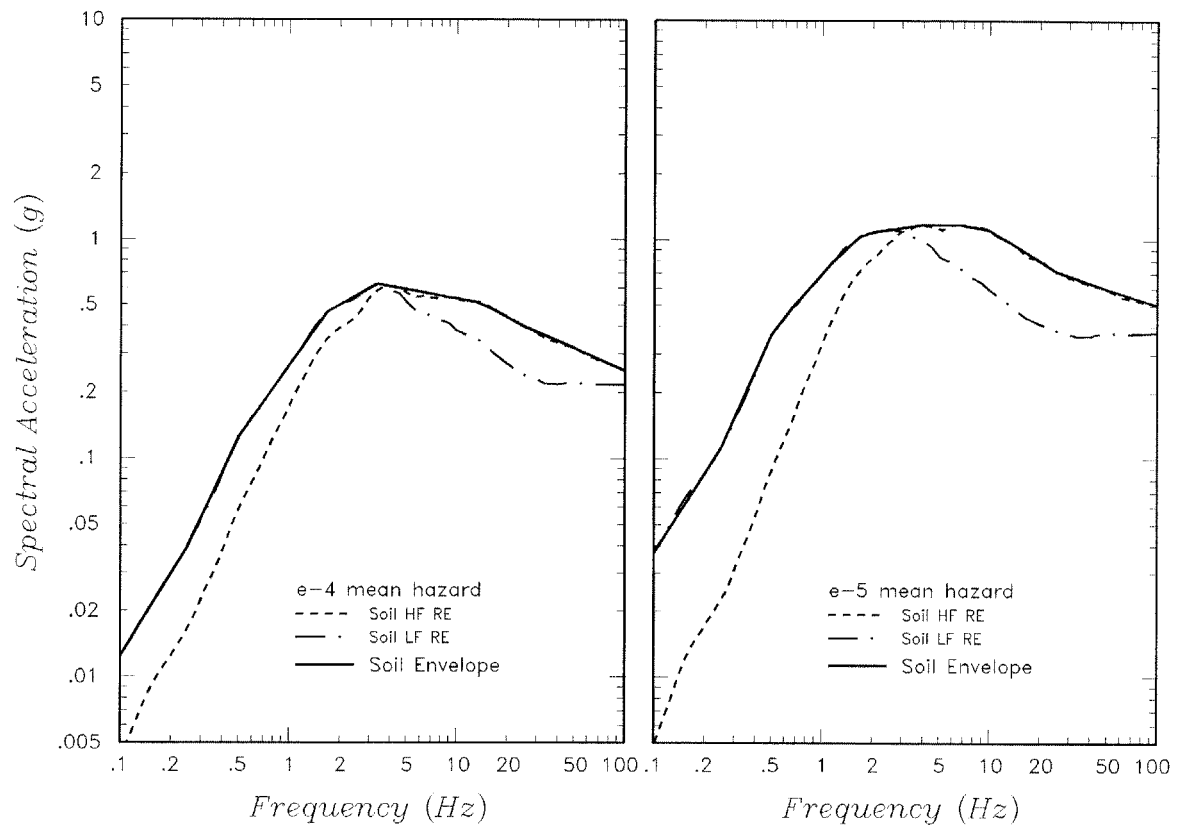
Figure
4.2-23

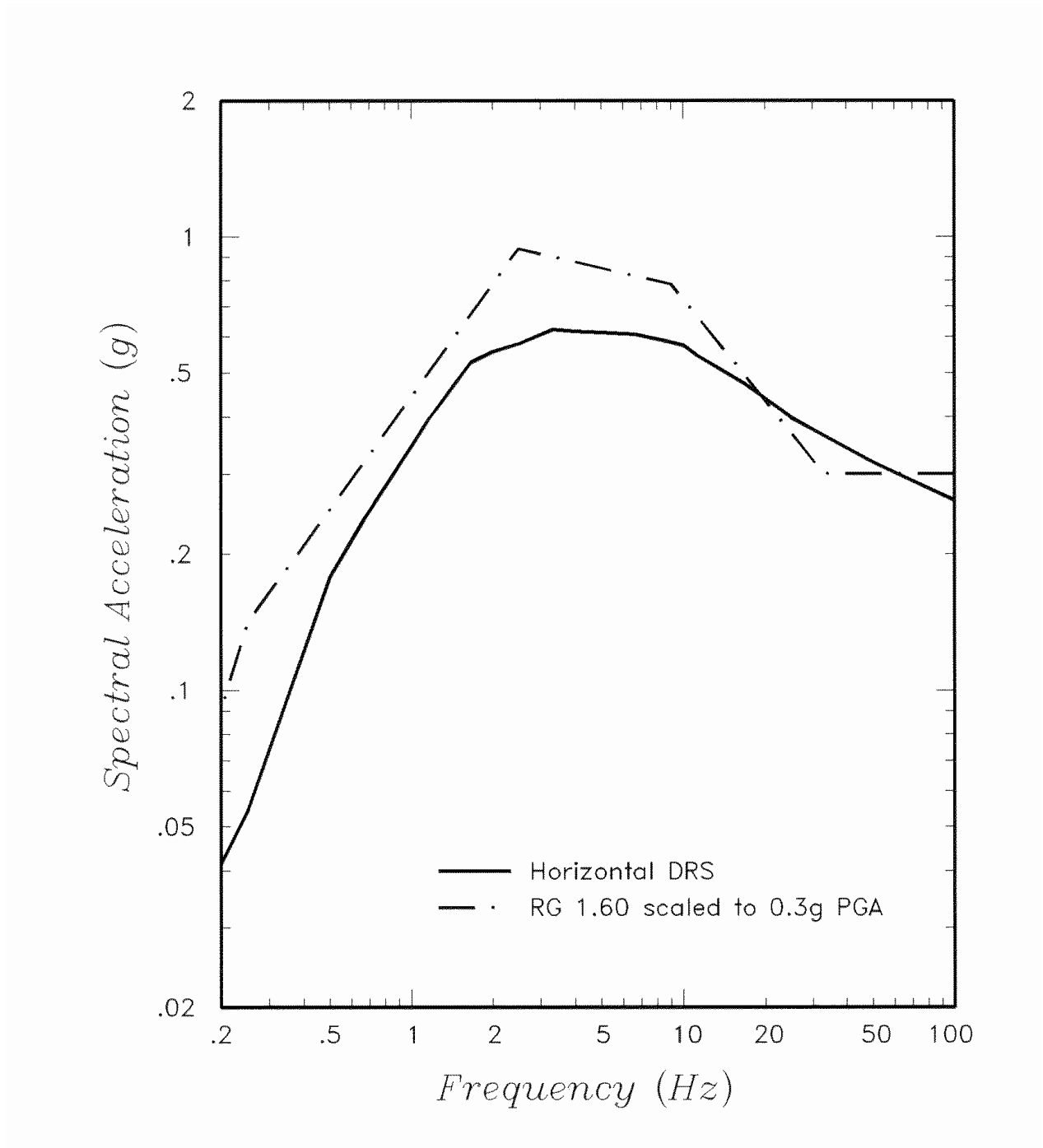


Seismic Hazards Report for the EGC ESP Site
Mean Site Amplification Functions for Deaggregation Earthquakes and Weighted Average Site Amplification Functions for Reference Earthquakes for Mean 10^{-5} Hazard

Figure
4.2-24

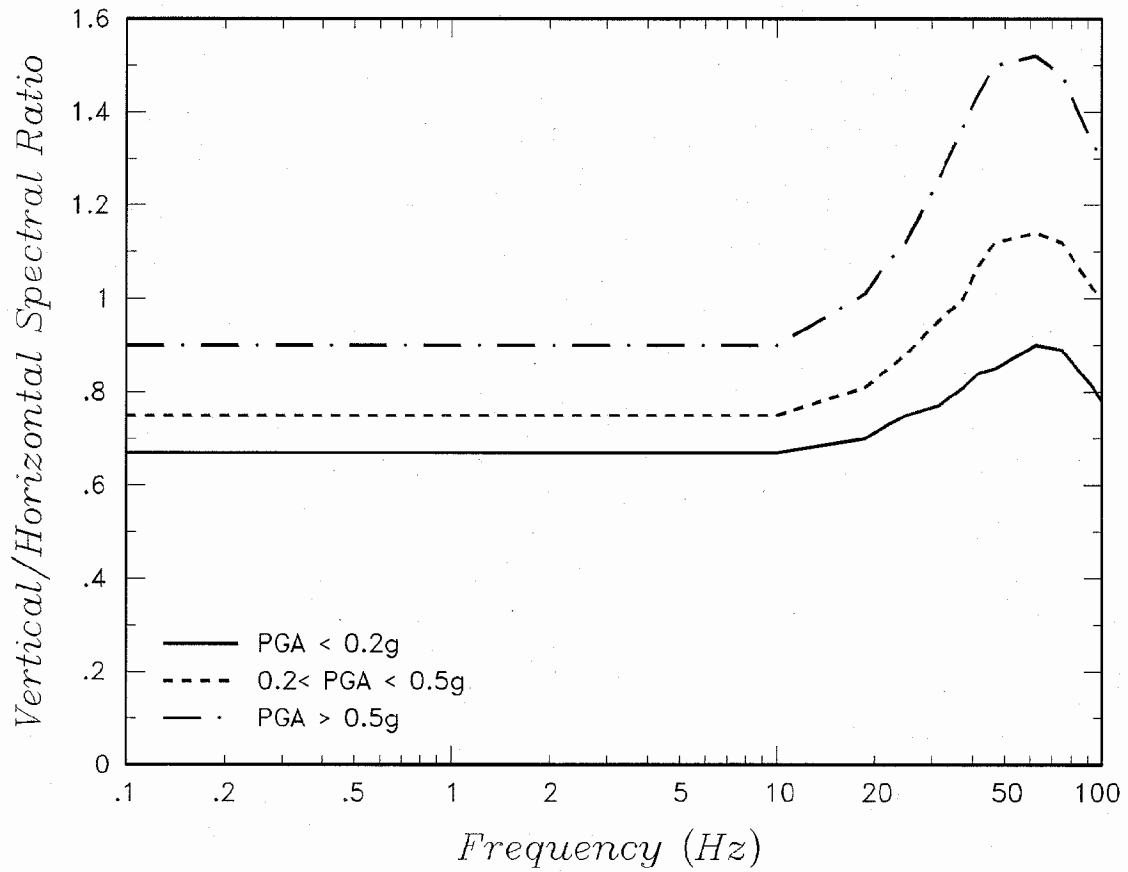


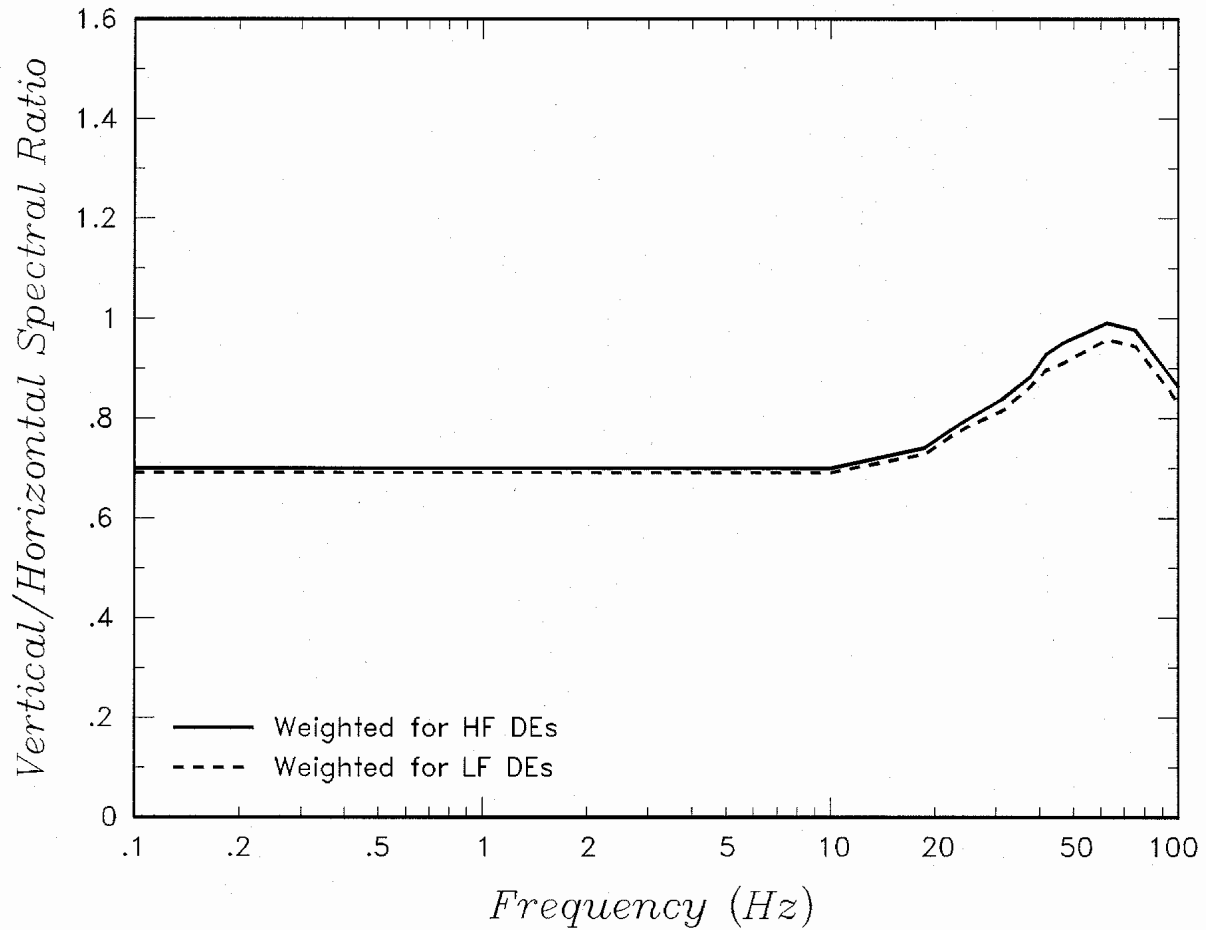




Seismic Hazards Report for the EGC ESP Site
Horizontal DRS Spectrum Defining Horizontal SSE

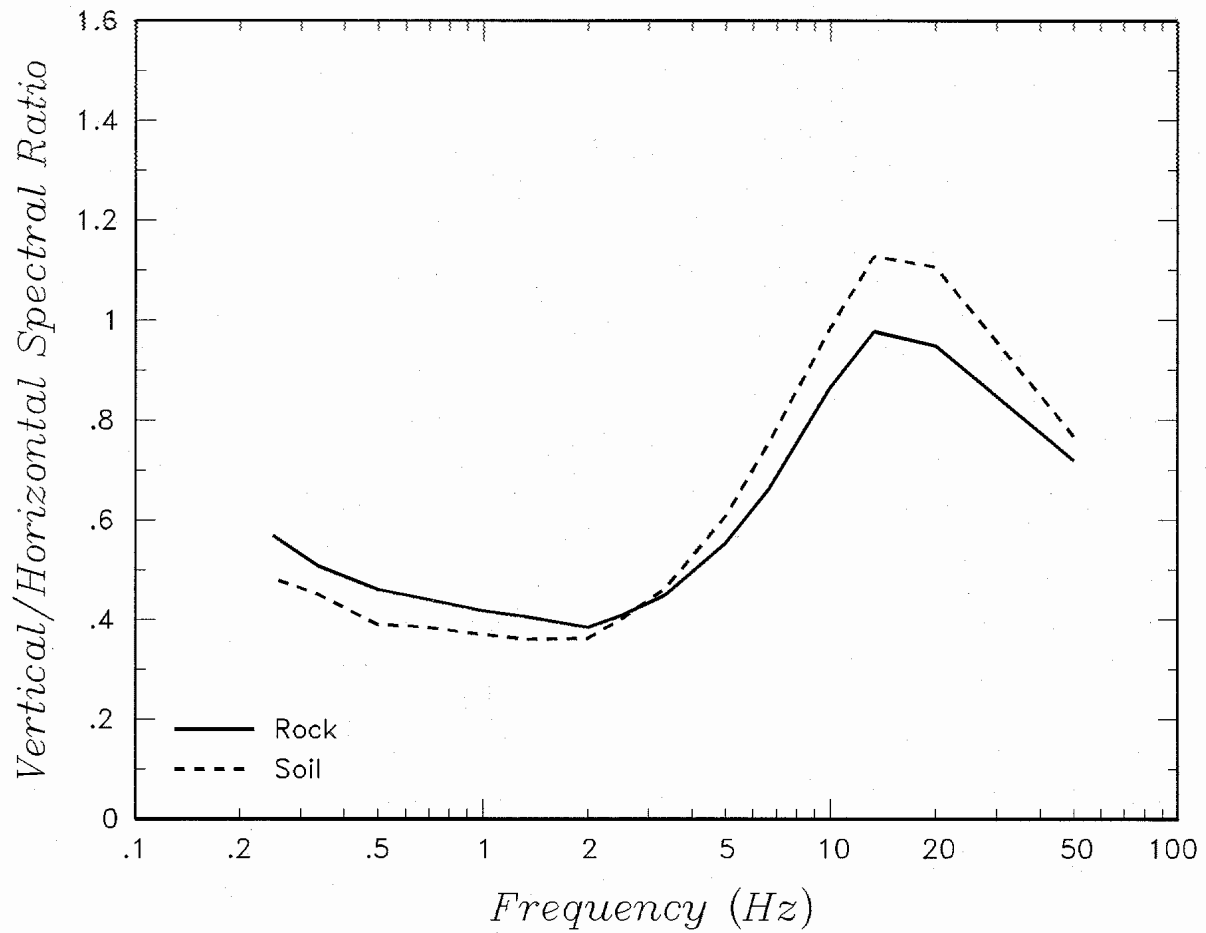
Figure
4.3-1





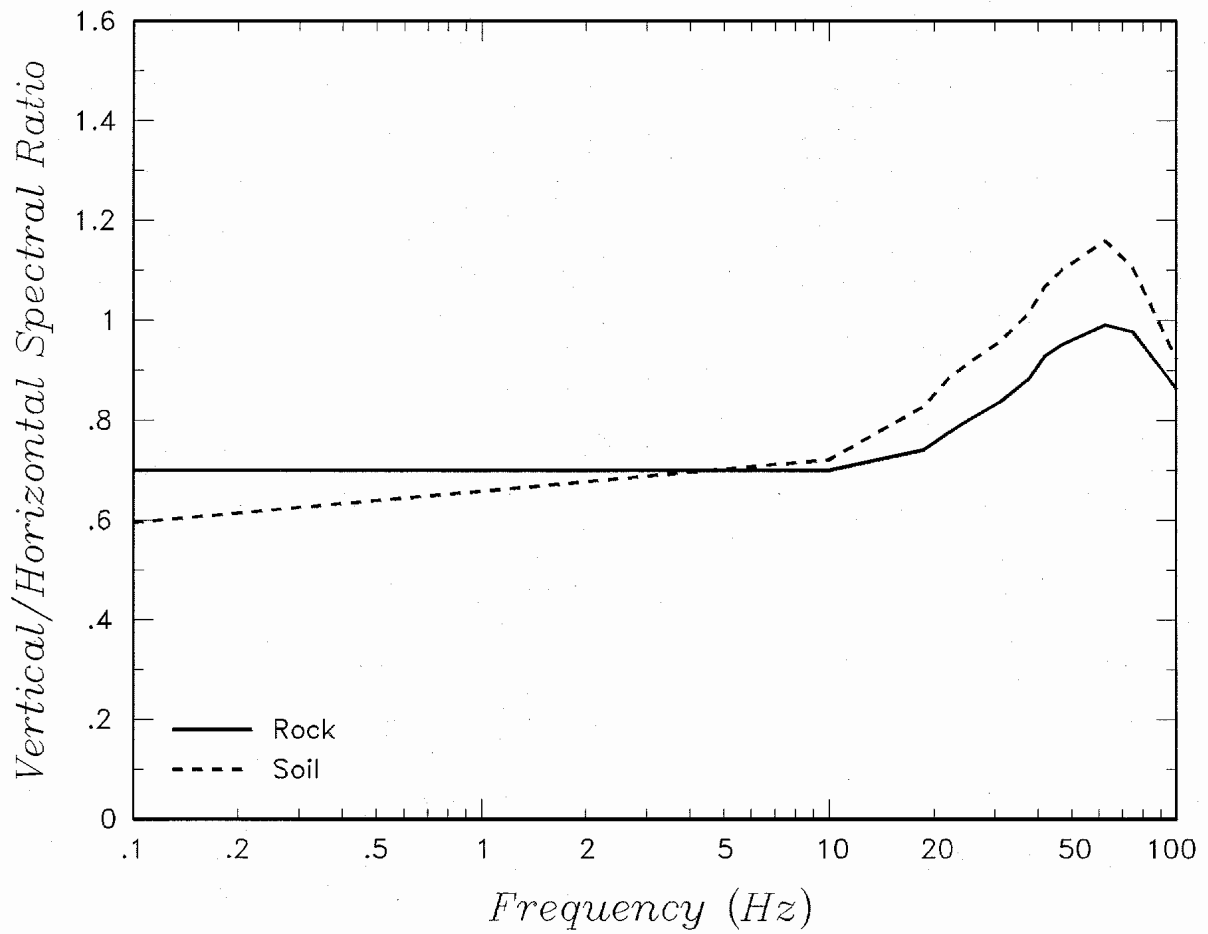
Seismic Hazards Report for the EGC ESP Site
**Weighted Average Vertical/Horizontal Response Spectral Ratios for Rock Site
Conditions for Mean 10^{-4} Hazard Level at EGC ESP Site**

Figure
4.3-3



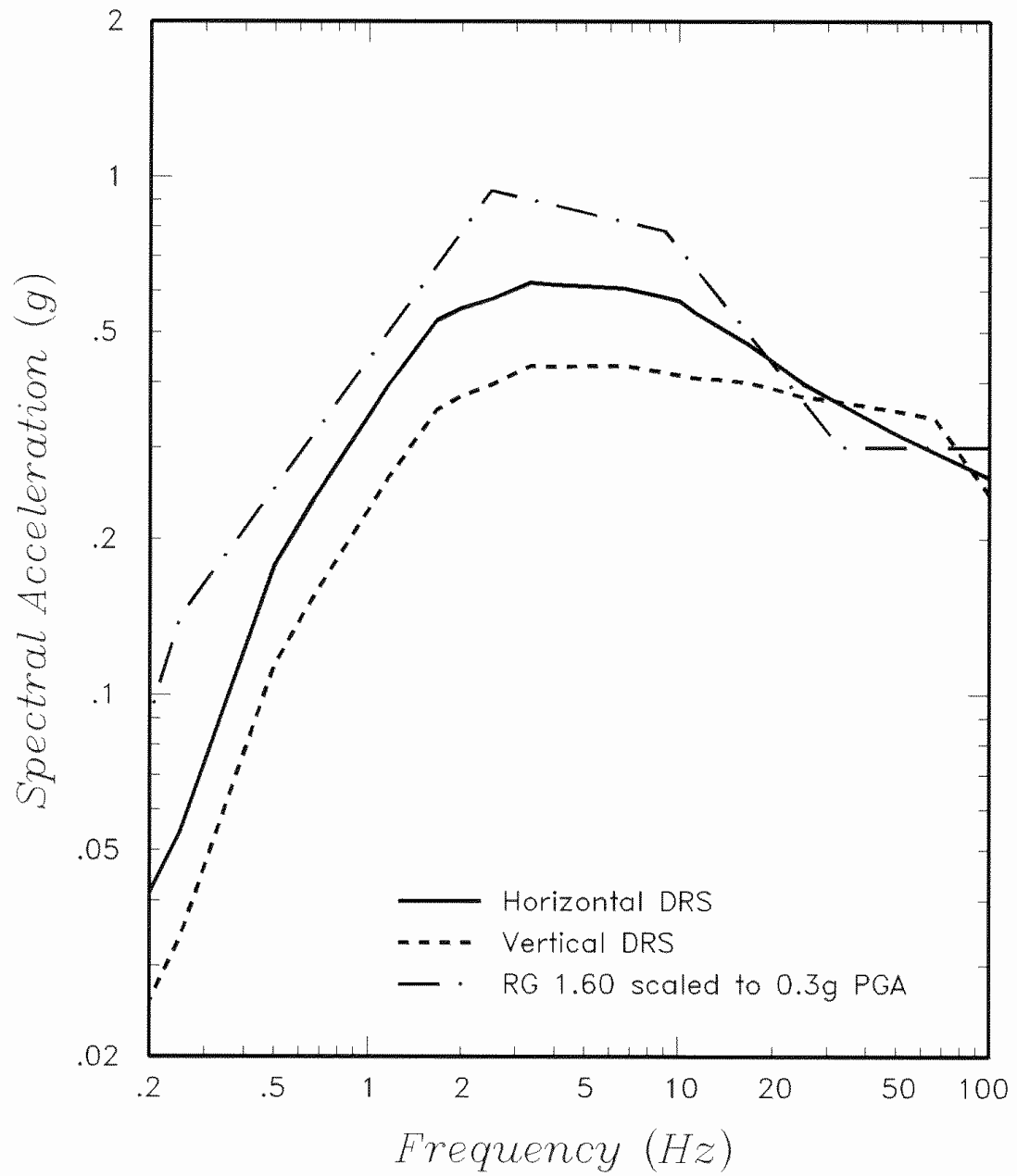
Seismic Hazards Report for the EGC ESP Site
**Vertical/Horizontal Response Spectral Ratios for WUS Rock and Soil Rock
 Site Conditions Based on Empirical Ground Motion Models**

Figure
4.3-4



Seismic Hazards Report for the EGC ESP Site
**Vertical/Horizontal Response Spectral Ratios for Rock and Soil Site
 Conditions Developed for Mean 10^{-4} Hazard Level at EGC ESP Site**

Figure
4.3-5



Seismic Hazards Report for the EGC ESP Site
Horizontal and Vertical DRS Spectra Defining EGC ESP SSE Spectra

Figure
4.3-6

Surface Faulting

This chapter describes the evidence gathered to date for faulting or the absence of faulting in the region of the EGC ESP Site. The following aspects of the geology and seismicity of the site region are discussed:

- geologic evidence, or lack thereof, for surface deformation (Section 5.1);
- earthquakes associated with capable tectonic sources (Section 5.2);
- ages of most recent deformation (Section 5.3);
- relationship between tectonic structures in the site area and regional structures (Section 5.4);
- characterization of identified capable tectonic sources (Section 5.5);
- identified zones of Quaternary deformation (Section 5.6); and
- the potential for surface tectonic deformation at the site (Section 5.7).

There is no evidence for surface faulting or fold deformation at the EGC ESP Site, and no earthquakes or capable tectonic sources have been identified within 25 miles of the site. Paleoliquefaction studies performed for this study identified locations that reveal evidence for possible paleoliquefaction (detailed in Attachment 1) possibly associated with prehistoric earthquakes. No evidence has been found for surface faulting or deformation that would pose a hazard to the EGC ESP Site. No evidence for tectonic Quaternary faulting or surface deformation was found during geologic reconnaissance for this study or in previous studies.

5.1 Geologic Evidence, or Absence of Evidence, for Surface Deformation

There is no evidence for surface faulting or fold deformation at the EGC ESP Site. Recent detailed geotechnical investigations of the site were used to develop a site-specific geologic cross section (Figure 5.1-1). Irregularities in the upper units (Illinoian glacial till and younger strata) are not reflected in the older units. In particular, the contact between a lacustrine unit and the overlying Illinoian till is flat-lying across the entire site.

5.2 Earthquakes Associated with Capable Tectonic Sources

There have been no historically reported earthquakes within 25 miles of the site that reasonably can be associated with a local structure.

Historical earthquakes have been postulated to be associated with faults and inferred structures at greater distances within the site region, as noted below. The evidence for

capable tectonic sources inferred from the historical seismicity is considered in the characterization of alternative seismic sources included in the probabilistic seismic hazard analysis (PSHA; Section 4).

A spatial association of recent small earthquakes has been postulated for the northern part of the Peru monocline (Larson, 2002). The southern part of this structure extends to within approximately 50 miles of the site (Plate 1).

The lower Wabash Valley surrounding and south of the Vincennes bend has long been recognized as slightly more active than surrounding regions. Historical earthquakes have occurred along the Commerce geophysical lineament (CGL) in this region (Langenheim and Hildenbrand, 1997). McBride et al. (2002a) report that the hypocenter for the largest historical earthquake in the site region (November 9, 1968, m_{bLg} 5.5) corresponds to the most prominent zone of dipping middle-crustal reflections, just west of the Wabash Valley fault system. McBride et al. (2002a) suggest that contemporary stress may be being released by the reactivation of Precambrian and/or Paleozoic structures. The width of the inferred fault system that underlies the CGL southwest of the Vincennes bend is approximately 1.5 to 3 miles, as imaged in deep seismic-reflection profiles (McBride et al., 2002a).

A spatial association of seismicity also is suggested along the trend of the Du Quoin monocline trend and Centralia fault zone in south-central Illinois. Su and McBride (1999) state that current deformation along this structure is suggested by earthquakes located near structural axes and having focal mechanisms consistent with strike slip along north-trending structures. These structures also are associated with a basement-involved fault, as documented from seismic-reflection profiles.

5.3 Ages of Most Recent Deformation

The evidence for possible Pleistocene and Holocene surface deformation and the association of seismicity with the structures described above suggest that there may be capable tectonic sources within the study region (the 200-mile radius of the site). The ages of most recent deformation on faults and folds within the study region are summarized on Tables 2.1-1 and 2.1-2.

Paleoliquefaction studies were conducted as part of this study to search for evidence of nearby prehistoric earthquakes. The results of these investigations (Section 2.1.4 and Attachment 1) suggest that no repeated moderate to large events (comparable to the postulated **M** 6.2 to 6.8 Springfield earthquake) occurred in the site vicinity in latest Pleistocene to Holocene time that would indicate a capable tectonic structure within 25 miles of the EGC ESP Site. The late Holocene record in particular is sufficient to demonstrate the absence of such events in the past approximately 6 to 7 ka. The latest Pleistocene/early Holocene record is less complete. The significance of the latest Pleistocene/early Holocene features recorded at location SC 25, approximately 17 miles from the site, is less certain. Only a limited number of features were found, providing insufficient information to estimate a location or magnitude if these features were caused by an earthquake. The presence of these features was considered in developing the range in maximum magnitude assigned to a random background earthquake in the probabilistic seismic hazard analysis.

5.4 Relationship of Tectonic Structures in the Site Area to Regional Tectonic Structures

Recent compilations of geologic structural data for the State of Illinois (i.e., Nelson, 1995) show no faults within a 25-mile radius of the site. Folds within the La Salle anticlinorium do lie within the 25-mile radius. Based on available data, as outlined in previous studies for the CPS (Section 2.5.1.2.3 of the CPS USAR), there is no evidence for tectonic surface deformation within 25 miles of the site that is associated with these structures. No reported evidence for tectonic surface deformation in the site region was found in the recent literature.

No active faults are postulated to be associated with the folds mapped within a 25-mile radius of the site (Nelson, 1995). In other regions reverse faults in the basement, imaged in deep seismic-reflection profiles, may be associated with historical seismicity (e.g., Wabash Valley seismic zone, McBride et al., 2002a). There is, however, no recorded historical seismicity associated with folds within 25 miles of the site.

5.5 Characterization of Capable Tectonic Sources

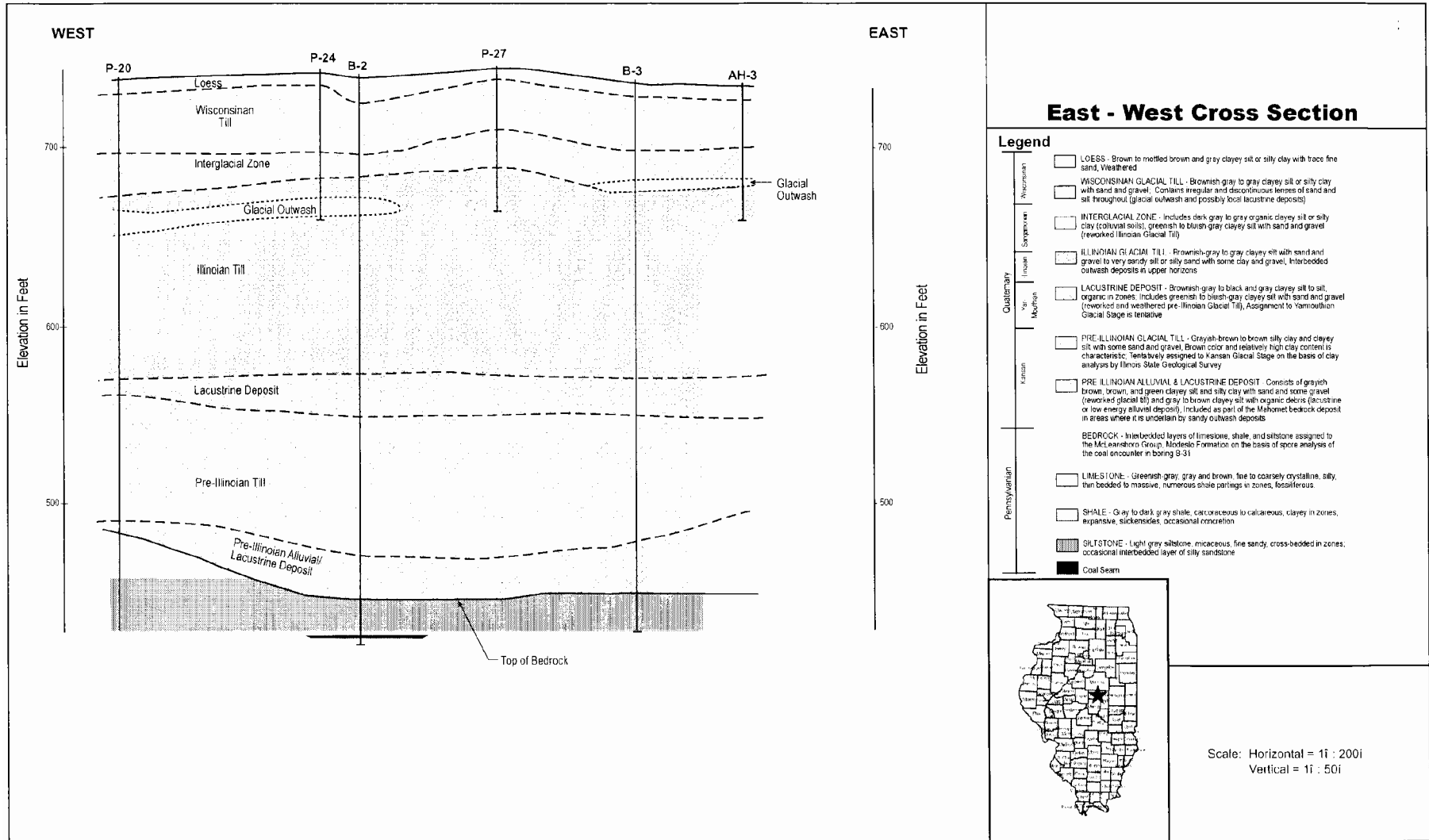
As noted in previous sections, no capable tectonic sources have been identified within 25 miles of the site.

5.6 Designation of Zones of Quaternary Deformation in Site Region

Geologic investigations of the CPS site identified no evidence of capable faulting in the site region (CPS USAR). Paleoliquefaction studies conducted in connection with the preparation of this ESP application identified locations that reveal possible evidence for paleoliquefaction (Attachment 1 to this Appendix). These features are indicative of possible seismic ground shaking associated with prehistoric earthquakes. No evidence for tectonic Quaternary faulting or surface deformation was observed during the field reconnaissance conducted along selected rivers in the study region as part of these investigations. No reported evidence for Quaternary deformation in the site region was found in the recent literature.

5.7 Potential for Surface Tectonic Deformation of Site

Previous investigations of the CPS site described in the CPS USAR, post-CPS USAR studies (e.g., published literature), and investigations conducted for this study have identified no evidence for surface faulting or deformation that would pose a hazard to the EGC ESP Site.



Seismic Hazards Report for the EGC ESP Site
Site-Specific Geologic Cross Section (from SSAR, Appendix A, 2003)

Figure
5.1-1

References

Abrahamson, N. A., and W. J. Silva. "Empirical Response Spectral Attenuation Relations for Shallow Crustal Earthquakes." *Seismological Research Letters*. Vol. 68, No. 1, pp. 9-23. 1997.

Ambraseys, N.N. "Engineering Seismology: Earthquake Engineering and Structural Dynamics." *Journal of the International Association of Earthquake Engineering*. Vol. 17. pp. 1-105. 1988.

American Society of Civil Engineers (ASCE). "Seismic Design Criteria for Structures, Systems, and Components in Nuclear Facilities and Commentary." ASCE Standard XXX, Approval Draft, July 25, 2003. American Society of Civil Engineers, Reston, VA. 2003.

Anderson, J.G. and S.E. Hough. "A Model for the Shape of the Fourier Amplitude Spectrum of Acceleration at High Frequencies." *Bulletin of the Seismological Society of America*. Vol. 74, No. 5. pp. 1969-1993. 1984.

Atkinson, G.M., and I.A. Beresnev. "Ground Motions at Memphis and St. Louis from M 7.5-8.0 Earthquakes in the New Madrid Seismic Zone." *Bulletin of the Seismological Society of America*. Vol. 92, No. 3. pp. 1015-1024. 2002.

Atkinson, G.M. and D.M. Boore. "Ground Motion Relations for Eastern North America." *Bulletin of the Seismological Society of America*. Vol. 85, No. 1. pp. 17-30. 1995.

Atkinson, G.M., and T.C. Hanks. "A High Frequency Magnitude Scale." *Bulletin of the Seismological Society of America*. Vol. 85, No. 3. pp. 825-833. 1995

Bakun, W.H., and M.G. Hopper. "The 1811-12 New Madrid, Missouri, and the 1886 Charleston, South Carolina, Earthquakes." *Bulletin of the Seismological Society of America*. 2003 (in press).

Bakun, W.H., and A. McGarr. "Differences in Attenuation among the Stable Continental Regions." *Geophysical Research Letters*. Vol. 29, No. 23. 4 pp. 2002.

Bakun, W.H., A.C. Johnston, and M.G. Hopper. "Estimating Locations and Magnitudes of Earthquakes in Eastern North America from Modified Mercalli Intensities." *Bulletin of the Seismological Society of America*. Vol. 93, No. 1. pp. 190-202. 2003.

Baldwin, J.N., A.D. Barron, K.I. Kelson, J.B. Harris, and S. Cashman. "Preliminary Paleoseismic and Geophysical Investigation of the North Farrenburg Lineament: Primary Tectonic Deformation Associated with the New Madrid North Fault." *Seismological Research Letters*. Vol. 73, No. 3. pp. 393-413. 2002.

Barnes, A.A. "An Interdisciplinary Study of Earthquake-Induced Liquefaction Features in the New Madrid Seismic Zone, Central United States." M.S. Thesis. Auburn University, Alabama, 266 pp. 2000.

Bauer, Robert. Illinois State Geological Survey. Written Communication. November 21, 2002.

Baxter, J.W., and G.A. Desborough. *Areal Geology of the Illinois Fluorspar District, Part 2 – Karbers Ridge and Rosiclare Quadrangles*. Illinois State Geological Survey Circular 385. 40 pp. 1965.

Bear, G.W., J.A. Rupp, and A.J. Rudman. "Seismic Interpretation of the Deep Structure of the Wabash Valley Fault System." *Seismological Research Letters*. Vol. 68, No. 4. pp. 624-640. 1997.

Becker, L.E., Head, Petroleum Section, Indiana Geological Survey, Letter to A. K. Yonk, Sargent & Lundy Senior Geologist, May 22, 1975: CPS USAR Attachment D2.5. 1975.

Bell, A.H., E. Atherton, T.C. Buschbach, and D.H. Swann. *Deep Oil Possibilities of the Illinois Basin*. Illinois State Geological Survey Circular 368. 38 pp. 1964.

Boore, D.M., and G.M. Atkinson. "Stochastic Prediction of Ground Motion and Spectral Response Parameters at Hard-Rock Sites in Eastern North America." *Bulletin of the Seismological Society of America*. Vol. 77, No. 2. pp. 440-467. 1987.

Braile, L.W., W.J. Hinze, J.L. Sexton, R.G. Keller, and E.G. Lidiak. *The Northeastern Extension of the New Madrid Seismic Zone*. U.S. Geological Survey Professional Paper 1236. pp. 175-184. 1982.

Braile, L.W., W.J. Hinze, G.R. Keller, E.G. Lidiak, and J.L. Sexton. "Tectonic Development of the New Madrid Rift Complex, Mississippi Embayment, North America." *Tectonophysics*. Vol. 131, pp. 1-21. 1986.

Braile, L.W., W.J. Hinze, and G.R. Keller. "New Madrid Seismicity, Gravity Anomalies and Interpreted Ancient Rift Structures." *Seismological Research Letters*. Vol. 68, No. 4. pp. 599-610. 1997.

Bristol, H.M., and R. Prescott. *Geology and Oil Production in the Tuscola Area, Illinois*. Illinois State Geological Survey Circular 424. 34 p. 1968.

Bristol, H.M., and J.D. Treworgy. *The Wabash Valley Fault System in Southeastern Illinois*. Illinois State Geological Survey Circular 509. 19 pp. 1979.

Broster, B.E. "Glacitectonic Deformation in Sediment and Bedrock, Hat Creek, British Columbia." *Geographie Physique et Quaternaire*. Vol. 45, No. 1. pp. 5-20. 1991.

Brune, J.N. "Tectonic stress and the spectra of seismic shear waves from earthquakes." *Journal of Geophysical Research*. Vol. 75, pp. 4997-5009. 1970.

Brune, J.N. "Correction." *Journal of Geophysical Research*. Vol. 76, pp. 5002. 1971.

Bunker, B.J., G.A. Ludvigson, and B.J. Witzke. *The Plum River Fault Zone and the Structural and Stratigraphic Framework of Eastern Iowa*. Iowa Geological Survey Technical Information Series Report 13. 126 pp. 1985.

Buschbach, T. C. Unpublished Notes, Attachment D2.5, Clinton Power Station Updated Safety Analysis Report (CPS-USAR). 1973.

- Buschbach, T. C., and G.E. Heim. *Preliminary Geologic Investigations of Rock Tunnel Sites for Flood and Pollution Control in the Greater Chicago Area*. Illinois State Geological Survey, Environmental Geology Note 52. 35 pp. 1972.
- Campbell, K.W. "Empirical near-source attenuation relationships for horizontal and vertical components of peak ground acceleration, peak ground velocity, and pseudo-absolute acceleration response spectra." *Seismological Research Letters*. Vol. 68, pp. 154-179. 1997.
- Campbell, K. W. Development of Semi-Empirical Attenuation Relations for the CEUS, USGS Annual Technical Summary. Available: <http://erp-web.er.usgs.gov/reports/annsum/vol43/ni/g0011.pdf>. 2001.
- Campbell, K.W. "Prediction of Strong Ground Motion Using the Hybrid Empirical Method and its Use in the Development of Ground-Motion (attenuation) Relations in Eastern North America." *Bulletin of the Seismological Society of America*. Vol. 93, No. 3. pp. 1012-1033. 2003.
- Chadwick, D.L. "Investigation of Recent Movement within the Rough Creek Fault Zone in McLean and Daviess Counties, Kentucky." Unpublished M.S. Thesis. Eastern Kentucky University, Richmond. 99 pp., 5 pl. Scale = 1:150. 1989.
- Champion, J., K. Mueller, A. Tate, and M. Guccione. "Geometry, Numerical Models, and Revised Slip Rate for the Reelfoot Fault and Trishear Fault-Propagation Fold, New Madrid Seismic Zone." *Engineering Geology*. Vol. 62. pp. 20-31. 2001.
- Chester, J. S., and M.P. Tuttle. "Paleoseismology in the Cache River Valley, Southern Illinois." *Technical Progress Report Submitted to U.S. Geological Survey National Earthquake Hazards Reduction Program*. U.S.G.S. External Grant Nos. 1434-HQ-98-GR-00013 and 1434-HQ-98-GR-00015. 2000.
- Chiu, S-C. C., J-M. Chiu, and A.C. Johnston. "Seismicity of the Southeastern Margin on Reelfoot Rift, Central United States." *Seismological Research Letters*. Vol. 68. pp. 785-796. 1997.
- Clegg, K.E. *Subsurface Geology and Coal Resources of the Pennsylvanian System in Clark and Edgar Counties, Illinois*. Illinois State Geological Survey Circular 380. 28 pp. 1965.
- Clegg, K.E. *Subsurface Geology and Coal Resources of the Pennsylvanian System in De Witt, Mclean, and Piatt Counties, Illinois*. Illinois State Geological Survey Circular 473. 25 pp. 1972.
- Clendenin, C.W., G.R. Lowell, and C.A. Niewendorp. "Sequencing Reelfoot Extension Based on Relations from Southeast Missouri and Interpretations of the Interplay between Offset Preexisting Zones of Weakness." *Tectonics*. Vol. 12. pp. 703-712. 1993.
- Cox, R.T., R.B. Van Arsdale, J.B. Harris, and D. Larsen. "Neotectonics of the Southeastern Reelfoot Rift Zone Margin, Central United States, and Implications for Regional Strain Accommodation." *Geology*. Vol. 29, No. 5. pp. 419-422. 2001.
- Cramer, C.H. "A Seismic Hazard Uncertainty Analysis for the New Madrid Seismic Zone." *Engineering Geology*. Vol. 62. pp. 251-266. 2001.
- Cramer, C.H., R.L. Wheeler, and C.S. Mueller. "Uncertainty Analysis for Seismic Hazard in the Southern Illinois Basin." *Seismological Research Letters*. Vol. 73, No. 5. pp. 792-805. 2002.

- Craven, J.A. *Paleoseismological Study in the New Madrid Seismic Zone using Geological and Archeological Features to Constrain Ages of Liquefaction Deposits*. Unpublished M. S. Thesis. University of Memphis. 51 pp. 1995.
- Crone, A.J. "Defining the Southwestern End of the Blytheville Arch, Northeastern Arkansas: delimiting a Seismic Source Zone in the New Madrid Region." *Seismological Research Letters*. Vol. 69, No. 4. pp. 350-358. 1998.
- Crone, A.J., and R.L. Wheeler. "Data for Quaternary Faults, Liquefaction Features, and Possible Tectonic Features in Central and Eastern United States, East of the Rocky Mountain Front." U.S. Geological Survey Open File Report 00-260, 332 pp. 2000.
- Dart, R.L., and H.S. Swolfs. "Contour Mapping of Relic Structures in the Proterozoic Basement of the Reelfoot Rift, North American Midcontinent." *Tectonics*. Vol. 17, No. 2. pp. 235-249. 1998.
- Dreimanis, A. "Downward Injected Till Wedges and Upward Injected Till Dikes." In Robertson, A.M., B. Ringberg, U. Miller, and L. Brunnberg (eds.). *Quaternary Stratigraphy, Glacial Morphology, and Environmental Changes*, Research paper. Geological Survey of Sweden, Serie Ca81. pp. 91-96. 1992.
- Dreimanis, A., and M. Rappol. "Late Wisconsinan Sub-Glacial Clastic Intrusive Sheets along Lake Erie Bluffs at Bradtville, Ontario, Canada." *Sedimentary Geology*. Vol. 111. pp. 225-248. 1997.
- DuBois, E.P., and R. Siever. *Structure of the Shoal Creek Limestone and Herrin (No. 6) Coal in Wayne County, Illinois*. Illinois State Geological Survey Report of Investigations 182. 7 pp. 1955.
- Eardley, A.J. *Structural Geology of North America*. Harper & Brothers, New York, New York. 624 pp. 1951.
- Electric Power Research Institute (EPRI). *Probabilistic Seismic Hazard Evaluations at Nuclear Power Plant Sites in the Central and Eastern United States*. NP-4726. 9 Vol. 1989-1991.
- Electric Power Research Institute (EPRI). *Guidelines for Determining Design Basis Ground Motions*. Electric Power Research Institute. Vol. 1, No. 5, EPRI TR-102293. Palo Alto, California. 1993.
- Electric Power Research Institute (EPRI). *CEUS Ground Motion Project – Model Development and Results*. EPRI Technical Report 1008910. 2003.
- Ellis, W.L. *Summary and Discussion of Crustal Stress Data in the Region of the New Madrid Seismic Zone*. in Shedlock, K.M., and A.C. Johnston, *Investigations of the New Madrid Seismic Zone*. U. S. Geological Survey Professional Paper 1538-B. pp. B1-B12. 1994.
- Evans, T.J., K.M. Massie-Fereh, and R.M. Peters. "Bedrock Geology of Walworth, Kenosha, Racine, Waukesha, Milwaukee, Ozaukee, and Washington Counties, Wisconsin." Wisconsin Geological and Natural History Survey. 2003 (in preparation).
- Folmer, Leon. Illinois Geological Survey. Personal Communication. October 15, 2002.

Frankel, A., C. Mueller, T. Barnhard, D. Perkins, E.V. Leyendecker, N. Dickman, S. Hanson, and M. Hopper. *National Seismic-Hazard Maps*. Documentation June 1996. U. S. Geological Survey Open-File Report 96-532. 1996.

Frankel, A.D., M.D. Petersen, C.S. Mueller, K.M. Haller, R.L. Wheeler, E.V. Leyendecker, R.L. Wesson, S.C. Harmsen, C.H. Cramer, D.M. Perkins, and K.S. Rukstales. *Documentation for the 2002 Update of the National Seismic Hazard Maps*. U. S. Geological Survey Open-File Report 02-420. 33 pp. 2002.

Fraser, G.S., T.A. Thompson, G.A. Olyphant, L. Furer, and S.W. Bennett. "Geomorphic Response to Tectonically-Induced Ground Deformation in the Wabash Valley." *Seismological Research Letters*. Vol. 68, No. 4. pp. 662-674. 1997.

Fuller, Mossbarger, Scott & May Engineers. *J. T. Myers Locks and Dam Seismological Study, Summary of Deterministic and Probabilistic Seismic Hazard Analyses and Generation of Time Histories Report*. Prepared for U.S. Army Corps of Engineers, Louisville, Kentucky. August 2001.

Gordon, D.W. *Revised Instrumental Hypocenters and Correlation of Earthquake Locations and Tectonics in the Central United States*. U.S. Geological Survey Professional Paper 1364. 69 pp. 1988.

Gray, H.H., Head Stratigrapher, Indiana Geological Survey. *Letter to G. E. Heim, Sargent & Lundy Senior Geologist*. CPS-USAR Attachment D2.5. October 15, 1974.

Green, D.A. "Trenton Structure in Ohio, Indiana, and Northern Illinois." *Bulletin of the American Association of Petroleum Geologists*. Vol. 41. pp. 627-642. 1957.

Green, R.A. *Energy-Based Evaluation and Remediation of Liquefiable Soils*. Ph.D. Dissertation. Virginia Polytechnic Institute and State University. 394 pp. 2001.

Grollimund, B., and M.D. Zoback. "Did Deglaciation Trigger Intraplate Seismicity in the New Madrid Seismic Zone?" *Geology*. Vol. 29, No. 2. pp. 175-178. 2001.

Hajic, E.R., M.D. Wiant, and J.J. Oliver. *Distribution and Dating of Prehistoric Earthquake Liquefaction in Southeastern Illinois, Central U. S.* Final Technical Report Submitted to the U. S. Geological Survey National Earthquake Hazards Reduction Program. Contract No. 1434-93-G-2359. 33 pp. 1995.

Hamburger, M.W., V. Rybakov, A. Lowry, B. Shen-Tu, and J.A. Rup. "Preliminary Results from a GPS Geodetic Network in the Southern Illinois Basin." *Seismological Research Letters*. Vol. 73, No. 5. pp. 762-775. 2002.

Hansel, A.K., and W.H. Johnson. *Wedron and Mason Groups: Lithostratigraphic Reclassification of Deposits of the Wisconsin Episode, Lake Michigan Lobe Area*. Department of Natural Resources Illinois State Geological Survey Bulletin 104. 116 pp. 1996.

Harris, S.E. Jr., and M.C. Parker. *Stratigraphy of the Osage Series in Southeastern Iowa*. Iowa Geological Survey, Report of Investigations 1. 52 pp. 1964.

Harrison, R.W., and A. Schultz. "Strike-Slip Faulting at Thebes Gap, Missouri and Illinois, Implications for New Madrid Tectonism." *Tectonics*. Vol. 13, No. 2. pp. 246-257. 1994.

Harrison, R.W., and A. Schultz. "Tectonic Framework of the Southwestern Margin of the Illinois Basin and its Influence on Neotectonism and Seismicity." *Seismological Research Letters*. Vol. 73, No. 5. pp. 698-731. 2002.

Harrison, R.W., D. Hoffman, J.R. Palmer, J.D. Vaughn, and A. Schultz. "Late Quaternary Deformation on the English Hill Fault, Southeast Missouri." (abs.) *Geological Society of America Abstracts with Programs*. Vol. 26, No. 6. p. A-389. 1995.

Harrison, R.W., D. Hoffman, J.R. Palmer, J.D. Vaughn, J.R. Palmer, C.L. Wiscombe, J.P. McGeehin, W.J. Stephenson, J.K. Odum, R.A. Williams, and S.L. Forman. "An Example of Neotectonism in a Continental Interior – Thebes Gap, Midcontinent, United States." *Tectonophysics*. Vol. 305. pp. 399-417. 1999.

Heigold, PP. C. *Notes on the Earthquake of September 15, 1972, in Northern Illinois*. Illinois State Geological Survey Environmental Geology Note 59. 15 pp. 1972.

Heigold, PP. C., and D.R. Kolata. "Proterozoic Crustal Boundary in the Southern Part of the Illinois Basin." *Tectonophysics*. Vol. 217. pp. 307-319. 1993.

Heigold, PP. C., and T.H. Larson. *Geophysical Investigations of Possible Recent Ground Deformation and Neotectonism in White County, Illinois*. Illinois State Geological Survey Open File Series 1994-5, Final Report to the National Earthquake Hazard Reduction Program, U. S. Geological Survey. 22 pp. 1994.

Herrmann, R.B. "Surface Wave Focal Mechanisms for Eastern North American Earthquakes with Tectonic Implications." *Journal of Geophysical Research*. Vol. 84, No. B7. pp. 3543-3552. 1979.

Herrmann, R.B., C.J. Ammon, F. Leyton, F., and A. Fatchi. "Focal Mechanisms for Recent Earthquakes in the ANSS Mid-America Region" (abs.). *American Geophysical Union EOS Transactions*. Vol. 83, No. 47. Fall Meeting Supplement. p. F1069. 2002.

Heyl, A.V., Jr. "The 38th Parallel Lineament and its Relationship to Ore Deposits." *Economic Geology*. Vol. 67, No. 7, pp. 879-894. 1972.

Heyl, A.V. Jr., A.F. Agnew, E.J. Lyons, and C.H. Behre Jr. *The Geology of the Upper Mississippi Valley Zinc-Lead District*. U. S. Geological Survey Professional Paper 309, 310 pp. 1959.

Hildenbrand, T.G., and J. Hendricks. *Geophysical Setting of the Reelfoot Rift and Relations between Rift Structures and the New Madrid Seismic Zone*. U. S. Geological Survey Professional Paper 1538-E. 1995.

Hildenbrand and Kucks, 1992. Hildenbrand, T.G., and R.P. Kucks. "Filtered Magnetic Anomaly Maps of Missouri." U.S. Geological Survey Geophysical Investigations Series Map GP-1000, 2 sheets, scale 1:1,000,000. 1992.

Hildenbrand, T.G., and D. Ravat. "Geophysical Setting of the Wabash Valley Fault System." *Seismological Research Letters*. Vol. 68, No. 4, pp. 1997.

Hildenbrand, T.G., R.P. Kucks, and R.E. Sweeney. "Digital Magnetic-Anomaly Map of Central United States: Description of Major Features." U.S. Geological Survey Geophysical Investigations Map GP-955, scale 1:2,500,000. 1983.

- Hildenbrand, T.G., W.D. Stuart, and P. Talwani. "Geologic Structures Related to New Madrid Earthquakes Near Memphis, Tennessee, Based on Gravity and Magnetic Interpretations." *Engineering Geology*. Vol. 62. pp. 105-121. 2001.
- Hildenbrand, T. G., J. H. McBride, and D. Ravat. The Commerce Geophysical Lineament and its Possible Relation to Mesoproterozoic Igneous Complexes and Large Earthquakes in the Central Illinois Basin. *Seismological Research Letters*. Vol. 73, No. 5, pp. 640-659. 2002.
- Hough, S., J.G. Armbruster, L. Seeber, and J.F. Hough. "On the Modified Mercalli Intensities and Magnitudes of the 1811-1812 New Madrid, Central United States, Earthquakes." *Journal of Geophysical Research*. Vol. 105, No. B10. pp. 23,839-23,864. 2000.
- Hwang, H., and J. R. Huo. "Attenuation Relations of Ground Motion for Rock and Soil Sites in Eastern United States." *Soil Dynamics and Earthquake Engineering*. Vol. 16, pp. 363-372. 1997.
- Indiana Geological Survey. Structural_Features_SW: Structural Features of Southwestern Indiana (Indiana Geological Survey, Line Shapefile). Available: http://igs.indiana.edu/arcIMS/southwest/Metadata/Structural_Features_sw.html. [29.05.2003]. 2001.
- Johnston, A.C. "Seismic Moment Assessment of Earthquakes in Stable Continental Regions – III. New Madrid 1811-1812, Charleston 1886, and Lisbon 1755." *Geophysical Journal International*. Vol. 126. pp. 314-344. 1996.
- Johnston, A.C., and E.S. Schweig. "The Enigma of the New Madrid Earthquakes of 1811-1812." *Annual Review of Earth and Planetary Sciences*. Vol. 24. pp. 339-384. 1996.
- Johnston, A.C., K.J. Coppersmith, L.R. Kanter, and C.A. Cornell. *The Earthquakes of Stable Continental Regions, Volume 1; Assessment of Large Earthquake Potential, Final Report* Submitted to Electric Power Research Institute (EPRI). TR-102261-VI. 1994.
- Kane, M.F., T.G. Hildenbrand, and J.D. Hendricks. "Model for the Tectonic Evolution of the Mississippi Embayment and its Contemporary Seismicity." *Geology*. Vol. 9. pp. 563-568. 1981.
- Kelson, K.I., R.B. Van Arsdale, G.D. Simpson, and W.R. Lettis. "Assessment of the Style and Timing of Surficial Deformation along the Central Reelfoot Scarp, Lake County, Tennessee." *Seismological Research Letters*. Vol. 63, No. 3. pp. 349-356. 1992.
- Kelson, K.I., G.D. Simpson, R.B. Van Arsdale, C.C. Haraden, and W.R. Lettis. "Multiple Late Holocene Earthquakes along the Reelfoot Fault, Central New Madrid Seismic Zone." *Journal of Geophysical Research*. Vol. 101, No. B3. pp. 6151-6170. 1996.
- Kenner, S., and P. Segall. "A Mechanical Model for Intraplate Earthquakes: Application to the New Madrid Seismic Zone." *Science*. Vol. 289. pp. 2329-2332. 2000.
- Kolata, D.R., and T.C. Buschbach. *Plum River Fault Zone of Northwestern Illinois*. Illinois State Geological Survey Circular 491. 20 pages. 1976.

- Kolata, D.R., and Hildenbrand, T.G. "Structural Underpinnings and Neotectonics of the Southern Illinois Basin: An Overview." *Seismological Research Letters*. Vol. 68, No. 4. pp. 499-510. 1997.
- Kolata, D.R., and W.J. Nelson. "Tectonic History of the Illinois Basin." In Leighton, M.W., D.R. Kolata, D.F. Oltz, and J.J. Eidel (eds.). *Interior Cratonic Basins. American Association of Petroleum Geologists Memoir*. Vol. 51. pp. 263-285. 1991.
- Kolata, D.R., and W.J. Nelson. "Role of the Reelfoot Rift/Rough Creek Graben in the Evolution of the Illinois Basin." In Ojakangas, R.W., A.B. Dickas, and J.C. Green (eds.). *Middle Proterozoic to Cambrian Rifting, Central North America*. Geological Society of America Special Paper 312. pp. 287-298. 1997.
- Kolata, D.R., T.C. Buschbach, and J.D. Treworgy. *The Sandwich Fault Zone of Northern Illinois*. Illinois State Geological Survey Circular 505. 26 pp. 1978.
- Langenheim, V.E., and T.G. Hildenbrand. "Commerce Geophysical Lineament – Its Source, Geometry, and Relation to the Reelfoot Rift and New Madrid Seismic Zone." *Geological Society of America Bulletin*. Vol. 109, No. 5. pp. 580-595. 1997.
- Langer, C.J., and G.A. Bollinger. "The Southeastern Illinois Earthquake of 10 June 1987: The Later Aftershocks." *Bulletin of the Seismological Society of America*. Vol. 81. pp. 423-445. 1991.
- Larson, T.H. "The Earthquake of September 2, 1999, in Northern Illinois: Big Lessons from a Small Earthquake." Illinois State Geological Survey. *Environmental Geology* 153. pp. 1-22. 2001.
- Larson, T.H. "The Earthquake of 2 September 1999 in Northern Illinois: Intensities and Possible Neotectonism." *Seismological Research Letters*. Vol. 73, No. 5. pp. 732-738. 2002.
- Li, Y., E.S. Schweig, M.P. Tuttle, and M.A. Ellis. "Evidence for Large Prehistoric Earthquakes in the Northern New Madrid Seismic Zone, Central United States." *Seismological Research Letters*. Vol. 69. pp. 270-276. 1998.
- Marshak, S., and T. Paulsen. "Structural Style, Regional Distribution, and Seismic Implications of Midcontinent Fault-and-Fold Zones, United States." *Seismological Research Letters*. Vol. 68, No. 4. pp. 511-520. 1997.
- Mateker, E. J., and R.L. Segar. "Gravity investigation along the eastern flank of the Ozark uplift." *EOS Transactions, American Geophysical Union*, Vol. 46, pp. 160. 1965.
- Mateker, E.J., M.J. Phelan, and L. Scharon. "Geophysical Evidence for a Northeast Crustal Lineament near St. Louis." *Transactions of the American Geophysical Union*. Vol. 47. pp. 192. 1966.
- McBride, J.H., and D.R. Kolata. "Upper Crust beneath the Central Illinois Basin, United States." *Geological Society of America Bulletin*. Vol. 111. pp. 372-394. 1999.
- McBride, J. H., and W.J. Nelson. "Style and Origin of Mid-Carboniferous Deformation in the Illinois Basin, USA – Ancestral Rockies Deformation?" *Tectonophysics*. Vol. 305. pp. 249-273. 1999.

- McBride, J.H., and W.J. Nelson. "Seismic Reflection Images of Shallow Faulting, Northernmost Mississippi Embayment, North of the New Madrid Seismic Zone." *Bulletin of the Seismological Society of America*. Vol. 91. pp. 128-139. 2001.
- McBride, J.H., M.L. Sargent, and C.J. Potter. "Investigating Possible Earthquake-Related Structure Beneath the Southern Illinois Basin from Seismic Reflection." *Seismological Research Letters*. Vol. 68, No. 4, pp. 641-649. 1997.
- McBride, J.H., T.G. Hildenbrand, W.J. Stephenson, and C.J. Potter. "Interpreting the Earthquake Source of the Wabash Valley Seismic Zone (Illinois, Indiana, and Kentucky) from Seismic Reflection, Gravity, and Magnetic Intensity." *Seismological Research Letters*. Vol. 73, No. 5. pp. 660-686. 2002a.
- McBride, J.H., W.J. Nelson, and W.J. Stephenson. "Integrated Geological and Geophysical Study of Neogene and Quaternary-Age Deformation in the Northern Mississippi Embayment." *Seismological Research Letters*. Vol. 73, No. 5. pp. 597-627. 2002b.
- McBride, J.H., D.R. Kolata, and T.G. Hildenbrand. "Geophysical Constraints on Understanding the Origin of the Illinois Basin and its Underlying Crust." *Tectonophysics*. Vol. 363. pp. 45-78. 2003.
- McCracken, M.H. *Structural Features of Missouri*. Missouri Geological Survey and Water Resources Report of Investigations No. 49. 99 pp. 1971.
- McGinnis, L.D. *Crustal Tectonics and Precambrian Basement in Northeastern Illinois*. Illinois State Geological Survey Report of Investigations 219. 29 pp. 1966.
- McGuire, R.K., G.R. Toro, and W.J. Silva. *Engineering Model of Earthquake Ground Motion for Eastern North America*. Electric Power Research Institute Technical Report NP-6074. 1988.
- McGuire, R.K., W.J. Silva, and C.J. Costantino. "Technical Basis for Revision of Regulatory Guidance on Design Ground Motions: Hazard- and Risk-Consistent Ground Motion Spectra Guidelines." U.S. Nuclear Regulatory Commission Technical Report NUREG/CR-6728. 2001.
- McGuire, R. K., W. J. Silva, and C. J. Costantino "Technical Basis for Revision of Regulatory Guidance on Design Ground Motions: Development of Hazard-and Risk-Consistent Seismic Spectra for Two Sites." U.S. Nuclear Regulatory Commission Technical Report NUREG/CR-6769. 2002.
- McKeown, F.A., R.M. Hamilton, S.F. Diehl, and E.E. Glick. "Diapiric Origin of the Blytheville and Pascola Arches in the Reelfoot Rift, East Central United States: Relation to the New Madrid Seismic Zone." *Geology*. Vol. 18. pp. 1158-1162. 1990.
- McNulty, W.E., and S.F. Obermeier. "Liquefaction Evidence for at least Two Strong Holocene Paleoearthquakes in Central and Southwestern Illinois, USA." *Environmental and Engineering Geoscience*. Vol. 5, No. 2, pp. 133-146. 1999.
- McQueen, H.S., N.S. Hinchey, and K. Aid. *The Lincoln Fold in Lincoln, Pike, and Ralls, Counties, Northeastern Missouri*. Missouri Geological Survey and Water Resources, Report of Investigations No. 27. pp. 81-85. 1961.

Melhorn, W.N., and N.M. Smith. *The Mt. Carmel Fault and Related Structural Features in South-Central Indiana*. Indiana Geological Survey Report of Progress No. 16,,29 pp. 1959.

Mihills, R.K., and R.B. Van Arsdale. "Late Wisconsin to Holocene Deformation in the New Madrid Seismic Zone." *Bulletin of the Seismological Society of America*. Vol. 89. pp. 1019-1024. 1999.

Mueller, C., M. Hopper, and A. Frankel. "Preparation of Earthquake Catalogs for the National Seismic-Hazard Maps: Contiguous 48 States." U.S. Geological Survey Open-File Report 97-464. 1997.

Mueller, K. and J. Pujol. "Three-Dimensional Geometry of the Reelfoot Blind Thrust: Implications for Moment Release and Earthquake Magnitude in the New Madrid Seismic Zone." *Bulletin of the Seismological Society of America*. Vol. 91. pp. 1563-1573. 2001.

Mueller, K., J. Champion, M. Guccione, and K. Kelson. "Fault Slip Rates in the Modern New Madrid Seismic Zone." *Science*. Vol. 286. pp. 1135-1138. 1999.

Munson, PP. J., S.M. Obermeier, C.A. Munson, and E.R. Hajic. "Liquefaction Evidence for Holocene and Latest Pleistocene in the Southern Halves of Indiana and Illinois – A Preliminary Overview." *Seismological Research Letters*. Vol. 68, No. 4. pp. 523-536. 1997.

Nelson, W.J. "Structural Styles of the Illinois Basin." In Leighton, M.S., D.R. Kolata, D.F. Oltz, and J.J. Eidel (eds.). *Interior Cratonic Basins*. American Association of Petroleum Geologists Memoir 51, pp. 209-243. 1991.

Nelson, W.J. *Structural Features in Illinois*. Illinois State Geological Survey Bulletin 100. 144 pp. 1995.

Nelson, W.J., and R.A. Bauer. "Thrust Faults in Southern Illinois Basin – Results of Contemporary Stress?" *Geological Society of America Bulletin*. Vol. 98, pp. 302-307. 1987.

Nelson, W.J., and D.K. Lumm. *Structural Geology of Southeastern Illinois and Vicinity*. Illinois State Geological Survey Circular 538. 70 pages. 1987.

Nelson, K.D., and J. Zhang. "A COCORP Deep Reflection Profile across the Buried Reelfoot Rift, South-Central United States." *Tectonophysics*. Vol. 197. pp. 271-293. 1991.

Nelson, W.J., F.B. Denny, J.A. Devera, L.R. Follmer, and J.M. Masters. "Tertiary and Quaternary Tectonic Faulting in Southernmost Illinois." *Engineering Geology*. Vol. 46. pp. 235-258. 1997.

Nelson, W.J., F.B. Denny, L.R. Follmer, and J.M. Masters. "Quaternary Grabens in Southernmost Illinois: Deformation near an Active Intraplate Seismic Zone." *Tectonophysics*. Vol. 305, pp. 381-397. 1999.

Newman, A.S., J. Stein, J. Weber, J. Engeln, A. Mao, and T. Dixon. "Slow Deformation and Lower Seismic Hazard at the New Madrid Seismic Zone." *Science*. Vol. 284. pp. 622. 1999.

Newmark, N.M., and W.J. Hall. *Earthquake Spectra and Design*. Earthquake Engineering Research Institute. Berkeley, California. 1982.

Noger, M.C. (compiler) "Geologic Map of Kentucky." U.S. Geological Survey and Kentucky Geological Survey, 1 sheet, scale 1:500,000. 1988.

Nuttli, O.W. Letter to J.B. Savy. in Bernreuter, D., J. Savy, R. Mensing, J. Chen, and B. Davis. *Seismic Hazard Characterization of 69 Nuclear Plant Sites East of the Rocky Mountains: Questionnaires*. Prepared by the Lawrence Livermore National Laboratory. U.S. Nuclear Regulatory Commission Technical Report NUREG/CR-5250, UCID-21517. Vol. 7. 1989. Letter dated 1986.

Obermeier, S.F. "Using liquefaction-induced features for paleoseismic analysis." In J.P.P. McCalpin (ed.). *Paleoseismology*. Academic Press Inc., San Diego, pp. 331-396. 1996.

Obermeier, S.F. "Liquefaction Evidence for Strong Earthquakes of Holocene and Latest Pleistocene Ages in the States of Indiana and Illinois, USA." *Engineering Geology*. Vol. 50. pp. 227-254. 1998.

Obermeier, S.F., U. S. Geological Survey, Emeritus, Reston, Virginia; EqLiq Consulting. Written (electronic mail) Communication to Kathryn Hanson. January 10, 2003.

Obermeier, S.F., U. S. Geological Survey, Emeritus, Reston, Virginia; EqLiq Consulting. Written (electronic mail) Communication to Kathryn Hanson. May 13, 2003.

Obermeier, S.F., N.K. Bleuer, C.A. Munson, P.J. Munson, W.S. Marin, K.M. McWilliams, D.A. Tabaczynski, J.K. Odum, M. Rubin, and D.L. Eggeert. "Evidence of Strong Earthquake Shaking in the Lower Wabash Valley from Prehistoric Liquefaction Features." *Science*. Vol. 251. pp. 1061-1063. 1991.

Obermeier, S.F., J.R. Martin, A.D. Frankel, T.L. Youd, P.P. J. Munson, C.A. Munson, and E.C. Pond. *Liquefaction Evidence for One or More Strong Holocene Earthquakes in the Wabash Valley of Southern Indiana and Illinois, with a Preliminary Estimate of Magnitude*. U.S. Geological Survey Professional Paper 1536, 27 pp. 1993.

Obermeier, S.F., E.C. Pond, and S.M. Olson, with contributions by R.A. Green, T.D. Stark, and J.D. Mitchell. *Paleoliquefaction Studies in Continental Settings: Geologic and Geotechnical Factors in Interpretations and Back-Analysis*. U.S. Geological Survey Open-File Report 01-29, 75 pp. 2001.

Odum, J.K., W.J. Stephenson, K.M. Shedlock, and T.L. Pratt. "Near-Surface Structural Model for Deformation Associated with the February 7, 1812, New Madrid, Earthquake." *Geological Society of America Bulletin*. Vol. 110, No. 2. pp. 149-162. 1998.

Odum, J.K., W.J. Stephenson, R.A. Williams, J.A. Devera, and J.R. Staub. "Near-Surface Faulting and Deformation Overlying the Commerce Geophysical Lineament in Southern Illinois." *Seismological Research Letters*. Vol. 73, No. 5. pp. 687-697. 2002.

Olson, S.M., R.A. Green, and S.F. Obermeier. "Geotechnical Analysis of Paleoseismic Shaking Using Liquefaction Features: Part I. Major Updating of Analysis Techniques." U. S. Geological Survey Open-File Report 03-307. 33 pp. 2003.

Ostrom, M.E. *Geology Field Trip-Southwestern Dane County*. University of Wisconsin Geological and Natural History Survey. Madison, Wisconsin. 10 pp. 1971.

Ostrom, M.E., Director and State Geologist, Wisconsin Geological and Natural History Survey, Letter to G.E. Heim, Sargent & Lundy Geotechnical Division Head. CPS USAR Attachment D2.5. April 8, 1975.

Palmer, J.R., D. Hoffman, W.J. Stephenson, J.K. Odum, and R.A. Williams. "Shallow Seismic-Reflection Profiles and Geological Structure in the Benton Hills, Southeast Missouri." *Engineering Geology*. Vol. 46. pp. 217-233. 1997a.

Palmer, J.R., M. Shoemaker, D. Hoffman, N.L. Anderson, J.D. Vaughn, and R.W. Harrison. "Seismic Evidence of Quaternary Faulting in the Benton Hills Area Southeast Missouri." *Seismological Research Letters*. Vol. 68, No. 4. pp. 650-661. 1997b.

Pavlis, G.L., A.J. Rudman, B.M. Pope, M.W. Hamburger, and G.W. Bear. "Seismicity of the Wabash Valley Seismic Zone Based on a Temporary Seismic Array Experiment." *Seismological Research Letter*. Vol. 73, No. 5. pp. 751-761. 2002.

Peters, Roger. Wisconsin Geological and Natural History Survey. Written Communication. May 2, 2003.

Peters, Roger. Wisconsin Geological and Natural History Survey. Written Communication. May 14, 2003.

Pond, E.C., and J.R. Martin. "Estimated Magnitudes and Accelerations Associated with Prehistoric Earthquakes in the Wabash Valley Region of the Central United States." *Seismological Research Letters*. Vol. 68, No. 4. pp. 611-623. 1997.

Potter, C.J., J.A. Drahovzal, M.L. Sargent, and J.H. McBride. "Proterozoic Structure, Cambrian Rifting, and Younger Faulting as Revealed by a Regional Seismic Reflection Network in the Southern Illinois Basin." *Seismological Research Letters*. Vol. 68, No. 4, pp. 537-552. 1997.

Pratt, T.L., R. Culotta, E.C. Hauser, K.D. Nelson, L. Brown, S. Kaufman, J. Oliver, and W. Hinze. "Major Proterozoic Basement Features of the Eastern Midcontinent of North America Revealed by Recent COCORP Profiling." *Geology*. Vol. 17. pp. 505-509. 1989.

Pujol, J., A. Johnston, J. Chiu, and Y. Yang. "Refinement of Thrust Faulting Models for the Central New Madrid Seismic Zone." *Engineering Geology*. Vol. 46. pp. 281-298. 1997.

Rhea, S., and R.L. Wheeler. *Map Showing Seismicity in the Vicinity of the Lower Wabash Valley, Illinois, Indiana, and Kentucky*. U. S. Geological Survey Geologic Investigations Map I-2583-A, scale 1:250,000. 11 pp. 1996.

Rubey, W.W. *Geology and Mineral Resources of the Hardin and Brussels Quadrangles (in Illinois)*. U.S. Geological Survey Professional Paper 218. 1952.

Russ, D.P. "Style and Significance of Surface Deformation in the Vicinity of New Madrid, Missouri." *in* McKeown, F.A., and L.C. Pakiser (eds.) *Investigations of the New Madrid Missouri, Earthquake Region*. U.S. Geological Survey Professional Paper 1236. pp. 95-114. 1982.

Saucier, R.T. "Geoarchaeological Evidence of Strong Prehistoric Earthquakes in the New Madrid (Missouri) Seismic Zone." *Geology*. Vol. 19, pp. 296-298. 1991.

Schnabel, P.B., J. Lysmer, and H.B. Seed. "SHAKE: A Computer Program for Earthquake Response." EERC 72-12. Earthquake Engineering Research Center, University of California at Berkeley. 1972.

Schneider, J., B. Camp, and P.W. Mayne. "Soil Liquefaction Assessment in Mid-America by Seismic Piezocone Tests." Seismological Society of America, Eastern Section Meeting, Program and Abstracts. pp. 19-20. 1999.

Schweig, E.S., and M.A. Ellis. "Reconciling Short Recurrence Intervals with Minor Deformation in the New Madrid Seismic Zone." *Science*. Vol. 264. pp. 1308-1311. 1994.

Schweig, E.S., and R.B. Van Arsdale. "Neotectonics of the Upper Mississippi Embayment." *Engineering Geology*. Vol. 45, No. 1-4. pp. 185-203. 1996.

Seeber, L., and J.G. Armbruster. The NCEER-91 Earthquake Catalog: Improved Intensity-Based Magnitudes and Recurrence Relations for U.S. Earthquakes East of New Madrid, *Technical Report NCEER-91-0021*, National Center for Earthquake Engineering Research, Buffalo, New York. 1991.

Senior Seismic Hazard Analysis Committee (SSHAC). "Recommendations for Probabilistic Seismic Hazard Analysis: Guidance on Uncertainty and Use of Experts." NUREG/CR-6372, Volume 1, Washington, D.C., U.S. Nuclear Regulatory Commission. 1997.

Sexton, J.L., and P.B. Jones. "Evidence for Recurrent Faulting in the New Madrid Seismic Zone from Mini-Sosie High-Resolution Reflection Data." *Geophysics*. Vol. 51. pp. 1760-1788. 1986.

Sexton, J.L., L.W. Braile, W.J. Hinze, and M.J. Campbell. "Seismic Reflection Profiling Studies of a Buried Precambrian Rift beneath the Wabash Valley Fault Zone." *Geophysics*. Vol. 51, No. 3. pp. 640-660. 1986.

Silva, W.J. and R. Darragh. "Engineering Characterization of Earthquake Strong Ground Motion Recorded at Rock Sites." Electric Power Research Institute TR-102261. Palo Alto, California. 1995.

Silva, W.J. and K. Lee. "WES RASCALS Code for Synthesizing Earthquake Ground Motions." State-of-the-Art for Assessing Earthquake Hazards in the United States Report 24, Miscellaneous Paper S-73-1, U.S. Army Engineers Waterways Experiment Station. 1987.

Silva W.J., N. Abrahamson, G. Toro, and C. Costantino. "Description and Validation of the Stochastic Ground Motion Model." Report prepared by Pacific Engineering and Analysis, El Cerrito, CA for the Engineering Research and Applications Division, Department of Nuclear Energy, Brookhaven National Laboratory, Contract No. 770573. 1996.

Silva, W. J., N. Gregor, and R. Darragh, *Development of Regional Hard Rock Attenuation Relations for Central and Eastern North America*, Pacific Engineering and Analysis, El Cerrito, CA. 2002.

Sims, P.K. *Precambrian Basement Map of the Northern Midcontinent, U.S.A.* U.S. Geological Survey Miscellaneous Investigations Series Map I-1853A, scale 1:1,000,000. 1 sheet. 1990.

- Sims, P.K., and Z.E. Peterman. "Early Proterozoic Central Plains Orogen: A Major Buried Structure in the North-Central United States." *Geology*. Vol. 14. pp. 488-491. 1986.
- Sims, P.K., E.B. Kisvarsanyi, and G.B. Morey. *Geology and Metallogeny of Archean and Proterozoic Basement Terranes in the Northern Midcontinent, U.S.A. – An Overview*. U.S. Geological Survey Bulletin 1815. 51 pp. 1987.
- Snay, R.A., J.F. Ni, and H.C. Neugebauer. *Geodetically Derived Strain Across the Northern New Madrid Seismic Zone*. U. S. Geological Survey Professional Paper 1538-F. 1994.
- Somerville, P., N. Collins, N. Abrahamson, R. Graves, and C. Saikia. "Ground Motion Attenuation Relations for the Central and Eastern United States." Final Report to U.S. Geological Survey. 2001.
- Stephenson, W.J., J.K. Odum, R.A. Williams, T.L. Pratt, R.W. Harrison, and D. Hoffman. "Deformation and Quaternary Faulting in Southeast Missouri across the Commerce Geophysical Lineament." *Bulletin of the Seismological Society of America*. Vol. 89. pp. 140-155. 1999.
- Stickney, J.F. "Investigation of Recent Movement Along the Rough Creek Fault System in Webster and McLean Counties, Kentucky." Unpublished M.S. Thesis. 95 p., 5 pls, scale 1:150. 1985.
- Su, W.J., and J.H. McBride. *Final Technical Report – Study of a Potential Seismic Source Zone in South-Central Illinois (abs.)*. Technical Report Submitted to the U.S. Geological Survey under USGS External Grant Number 99HQGR0075. 1999.
- Taylor, K.B., R.B. Hermann, M.W. Hamburger, G.L. Pavlis, A. Johnston, C. Langer, and C. Lam. "The Southeastern Illinois Earthquake of 10 June 1987." *Seismological Research Letters*. Vol. 60, No. 3. pp. 101-110. 1989.
- Templeton, J.S., and H.B. Willman. *Guidebook for the Sixteenth Annual Field Conference of the Tri-State Geological Society*. Guidebook Series 2. Illinois State Geological Survey, Urbana, Illinois. 47 pp. 1952.
- Thwaites, F.T. *Map of the Buried Pre-Cambrian of Wisconsin*. Wisconsin Geological and Natural History Survey. 1957.
- Toro, G. "Probabilistic Models of Site Velocity Profiles for Generic and Site-Specific Ground Motion Amplification Studies." Appendix C of Silva et al. (1996). 1996.
- Toro, G.R., and W.J. Silva. *Scenario Earthquakes for Saint Louis, MO, and Memphis, TN, and Seismic Hazard Maps for the Central United States Region including the Effect of Site Conditions*. Final Technical Report Submitted to the U.S. Geological Survey under USGS External Grant Number 1434-HQ-97-GR-02981. 2001.
- Toro, G., N. Abrahamson, and J. Schneider. "Model of Strong Ground Motions from Earthquakes in the Central and Eastern North America: Best Estimates and Uncertainties." *Seismological Research Letters*. Vol. 68, pp. 41-57. 1997.
- Tuttle, M. *Implications for Tectonics, Paleoseismicity, and Ground Failure from Soft-Sediment Deformation in the Marked Tree Area of the New Madrid Seismic Zone*. Annual Report Submitted

to the U.S. Geological Survey under USGS External Project No. 14080001-G62001. 25 pp. 1993.

Tuttle, M.P. *Late Holocene Earthquakes and their Implications for Earthquake Potential of the New Madrid Seismic Zone, Central United States*. Ph.D. Dissertation. University of Maryland. 250 pp. 1999.

Tuttle, M.P. "The Use of Liquefaction Features in Paleoseismology: Lessons Learned in the New Madrid Seismic Zone, Central United States." *Journal of Seismology*. Vol. 5. pp. 361-380. 2001.

Tuttle, Martitia P. M. Tuttle & Associates. Written (Electronic) Communication. September 3, 2002.

Tuttle, Martitia P. M. Tuttle & Associates. Written (Electronic) Communication. February 11, 2003.

Tuttle, Martitia P. M. Tuttle & Associates. Written (Electronic) Communication. February 27, 2003.

Tuttle, M.P., and E.S. Schweig. "Recognizing and Dating Prehistoric Liquefaction Features: Lessons Learned in the New Madrid Seismic Zone, Central United States." *Journal of Geophysical Research*. Vol. 101, No. B3. pp. 6171-6178. 1996.

Tuttle, M.P., and E.S. Schweig. "The Earthquake Potential of the New Madrid Seismic Zone." *American Geophysical Union, EOS Transactions*. Vol. 81, No. 19, p. S308. 2000.

Tuttle, M.P., and E.S. Schweig. *Towards a Paleoearthquake Chronology for the New Madrid Seismic Zone*. Collaborative Research, M. Tuttle & Associates and Eastern Region Hazards Team, U.S. Geological Survey. Annual Report Submitted to the U.S. Geological Survey. USGS External Project No. 1434-99HQGR0022. 18 pp. 2001.

Tuttle, M.P., and L.W. Wolf. *Towards a Paleoearthquake Chronology for the New Madrid Seismic Zone*. Progress Report Submitted to the U.S. Geological Survey NEHRP. USGS External Project No. 1434-01HQGR0164. 36 pp. 2003.

Tuttle, M.P., R.H. Lafferty, R.F. Cande, J.S. Chester, and M. Haynes. "Evidence of Earthquake-Induced Liquefaction North of the New Madrid Seismic Zone, Central United States" (abs.). *Seismological Research Letters*. Vol. 67, No. 2. page 58. 1996.

Tuttle, M.P., R.H. Lafferty III, and E.S. Schweig III. *Dating of Liquefaction Features in the New Madrid Seismic Zone and Implications for Earthquake Hazard*. U. S. Nuclear Regulatory Commission Report NUREG/GR-0017. 77 pp. (plus appendices). 1998.

Tuttle, M.P., J. Chester, R. Lafferty, K. Dyer-Williams, and R. Cande. *Paleoseismology Study Northwest of the New Madrid Seismic Zone*. U. S. Nuclear Regulatory Commission Report NUREG/CR-5730, 96 pp. 1999a.

Tuttle, M.P., J. Collier, L.W. Wolf, and R.H. Lafferty. "New Evidence for a Large Earthquake in the New Madrid Seismic Zone between A. D. 1400 and 1670." *Geology*. Vol. 27, No. 9. pp. 771-774. 1999b.

Tuttle, M.P., J.D. Sims, K. Dyer-Williams, R.H. Lafferty III, and E.S. Schweig III. *Dating of Liquefaction Features in the New Madrid Seismic Zone*. U. S. Nuclear Regulatory Commission Report NUREG/GR-0018. 42 pp. (plus appendices). 2000.

Tuttle, M.P., E.S. Schweig, J.D. Sims, and R.H. Lafferty. "Recurrence of Clustered Major Earthquakes in the New Madrid Seismic Zone." *Seismological Research Letters*. Vol. 72, No. 2. pp. 265. 2001.

Tuttle, M.P., E.S. Schweig, J.D. Sims, R.H. Lafferty, L.W. Wolf, and M.C. Haynes. "The Earthquake Potential of the New Madrid Seismic Zone." *Bulletin of the Seismological Society of America*. Vol. 92, No. 6. pp. 2080-2089. 2002.

University of Missouri, 1991. Department of Geology. State Geologic Faults of Missouri. Available: <http://msdis.missouri.edu/html/sfault.html>. [15.08.2002].

U.S. Department of Energy (DOE). *Natural Phenomena Hazards Design and Evaluation Criteria for Department of Energy Facilities*. DOE Standard DOE-STD-1020-94. U.S. Department of Energy, Washington D.C. 1996.

U.S. Nuclear Regulatory Commission (USNRC). "Safety Goals for the Operation of Nuclear Power Plants: Policy Statement", *Federal Register*, 10 CFR Part 50, Vol. 51, No. 149. 1986.

U.S. Nuclear Regulatory Commission (USNRC). "Identification and Characterization of Seismic Sources and Determination of Safe Shutdown Earthquake Ground Motion." Regulatory Guide 1.165, U.S. Nuclear Regulatory Commission, Washington, DC. 1997.

U.S. Nuclear Regulatory Commission (USNRC). "An Approach for Using Probabilistic Risk Assessment in Risk-Informed Decisions on Plant-Specific Changes to the Licensing Basis." Regulatory Guide 1.174, U.S. Nuclear Regulatory Commission, Washington, DC. 1998.

U.S. Nuclear Regulatory Commission (USNRC). "White Paper on Risk-Informed, Performance-Based Regulation." SECY-98-144, U.S. Nuclear Regulatory Commission, Washington, DC. 1999.

U.S. Nuclear Regulatory Commission (USNRC). "Modified Reactor Safety Goal Policy Statement." SECY-01-0009, U. S. Nuclear Regulatory Commission, Washington, DC. 2001.

U.S. Nuclear Regulatory Commission (USNRC). "Update of the Risk-Informed Regulation Implementation Plan." SECY-02-0131, U.S. Nuclear Regulatory Commission, Washington, DC. 2002.

Van Arsedale, R.B. Displacement History and Slip Rate on the Reelfoot Fault of the New Madrid Seismic Zone." *Engineering Geology*. Vol. 55. pp. 219-226. 2000.

Van Arsedale, R., and A. Johnston. *Geological and Seismological Setting of the New Madrid Seismic Zone and the Wabash Valley Seismic Zone, Appendix A*. in Risk Engineering, Inc. "Revision 3 to Updated Probabilistic Seismic Hazard Analysis for the Paducah Gaseous Diffusion Plant, Paducah, Kentucky." Final Report (Revision 3), Risk Engineering, Inc., Boulder Co., USEC Contract Number USEC-96C-0001. Prepared for Lockheed-Martin Utility Services. Available through USNRC Public Documents Library. Accession Number 9905140175. Docket No. 07007001. pp. A1-A51. 1999.

Van Arsdale, R.B., R.T. Cox, A.C. Johnston, W.J. Stephenson, and J.K. Odum. "Southeastern Extension of the Reelfoot Fault." *Seismological Research Letters*. Vol. 70, No. 3, pp. 348-359. 1999.

Van Schmus, W.R., M.E. Bickford, and A. Turek. "Proterozoic Geology of the East-Central Midcontinent Basement. In Van der Pluijm, B.A., and P.A. Catacosinos (eds.). *Basement and Basins of Eastern North America*. Boulder, Colorado. Geological Society of America Special Paper 308. pp. 7-32. 1996.

Vaughn, J.D. *Paleoseismological Studies in the Western Lowlands of Southeast Missouri*. Report to National Earthquake Hazards Reduction Program Annual External Program. Contract Number 14-08-0001-G1931, 27 pp. 1994.

Weber, J., S. Stein, and J. Engeln. "Estimation of Strain Accumulation in the New Madrid Seismic Zone from GPS Geodesy." *Tectonics*. Vol. 17. pp. 250-266. 1998.

Wheeler, R. "Boundary Separating the Seismically Active Reelfoot Rift from the Sparsely Seismic Rough Creek Graben, Kentucky, and Illinois." *Seismological Research Letters*. Vol. 68. pp. 586-598. 1997.

Wheeler, R.L., and C.H. Cramer. "Updated Seismic Hazard in the Southern Illinois Basin – Geological and Geophysical Foundations for Use in the 2002 USGS National Seismic-Hazard Maps." *Seismological Research Letters*. Vol. 73, No. 5. pp. 776-791. 2002.

Wheeler, R.L., and A.J. Crone. "Known and Suggested Quaternary Faulting in the Midcontinent United States." *Engineering Geology*. Vol. 62. pp. 51-78. 2001.

Wheeler, R.L., S. Rhea, S.F. Diehl, J.A. Drahovzal, G.W. Bear, and M.L. Sargent. *Seismotectonic Map Showing Faults, Igneous Rocks, and Geophysical and Neotectonic Features in the Vicinity of the Lower Wabash Valley, Illinois, Indiana, and Kentucky*. U.S. Geological Survey Geologic Investigations Series I-2583-D. 1997.

Willman, H.B., E. Atherton, T.C. Buschbach, C. Collinston, J.C. Frye, M. Hopkins, J.A. Lineback, and J.A. Simon. *Handbook of Illinois Stratigraphy*. Illinois State Geological Survey Bulletin 95. 261 pp. 1975.

Woolery, E.W., and R. Street. "Quaternary Fault Reactivation in the Fluorspar Area Fault Complex of Western Kentucky: Evidence from Shallow SH-Wave Reflection Profiles." *Seismological Research Letters*. Vol. 73, No. 5. pp. 628-639. 2002.

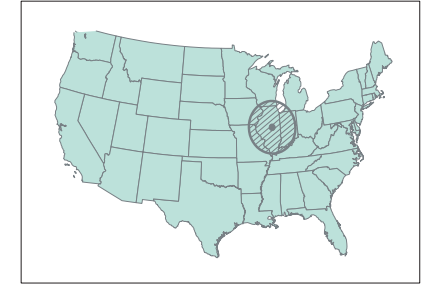
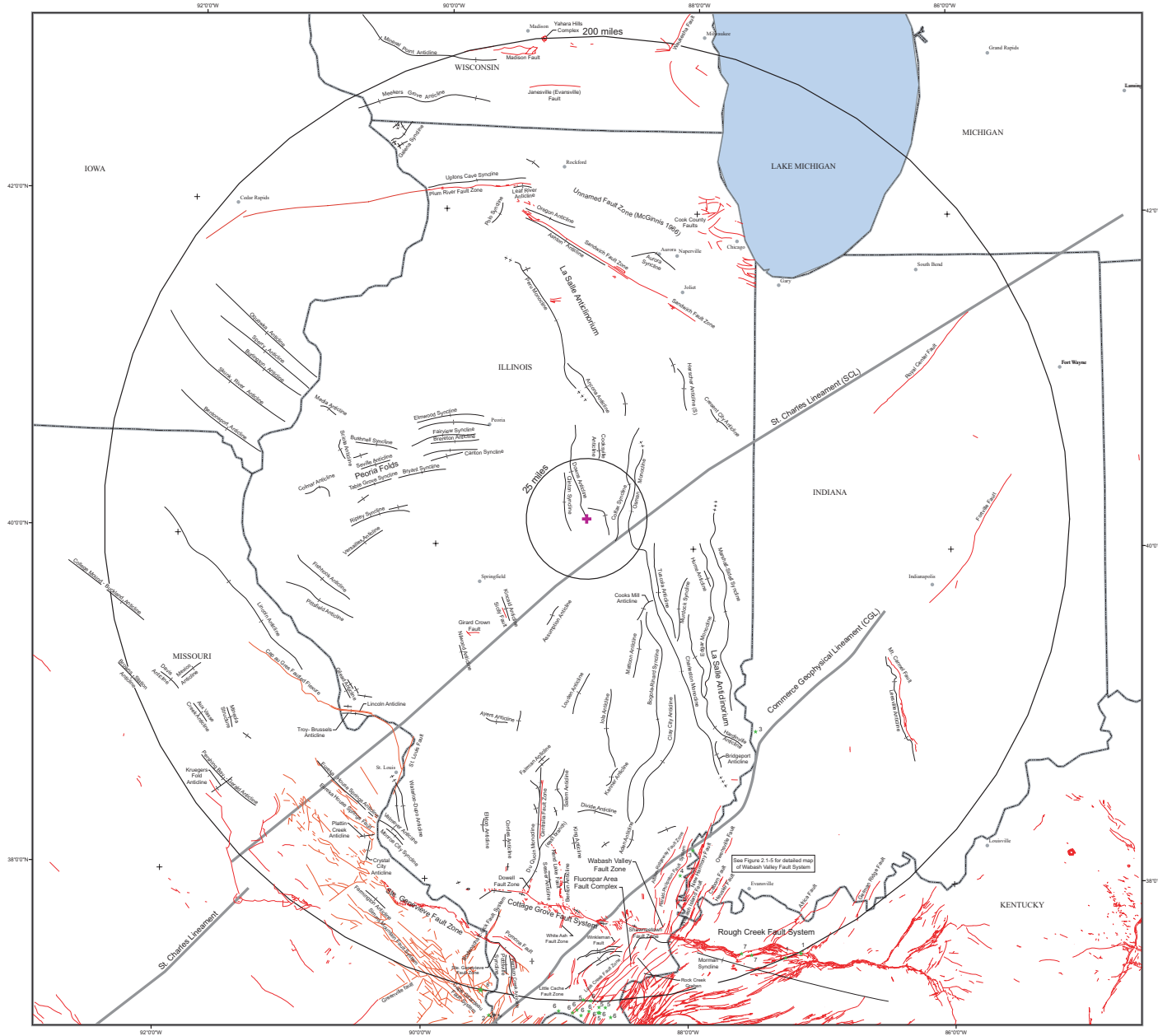
Working Group on California Earthquake Probabilities. "Earthquake Probabilities in the San Francisco Bay Region: 2000 to 2030 - A Summary of Findings." U.S. Geological Survey, Open File Report 99-517. 1999.

Working Group on California Earthquake Probabilities. "Earthquake Probabilities in the San Francisco Bay Region: 2002-2031." U.S. Geological Survey Open-File Report 03-214. 2003.

Youngs, R.R., and K.J. Coppersmith. "Implications of Fault Slip Rates and Earthquake Recurrence Models to Probabilistic Hazard Estimates." *Bulletin of the Seismological Society of America*. Vol. 75. pp. 939-964. 1985

Youngs, R.R., F.H. Swan, and M.S. Power. "Use of detailed geologic data in regional PSHA: an example from the Wasatch Front, Utah" In "Earthquake Engineering and Soil Dynamics II – Recent Advances in Ground Motion Evaluation," J.L. Von Thun (Ed.). pp. 156-172. 1988.

Zoback, M.L., and M.D. Zoback. "Tectonic Stress Field of the Continental United States." in Pakiser, L.C., and W.D. Mooney (eds.). *Geophysical Framework of the Continental United States*. Geological Society of America Memoir 172. pp. 523-539. 1989.



Legend

- + EGC ESP Site
- Faults
- Well documented, significant faults, faulted flexures and graben.
- Folds
- Well documented, significant fold structures that deform Mesozoic and older rocks.
- Anticline
- Syncline
- Monocline
- + Neotectonic Point
- + Locations of known or suspected recent faulting or tectonic deformation. Features identified in trenches, auger holes, wells, or on the surface.

Source	Age of Youngest Deformation	Comments
1. Harrison and Schultz (2002)	Quaternary (New Wisconsin?)	Quaternary faulting evidence often identified from shallow geophysics and auger hole data.
2. Harrison and Schultz (2002)	Quaternary	Quaternary faulting evidence for regional westward tilt of modern level surface. Southern evidence approximately southern and southern border.
3. Finner and others (1997)	Quaternary and Holocene	Quaternary evidence for regional westward tilt of modern level surface. Southern evidence approximately southern and southern border.
4. Hargrett and Lauen (1994)	1811-1812	Quaternary and Holocene
5. Nelson and others (1995)	Quaternary and Holocene	Quaternary and Holocene
6. Nelson and others (1995)	Quaternary and Holocene	Quaternary and Holocene
7. Doherty (1985)	Quaternary and Holocene	Quaternary and Holocene
8. Harrison and Schultz (2002)	Quaternary and Holocene	Quaternary and Holocene

Geophysical Lineaments
Data Sources:
Harrison and Schultz (2002)
Hilbert and others (2002)
Milne and Kozala (1999)

Major Cities (Population greater than 100,000)
St. Louis
St. Charles
St. Louis

Sources of Map Data

- Nelson (1995) (Faults and folds in Illinois)
- Indiana Geological Survey (2001)
- Kentucky Geological Survey (2002), Geologic Faults in Kentucky
- State Geological Survey of Missouri, Department of Geology, University of Missouri, Columbia (1991)
- Harrison and Schultz (2002) (Faults and Folds in Southeastern Missouri and Southwestern Illinois)
- CPS USAR, (Folds in Iowa, Wisconsin, and Missouri)
- Evans et al. (2003, in preparation) (Faults in Wisconsin)
- Brown et al. (2003, in preparation) (Faults in Wisconsin)

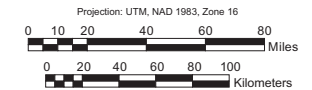


Plate 1
Seismic Hazards Report for the EGC ESP Site
Structural Features Map